School of Chemical and Petroleum Engineering

Department of Chemical Engineering

Photocatalytic Oxidation of Air Toxics via Visible Light Irradiation and Nano-Photocatalysts

Ruh Ullah

This thesis is presented for the degree of

Doctor of Philosophy

of

Curtin University

June 2012

Declaration

To the best of my knowledge and belief this thesis contains no material previously published by any other person except where due acknowledgment has been made. This thesis contains no material which has been accepted for the award of any other degree or diploma in any university.

Signature:…….

Date: …….

This thesis is dedicated in the loving memory to my parents

Acknowledgement

I heartily owe my deepest gratitude to Associate Professor Shaobin Wang who has provided me exceptionally worthy supervision with great patient and proper directions; and fortified me throughout this research work. I must say that this thesis would have not been completed without his friendly encouragement that he has extended toward me all the time.

My enthusiastic gratitude must also go to my co-supervisor Prof. Ming Ang who has always paid considerable attention to my requests and resolved my issues on top priority basis and with great pleasure. This was his greatness that I never need to make prior appointment for meeting with him. I am really thankful to him for his encouragement and worthy support throughout my stay in Curtin University.

I am also grateful to Porf. Moses Tade being the head of the School and my thesis chairman, who has always praised my work, supported me morally and financially. I sincerely express my thanks to him for his guidance and strong motivation.

I would like to thank Prof. Ravi Naidu, Managing Director of Cooperative Research Centre for Contamination Assessment and Remediation of the Environment (CRC-CARE), and Chemical Engineering Department, Curtin University, for providing me the financial support for completion of this research work.

I also express my sincere thanks to Dr. Hung Pham and Dr. Hongqi who have always helped me and gave me trainings on various equipments that were required for completion of this work.

I am also grateful to my senior colleagues, Dr. Pradeep Shukla, and Dr. Fay Chong with whom I started my research work. I am really thankful for their help which they provided me in the initial stages of this research work.

My gratitude must also go to my colleagues and friends, particularly Hussein, Yash, Eddy, Syaifullah and Manzar Sohail who have helped me on various occasions for the fulfilment of this thesis.

I must gratitude the Department of Imaging and Applied Physics of Curtin University and particularly Dr. Rob Hart, and Ms Elaine Millar who have trained me on XRD, SEM and TEM, and helped me using these characterization facilities.

I am also thankful to all laboratory technical staff, Karen Haynes, Jason Write, and Ann Carrol for their great and valuable help in the safe use of laboratory equipment and providing the required items.

I am also thankful to those master and undergraduate students who have worked with me on this project.

I am also thankful to my father, brothers, and sisters who have always kept in touch with me via telephone, and encouraged me through various means to continue my learning and research endeavours. They gave me their unequivocal support throughout, as always, for which my mere expression of thanks likewise does not suffice.

At last special thanks and gratitude go to my lovely wife and three kids, Fida Ullah, Ibad Ullah and Raeesa, who joined me here for this interesting and hardworking time with great patient which makes this thesis a success. I must say that without the great help of my wife and everlasting love of my kids this work would never be completed.

Abstract

This thesis explores synthesis of various types of metal oxide nanoparticles through a wet-chemical synthesis route. The materials were used for photocatalytic oxidation of gaseous toluene irradiated with UV, artificial solar light, and pure visible light. Tantalum based compounds like $BiTaO_4$: La, $BiNbO_4$: Ga and Ta_2O_5 have shown better performance than a commercial TiO_2 under UV and solar light. Ta_2O_5 and nitrogen doped Ta_2O_5 have shown excellent performance for toluene oxidation with solar and visible light.

Summary

This scholarly research work explores the preparation of metal oxide nano-photocatalysts and their application for decomposition of gaseous volatile organic compounds through advanced oxidation techniques. Enormous volatile organic compounds such as toluene, acetaldehyde, formaldehyde and benzene are continuously emitting from various sources and polluting the indoor air. Photocatalytic oxidation is an advanced technology, where the photo-excited electron-hole pairs at the conduction and valence band participates in a redox reaction and produces powerful hydroxyl radicals. The hydroxyl radicals on photocatalyst surface undergo reactions with adsorbed VOCs and consequently disintegrate them in water, CO_2 and mineral salt.

This dissertation reports synthesis of various photocatalyst materials prepared with a solution method and their application for removal of toluene both with UV and artificial solar light. We successfully prepared pristine, cation and anion doped materials which include $InTaO_4$, $InNbO_4$, $AgNbO_3$, $EuTaO_4$, $AgTaO_3$, $Cd_2Ta_2O_7$, $CeTaO_4$, $CoTa_2O_6$, $BiTaO_4$, $AgVO_3$, Bi_2WO_6, $BiNbO_4$, Nb_2O_5 and Ta_2O_5. Metal ions such as Ag, Ni, Fe, Co, Cu, Nd, W, Ga, Ba, Sn, La and Pt, were doped at 2 wt% ratio in $InTaO_4$, $BiTaO_4$ and $BiNbO_4$, which consequently modified the optical and photocatalytic properties of these materials. Gaseous toluene was decomposed with these materials using a continuous flow reactor irradiated with both ultraviolet and visible light. All of the newly prepared materials were capable to decompose toluene with ultraviolet light. However, materials like La doped $BiTaO_4$, Ga doped $BiNbO_4$ and Ni doped $InTaO_4$ were more efficient than TiO_2 (P25) under UV light irradiation. Most of the newly prepared materials are quite stable under UV irradiation. Neither their photocatalytic performance reduces in repeated tests nor the photo-corrosion degrades the structure of these materials. Unlike TiO_2, intermediate adsorption was not observed for the newly prepared materials indicating the appropriateness of these materials for commercialization.

Pristine $BiTaO_4$, $BiNbO_4$, $AgTaO_3$, $Cd_2Ta_2O_7$ and Ta_2O_5 are capable to degrade toluene under artificial solar light irradiation with much faster rate than TiO_2. The

higher photocatalytic performance of these metal oxide nanomaterials are attributed to large number of defect states at lower energy levels, which can easily photo-generate electron-hole pairs under visible light irradiation. Metal ion doping in $BiTaO_4$ and $BiNbO_4$ has significantly improved toluene decomposition with artificial solar light.

The last task of this thesis is devoted to the most efficient nitrogen doped Ta_2O_5. This material has the highest activity for gaseous toluene decomposition both in undoped and nitrogen doped form. Nitrogen doped Ta_2O_5 is capable to decompose more than 70% of gaseous toluene continuously for long time without any significant reduction in the performance. Among the various newly synthesized materials, nitrogen doped Ta_2O_5 has shown excellent performance with high and long-time stability and re-usability without malfunctioning. This thesis suggests that nitrogen doped Ta_2O_5 is an efficient photocatalyst material and can be further examined for other VOCs such as formaldehyde and acetaldehyde to check the applicability of this material on a large scale.

Publications by author

Referred Journals

Ruh Ullah, Shaobin Wang, H. Ming Ang, Moses O Tade, " Synthesis of Doped $BiNbO_4$ Photocatalysts for Removal of Gaseous Volatile Organic Compounds with Artificial Sunlight (Under review), Chemical Engineering Journal, 185-186(2012) 328-336.

Ruh Ullah, Hongqi Sun, Shaobin Wang, H. Ming Ang, Moses O Tade," Visible Light Photocatalytic Degradation of Organics on Nanoparticles of Bi-Metallic Oxides, Separ & Puri Technology, 89 (2012) 98-106.

Hongqi Sun, Ruh Ullah, Chong Siewhui, Shaobin Wang, H. Ming Ang, Moses O Tade, "Room-Light-Induced Indoor Air Purification", Appl. Catal. B Environment, 108-109 (2011) 127-133

Ruh Ullah, Hongqi Sun, Shaobin Wang, H. Ming Ang, Moses O Tade, Wet-chemical Synthesis of $InTaO_4$ for Photocatalytic Decomposition of Organic Contaminants in Air and Water (Journal of Industrial & Engineering Chemistry Research (I&EC Research). Ind. Eng. Chem. Res. 51 (2012) 1563–1569**.**

S. Rehman, Ruh Ullah, A. M. Butt, and N. D. Gohar "Strategies of making TiO_2 and ZnO visible light active", Journal of Hazardous Materials 170 (2009)560-569.

R. Ullah, J. Dutta, "Photodegradation of Organic Dyes with Manganese Doped ZnO Nanoparticles" Journal of Hazardous Materials 156(2008)194-200.

Submitted papers

Ruh Ullah, Hongqi Sun, Shaobin Wang, H. Ming Ang, Moses O Tade, "Photocatalytic Decomposition of Water and Air Contaminants with Metal Doped $BiTaO_4$ Irradiated with visible light" In press, Catalysis Today.

Hongqi Sun, Ruh Ullah, Siewhui Chong, Ha Ming Ang, Moses O Tadé, Shaobin Wang "Visible light titania photocatalysts co-doped by nitrogen and metals for remediation of aqueous and gaseous pollutants" (Submitted) Photochem Photobiol A Chem

Ruh Ullah, Shaobin Wang, H. Ming Ang, Moses O Tade, "Effect of nitrogen doping on the photocatalytic activities of Ta_2O_5 and Nb_2O_5 nanoparticles" (In submission)

Referred Conference Presentations

Ruh Ullah and Shaobin Wang, "Preventing indoor air pollution with nanotechnology, Collaborate Innvate, Adelaide May 15—17 2012, Organized by CRC-CARE. Cooperative Research Centres Association 2012 Conference.

Ruh Ullah, Hongqi Sun, Shaobin Wang, H. Ming Ang, Moses O Tade, Photocatalytic oxidation of gaseous toluene with nitrogen doped Ta_2O_5, 7th International Conference on Environmental Catalysis (ICEC 2012), Lyon – France, 2 - 6 September 2012.

Ruh Ullah, Hongqi Sun, Shaobin Wang, H. Ming Ang, Moses O Tade, Alternative photocatalysts to TiO_2 for catalytic reactions by UV-vis light, 15th International Congress on Catalysis (ICC 2012), Munich/Germany from July 01-06, 2012.

Ruh Ullah, Shaobin Wang, H. Ming Ang, Moses O Tade, Visible Light Photocatalytic Decomposition of Toluene with $BiMO_4$ (M = Ta, Nb) Presented in CleanUp 2011, 4th International Contaminated Site Remediation Conference 11–15 September, 2011.

Ruh Ullah, Hongqi Sun, Shaobin Wang, H. Ming Ang, Moses O Tade, Photocatalytic decomposition of organic contaminants with $InTaO_4$ synthesised with wet-chemical techniques, Presented in Asia Pacific Conference on Sustainable Energy & Environmental Technologies (APCSEET 10-13th July 2011).

Ruh Ullah, Shaobin Wang, Hongqi Sun, H. Ming Ang, Moses O Tade, “Synthesis, Characterization and Applications of Vanadium, Tantalum and Niobium Based Oxides for Photocatalytic Presented in VII International Symposium on Group Five Elements held in Italy 8th -11th May 2011.

Ruh Ullah, Dr. Shaobin Wang, Dr. Hongqi Sun, Dr. Pradeep Shukla, Professor Ming Ang, and Professor Moses Tade, "Photocatalytic Oxidation of Toluene Under visible Light Irradiation" Communicate 10 Conference (21-22nd July 2010) Organised by Cooperative Research Centre for Contamination Assessment and Remediation of the Environment (CRC CARE) Adelaide South Australia

Siewhui Chong, Pradeep Shukla, Hongqi Sun, Ruh Ullah, Gia Hung Pham, Shaobin Wang, Ming Ang, Vishnu Pareek, Moses Tade, "Visible-light photocatalytic oxidation of toluene on N,Pt-TiO_2 using a flat-plate reactor", Asia Pasific conference on Sustainable Energy and Environment Technology (APCSEET2009). Organizer: China University of Petroleum Research Centre of Eco-Environmental Sciences, China Academy of Sciences.

Ruh Ullah and Dr. Joydeep Dutta, “Photocatalytic activities of ZnO nanoparticles synthesized by wet chemical techniques”, Proceedings of Second International Conference on Emerging Technologies Peshawar, November 2006 (ICET -2006 Peshawar) 353-358.

Ruh Ullah, Joydeep Dutta, “Synthesis and Optical Properties of Transition Metal Doped ZnO Nanoparticles” Proceedings of International Conference on Emerging Technologies Islamabad, November 2007 (ICET -2007) 306-311.

Ruh Ullah, Joydeep Dutta, Photocatalysis with Mn-doped ZnO nanoparticles (Presented in nano2006 international conference, Bangalore, India)

Ruh Ullah, Sunandan Baruah, Faizur Rafique Rahman, and Joydeep Dutta "ZnO nanoparticles and Nanowires semiconductor doping, a way towards visible light photocatalysis", ISNEPP 2007, International Symposium on

Nanotechnology in Environmental Protection and Pollution, 11-13 December 2007, The Bahia Mar Beach Resort and Yachting Hotel, Ft. Lauderdale, Florida, USA, (Asia Pacific Nanotechnology Forum)

Scholarly Articles

Ruh Ullah, Shaobin Wang, 'Removing VOCs through Photocatalytic Oxidation", Remediation Australia, Issue# 7 Sep 2011 (12-14)

CONTENTS

List of Figures

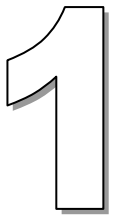

1 -Introduction

1.1 Motivation

Concerns about the severe health effects resulted from indoor air pollution have increased in recent decades since the concentrations of indoor air pollutants in modern buildings have risen to relatively high levels. In this advanced technological era both in developed and developing countries people spent most of their time in enclosed environment such as offices, homes, vehicles and others indoor conditions. It has been estimated that the people in developed countries like USA, Australia and Europe spend averagely more than 90% of their time indoors. As per the U.S Environmental Protection Agency (EPA), indoor air pollution is one of the top-five environmental issues.

There are mainly two types of air pollution; i) biologicals; which include measles, influenza, molds, viruses, dust mites and bacteria and ii) chemicals; which consist of carbon monooxide, ozone, tobacco and other smokes, radon, pesticides, asbestos and volatile organic compounds (VOCs). Among the numerous air pollutants, volatile organic compounds have been identified as the major contributors to the extremely high risks associated with air pollution. An EPA investigation revealed that the concentration of organic pollutants inside homes is about 20 times higher than outside environment[1]. The outdoor air pollutants and large number of indoor sources are the major components contributing to the poor indoor air quality[2]. Many VOCs, which are the roots for fatal diseases like carcinoma and mutagenicity, have a very close relationship to sick building syndrome (SBS) i.e. excess of chronic symptoms[3]. Even though the average concentration of individual VOC is usually lower than 50 $\mu g/m^3$, the total VOCs are much higher and therefore, assumed to be the sources of above various fatal diseases.

The common air purification techniques like ventilation and its advanced forms such as air filtration, High Efficiency Particulates Air (HEPA) filter, electronic air filters, dust filters, ionic purifiers, adsorption filters and thermo-catalytic combustors have been successful in mitigating the biological pollutants,

however, these techniques neither perfectly reduce the concentrations of chemical pollutants nor mitigate their severe health effects[4].

However, advanced oxidation techniques like heterogeneous photocatalysis have been proven as efficient purification technologies, which can completely mineralize various toxic VOCs and reduce the risks associated with these compounds. This research therefore, focuses on the preparation of suitable photocatalytic materials and their application for photocatalytic mineralization of various VOCs detected inside the buildings.

1.1.1 Major volatile organic compounds (VOCs) in air

A large number of home items including furniture, wall paints, carpets, detergents, aerosol products, air-fresheners, cigarettes smokes and many more emit various types of gaseous VOCs. National Asthma Council of Australia (NAC) and other World Health Organizations have indentified through various research studies that the most abundantly emitted VOCs are; formaldehyde, acetaldehyde, benzaldehyde, toluene, phenol, benzene, styrene, xylenes, trichloroethylene and acetone. Since different types of sources emit large number of volatile organic compounds and it is very challenging and complicated to identify and measure the concentration of each VOC. Therefore, in a recent report by the European Collaborative Action (ECA) the total concentration and wide range of VOCs were termed to be identified by "total volatile organic compounds" TVOCs. The total volatile organic compounds consisted of about 64 different types of VOCs emitted by various sources and were detected by advanced analytical techniques. Among the various VOCs, formaldehyde has been found as the most abundantly occurring hydrocarbon which is emitted by large number of sources. The above chemicals are the main indoor pollutants which have serious effects on the health[5].

1.1.2 Effects of poor indoor air quality (IAQ)

The systematic investigation of health effects caused by IAQ has not been performed so far which could be helpful in identifying specific health problems associated with VOCs. However, the occupants of buildings with poor IAQ can suffer from various types of effects ranging from irritation (of eyes, nose, and throat) to dizziness and nausea to even more severe issues like asthma, allergic response, cancer and damage to the central nervous system. The level of toxicity varies with the quantities and types of VOCs. Even though the concentrations of some toxic VOCs are very low and would not cause immediate concerns, however, the long term health effects associated with these compounds are even more treacherous.

EPA case studies have envisaged that some VOCs like trichloroethylene, toluene, xylene, styrene and methyl chloride could be the sources of leukaemia in children, neurological difficulties and development growth in infants and cancer in animals. Formaldehyde which is the mostly emitted hydrocarbon of various indoor and outdoor items has been identified to be the source of adverse health effects like dizziness, asthma, respiratory and lung diseases, and even malignance.

1.1.3 Removal of VOCs via photocatalytic oxidation

Although some air purification technologies such as ventilation through HEPA, destructs micro-organism such as germs, bacteria and molds via germicidal UV lamps, ionizer and anti-bacterial filters are relatively useful, however, these and some other advanced level air purification technologies are inadequate for removal of VOCs.

Since its discovery, oxidation of VOCs via photocatalytic process has been introduced as a vital technology for indoor and outdoor air purification. Some successful results have been shown for photocatalytic degradation of VOCs in gaseous forms using pure and modified TiO_2 irradiated with black light ($\lambda<380$

nm) however, these systems have some other related issues like humidity effect, low adsorption and reduced efficiency at low ppm level of contaminants. The competitive adsorption of water and VOCs molecules[6] on the photocatalyst surface has significant effects on the oxidation rate. It has been observed that the photocatalytic oxidation efficiency decreased with decreasing the pollutant concentration [7]. Many investigations have described the enhanced photocatalytic properties of nitrogen doped TiO_2, however, its potential application is very limited and doping and/or modification with additional elements or compounds will further promote the catalytic activity[3]. The experiments showed that instead of decomposition, many VOCs such as formaldehyde, acetone, and acetaldehyde were generated during normal and UVA light irradiation suggesting the malfunctioning of paints mixed photocatalysts. The complete mineralization of indoor VOCs through visible light radiated photocatalyst is still under way to be investigated.

The Interim national indoor air quality goals recommended by the Australian National Health and Medical Research Council have suggested the permissible levels of various pollutants in air including formaldehyde in the range of 0.1 ppm (120 $\mu mol/m^3$), which is similar to the World Health Organization (WHO) guidelines for formaldehyde exposure. The applicability of the process becomes more and more difficult due to the UV light requirements in huge amounts. Therefore, a lot of research is required to develop such a photocatalyst, which can be operated efficiently at the available artificial light and/or sun light in the intensity range of 0.1-0.2 mW/cm^2. This research particularly focused on the development of new photocatalysts, which will be capable to operate through indoor lightening and will not demand for UV light and/or high intensity radiation.

1.2 Scope and objectives of thesis

The main objective of this research was to decompose gaseous volatile organic compounds with nanomaterials and visible light irradiation. The disintegration

of gaseous VOCs takes place via oxidation processes. Electron-hole pairs are generated at the conduction and valence band of metal oxide nanoparticles upon visible light irradiation. The photo-generated carriers migrate quickly to the particle surface and participate in redox reactions to produce powerful hydroxyl radicals at the valence band and super oxide at the conduction band. The hydroxyl radicals produced by photo-generated carrier have the proper potential and can mineralize large number of VOCs. The overall research work aimed

i) To synthesize a novel nano-photocatalyst being capable of degrading indoor air toxins at room temperature.
ii) To synthesize and develop semiconductor metal oxide nano-photocatalysts via wet-chemical routes.
iii) To evaluate the photocatalytic activities of newly synthesized materials irradiated with visible light at room temperature.
iv) To investigate the performance of newly developed photocatalysts, immobilized on a suitable support using an enclosed controllable reactor for the practical applications

1.3 Thesis organization

Chapter one of this work mainly introduced the overall scenario of the air pollution associated worse effect on human health. Chapter one also briefly described the main sources and types of VOCs, their associated health risks. Scope of the thesis and chapter wise summary of the thesis are also a part of chapter one.

In chapter two detailed literature review has been given on the types, sources, and health effects of VOCs and their mitigation techniques, particularly on advanced oxidation techniques. In this chapter synthesis, structure and photocatalytic properties of various types of material will be discussed in details. The objectives of this detail literature survey were to select suitable materials that can decompose VOCs more efficiently than the commercial photocatalysts.

Chapter three is one of our first efforts in synthesis, characterization and photocatalytic activities of $InTaO_4$, $InNbO_4$, and $AgNbO_3$. This chapter highlights the possible applications of pristine $InTaO_4$ and metal ion doped $InTaO_4$ as efficient visible light photocatalytic materials. The chapter also discusses and compares the photocatalytic activities of non-doped and doped $InTaO_4$ with homemade photocatalysts such as $InNbO_4$ and $AgNbO_3$ and commercial photocatalyst P25.

Chapter 4 is composed of synthesis, characterization and photocatalytic properties of undoped and metal ion doped $BiTaO_4$. Crystal structure of undoped and metal doped $BiTaO_4$ has been discussed with details along with the effect of doping on the photo-physical properties of the newly prepared materials. Among the various metal dopants, Sn, Ba, and La, have significantly modified the photocatalytic performance of $BiTaO_4$. Variation in band gap and optical absorption of the material with doping has been also discussed in connection with the effects on the photocatalytic property of the materials.

Chapter 5 describes the wet-chemical synthesis of various ternary metal oxide nano-particles which include Bi_2WO_6, $AgVO_3$, $AgTaO_3$, $BiTaO_4$, $Cd_2Ta_2O_7$, $InTaO_4$, $CoTa_2O_6$, $CeTaO_4$ and $EuTaO_4$. Photocatalytic activities of all these materials examined with UV and visible light irradiation and compared with a commercial photocatalyst i.e. P25 have been discussed in details. These materials have also been examined for decomposition of water contaminants where methylene blue has been used as a model organic dye. Different materials respond differently for decomposition of VOCs in aqueous and gaseous forms. The trend of photocatalytic properties for aqueous and gaseous reactions was neither similar under UV light nor with visible light irradiation.

Chapter 6 refers to the synthesis and photocatalytic properties of undoped and metal ion doped $BiNbO_4$. This material has been tested only for the decomposition of toluene with UV and visible light irradiation. This chapter highlights the effects of various dopants on the photo-physical properties,

optical and structural behaviour of $BiNbO_4$ and the photocatalytic activities. In this chapter we have also discussed possibility of nitrogen doping in $BiNbO_4$ and have attempted to modify the optical and photocatalytic properties with anion doping.

Chapter 7 discusses nitrogen doping both in Ta_2O_5 and Nb_2O_5. Photocatalytic decomposition of toluene with visible light irradiation on undoped and nitrogen doped Ta_2O_5 and Nb_2O_5 have been detailed in this chapter. Photocatalytic performance of the nitrogen doped Ta_2O_5 were much higher than that of nitrogen doped Nb_2O_5 and commercial Ta_2O_5. We have found that annealing commercial Ta_2O_5 in nitrogen environment can also modify the photo-physical properties of the material and increase its photocatalytic activities.

Chapter 8 summarizes the overall thesis and discusses the performance of all the materials, which were synthesized during the research work. This chapter also highlights the major outcomes of entire research work and pinpoints the best materials among the various newly synthesized metal oxide nanomaterials. The last part of the chapter is devoted to the possible suggestions and future work.

1.4 References

1. Kumar, R., et al., *Association of indoor and outdoor air pollutant level with respiratory problems among children in an industrial area of Delhi, India.(Clinical report)* Archives of Environmental and Occupational Health, 2007.
2. Brown, B.S., *Assessment and control of volatile organic compounds and house dust mites in Australian building.* Proceedings of the 13th International Clean Air and Environment Conference, Adelaide, Australia, 1996. **649**.
3. Wang S, Ang HM, and T. MO., Volatile organic compounds in indoor environment and photocatalytic oxidation: state of the art. Environmental International 2007. 33 (5): p. 694-705.
4. B.C.Wolverton, D., *How to Grow Fresh Air.* Book, 1997.

5. Beach, et al., *The effects on asthmatics of exposure to a conventional water-based and a volatile organic compound-free paint.* European Respiratory Journal, 1997. **10**(3): p. 563-566.

6. Obee T. N, B.R.T., *TiO_2 photocatalysis for indoor air applications : effects of humidity and trace contaminant levels on the oxidation rates of formaldehyde, toluene, and 1,3-butadiene.* Environmental science & technology, 1995. **29**(5): p. 1223-1231

7. Shiraishi, F., et al., *Decomposition of gaseous formaldehyde in a photocatalytic reactor with a parallel array of light sources: 1. Fundamental experiment for reactor design.* Chemical Engineering Journal, 2005. **114**(1-3): p. 153-159.

2 -Literature Review

2.1 Introduction

Since the era of industrialization, toxic compounds such as sulphur dioxide, nitrogen oxide, carbon monoxide and various volatile organic compounds (VOCs) have been continuously polluting the whole environment. In addition, the presence of VOCs in air has been identified as extremely perilous and could be the sources of incurable diseases like carcinoma. The World Health Organization (WHO) has estimated that 2.8 millions people lose their lives each year as consequences of polluted indoor air [1]. According to WHO, chemicals containing hydrogen and oxygen which have a boiling point in the range of 50 -260 °C are defined as volatile organic compounds (VOCs). These compounds can be easily evaporated at normal temperature and pressure, and contribute to the surrounding air [2]. According to Australian Government standards (National Pollutant Inventory) a large number of substances including aromatic hydrocarbons (benzene, toluene), aliphatic hydrocarbons (hexane, formaldehyde) and oxygenates are termed as VOCs. Various investigations by WHO, NICNAS (Australia) and EPA (USA) have confirmed that substantial sources of VOCs are constantly polluting indoor and outdoor air. In developed countries like USA, Europe, and Australia people spend more than 90% of their time in closed environment, such as homes, rooms, offices, cars, etc[3]. EPA studies have shown that, indoor concentration of VOCs is 20% higher than outdoor environment. Therefore, risks associated with the exposure to VOCs becoming more severe and can cause serious health issues[4]. Further, long-term exposure to VOCs is detrimental to human health since it can cause sick building syndrome (SBS)[5, 6]. Although the average concentration of individual VOC is usually lower but the concentrations of total VOCs are really higher and therefore assumed to be the sources of various diseases. Building materials such as adhesives, paints, carpets, furniture and coverings are the main contributors of VOCs to the indoor environment [7]. It is reported by the Australian Government Department of Health and Ageing, (NICNAS) that formaldehyde is one of the most persistent VOCs in indoor air and can be the major source of cancer in animals. The report

further detailed that occupants of mobile homes and demountable buildings may face serious health issues in exposure to formaldehyde.

It has been confirmed by various studies, departmental reports (NINCAS, EPA,), and various health organizations (WHO) surveys that VOCs are the main contributors to the indoor and outdoor pollution. Therefore, various air purification techniques such as air filtration[8], high efficiency particulates air (HEPA) filter, electronic air filters, dust filters[9], ionic purifiers, adsorption filters, thermo-catalytic combustors[10] and photocatalytic filtrations[1] have been developed to mitigate the indoor pollutants and reduce their possible health risks. All of the above air purification techniques have specific limitations associated with each technology. However, researchers have a consensus that further investigation is highly required in order to purify indoor air from hazardous VOCs and provide clean indoor environment to the occupants. Removal of VOCs through photocatalytic oxidation has been extensively studied as an efficient, air purification technology based on its various benefits over the conventional technologies[7],[11, 12]. Here we will review the main sources of VOCs, the risks, hazards and serious health issues associated with existence of VOCs in both outdoor and indoor environment. We will also comparatively study the VOCs removal technologies and will suggest the best way to mitigate the deadly effect of VOCs.

2.2 Sources of VOCs

We daily encounter with thousands of volatile organic compounds (VOCs) produced either through biogenic[13] or anthropogenic processes. These VOCs are mostly oxidized by the powerful hydroxyl radicals present in the atmosphere[14] and become secondary VOCs. Primary VOCs like ethanol and acetaldehyde emitted from fresh leaf mulch and wood chips can last for 20-30 hours[13]. Domestic heating and hot weather were identified as the two main sources for the enhancement of photo-chemical process which subsequently increase the outdoor VOCs[15]. However, some common VOCs such as acetone, benzene, ethylene glycol, methylene chloride, toluene, xylene, 1, 3-butadien, formaldehyde, and

acetaldehyde[16] are mostly emitted from building and finishing materials substantially polluting the indoor air[17]. It has been identified that a single type of volatile organic chemical can be produced by various sources[18]. Therefore, it's more complicated to assign emission of a particular VOC to a particular source[18]. Newly constructed buildings consisted of paints, varnishes, adhesives, vinyl wallpaper and plywood with no furniture have considerable amount of benzene, toluene, methylbenzene, xylene, styrene and formaldehyde[17], where building renovations also produce high levels of methyle isobutyle ketone, tetrahydrofuran, and alkanes[19]. In a case study on outdoor and indoor VOCs, benzene, toluene and xylene have been detected in both the environment with high concentration in urban, suburban, and industrial areas[19]. Along with the building materials and occupant's activities, ventilation has been identified as one of the potential sources of various types of VOCs[20]. Mølhave et al. have found that ventilation enhanced the concentration of VOCs 4 and 16 times for open and close buildings, respectively[21]. Formaldehyde and aldehyde emissions from flooring, flooring with adhesive and only adhesive were temperature dependant, however, emission rate of formaldehyde was maximum at 32 °C[22]. Room furnishing carpets, wall plasters, and consumers like nail polishes have been found to be the causes of toluene, xylene and acetone emissions, respectively[23]. All-purpose cleaners, disinfecting cleaners, and spot removers are potential sources of carbonyls, hydrocarbons, glycol ethers, 4-nonylphenol and nonylphenol ethoxylates[24]. Garages attached to the residential units are the potential sources of various VOCs with the highest concentration of benzene[25]. Most of the fuels are related to aromatic VOCs (such as toluene, ethyl-benzene, xylene, and trimethylbenzene) and almost all of the benzene detected in the garage-attached houses are originated from the items stored in the garages[26]. Although quantity and type of VOCs vary from house to house, various studies[27] have identified formaldehyde as one of the major air pollutants in most of the public facilities like subway stations, underground shopping centres, medical centres, public childcare facilities, libraries, large stores, funeral homes, and indoor parking. Home kitchens, which use LPG and town gases as fuels, have been reported as potential sources of

more than 50 different types of VOCs, where formaldehyde, acetaldehyde and benzene were found in abundance[28]. Significant amounts of benzene and toluene have been detected in open and closed kitchens, where solid biomass fuels such as dung and wood were used as fuels[29]. Various investigations have shown that cigarettes smoke contains toluene, xylene, benzene, limonene, styrene, ethylbenzene, xylene, and other aromatic compounds [30, 31]. Detailed investigations have further revealed that cigarettes smoke increases the concentration of total VOCs at 10 times in a closed environment [31]. Additionally a recent study[32] has identified that shisha (water pipes) smoke has aldehydes four times higher than a single cigarettes.

It can be concluded that there are various sources such as building materials, home consumers, cleaning detergents, kitchen smokes, plants, cigarette, fuels, vehicle exhausts, LPG, home furnishing materials, carpets, paints, and many more which emit lots of volatile organic compounds. However, the most common VOCs detected in different environment and produced by various sources were benzene, formaldehyde, aldehydes, toluene, xylene, 1, 3-butadeien, and acetaldehyde. In the following section we will briefly highlight the serious health effects of the above mentioned VOCs.

2.3 Health issues associated with VOCs

VOCs emitted from most of the substances and human activities, spread rapidly in the environment and become a significant fraction of the air. Exposure to these toxic compounds via ingestion, dermal contact and inhalation eventually causes various types of dreadful disease. Among the three routes of ingestion, dermal contact and inhalation, the latter has been identified as a main process through which human can be adversely affected by VOCs. Various acute and chronic health effects, which include respiratory effects, neurological toxicity, lung malignancy, throat and eye irritations[33], neurological symptoms, headaches, dizziness, depression, and even cardiovascular diseases, can be associated to various types of VOCs. Benzene, one of the abundant VOCs emitted by most of the substances, is

known to be carcinogenic and causes leukaemia[30], [34]. It is reported that acetaldehyde and aldehyde emitted by the cigarettes smoke are potential sources of cyto-toxicity and increase geno-toxicity since these VOCs reduce activity of DNA repair readily[35]. The estimated life time risks of cancer associated with the 8 hour exposure to seven selected VOCs (which include benzene, 1,1-dichloroethene, tri-chloro-ethene, and tetra-chloro-ethene) for various groups of people showed that, housewives, food workers and office workers are at the highest risks of cancer[34]. Most often the residential cooking facilities are operated by women; therefore they are more exposed to formaldehyde, acetaldehyde and benzene (the three main VOCs of kitchens). The cancer risk assessments for these women indicated that formaldehyde and acetaldehyde have the highest life time cancer risks [28]. Aromatic VOCs (benzene, toluene, xylenes) detected in a closed building have been found to originate ophthalmic symptoms, tiredness and headache in the office workers. Various others SBS symptoms like eye dryness, runny nose, dry throat, congestion symptoms, and lethargy were also observed by the occupants of the buildings[36]. The average concentration of formaldehyde in homes and offices is about 0.05 mg/m^3, where the odour of formaldehyde can be perceived at 0.1 mg/m^3, eye irritation can occur at 0.36 mg/m^3, and lungs may be affected at concentration of 1.0 mg/m^3[37]. A panel of experts has recommended occupational exposure limit of 0.3 -1.00 ppm for formaldehyde, 2.0-3.0 ppm formaldehyde could cause severe eye, throat and nose irritations[33], and above 5 ppm lower airway and pulmonary effects can be resulted in [38]. However, European Commission has advised concentration of indoor formaldehyde as 1.0 $\mu g/m^3$(0.8 ppb) based on the nose and throat irritation limits of 0.1 mg/m^3(0.08 ppm). Nose and throat irritation are the manifestations of trigeminal nerve stimulation (sensory irritation), which can be caused by formaldehyde at very low level of 0.04-0.4 ppm[39].

It has been reported that increasing asthma in children is due to the presence of VOCs in the cleaning products, solvents[40] and indoor air[38]. Prevalence of asthma, exacerbations of asthma and other chronic respiratory disorders in children near industrial regions with copious VOCs were much higher as compared to those

in non-industrial area[41]. The most serious effect of VOCs on human health has been demonstrated between exhaled VOCs and lung cancers[42]. Samples of breath collected from the cancer patients showed that there were 22 different types of VOCs including benzene, derivatives of benzene and alkane derivatives, indicated a strong relationship of these toxic compounds to carcinoma[43]. It has been reported that exposure to microbial VOCs (such as 1-octen-3-ol) can be associated to sensory irritation of nose, eye and throat mucous membrane of the inhabitants[44]. It can be deduced that indoor/outdoor VOCs are not only the main source of sick building syndromes (SBS), which causes serious health risks, but can also be the source of asthma and respiratory effects, eye, nose, and throat irritations, physical fatigue, and may impose more severe health issues like carcinogenic effects. In the recent technological era, human exposure to VOCs is a realistic concern. Therefore, it requires much attention from both scientific community and public to eradicate and/or mitigate the toxicity and severe health effects of VOCs.

2.4 VOCs Removal Techniques

Removal of VOCs from both indoor and outdoor environments is not only highly recommended but on the top priority of various health organizations (WHO), owing to the severe toxicity associated with VOCs. A range of techniques have been introduced to reduce the potential adverse effects either by preventing exposure to VOCs or by partial reduction of these compounds. Ventilation being an old technology is still in use to control the concentration of total volatile organic compounds in indoor environment. This technology uses a large number of modern and sophisticated equipment extracting polluted air from indoor and allowing fresh purified air from outside environment. However, some issues are associated with this process, which include persistence sources of indoor VOCs, highly polluted outdoor air, inefficient working capacity of the ventilators, limited applicability[21], and energy consumption. Although advanced ventilation (High Efficient Particulate Air Filter) and its modified forms have been proven to be effective for the reduction of particulate matter, NO, SOx, greenhouse gases etc. This technique was not useful

to mitigate the concentration of total VOCs to the lower magnitudes as recommended by international health organizations.

Plasma [45] technology requires high pressure and power to produce radicals, which subsequently react with the pollutant gases and reduce their concentrations. This technology is useful to minimize the concentration of hazardous air pollutants produced in industries but could not be applicable to public places and residential areas due to the requirements of high power and other associated limitations. Thermal oxidation[46] or combustion of VOCs is an oxidation technique which can completely disintegrate various VOCs into non-hazardous compounds. However, the main drawbacks of this method are: requirement of elevated temperature (900 - 1500 °C) and by products of NO. Addition of a catalyst to the thermal oxidation process definitely reduces the temperature down to 400 °C, but the system only works for VOCs at a concentration of above 1000 ppm. While the indoor concentration of VOCs is only a few ppms or less, thus neither the thermal oxidation nor the thermal catalytic oxidation process is suitable for removal of such as lower concentration of indoor VOCs. Catalytic oxidation of VOCs over ozone/zeolite mixed system was not successful owing to the lower efficiency and production of toxic by-products like aldehydes[47].

Condensation[48], absorption[49], [50] and adsorption[51] are some other important physical techniques for VOCs removal, however these technologies possess limitations of temperature, concentration and boiling points of VOCs (varies for different types of VOCs), solubility of VOCs, surface area, and selectivity of adsorbents respectively. Physical adsorption, chemosorption by activated carbons and zeolites are under investigations for effective removal of VOCs. Adsorption by activated carbon [15] is not very helpful, since the competitive adsorption of different volatile organic gases reduces the effectiveness of the process. The most challenging and crucial limitations of adsorption process are material re-useability, low efficiency[52] for specific volatile compounds and impracticality[53] at high temperature. Bio-filtration[54] is an effective way to remove and/or mitigate VOCs on a large scale (at industrial sites), however, this

technique is extremely temperature sensitive and the removal efficiency of VOCs dropped rapidly for a very small increase of temperature (from 30 °C to 40 °C). Furthermore this technique is not capable to remove all types of VOCs[55]. A comparison of VOCs removal techniques has suggested that photocatalytic oxidation of volatile organic compounds can be the best alternative based on the efficiency and cost[46].

2.5 Photocatalytic oxidation of VOCs

Technical attributes like feasibility[11], compatibility to work at ambient temperature and pressure, suitability for lower concentration of VOCs (at ppb levels), extremely low energy requirements, better removal efficiency, re-useability and longer life time of photocatalysts make photocatalytic oxidation a unique process for VOCs decomposition. Photocatalytic oxidation techniques can be operated at very low power and sun light will be enough to completely decompose hazardous VOCs to mineral salt, CO_2 and water. Figure 2.1 briefly explains the photocatalysis process which can be used for hydrogen production via water splitting along with VOCs disintegration in water and air. Since 1972, heterogeneous photocatalysis has been under investigation for VOCs removal, and hydrogen production via UV light irradiation using TiO_2 as a photocatalyst.

Highly oxidative species i.e. hydroxyl radicals ($^{\cdot}OH$) and super oxide ($^{\bullet}O_2$) are produced when metal oxide and/or sulphide (such as TiO_2, ZnO, CdS etc) is exposed to UV light in the presence of water and oxygen. These two species possess high oxidative power and are capable to decompose most of the VOCs residing on the surface of materials (or in the near vicinity of the materials). The photocatalytic mechanism for the generation of active species is given as

$$TiO_2 + \mathrm{h} \rightarrow \mathrm{h}^+ + \mathrm{e}^-$$

$$\mathrm{h}^+ + \mathrm{OH}^- \rightarrow {}^{\bullet}\mathrm{OH}$$

$$Ti^{4+} + \mathrm{e}^- \rightarrow \mathrm{Ti}^{3+}$$

$$Ti^{3+} + O_{2ads} \rightarrow Ti^{4+} + e^{-}_{2ads}$$

$$^{\bullet}OH + \text{Pollutant} \rightarrow \text{Oxidized pollutant}$$

$$h^{+} + e^{-} \rightarrow \text{Thermal heat or luminescence}$$

Or in general the above mechanism can be expreseed as follows

$$RX_{ads} + H_2O + O_2 \rightarrow \frac{h}{TiO_2} \rightarrow H_2O + CO_2 + \text{Mineral acid}$$

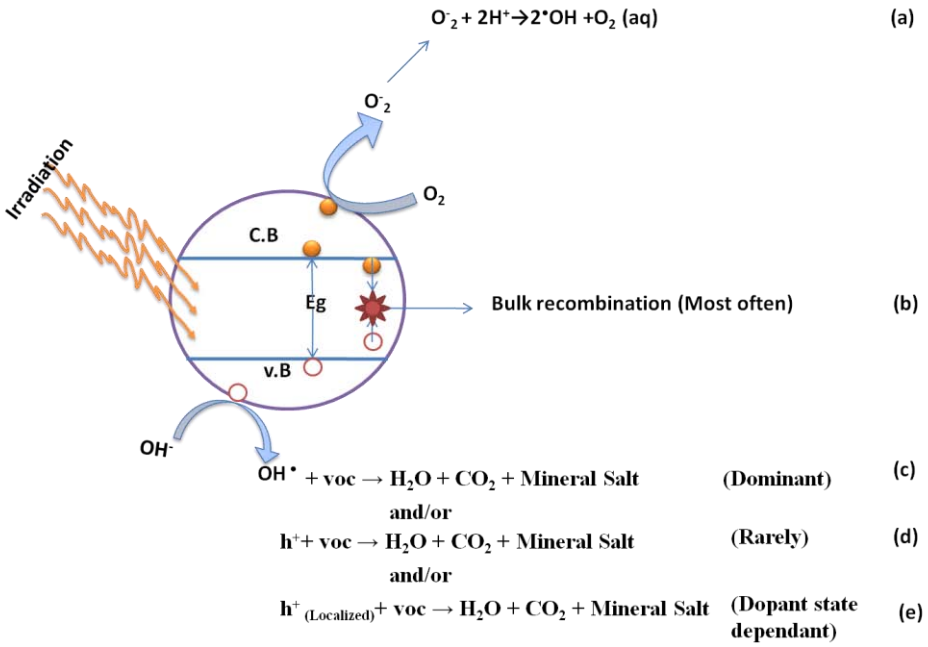

Figure: 2.1 Mechanism of Photocatalysis Process

Some successful results on the photocatalytic degradation of VOCs in gaseous forms with non-doped, cation doped and anion doped TiO_2 irradiated with black light (λ<380 nm) have shown that, this technique is viable and can be used on a large scale. However, the system has technical issues like humidity effect, low adsorption of VOCs, lower efficiency at low ppm of VOCs, competitive adsorption of water and VOCs molecules [56] and photocatalyst life time[57]. To overcome the above issues extensive efforts have been made to modify and/or substitute the most credible material i.e. TiO_2 and make the system capable to work with visible

light (λ>400 nm) irradiation. Various techniques such as doping, co-doping, coupling of the photocatalysts (TiO_2/ZnO, TiO_2/SnO_2 and ZnO/SnO_2) and surface modification have been applied to achieve the required results. Until now, nitrogen doped TiO_2 has shown excellent performance [58], [59] for photocatalytic decomposition of VOCs owing to the synergetic effect of high porosity, acidic surface, and band gap miniaturization by anion ions like nitrogen and sulphur. However, humidity and competitive adsorption of water and intermediates have a negative effect on the photocatalytic oxidation of VOCs.

The rate of VOCs degradation depends on both the concentration of OH radicals produced by the light irradiation and concentration of VOCs present in the vicinity[60]. Higher intensity of suitable light radiation generates large number of reactive species to decompose those VOCs molecules which are in contact with the photocatalytic material. In a typical office the intensity[61] of artificial visible light is about 0.1-0.2 mW/cm^2, while the photocatalytic reactors developed so far requires intense light (1.0-10.0 mW/cm^2) in the range of UV_A to UV_B. Light intensity of 0.25 mW/cm^2 has been recommended for degradation of 2 ppm (81.89 μmol/m^3) of formaldehyde at normal temperature and pressure[62]. Investigations on the formaldehyde concentration in various buildings have shown that the formaldehyde level is (4.2 ppm) 500 μg/m^3 in homes, about half of that in offices [37] and 34 ppm in newly manufactured homes. The Australian National Health and Medical Research Council has suggested the permissible levels of various pollutants in air including formaldehyde in the range of 0.1 ppm (120 μg/m^3), which is similar to the World Health Organization (WHO) guidelines for formaldehyde exposure. To reduce the concentration of VOCs and formaldehyde in particular to the WHO recommended level of 0.1 ppm, through commercialized photocatalysts, a large amount of UV light irradiation is required. The applicability of the process becomes difficult due to the UV light requirements in huge amount. Indeed further investigation is required to develop new photocatalysts, which can operate efficiently at the available artificial light and/or sun light in the intensity range of 0.1-0.2 mW/cm^2. We eventually have focused on synthesis of photocatalysts such

as $InTaO_4$[63], $BiTaO_4$, $AgNbO_3$, and $BiNbO_4$, which are capable to operate at room temperature under sun light irradiations and have a longer life time than commercial photocatalyst materials.

2.6 Selection of photocatalytic materials

Since 1973, heterogeneous photocatalysis has been well thought-out as a prevailing solution to the environmental purification and supply of inexpensive energy. In a photocatalysis process, same materials and energy resources (visible light) can be utilized for two different purposes i.e. environmental detoxification and water splitting into H_2 and O_2. Although a single material can perform these tasks efficiently, selection of a visible light active photocatalytic material is not remarkably successful until now. Some fundamental requirements must be fulfilled in order to make photocatalytic process viable and achieve the goals of green energy and cleaner environment. These basic factors are i) a photocatalyst must be inert, ii) must be excited with UV/visible light to generate electron hole pairs, iii) conduction band/valence band level of a photocatalyst must be more negative/positive than the reduction/oxidation potential of decomposing substances, iv) photo-generated carriers (electron, hole) can be efficiently and quickly migrated to the surface, v) recombination of photo-generated carriers must be suppressed, vi) there must exist sufficient and separated active sites for redox reactions. Some traditionally well-known metal oxides such as TiO_2, ZnO, and WO_3 obey one or more of the above criteria in their pure and/or modified forms; therefore most attention has been paid to these materials to achieve the desired visible light activity. Nevertheless, some of these efforts like doping TiO_2 with metals such as platinum[64, 65], non - metals particularly with nitrogen [66], and depositing metals like Ag [67] on TiO_2 surface were moderately successful. In order to enhance efficiency of the system, various other ways have been searched out which include; compositing TiO_2 with other metal oxides [68], metal sulfide, co-doping with metals and non-metals (Ag, S) [69]. More attention has been devoted to investigate inert, reliable, non-toxic, and environmentally friendly photocatalysts, which can operate efficiently under visible light irradiation and can split water into H_2/O_2 and

also decompose air and water contaminants faster than the traditional photocatalysts. In this context a range of materials (detailed in Table 1 of appendices 1) such as niobium based compounds like Nb_2O_5[70, 71], vanadates like $BiVO_4$, tantalates like $InTaO_4$, bismuth based compounds such as $Sr_2Bi_2O_5$, $SrBi_2O_4$, $NaBiO_3$ and many more have been investigated. This study has been devoted to critically review photocatalytic performance of these promising materials and in view of this to suggest the best alternative photocatalysts for further exploration.

2.7 Photocatalytic decomposition of VOCs with TiO_2

Since 1972, TiO_2 has been extensively studied for the photocatalytic decomposition of volatile organic compounds due to its versatile properties. Some successful results have shown photocatalytic degradation of VOCs in gaseous forms with pure and modified TiO_2 irradiated with black light (λ<380 nm), however, these systems have some issues like humidity effect, low adsorption and reduced efficiency at low ppm level of contaminants. The competitive adsorption of water and VOCs molecules[72] on the photocatalyst surface significantly modify the oxidation rate of VOCs. A considerable decline in the oxidation rate has been observed at decreasing the pollutant concentration[73]. In order to avoid the use of UV light extensive efforts have been made so far to modify and/or substitute the most credible material i.e. TiO_2 to generate e-h pairs upon solar light irradiation[74]. Extremely lower concentration (3 to 5%) of UV light in the solar spectrum made such systems ineffective for indoor applications. Therefore, most attention has been paid to make photocatalysts capable of absorbing visible light (47% of the solar spectrum) and generate electron-hole pairs with longer wavelength irradiation. Various techniques such as doping with metals[75], transition metals[76], lanthanide, anions[77], co-doping (anion and cation both)[78], metal deposition[79] (such as gold, silver, Pt, and Fe), coupling of the photocatalysts[80-83] (TiO_2/ZnO, TiO_2/SnO_2 and ZnO/SnO_2) and surface modification have been applied to achieve the required results. Among these, nitrogen doped TiO_2 has been found to be the most excellent photocatalyst so far as the optical absorption in the visible region is

concerned[84]. Ihara et al [59] has described high photocatalytic activity of TiO_2 as the synergetic effect of porosity, acidic surface, and effect of N ion and F ion co-doping.

The nano sized TiO_2 has a very low contact angle and possess high hydro-philicity[85], therefore, humidity and competitive adsorption of water have negative effects on the photocatalytic oxidation of VOCs. More attention is needed to make TiO_2 capable to adsorb contaminants more efficiently than water. However, very low humidity may suppress the oxidation process as well. The rate of VOCs degradation depends upon the concentration of OH radicals and the concentration of VOCs[60]. Sulphur doped TiO_2 [86] was used as visible light active photocatalysts for the decomposition of trichloroethylene (TCE) and dimethyl sulphide (DMS). The comparative study has confirmed that Degussa P25 can work better than S-TiO_2 under UV light irradiation while the latter was much efficient under visible light irradiation and no activity for Degussa P25 under the similar conditions. The improved photocatalytic activity of S-TiO_2 was attributed to the band gap narrowing effect induced by S doping. Many investigations have described the enhanced photocatalytic properties of nitrogen doped TiO_2, however, its potential application is very limited and doping and/or modification with additional elements or compounds will further promote the catalytic activity. A detailed study [87] on the photocatalytic removal of VOCs using photocatalytic paints mixed with six different binder systems has indicated some strange results [6]. The investigation showed that instead of decomposition, many VOCs such as formaldehyde, acetone, and acetaldehyde were generated during UVA light irradiation suggesting the malfunctioning of paints mixed photocatalysts. The complete mineralization of indoor VOCs through visible light radiated photocatalyst is still to be investigated.

Salthammer et al. [61] have demonstrated that in a typical office the intensity of artificial visible light is about 0.1-0.2 mW/cm^2, while the photocatalytic reactors developed so far require light intensity of 1.0-10.0 mW/cm^2 in the range of UV_A to UV_B. Light intensity of 0.25 mW/cm^2 has been recommended for degradation of 2 ppm (81.89 $\mu mol/m^3$) of formaldehyde at normal temperature and pressure[88]. We

have shown that nitrogen and Pt co-doped TiO_2 can be excited with indoor lightening which can decompose toluene very efficiently[89]. However, photocatalyst regeneration, life time of the photocatalyst, and strong adsorption of intermediates have worse effects on the photocatalyst performance[89]. In our recent study for the search of alternative photocatalysts [90], we have found that Ni doped $InTaO_4$ has lower performance initially but it has a much longer life time than that of commercial TiO_2 for toluene decomposition under UV irradiation[63].

It can be deduced from the above discussion that, nitrogen doped and metal doped TiO_2 catalysts have shown significant improvement both in the visible light absorption due to band gap miniaturization and efficiency of VOCs removal with visible light irradiation. However, rapid decrease in the activity due to intermediate adsorption and other related issues are still the major challenges that require much attention for the improved photocatalytic activity of TiO_2. In the preceding sections we will review photocatalytic performance of non-TiO_2 materials for VOCs decomposition via UV/visible light irradiation.

2.8 Performance of lanthanide oxides

Bamwenda et al. [91] have reported decomposition of water into O_2 and H_2 through irradiation of CeO_2 with UV/Vis light (λ>330 nm) in the presence of electron acceptors such as Ce^{4+} and Fe^{3+} ions. It was suggested that photo-excited electron transferred from CeO_2 conduction band to the adsorbed Ce^{4+} and/or Fe^{3+}, reducing these ions to Ce^{3+} and Fe^{2+} and evolve O_2 via following reaction pathway.

$$4h_{VB}^{+} + 2H_2O \rightarrow 4H_{aq}^{+} + O_{2(gas)} \qquad (1)$$

However, oxygen evolution rate (66.8 μmol/h) with CeO_2 was much slower than (326.4 μmol/h) with TiO_2 P25 under similar condition. Additionally, upon prolonged irradiation this rate was further decreasing owing to the continuous consumption of electron acceptors (Ce^{4+} and/or Fe^{3+}) into their reduced forms (Ce^{3+} and Fe^{2+}) which subsequently promote recombination of electron-hole pairs and affect the photocatalytic activities. Photocatalytic oxidation rate of toluene with

CeO_2 was also found to be lower than that with TiO_2-P25. However, complete mineralization of toluene, apparent lack of deactivation [92] and increase in activity at high temperature were observed with CeO_2, while intermediates like benzaldehyde were detected in case of TiO_2-P25. It was suggested [92] that oxygen vacancies and superoxide species formed on CeO_2 contributed to the photo-degradation of toluene. Since existence of surface vacancies is one of the key factors, influencing photocatalytic behaviour of materials, therefore, Coronado et al. [93] have investigated routes for the formation of photo-generated radicals on the surface of CeO_2 using EPR techniques. EPR spectra of CeO_2 with adsorbed oxygen at room temperature and already outgassed sample at 473k has shown some signals which were corresponded to superoxide radicals adsorbed on the cerium cations. Formation of superoxide radicals on CeO_2 surface was attributed to the interaction of Ce^{3+} and oxygen vacancies (V_o) according to the following reaction.

$$"Ce^{3+} - V_O{\bullet\bullet} \rightarrow Ce^{4+} - O_2^- \text{ "} \qquad (2)$$

After irradiation with UV light and subsequent oxygen adsorption at 77K three other signals observed on CeO_2 surface were assigned as the characteristics of $Ce^{4+} - O_2^-$ complexes. Similar characteristic peaks for $Ce^{4+} - O_2^-$ species have been observed by Alosnon et al. [92], which were presumably responsible for the toluene decomposition. Contrary to this, Yuliati et al. [94] demonstrated that Ce (III) ion of cerium oxide supported on silica and alumna was the photocatalytic active site to produce hydrogen and ethane through non-oxidative coupling of methane (NOCM).

Particle size of single crystalline nanoparticles of CeO_2 prepared through hydrothermal techniques [95] was increasing with increase in calcination temperature. However, morphology of particles was controlled through water content, legend concentration and types of amines (hexadecylamine) [96]. Particles dispersed in polyethylene glycol 1000 have an average size of about 30 nm [95] and strong absorption in wavelength range of 28 -365 nm. Acidic black 10B and

MO dyes were degraded (up to 72%) with the newly synthesized nanoparticles under solar and UV irradiation respectively.

In short, cerium oxide i.e. CeO_2 or Ce_2O_3 is not a candidate for further exploration owing to i) the reduction in the active sites (oxygen vacancies), ii) structure dependence on Ce content, and iii) extreme effect of calcination temperature on particle size. Lessening of the active sites is a major detrimental effect which subdues usefulness of this material over P25.

2.9 Activities of niobium based compounds and alkali niobates

Ohuchi et al. [97] have investigated photo-oxidation of 1-pentanol (in the presence of molecular oxygen) to pentanal (RCHO), pentonic acid (RCOOH), and carbon dioxide using TiO_2, ZnO, and Nb_2O_5. Although, photo-conversion efficiency of TiO_2 was about 3.5 times higher than that of Nb_2O_5; the latter has a better selectivity (to partial oxidation products) than TiO_2. Further investigation of photo-physical properties unveiled that, BET surface area of Nb_2O_5 decreases (from 132 to 48 m^2/g) with calcination; however its pentanol conversion efficiency and selectivity to partial oxidation products were significantly increased at optimum calcination temperature of 773K. Contrary to this, calcination of Nb_2O_5 has a converse effect on water splitting and H_2 evolution [98]. Higher photo-oxidation of 1-pentanol with Nb_2O_5 calcined at 773K was attributed to the better crystalline structure and high surface area, since modification of crystal structure and drastic decrease in surface area were found when the samples were calcined at higher temperatures.

Various studies ([71] -[99]) have investigated the effect of synthesis routes and/or calcination temperature on photocatalytic properties of niobates type compounds. Zhang et al. [100] have reported that, potassium niobate ($K_6Nb_{10.8}O_{30}$) prepared with wet-chemical techniques has smaller particle size, slight larger band gap, larger surface area and more number of Nb^{4+} in crystal structure than the sample prepared with solid state reaction techniques. However, surface area of newly prepared sample was much larger than the surface area of TiO_2. Sun et al. [99] also

demonstrated that calcium niobate ($CaNb_2O_6$) prepared with a solvothermal (SV) method has smaller particle size (30-40 nm), lower band gap (3.46 eV) and very high surface area (51.9 m^2/g) than the similar material prepared with a solid state (SS) method, which has 1-3 μm particle size and 1.1 m^2/g surface area. Higher photocatalytic degradation of acid red G with samples ($K_6Nb_{10.8}O_{30}$, $CaNb_2O_6$) prepared through wet-chemical techniques were attributed to the nano-crystalline structure, uniform particle shape, existence of various valence states [100], high absorption in the optical range and high surface area of nano-photocatalyst [99].

As a common strategy for improving photocatalytic properties of materials, band gap engineering of alkali niobates ($NaNbO_3$) has been attempted by making solid solution of $(AgNbO_3)_{1-x}(NaNbO_3)_x$ [70] and doping nitrogen in $NaNbO_3$ [71] respectively. Li et al. [70] have reported an increase in oxidation power of $AgNbO_3$ by shifting its valence band toward more positive position. Blue shift in the optical absorption of the solid solution ($(AgNbO_3)_{1-x}(NaNbO_3)$) suggested that contribution of Ag 4d orbital to the valence band of $AgNbO_3$ was reduced due to $NaNbO_3$ addition. Particle size of the solid solution was also reduced which leads to enhanced surface area. These two modifications introduced by the solid solution boosted up photocatalytic activities, which resulted in faster decomposition of 2-isopropanol [101] into acetone (2.8 ppm/h) and CO_2. Shi et al. [71] have recently doped nitrogen into $NaNbO_3$ via a solid state reaction in order to completely mineralize gaseous 2-isopropanol with only visible light irradiation. IPA decomposition into acetone and CO_2 was simple and quick process, complete mineralization of acetone into CO_2 and water was a more complex process since it took about 118 hours to mineralize only 40% of IPA under visible light irradiation (>400 nm). UV-Vis diffuse reflectance spectra of nitrogen doped $NaNbO_3$ has shown red-shift in optical absorption from 365 to 480 nm. Enhancement in optical absorption and its effect on photocatalytic performance were attributed to the formation of new band just above the valence band of $NaNbO_3$ introduced by N 2p orbital.

We can deduce from above discussion that none of the attempts (wet-chemical synthesis routes, impregnation with LiOH, coating with Pt, band gap modification with cation (Ag), and anion (N), and low temperature calcination) were successful to improve the photocatalytic properties of niobium based compounds. Some of these processes were relatively useful but overall performance of niobium based compounds (as detailed in above section) was much lower than that of TiO_2 P25.

2.10 Photocatalytic activities of tantalates

Moment of photo-generated carriers and position of conduction/valence band levels are two important parameters which differentiate photocatalytic properties of materials with similar band gaps and crystal structures. The more negative/positive of the conduction/valence band the higher the redox potential and consequently the higher photocatalytic activity of the material is, even though the material might have lower absorption due to a large band gap. Photo-generated carrier moments have a strong relationship with M-O-M angle in mixed metal oxide catalysts such as $InTaO_4$ and $InNbO_4$. It has been reported [102] that both $InTaO_4$ and $InNbO_4$ are consisted of two octahedrons InO_6, and NbO_6 (TaO_6), where variation in volumes of NbO_6 and TaO_6 induces differences in lattice parameters of the two materials. Conduction bands which are made of empty 5d and 4d orbitals of Ta and Nb in $InTaO_4$ and $InNbO_4$, respectively, are positioned at different levels (as shown in Figure 2.3), while valence bands which are made of O 2p orbitals of InO_6 in both the materials have the same potential level.

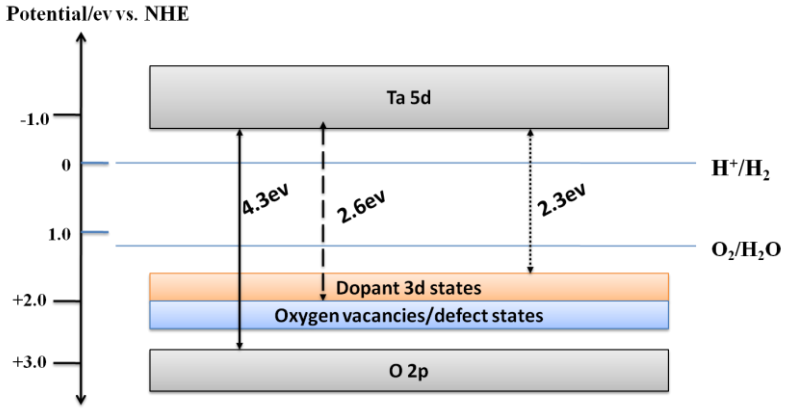

Figure: 2.2 Band gap of pristine and N, Ni doped $InTaO_4$

Band gap modification of $InTaO_4$ through doping was explored by Chang et al. [103] using simulation techniques and by Matsushima et al. [80], [104] using also modelling, such as CASTEP code, generalized gradient approximation (GGA), and full-potential linearized augmented plane-wave (FLAPW) method. Both the studies concluded that undoped $InTaO_4$ has wolframite-type structure with indirect-band gap of 4.3 eV (as shown in Figure 2.2). However, diffuse reflectance spectroscopy of $InTaO_4$ [105] suggested two onsets in the absorption spectra; at 4.3 eV and 2.6 eV which were originated from gap transition (between VB and CB) and the excitation of the gap states (defect states) respectively.

Chang et al. [103] and Irei et al. [105] have assigned the lower band gap of 2.6 eV to the gap states between the VB and CB, where the dominant contribution to these gap states was from In 5s, and 5p hybridized with some Ta 5d and O 2p states. Ye et al. [106] have also estimated the similar band gap of 2.6 eV for undoped $InTaO_4$. It was predicted [103] and proved [106] that these gap states further increased with cation (Ni) and anion (N) doping. The doping states/oxygen vacancies/gap states are the consequences of hybridization of Ni 3d, O 2p, and Ta 5d levels. Cation (Ni) and anion (N) doping in $InTaO_4$ introduced doping states/new energy level just above the VB (as shown in Figure 2.2), which were mainly originated from occupied Ni 3d states and N 2p states respectively, and unoccupied 3d states above the gap

states. The analysis of total density of states (TDOS) and partial density of states (PDOS) suggested that valence band is mainly consisted of O 2p orbital's, with a small contribution from In 4d, 5s, 5p and Ta 5d orbitals. Conduction band is mainly composed of Ta 5d orbitals with a small contribution from In and O orbitals.

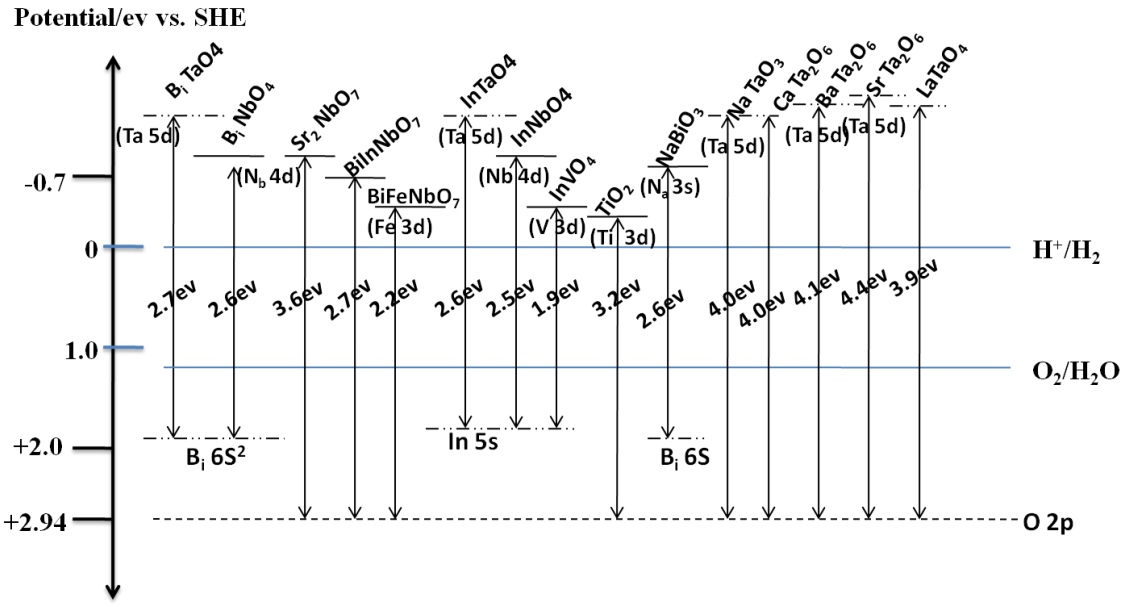

Figure: 2.3 Band gaps of various photocatalytic materials

Contrary to the above investigations, Irei et al. [105] have reported that anion (nitrogen) and cation (vanadium) doping of $InTaO_4$ was not helpful to reduce the native band gap of 4.3 eV but introduced defect/dopant levels above the valence band and below the conduction band, which served as recombination centres and worsen photocatalytic degradation activity of $InTaO_4$ when irradiated with UV light. Further investigation revealed that undoped $InTaO_4$ could not decompose IPA into CO_2 and acetone, when irradiated with visible light, while weak activity was observed for N and V doped $InTaO_4$ under the similar condition. However, under UV light irradiation $InTaO_4$ decomposed IPA more efficiently than N and V doped $InTaO_4$. The origin for visible light activity of the doped $InTaO_4$ was due to the formation of narrow bands from V 3d and N 2p orbitals within the forbidden energy

gap where the mobility of the carriers (electrons and holes) was much lower. Therefore, N-doped and V-doped $InTaO_4$ has shown very limited activity under visible light irradiation for decomposition of IPA. Nevertheless photocatalytic CO_2 conversion to methanol, and hydrogen evolution on $InTaO_4$ [107] synthesized through sol-gel[108] and laser ablation techniques[109] have been compared with the sample prepared through a solid state reaction method. These studies indicated that $InTaO_4$ synthesized with the sol-gel (SG) method has smaller particle size (17.1 nm) and smaller band gap (2.62 eV) than that (24.2 nm and 2.73 eV) prepared with solid state (SS) method. Photocatalytic activity of the sample prepared by the SG method was increased with increase in calcination temperature, since the crystallinity of the material was increasing and the particle size was reducing at high calcination temperature. Higher photocatalytic conversion of CO_2 to methanol by irradiating NiO loaded $InTaO_4$ with only visible light was attributed to the small and uniform crystal structure of the material. Youshida et al.[109] demonstrated that $InTaO_4$ has an indirect band gap where Ni substitution in the nano-structure synthesized by laser ablation method could not narrow down the band gap since no evidence of sub band absorption and/or band narrowing was observed.

It can be deduced from above detailed discussion that $InTaO_4$ is a proficient photocatalyst for visible light photocatalytic activation. It absorbs more visible light than TiO_2 and has more reduction potential because its conduction band level is at more negative position than TiO_2. However, more insight is required to determine its actual effective band gap, the effect of doping on band gap narrowing and effect of loading metal and/or metal oxide on modification of surface active sites. These and some other basic queries must be investigated in detail in order to use this material as visible light active photocatalyst.

2.11 Photocatalytic activities of alkali tantalates

As stated earlier, M-O-M angle and position of conduction band are other two governing factors which influence photocatalytic properties of metal tantalates such as $AgTaO_3$ and various alkali tantalates such as $NaTaO_3$, $KTaO_3$, and $LiTaO_3$, since

these compounds contain octahedral structures of TaO_6 with Ta-O-Ta angle. Hu et al. [110] have reported that $NaTaO_3$ prepared with sol-gel techniques has higher surface area (23 m^2/g), smaller particle size (30-5.0 nm), monoclinic type structure, and indirect band gap (3.9 eV), while the one prepared with solid state reaction techniques has smaller surface area (0.6 m^2/g), larger particle size (2-3 μm) orthorhombic type structure and direct band gap (4.1 eV). Further exploration of the samples discovered that the sol-gel prepared $NaTaO_3$ has (Ta-O-Ta) bond angle closure to 180°, more negative conduction band edge, and more number of effective states in the valence and conduction bands as compared to the sample prepared with solid state reaction method. Kato et al. [111] have investigated three different alkali tantalates, $LiTaO_3$, $NaTaO_3$ and $KTaO_3$, with and without co-catalysts loading. The Ta-O-Ta bond angles were 143°, 163° and 180° in $LiTaO_3$, $NaTaO_3$, $KTaO_3$ respectively, and band gaps (shown in Figure 2.3) which were calculated from the onset of the absorption edge were 4.7 eV, 4.0 eV, and 3.6 eV, respectively. It was suggested that the larger bond angle facilitates migration of the excited energy and makes the band gap smaller.

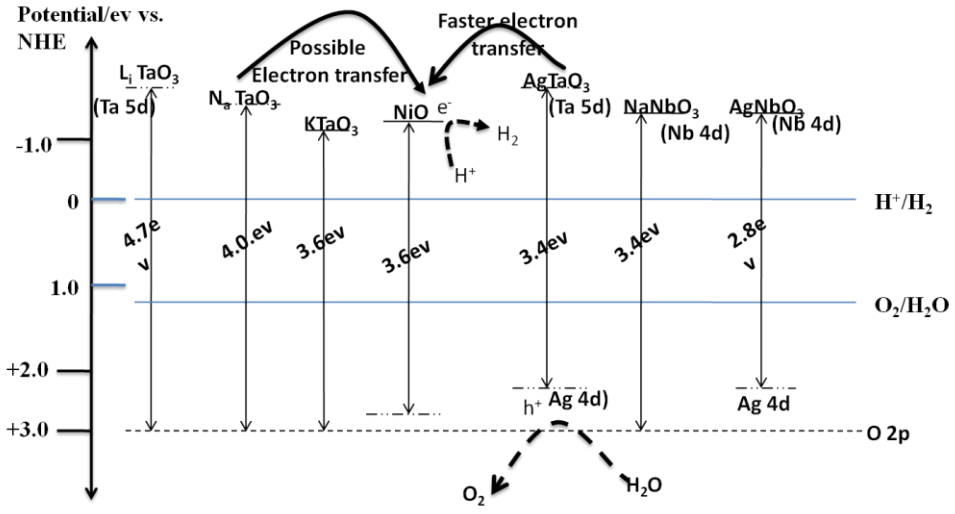

Figure: 2.4 Schematic of band gap modification with doping

Nevertheless, Kato et al. [112] found that substitution of Ag^+ modified the bond (Ta-O-Ta) angle and also reduced the band gap of alkali tantalate and alkali niobate to 3.4 eV for $AgTaO_3$ and 2.8 eV for $AgNbO_3$ as shown in Figure 2.4. The valence bands of $NaTaO_3$ and $NaNbO_3$ made of only O 2p orbital were hybridized with Ag 4d orbital and were shifted to more negative position than O 2p orbital in case of $AgTaO_3$ and $AgNbO_3$. A slight down shift in the conduction band was also observed due to Ag^+ substitution. Even though the reduction of Ag^+ was excluded; an unreasoned gradual decrease in photocatalytic activities of $Pt/AgNbO_3$ was another shortcoming of Ag^+ modified niobates. Nevertheless, unlike valence band up shifting (band gap miniaturization) [33], valence band down shifting (of $AgNbO_3$) was apparently successful[70]. However, visible light photocatalytic oxidation of IPA was attributed not only to the broadening of valence band, but was assumed to be the synergetic effect of blue shift in band gap, higher surface area (smaller particle size) and enhanced adsorption properties of $NaNbO_3$. Go et al. [113] recently reported band gap diminution of $NaTaO_3$ with vanadium, which consequently enhanced absorption in the optical region and improved photocatalytic decomposition of Rhodamine B (RB) under visible-light irradiation.

Nitrogen doping in $NaTaO_3$ changed the electronic structure, shifted the absorption edge from 320 nm (undoped: $NaTaO_3$) to 620 nm (doped: $NaTaO_{3-x}N_x$) and contributed in narrowing down the band gap from 3.9 to 3.69 eV, due to N 2p levels incorporated to valence band. Although size of nitrogen (0.171 nm) ion is larger than its substituent oxygen ion (0.132 nm) [114], it only brings in an up-shift of the conduction band of $NaTaO_3$[34], similar to cation doping [35] and could not modify the crystal structure. Nitrogen doping and band gap narrowing made this material to degrade formaldehyde only at visible light (>400 nm) irradiation whereas undoped $NaTaO_3$ could not degrade formaldehyde under similar condition. A similar effect of band gap miniaturization was also observed in case of nitrogen doped $LaTaO_4$ [115], but photocatalytic performance of the material remained unchanged.

2.12 Performance of Bi containing compounds

High surface area is one of the desired requirements for enhanced photocatalytic reaction since it provides more active sites, and a large number of electron-hole pairs can be generated. It is generally believed that particle size and surface area of materials can be controlled through a wet-chemical synthesis process. Lin et al.[116] have reported morphology and assembly-controllable synthesis of 3 dimensional nano-structured Bi_2O_3 through a precipitation technique. The band gap (3.02 eV) and maximum surface area (72.8 m^2/g) of the newly prepared Bi_2O_3 vary for different VO^{3-} concentration and temperatures. Nano-structured Bi_2O_3 degraded RhB with visible light irradiation about 6 times faster than the commercial Bi_2O_3. Higher photocatalytic activities were mostly attributed to the large surface area of newly synthesized Bi_2O_3. However, Kako et al.[117] believed that materials containing Bi (III) ion such as Bi_2O_3, $CaBi_2O_4$ and $BiVO_4$ have narrow conduction and valence bands where mobility of electrons is slower leading to recombination of photo-generated carriers. Visible light photocatalytic activities of $NaBiO_3$ were compared with $BiVO_4$ and N-doped TiO_2 by decomposition of methylene blue (MB) and gaseous 2-propanol. Results demonstrated that $NaBiO_3$ has better performance than both the nitrogen doped TiO_2 and Bi (III) containing compounds (Bi_2O_3, $CaBi_2O_4$, $BiVO_4$). Photocatalytic degradation of aqueous MB and gaseous 2- propanol was mainly attributed to the hybridized conduction band of $NaBiO_3$. Density function theory (DFT) analysis of the sample indicated that unlike Bi (III) materials (Bi_2O_3, $CaBi_2O_4$) where the valence band consisted of hybridized Bi 6s and O 2p orbitals (as shown in Figure 2.5) and conduction band mainly made up of Bi 6p orbital, $NaBiO_3$ has its broad valence band mainly consisted of O 2p orbitals and conduction band composed of hybridized Na 3s and O 2p orbitals. Large dispersion in hybridized conduction band of $NaBiO_3$ enhances mobility of photo-generated electrons and also suppresses electron-hole pair's recombination, which leads to the improved photocatalytic performance [118], [42]. However, Chang et al. [118] argued that the conduction band is very close to the reduction potential (O_2/O_2^-) level, which could hardly reduce O_2 to O_2^- while strong oxidation potential

at the top of valence band generates large number of powerful $^{\bullet}OH$ which then subsequently oxidize penta-chloro-phenate (PCP-Na) molecules. Decomposition of PCP-Na by $^{\bullet}OH$ was further justified since addition of radical ($^{\bullet}OH$) scavenger to the aqueous solution drastically reduced the visible light photocatalytic degradation of PCP-Na. It must be noted that along with nitrogen-de-ethylation process, Yu et al. [119] also laid emphasis on attack of ($^{\bullet}OH$) radical on the RhB chromospheres, which resulted in complete mineralization of the organic dye. Although, $NaBiO_3$ has a band gap of 2.6 eV, which lies within the visible range, it could not decompose 2-propanol with wavelength >460 nm, suggesting that oxidation beyond this wavelength is only originated from the lattice defects not from the native band gap excitation of $NaBiO_3$ [39].

Some researchers[119, 120] have reported that de-hydrated $NaBiO_3$ can decompose polycyclic aromatic hydrocarbons like anthracene and benz[a] anthracene [121] and degrade RhB dye [122] very efficiently under visible light irradiation. However, some biodegradable by-products such as anthraquinone and anthron were detected showing incomplete mineralization of the contaminants. Contrary to Kou et al. [123] findings, Yu et al. [119] demonstrated that non-hydrated $NaBiO_3.xH_2O$ decomposed RhB dye through visible light irradiation (λ>400 nm) with a much faster rate (97%) than P25 and Bi_2WO_6.

As discussed earlier, largely dispersed and hybridized conduction band of a photocatalyst material is beneficial because it not only enhances electron moment but also reduces recombination of photo-generated carriers. Anatase form of TiO_2 [43] is known to have thin conduction band and closed packing structures which affects electron moment and increases recombination. As an alternative to TiO_2, bismuth oxyhalides such as BiOCl [124], [125], BiOI [125] and BiOBr [124], [126] have highly dispersed and hybridized conduction band like $NaBiO_3$ and open structure along c-axis. These properties allow unrestricted moment of electrons in the conduction band. Zhang et al. [124] have indicated that Cl 3p and O 2p states make valence band largely dispersed whereas hybridized conduction band of BiOCl is made of O 2p, Cl 3p, Bi 6s, and Bi 6p orbitals. These bismuth oxyhalides (BiOCl

[124] [125]), BiOBr [124], [126] and BiOI [125] have been investigated as visible light photocatalysts because of smaller band gaps (3.22, 2.64, and 1.77 eV). Although, BiOCl, and BiOBr have shown better performance than the bench mark material P25 toward bleaching of methyl orange (MO) under UV light irradiation however, BiOI was found to be the most efficient among the three catalysts, because it degraded almost 95% of MO within 3 hours of visible light irradiation. In addition to dispersed conduction band in all of the three oxyhalides compounds (BiOI, BiCl, and BiOBr) the improved photocatalytic performance of these materials were attributed to the smaller band bap (1.77 eV) (BiOI), predominant photosensitization process (BiOCl) and unusual hierarchical mesoporous structure (BiOBr), respectively.

In order to control and stabilize direct formation of three dimension hierarchical structures of bismuth oxyhalides, some researchers [125], [126], [127] have used ethylene glycol as a solvent and structure controlling agent. Ethylene glycol due to its chelating characteristic insures formation of self-assembled, regular and hierarchical microspheres with 3 D flower like structure. All of these studies found similar (8-10 nm) sized plate like structures of BiOCl and BiOBr aggregated into final (2-10 μm) micro-spheres. Under UV-visible light irradiation, BiOBr was capable to remove 45% NO within 10 minutes, while TiO_2 could remove only 8% of NO under similar condition. However, NO removal rate was reduced when the system was irradiated with visible light (>420 nm). The better photocatalytic performance of BiOBr than P25 was attributed to the smaller band gap (2.5 eV), and hierarchical structure with a high surface area.

DFT analysis has shown that valence band of Bi_2WO_6 [128], [129] is also made of hybridized O 2p and Bi 6s orbitals, while conduction band is solely composed of W 5d orbital. As stated earlier, dispersive nature of valence band is advantageous for movement of photo-generated hole which further increases photo-oxidation process. However, Bi_2WO_6 has a valence band more positive than O_2 evolution level, while conduction band is lower than the H^+/H_2 reduction level, making it inappropriate for hydrogen production. Bi_2WO_6 has been synthesized through hydrothermal

techniques, where surface area, crystallinity and band gap were reaction temperature and time dependent. Samples prepared at 180 °C [128] have better crystallinity but lower surface area of 42.9 m^2/g than the sample prepared at 140 °C which has a surface area of 46.4 m^2/g. Although samples prepared at different temperatures show slight difference in the optical absorption, the band gap was estimated to be 2.7 eV. Shang et al. [130] observed a band gap of 2.5 eV and surface area of 51.5 m^2/g with high crystallinity for Bi_2WO_6 synthesized with 160 °C and 24 hour reaction time. Photocatalytic degradation of RhB with only visible light [128] or UV-vis [128] revealed that Bi_2WO_6 could degrade RhB dye more efficiently than N-doped TiO_2 at visible light; however, complete mineralization was only observed with UV irradiation of Bi_2WO_6. Contrary to Fu et al. [128] findings, the sample prepared at 160°C has complete disappearance of RhB under visible light irradiation, which was attributed to the smaller crystalline structure and high surface area. Fu et al. [128] and others (Li et al. [131], Zhang et al. [132]) have concluded that N-deethylation process was the main path for bleaching RhB dye with visible light irradiation while decomposition of RhB conjugated structure was only possible with UV irradiation. The same research group [128] also synthesized Bi_2WO_6, $ZnWO_4$ and $PbWO_4$ with surface areas of 46.4, 36.7 and 2.34 m^2/g and band gaps of 2.70, 2.43 and 3.31 eV, respectively. Their photocatalytic performance under UV light irradiation was lower than TiO_2 P25. However, under visible light irradiation Bi_2WO_6 has better activity than P25 and other two compounds attributing to the smooth mobility of photo-generated holes in hybridized valence band and to the faster electron transfer in highly distorted structure of WO_6 in Bi_2WO_6. In addition, fluorine ions (F^-) have been [129] substituted into Bi_2WO_6 in order to achieve complete decomposition of RhB dye with sun light irradiation. Results indicated that doping fluoride into Bi_2WO_6 reducing the band gap (as shown in Figure 2.5) creating more vacancies in the bulk and on the surface of the material and also increasing porosity and acidity of the material. These effects consequently amplify both the number of hydroxyl radicals on the surface and mobility of the intermediates, which subsequently enhance

photocatalytic property of fluorinated Bi_2WO_6 and increase the ratio of deethylation process to the decomposition of chromospheres.

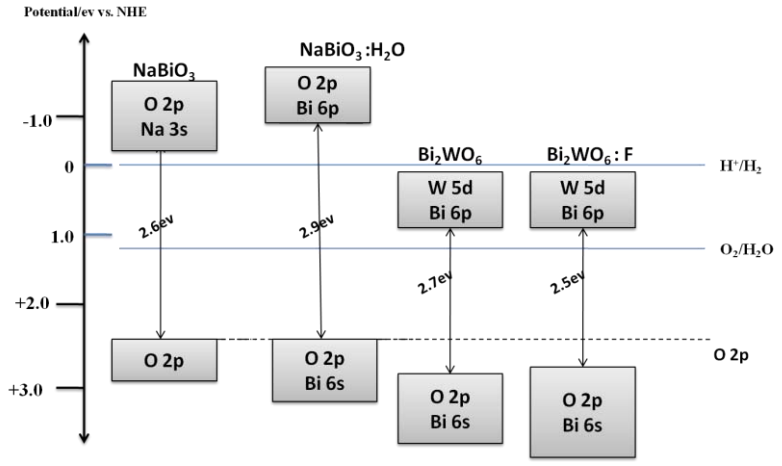

Figure: 2.5 Band gap modification of $NaBiO_3$ and Bi_2WO_6.

However, other bismuth containing mixed oxides such as Bi_2AlVO_7, Bi_2InTaO_7 [133], and Bi_2FeVO_7 [134] were capable to completely mineralize MB under visible light irradiation because they absorb more visible light with smaller band gaps of 2.06, 2.8 and 2.22 eV, respectively. Higher initial degradation rates of MB and higher removal of total organic carbon (TOC) obtained with these materials indicates their efficiency under visible light irradiation. Lower activity of Bi_2InTaO_7 was attributed to its large band gap. Although these materials were efficient to completely mineralize MB under visible light irradiation, they were unable to produce hydrogen and/or oxygen.

Similarly, Shan et al. [135] also compared photocatalytic activities of four Bi-based photocatalysts; $Sr_2Bi_2O_5$, $SrBi_2O_4$, $BiVO_4$, and Ag loaded $Sr_2Bi_2O_5$. Although the band gap of $Sr_2Bi_2O_5$ (2.87 eV) was larger than that of $SrBi_2O_4$ (2.51 eV) and $BiVO_4$ (2.34 eV), $Sr_2Bi_2O_5$ decomposed MO both under UV and visible light irradiation more efficiently than the latter two photocatalysts. Complete and faster mineralization of MO was observed with silver loaded $Sr_2Bi_2O_5$ when irradiated with UV light (λ = 365 nm), however, it took about 8 hours to completely mineralize MO at visible light (>420 nm). Higher photocatalytic activity of

$Sr_2Bi_2O_5$ was attributed to the higher dipole moment and lower packing fraction of the catalyst. It was argued that charge separation depends upon the distortion of crystal structure; the larger distorted local structure, higher dipole moment and higher charge separation capability, minimizing electron hole pair recombination and increasing photocatalytic activity. Loading silver onto the surface further reduces electron-hole pair recombination because of the trapping of photo-generated electrons by metallic silver as explained in Figure 2.6. Furthermore, mobility of the photo-generated electron-hole pair was suggested to be the packing fraction dependent. The smaller the packing fraction of the crystal structure, the higher the mobility of the carriers and thus the better activity it has. Therefore, $Sr_2Bi_2O_5$ has more distorted structure and less packing fraction than the other two catalysts and it has better activity than others. NiO co-assisted monoclinic $SrBi_2O_4$ was successful to decompose gaseous acetaldehyde and degrade coli (E. coli) under visible light irradiation [136]. Better photocatalytic performance of NiO coated material was mainly attributed to the efficient separation of electron hole pair before recombination and quick interfacial charge transfer.

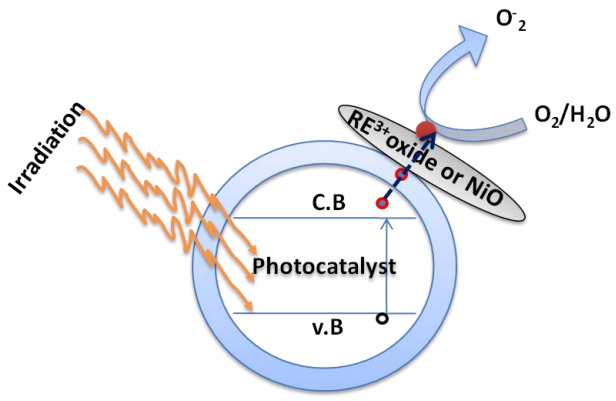

Figure: 2.6 Co-catalyst assisted photocatalytic degradation process

It can be concluded from above survey that neither of bismuth oxyhalides (BiOCl, BiOBr, and BiOI) is visible light active photocatalyst owing to their inability of complete mineralization of organic compounds, lower conduction band level than the redox potential, and weak selectivity. Mixed metal oxides such as $Sr_2Bi_2O_5$ loaded with metallic silver may have the opportunities but the electron capturing

property of the metallic silver reduces significantly if the material is used for multiple times.

2.13 Photocatalytic activities of vanadates

It is generally believed that hybridizing valence and/or conduction band of oxide semiconductors is beneficial for improvement of photocatalytic properties, because this enhances mobility of photo-generated carriers, suppresses recombination process, and swift carrier transfer to the active surface. Kudo et al. [137] prepared tetragonal and monoclinic $BiVO_4$ which have deep and hybridized valence bands, respectively. Conduction bands of the tetragonal and monoclinic $BiVO_4$ were made of V 3d orbitals, and valence bands were consisted of only O 2p orbital, and hybridized Bi 6s and O 2p orbitals, respectively. Therefore, due to hybridized valence band monoclinic $BiVO_4$ structure has a typical absorption band in visible region in addition to the UV band observed in tetragonal $BiVO_4$. Kohtani et al. [138] used the valence band hybridized $BiVO_4$ to reduce the estrogenic activity of 4-nonylphenol and octylphenol through visible light irradiation from a solar simulator. Results revealed that complete disappearance of the estrogenic properties of 4-alkylphenol was possible through the photocatalytic process, but it took longer time (about 140 minutes) and a series of non-degradable by-products were also observed. Ordered mesoporous and monoclinic scheelite $BiVO_4$[139] synthesized through nano-casting techniques using silica KIT-6 as replica parent template has also hybridized valence band consisted of Bi 6s and O 2p orbitals. It was assumed that the extended nature of valence band can facilitate mobility of photo-generated hole, which may subsequently improve photocatalytic activity. Due to the smaller crystalline size (7.5-8 nm) of mesoporous $BiVO_4$ a blue shift in the absorption edge was observed which leads to an increase in band gap from 2.05 to 2.2 eV. However, improved optical absorption of mesoporous $BiVO_4$ was mainly attributed to the higher surface area (59 m^2/g) because the conventional $BiVO_4$ has very lower surface area of (2 m^2/g). Photocatalytic removal rates of MB and NO were three and

two times higher than P25 under visible light irradiation. Further, mesoporous $BiVO_4$ exhibited strong stability since it did not lose its functionality after repeated use. Higher and stable photocatalytic activity of the mesoporous $BiVO_4$ was mainly attributed to the large surface area, smaller crystalline size, and hybridized valence band, since all of these were beneficial for separation of electron-hole pairs and efficient transfer of photo-generated carriers. In order to acquire large surface area and smaller crystalline size, certryl-tri-methyl-amonium bromide (CTAB) [140] was used as a capping agent to be selectively adsorbed on the surface of $BiVO_4$ nuclei at basic condition (pH=11). It was assumed that a lone pair of OH^- could strongly interact with the surface of $BiVO_4$ nuclei and can selectively adhere to some special crystalline faces and make these faces electronegative. Positively charged CTA^+ could adsorb hydroxyl ions by electrostatic effect, which acts as a capping agent and limits growth rate of crystal faces. It must be noted that samples with different morphologies such as flower, cuboid and square plate- like crystals were obtained at different pHs. Photodegradation of methyl orange under sunlight irradiation on $BiVO_4$ was much better than that of P25 under visible irradiation.

Various techniques such as doping with metals [141], [142] loading with transition metals [143],[144] and making composites[145],[137],[146] of $BiVO_4$ with oxide semiconductors have been attempted to reduce electron-hole pair recombination and enhance visible light photocatalytic activities. Long et al. [145] and Xue et al. [146] found that only monoclinic scheelite structure of $BiVO_4$ holds good photocatalytic property under visible light irradiation. Long et al. [145] synthesized a composite $CoO_3/BiVO_4$ material and Xue et al. [146] loaded transition metal oxides (Fe_2O_3, Co_3O_4 and CuO) on the surface of $BiVO_4$ through an impregnation method for water purification under visible light irradiation. Results [145] revealed that pristine $BiVO_4$ has an band gap in visible range (2.28 eV) but it could only degrade 6% of phenol when irradiated with visible light but decolorize methylene blue [146] under UV and visible light irradiation. However, photocatalytic activities were significantly increased with loading [145] transition metal oxide ($Fe_2O_3/BiVO_4$< $Co_2O_4/BiVO_4$< $CuO/BiVO_4$) and compositing[146] with Co_2O_3. Lower

photocatalytic activity and presence of photoluminescence in case of bared $BiVO_4$ [145], [146] were the consequences of electron-hole pair recombination. Co_2O_3 being a p-type semiconductor has a direct band gap of 2.07 eV and can build p-n hetero-junction when impregnated on $BiVO_4$ surface, which separated electron-hole pairs and reduced the recombination of carriers [146]. Reduction in the photoluminescence of composites $Co_2O_3/BiVO_4$, $Fe_2O_3/BiVO_4$, $Co_2O_4/BiVO_4$, $CuO/BiVO_4$ confirmed reduced recombination process, which subsequently enhanced their photocatalytic performance. Considerable decrease in TOC of phenol further confirmed that the composite materials are also capable to completely mineralize contaminants. Photocatalytic activity of the composites material found to be far better than both the Ag doped $BiVO_4$ and iodine doped TiO_2. It was argued that upon visible light irradiation separate electron-hole pair was generated both on Co_2O_3 and $BiVO_4$. Photo-generated holes were transferred (as shown in Figure 2.7 (II)) from $BiVO_4$ to Co_2O_3 due to the smaller valence band level of Co_2O_3 than that of $BiVO_4$; however, the photo-generated electrons cannot migrate from $BiVO_4$ to Co_2O_3 because of its higher conduction band level. It was further suggested that transition metal oxide on the surface of $BiVO_4$ captures photo-generated electrons (as shown in Figure 2.7 (II)), thus separating the electron hole pair, consequently increases photocatalytic activity.

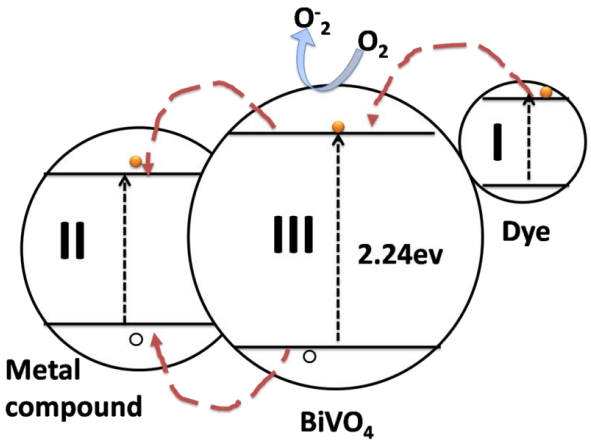

Figure: 2.7 (I) Dye sensitization, (II) Carrier capturing and EH pair separation and (III) Direct photocatalysis

Martinez-de la Cruz et al. [147] and Ge et al. [148] proposed three path ways; i) dye sensitization i.e. electron transfer from dye to photocatalyst (Figure 2.7 (I)), ii) photocatalyst excitation i.e. reduction of oxygen by photo-generated electron (Figure 2.7 (III)) and iii) electron trapping by deposited Pt (IV)Cl_4 (Figure 2.7 (II)) for photo-degradation of MO. Electron trapping (shown in Figure 2.7 (II)) was considered as the most dominant mechanism, because photo-degradation of MO was increasing with Pt concentration suggesting an increase in the trapping centres. It was also reported [143] that hydrothermally synthesized $PtCl_4/BiVO_4$ has monoclinic and distorted scheelite like structure which possess high activity under visible light irradiation. XPS analysis confirmed that Pt is not doped substitutionally and/or interstitially but deposited on the surface as platinum chloride compound ($PtCl_4$). It was found that only 42% MO was degraded by pure $BiVO_4$ within 15 hours under visible light irradiation, while 100% MO was degraded within the same time when $PtCl_4/BiVO_4$ was used as catalysts.

Silver (Ag) nanoparticles [149] of 10-20 nm size were deposited on $BiVO_4$ thin films to suppress electron hole recombination. Results revealed that Ag deposited films were more efficient than $BiVO_4$ film in removing phenol from water since migration of photo-generated electron to the surface deposited Ag particles isolates the photo-generated holes to oxidize phenol. In a recent study by Zhang et al. [150]

sliver was successfully doped into $BiVO_4$, rather than deposits metal and transition oxide on the surface [144], [137, 146]. Contrary to band broadening as reported earlier [144], [137], [146], silver doping was found to reduce the band gap of $BiVO_4$ and enhance its optical absorption improving photocatalytic degradation of MO under visible light irradiation. Higher photocatalytic activity and band gap reduction were mainly attributed to the increased surface defects caused by silver doping. Martinez-de la Cruz et al. [151] have recently reported that photocatalytic degradation of RhB with $BiVO_4$ varies with pH of the system. It was found that at lower pH (=6) less amount (60%) of RhB was bleached in longer time (6 hours) under visible light irradiation, on the other hand, large amount (90%) of RhB was bleached within 5 hours at higher pH level (= 10), while further increase in pH was detrimental to the photocatalytic activity. Three different ways; direct photolysis, dye photo-sensitization, and true heterogeneous photocatalysis were considered for degradation of RhB. Dye photo-sensitization as explained in Figure 2.7 (I), was considered to be the most favourable mechanism. However, degradation of dye through this mechanism doesn't require high pH, while true heterogeneous photocatalysis can be affected by pH variation, where photo-generated holes in a semiconductor can react with hydroxyl ion to generate hydroxyl radicals, which in turn oxidize dye molecules. Although the authors have emphasized on dye sensitization process, but we assumed that degradation of dye via heterogeneous process might be the possible reaction pathway because it depends on pH of the system. The lower activity of heterogeneous pathway upon UV irradiation can be attributed to the recombination of photo-generated electron-hole pairs owing to the small band gap (2.3 eV) of the material.

Various metals, transition metals and non-metals have been attempted to dope interstitially and/or substitutionally into $BiVO_4$ crystals to optimize optical properties and band levels for visible light photocatalysis. However, none of the efforts have shown significant improvement in photocatalytic activities of $BiVO_4$. Xu et al. [152] loaded various rare earth ions (La^{3+}, Ce^{3+}, Gd^{3+}, Yb^{3+}, Eu^{3+}, Ho^{3+}, Nd^{3+} and Sm^{3+}) on $BiVO_4$ surface and engineered its band gap for enhanced visible

light absorption and efficient degradation of water pollutants. It was assumed that instead of V^{5+} ion (which has smaller radii 0.59 Å), RE^{3+} ions with about similar radii as that of the Bi^{3+} ion can be substitutionally doped into $BiVO_4$. However, XRD analysis could not identify the existence of RE^{3+} ion doped into $BiVO_4$, but XPS investigation showed the presence of some rare earth oxides (RE_2O_3) on the surface. A blue shift in the absorption edge of RE^{3+} loaded $BiVO_4$ was observed; as a result the optical band gap of the material was shifted from 2.4 to 2.5 eV. Unlike metal and transition metal oxide loading all the samples loaded with various RE^{3+} ions have shown lower photocatalytic activity than pure $BiVO_4$ except Gd^{3+} loaded $BiVO_4$ which has 1.4 times better activity than pure $BiVO_4$. The blue shift in the optical absorption and smaller surface area might be the reasons for lower photocatalytic activities of RE^{3+} (La^{3+}, Ce^{3+}, Yb^{3+}, Eu^{3+}, Ho^{3+}, Nd^{3+} and Sm^{3+}) loaded $BiVO_4$. Higher activity of Gd^{3+} loaded $BiVO_4$ was attributed to its high efficiency of electron hole pair separation, which might be due to the fast electron transfer from Gd^{3+} to adsorbed oxygen. The lower crystallinity and number of hydroxyl radicals[153] on the surface of Ag_3VO_4 [154] were the two major factors which enhanced the visible light photocatalytic decomposition of gaseous IPA and benzene. The hydrothermally prepared Ag_3VO_4 was found to have 16.6 and 16.2 times higher activity for degradation of isopropanol and benzene than those of P25.

It can be deduced from above studies that $BiVO_4$ has two distinct properties of hybridized valence band and smaller band gap of 2.4 eV, and has a very lower reduction potential when irradiated with visible light. It is worth mentioning that modifying surface area and band gap, through doping and/or loading of metals and metal oxides, were also not a very successful strategy to enhance photocatalytic properties of $BiVO_4$.

2.14 Transition metal oxides and mixed oxide semiconductors

Kato et al. [155] have studied a large number of mixed oxide semiconductors mostly consisted of tantalates and modified forms and have set out some basic criteria for selecting best photocatalysts based on their findings. As per the

exploration of the research group, photocatalyst materials should have i) less distorted crystal structure, ii) more negative conduction band level, iii) M-O-M angle equal/closure to 180°, iv) and suitable crystal structure which possess high potential to transfer excited energy. It was reported that tantalates conduction band consisted of Ta 5d orbital, which is more negative than titanates Ti 3d and niobates Nb 4d orbitals, beneficial for hydrogen production in photocatalysis. Effect of 3d, 4d and 5d orbitals on the structural and photocatalytic properties of mixed oxides, $InVO_4$, $InNbO_4$ and $InTaO_4$, has been also investigated[155]. It was found that both 5d and 4d of transition metal compounds i.e. $InTaO_4$ and $InNbO_4$ have about similar structure which are made of two octahedrons InO_6 and $TaO_6(NbO_6)$, but the structure of 3d transition metal compound $InVO_4$ consisted of octahedron InO_6 and tetrahedron VO_4. Band gaps of $InTaO_4$, $InNbO_4$ and $InVO_4$ were 2.6, 2.5, and 1.9 eV, respectively, and all the three materials $InTaO_4$, $InNbO_4$, and $InVO_4$ evolved both hydrogen and oxygen by splitting water in the presence of sacrificial reagents and electrons acceptors.

Although Ta_2O_5 has a wide band gap of 4.00 eV, which is made up of O 2p orbital and Ta 5d orbital, but its highly porous structure [156] made this material beneficial for photocatalysis. Additionally NiO loading on Ta_2O_5 surface could enhance photocatalytic activity, the red shift in the absorption edge (from 315 to 285 nm) was observed by doping and/or coupling Ta_2O_5 with Eu_2O_3 [157] and TiO_2 [83]. This enhanced optical absorption and photocatalytic performance were presumably attributed to the interstitial Eu^{3+} ion residing on the surface of Ta_2O_5 in the form of Eu_2O_3. Substitution of Eu^{3+} was excluded due to the larger radius of Eu^{3+} ion. It was demonstrated that varying Eu^{3+} concentration and calcination temperature not only modify structure of Eu_2O_3/Ta_2O_5, but also vary mineralization rates of RB and 4-NP under UV light irradiation. Sample (Eu_2O_3/Ta_2O_5) prepared with 49% Eu and calcined at 200 °C was capable to mineralize RB and 4-NP at higher rate of 87%, larger than that of pure Ta_2O_5. Higher catalytic activities of the mixed system were attributed to the band gap miniaturization and electron trapping by Eu_2O_3, which reduces electron-hole pair recombination. It was also observed that increasing Ta

content decreases porosity of Ta_2O_5 and the porous structure could be maintained at high ratio a Ta:Ti. It can be deduced that reducing band gap through doping and/or coupling with metal/metal oxide can enhance photocatalytic property of Ta_2O_5 to a limited extent. In addition coupling of transition metal mixed oxide $LaVO_4$ with TiO_2 was successful to photo-catalytically degrade gaseous benzene with visible light irradiation[158]. As explained in Figure 2.8 the conduction band of $LaVO_4$ being more negative than that of TiO_2 facilitates electron transfer from $LaVO_4$ to TiO_2 upon visible light irradiation, which then participates in the redox reaction before recombination.

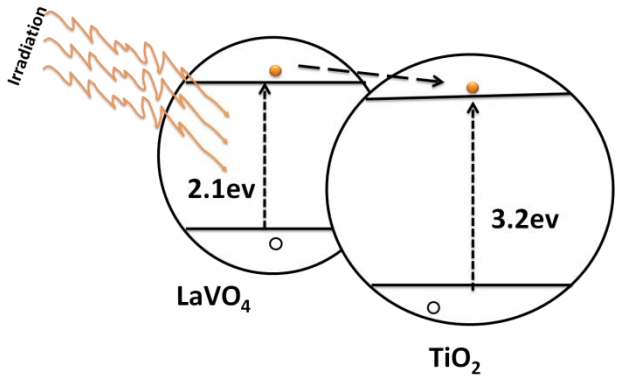

Figure: 2.8 Migration of photo-generated electron between two metal oxides.

CdS is another transition metal semiconductor photocatalyst which has been investigated for photocatalytic decomposition of contaminants under visible light irradiation based on its band gap (2.3 eV), which lies within the visible range of solar spectrum. Yanagida et al. [159] have reported synthesis of controlled sized nanoparticles of CdS using various solvents. CdS nanoparticles prepared in N, N-dimethyl-formamide were found to have the smallest crystallites size of 3-5 nm. The study revealed that, conduction band level of bulk CdS is at lower potential than required for reduction of CO_2, but the quantum size effect uplifts the conduction band level and the photo-excited electron can very easily transferred from conduction band to CO_2. Photo-generated electrons in conduction band of CdS-DMF are trapped by sulphur vacancies on CdS nanoparticles, whereas DMF

quenches photo-generated holes. This separation of carriers suppresses recombination of electron-hole pair and increases life time of photo-generated electrons which have enough potential to reduce the adsorbed CO_2 on CdS surface. Similarly, Xing et al. [160] have also discovered that positions of conduction band level and valence band level can be shifted toward more negative and positive potentials through doping Zn into CdS.

Highly dispersed quantum dots of CdS incorporated into the framework of ordered mesoporous TiO_2 [82] make a hetero-junction which facilitates charge separation and electron transfer between the two materials and enhances photocatalytic activities of the embedded system. Seeding CdO in the pore channels of TiO_2 followed by ion exchange of O with S introduced CdS quantum dots into the pores of TiO_2. Photoluminescence peaks of both TiO_2 and CdS/TiO_2 at 382 nm were apparently caused by the emission of surface oxygen vacancies and surface defects. Increase in the intensity of these peaks (in case of CdS/TiO_2) suggested that CdS quantum dots introduced in the ordered mesoporous TiO_2, increased both the number of oxygen vacancies and defect states on the surface and its ability of light absorption. Three different compounds; gaseous NO, MB and 4-chlorophenol in aqueous solution were tested as model contaminants under visible light irradiation. The study revealed that CdS/TiO_2 was more efficient than P25 in both the gas phase and aqueous media. Improvement in photocatalytic activity was attributed to the synergetic effect of high surface area, quick charge transfer, and more visible light absorption. Sun et al. [161] reported synthesis of a new Cd based photocatalyst ($Cd_2Sb_2O_{6.8}$) via a hydrothermal process, where the band gap, pore size and surface area of the material were found to be 3.9 eV, 3.5 nm and 163.8 m^2/gm. $Cd_2Sb_2O_{6.8}$ was found to be more efficient than P25 in degradation of gaseous benzene under UV irradiation in a continuous flow reactor. $Cd_2Sb_2O_{6.8}$ converted 51% benzene within initial 10 hours but the conversion was reduced to 13% after 40 hours; whereas P25 has very low initial conversion rate of 16% and it was reduced to 0% after 40 hours. However, $Cd_2Sb_2O_{6.8}$ was less efficient than P25 in degradation of

aqueous RhB and MO dyes. Higher photocatalytic activity of $Cd_2Sb_2O_{6.8}$ in gas phase condition was attributed to its large surface area than P25.

In summary, it is concluded from above discussion that, although CdS has smaller band gap than TiO_2 due to its photo-corrosion and its lower conduction band level than the reduction potential of water and/or other volatile organic compounds, this material may not be capable to decompose a large number of VOCs. In addition, $InVO_4$ has the smallest band gap and therefore can excite more electrons to the conduction band with visible light irradiation, however, high recombination of electron – hole pairs reduced its activity. Ni doped and coated $InTaO_4$ were found to be the most efficient photocatalysts as long as water splitting through visible light irradiation is concerned, we therefore attempted to prepare Ni doped $InTaO_4$ and examined its photocatalytic performance with gaseous toluene degradation under UV light irradiation[63, 141].

2.15 Conclusion

Numerous indoor and outdoor sources and human activities emit large amounts of extremely toxic VOCs. Among these, formaldehyde, acetaldehyde and benzene have been detected both in indoor and outdoor environment with very high concentrations, which can cause fatal diseases like asthma, irritation and carcinoma. Although various physical and chemical techniques have been suggested to mitigate the concentration of these toxic compounds and their prevailing effects, these techniques are not good enough to completely remove or disintegrate the VOCs. Photocatalytic decomposition via sunlight irradiation and suitable photocatalytic materials have been proven as a viable technology to completely mineralize VOCs at lower levels. This technology is capable to work at very lower power, and ambient temperature, and completely decompose VOCs to mineral salt, water and CO_2. However, this method of VOCs decomposition is in very preliminary stage and still needs much attention to be paid.

Fundamental objective of this chapter was to review photocatalyst materials which can operate more efficiently under visible light irradiation and can degrade water

and air contaminants and also generate hydrogen and oxygen via direct water splitting. In this context we have attempted a critical review of some mostly studied materials and their performance under UV/visible light irradiation. We inferred from vast literatures that achieving high efficiency under visible light irradiation is still a big challenge. We have identified the following prominent points from our study and concluded that;

i) Lanthanide oxides such as CeO_2 has a band gap (2.95 eV) in the visible range but overall performance of this material is inferior to TiO_2 because, neither can it operate with visible light nor it generates oxygen via water splitting. In addition it has photo-corrosion problem.

ii) Among various niobium based materials such as Nb_2O_5, $LiNbO_3$ and $NaNbO_3$, the former one calcined at lower temperature (400 °C) has thinner pore wall which facilitates electron transfer rate and suppresses electron hole pair recombination, however, TiO_2 has 3.5 times higher photo-conversion efficiency than the mesoporous Nb_2O_5. Nitrogen doping into alkali niobates such as $NaNbO_3$ was successful to achieve redshift in optical absorption from 365 to 400 nm but, it took long time to mineralize only 40% of IPA with visible light irradiation.

iii) Tantalates and niobates such as $NaTaO_3$ and $NaNbO_3$ consisted of octahedrons TO_6 and NbO_6 where, M-O-M angle is more closure to 180° in tantalates than in niobates which accelerates electron transfer, and enhances photocatalytic activities of tantalates. Among various (doped and non-doped) alkali tantalates ($NaTaO_3$, $LiTaO_3$, $KTaO_3$, etc.), both non doped and Sr doped $NaTaO_3$ loaded with NiO showed better performance under UV irradiation, however, reduction of NiO to metallic Ni, elution of Na^+, and recombination due to defect centres in the bulk of the material were detrimental for photocatalytic processes.

iv) Various bismuth containing materials such as bismuth oxide, (Bi_2O_3, $CaBi_2O_4$, BiOCl, BiOBr, and BiOI), bismuth containing mixed oxides (Bi_2WO_6, Bi_2InTaO_7, $BiCu_2VO_4$, $Sr_2Bi_2O_5$, $SrBi_2O_4$) and bismuth vanadates $BiVO_4$ have Bi 6s orbitals in structures which hybridize their valence bands and enhance

carrier mobility. Monoclinic $BiVO_4$, which has both the properties of lower band gap (2.4 eV) and hybridized valence band can be assisted with co-catalysts such as CoO_3, Fe_2O_3, Co_3O_4, $PtCl_4$ and CuO, doped with Ag and rare earth metals such as La^{3+}, Ce^{3+}, Gd^{3+}, Yb^{3+}, Eu^{3+}, Ho^{3+}, Nd^{3+} and Sm^{3+} to enhance its visible light photocatalytic activities. Despite of these modifications $BiVO_4$ did not show a significant improvement with visible light irradiation.

v) Transition metal oxides (Ta_2O_5) and sulfides have a large band gap of 4.0 eV which can only generate electron hole pairs with UV irradiation. Coupling and/or loading of NiO, Eu_2O_3, and TiO_2 on Ta_2O_5 were not successful to exclude UV excitation, however, it moderately enhanced the photocatalytic activity. Recombination can be suppressed by reducing the pore wall thickness in case of Nb_2O_5 but its photocatalytic performance is still lower than TiO_2.

vi) Large number of mixed oxide semiconductors such as Bi_2MNbO_7 (M^{3+} = Al^{3+}, Ga^{3+}, In^{3+}), $K_3Ta_3Si_2O_{13}$, $K_3Nb_3Si_2O_{13}$, $SrTa_2O_6$, $BaTa_2O_6$ $CaTa_2O_6$ in their native and/or modified forms through doping and/or loading with metals and metal oxides exhibited photocatalytic activity with visible light irradiation. Among these, $InTaO_4$ has shown tremendously efficient performance with both UV and visible and was found to be capable to split water into O_2 and H_2 with and without co-catalysts such as NiO. However, some more insight is still required to confirm actual band gap of the material, to investigate its capability for complete mineralization of air pollutants with visible light, and to explore routes for its low temperature synthesis.

2.16 References

1. Romero-Vargas Castrillón, S. and H.I. de Lasa, *Performance Evaluation of Photocatalytic Reactors for Air Purification Using Computational Fluid Dynamics (CFD).* Industrial & Engineering Chemistry Research, 2007. **46**(18): p. 5867-5880.

2. Maupin, I., et al., *Improved oxygen storage capacity on CeO2/zeolite hybrid catalysts. Application to VOCs catalytic combustion.* Catalysis Today. **In Press, Corrected Proof**.

3. Rumchev, K. and K. Rumchev, *Volatile organic compounds: do they present a risk to our health?* Reviews on environmental health, 2007. **22**(1): p. 39.

4. Beach J. R, et al., *The effects on asthmatics of exposure to a conventional water-based and a volatile organic compound-free paint.* European Respiratory Journal, 1997. **10**(3): p. 563-566.

5. Gallego, E., et al., *Assessment of Chemical Hazards in Sick Building Syndrome Situations: Determination of Concentrations and Origin of VOCs in Indoor Air Environments by Dynamic Sampling and TD-GC/MS Analysis*, in *Sick Building Syndrome*, S.A. Abdul-Wahab, Editor. 2011, Springer Berlin Heidelberg. p. 289-333.

6. Wang S, Ang HM, and T. MO., *Volatile organic compounds in indoor environment and photocatalytic oxidation: state of the art.* Environmental International 2007. **33** (5): p. 694-705.

7. Jo, W.-K. and K.-H. Park, *Heterogeneous photocatalysis of aromatic and chlorinated volatile organic compounds (VOCs) for non-occupational indoor air application.* Chemosphere, 2004. **57**(7): p. 555-565.

8. Ao, C.H. and S.C. Lee, *Indoor air purification by photocatalyst TiO2 immobilized on an activated carbon filter installed in an air cleaner.* Chemical Engineering Science, 2005. **60**(1): p. 103-109.

9. Jones, A.P., *Indoor air quality and health.* Atmospheric Environment, 1999. **33**(28): p. 4535-4564.

10. *Select the Best VOC Control Strategy.* Chemical engineering progress, 1993. **89**(28).

11. Jo, W.-K., J.-H. Park, and H.-D. Chun, *Photocatalytic destruction of VOCs for in-vehicle air cleaning.* Journal of Photochemistry and Photobiology A: Chemistry, 2002. **148**(1-3): p. 109-119.

12. Zhao, J. and X. Yang, *Photocatalytic oxidation for indoor air purification: a literature review.* Building and Environment, 2003. **38**(5): p. 645-654.

13. Fedele, R., et al., *Biogenic VOC emissions from fresh leaf mulch and wood chips of Grevillea robusta (Australian Silky Oak).* Atmospheric Environment, 2007. **41**(38): p. 8736-8746.

14. Gray, C. and C.M. Gray, *Emissions of volatile organic compounds during the decomposition of plant litter.* Journal of geophysical research, 2010. **115**(G3): p. G03015.

15. Lazaridis, M. and V. Aleksandropoulou, *Sources and Variability of Indoor and Outdoor Gaseous Aerosol Precursors (O₃, NOx and VOCs).* Water, Air, & Soil Pollution: Focus, 2009. **9**(1): p. 3-13.

16. Lewis, C.W. and R.B. Zweidinger, *Apportionment of residential indoor aerosol, voc and aldehyde species to indoor and outdoor sources, and their source strengths.* Atmospheric Environment. Part A. General Topics, 1992. **26**(12): p. 2179-2184.

17. Sim, S., et al., *Emission rates of selected volatile organic compounds and formaldehyde in newly constructed apartment.* Toxicology and Environmental Health Sciences, 2010. **2**(4): p. 263-267.

18. Seifert, B. and D. Ullrich, *Methodologies for evaluating sources of volatile organic chemicals (VOC) in homes.* Atmospheric Environment (1967), 1987. **21**(2): p. 395-404.

19. Jia, C., S. Batterman, and C. Godwin, *VOCs in industrial, urban and suburban neighborhoods, Part 1: Indoor and outdoor concentrations, variation, and risk drivers.* Atmospheric Environment, 2008. **42**(9): p. 2083-2100.

20. Zuraimi, M.S., K.W. Tham, and S.C. Sekhar, *A study on the identification and quantification of sources of VOCs in 5 air-conditioned Singapore office buildings.* Building and Environment, 2004. **39**(2): p. 165-177.

21. Mølhave, L. and M. Thorsen, *A model for investigations of ventilation systems as sources for volatile organic compounds in indoor climate.* Atmospheric Environment. Part A. General Topics, 1991. **25**(2): p. 241-249.

22. An, J.-Y., et al., *Emission behavior of formaldehyde and TVOC from engineered flooring in under heating and air circulation systems.* Building and Environment, 2010. **45**(8): p. 1826-1833.

23. Missia, D.A., et al., *Indoor exposure from building materials: A field study.* Atmospheric Environment, 2010. **44**(35): p. 4388-4395.

24. Nazaroff, W.W. and C.J. Weschler, *Cleaning products and air fresheners: exposure to primary and secondary air pollutants.* Atmospheric Environment, 2004. **38**(18): p. 2841-2865.

25. Batterman, S., G. Hatzivasilis, and C. Jia, *Concentrations and emissions of gasoline and other vapors from residential vehicle garages.* Atmospheric Environment, 2006. **40**(10): p. 1828-1844.

26. Batterman, S., C. Jia, and G. Hatzivasilis, *Migration of volatile organic compounds from attached garages to residences: A major exposure source.* Environmental Research, 2007. **104**(2): p. 224-240.

27. Lee, C., et al., *Pattern Classification of Volatile Organic Compounds in Various Indoor Environments.* Water, Air, & Soil Pollution, 2011. **215**(1): p. 329-338.

28. Huang, Y., et al., *Characteristics and health impacts of VOCs and carbonyls associated with residential cooking activities in Hong Kong.* Journal of Hazardous Materials, 2011. **186**(1): p. 344-351.

29. Sinha, S.N., et al., *Environmental monitoring of benzene and toluene produced in indoor air due to combustion of solid biomass fuels.* Science of The Total Environment, 2006. **357**(1-3): p. 280-287.

30. Chambers, D.M., et al., *Impact of cigarette smoking on Volatile Organic Compound (VOC) blood levels in the U.S. Population: NHANES 2003-2004.* Environment International. **In Press, Corrected Proof**.

31. Halios, C.H., et al., *Investigating cigarette-smoke indoor pollution in a controlled environment.* Science of The Total Environment, 2005. **337**(1-3): p. 183-190.

32. Daher, N., et al., *Comparison of carcinogen, carbon monoxide, and ultrafine particle emissions from narghile waterpipe and cigarette smoking: Sidestream smoke measurements and assessment of second-hand smoke emission factors.* Atmospheric Environment, 2010. **44**(1): p. 8-14.

33. Paustenbach, D., et al., *A RECOMMENDED OCCUPATIONAL EXPOSURE LIMIT FOR FORMALDEHYDE BASED ON IRRITATION.* Journal of Toxicology and Environmental Health, 1997. **50**(3): p. 217-264.

34. Guo, H., et al., *Risk assessment of exposure to volatile organic compounds in different indoor environments.* Environmental Research, 2004. **94**(1): p. 57-66.

35. Pouli, A.E., et al., *The cytotoxic effect of volatile organic compounds of the gas phase of cigarette smoke on lung epithelial cells.* Free Radical Biology and Medicine, 2003. **34**(3): p. 345-355.

36. Rios, J.L.d.M., et al., *Symptoms prevalence among office workers of a sealed versus a non-sealed building: Associations to indoor air quality.* Environment International, 2009. **35**(8): p. 1136-1141.

37. Wolkoff, P. and G.D. Nielsen, *Non-cancer effects of formaldehyde and relevance for setting an indoor air guideline.* Environment International, 2010. **36**(7): p. 788-799.

38. Jones, A.P., *Asthma and domestic air quality.* Social Science & Medicine, 1998. **47**(6): p. 755-764.

39. Arts, J.H.E., et al., *Setting an indoor air exposure limit for formaldehyde: Factors of concern.* Regulatory Toxicology and Pharmacology, 2008. **52**(2): p. 189-194.

40. *Asthma link: with VOCs in houses.* Focus on Surfactants, 2004. **2004**(11): p. 6-6.

41. Wichmann, F.A., et al., *Increased asthma and respiratory symptoms in children exposed to petrochemical pollution.* Journal of Allergy and Clinical Immunology, 2009. **123**(3): p. 632-638.

42. Dragonieri, S., et al., *An electronic nose in the discrimination of patients with asthma and controls.* Journal of Allergy and Clinical Immunology, 2007. **120**(4): p. 856-862.

43. Phillips, M., et al., *Volatile organic compounds in breath as markers of lung cancer: A cross-sectional study.* Lancet, 1999. **353**(9168): p. 1930-1933.

44. Araki, A., et al., *Relationship between selected indoor volatile organic compounds, so-called microbial VOC, and the prevalence of mucous membrane symptoms in single family homes.* Science of The Total Environment, 2010. **408**(10): p. 2208-2215.

45. Chang, J.-S., *Next generation integrated electrostatic gas cleaning systems.* Journal of Electrostatics, 2003. **57**(3-4): p. 273-291.

46. Khan, F.I. and A. Kr. Ghoshal, *Removal of Volatile Organic Compounds from polluted air.* Journal of Loss Prevention in the Process Industries, 2000. **13**(6): p. 527-545.

47. Kwong, C.W., et al., *Removal of VOCs from indoor environment by ozonation over different porous materials.* Atmospheric Environment, 2008. **42**(10): p. 2300-2311.

48. Gupta, V.K. and N. Verma, *Removal of volatile organic compounds by cryogenic condensation followed by adsorption.* Chemical Engineering Science, 2002. **57**(14): p. 2679-2696.

49. Ozturk, B. and D. Yilmaz, *Absorptive Removal of Volatile Organic Compounds from Flue Gas Streams.* Process Safety and Environmental Protection, 2006. **84**(5): p. 391-398.

50. Li, R., et al., *Reduction of VOC emissions by a membrane-based gas absorption process.* Journal of Environmental Sciences, 2009. **21**(8): p. 1096-1102.

51. Song, Y.-H., et al., *Effects of adsorption and temperature on a nonthermal plasma process for removing VOCs.* Journal of Electrostatics, 2002. **55**(2): p. 189-201.

52. Matsumoto, H., M. Shimizu, and H. Sato, *The contaminant removal efficiency of an air cleaner using the adsorption/desorption effect.* Building and Environment, 2009. **44**(7): p. 1371-1377.

53. Lin, C.-C., Y.-C. Lin, and K.-S. Chien, *VOCs absorption in rotating packed beds equipped with blade packings.* Journal of Industrial and Engineering Chemistry, 2009. **15**(6): p. 813-818.

54. Lu, Y., et al., *Study on the removal of indoor VOCs using biotechnology.* Journal of Hazardous Materials, 2010. **182**(1-3): p. 204-209.

55. Gironi, F. and V. Piemonte, *VOCs removal from dilute vapour streams by adsorption onto activated carbon.* Chemical Engineering Journal. **In Press, Corrected Proof**.

56. OBEE T. N and B.R. T, *TiO2 photocatalysis for indoor air applications : effects of humidity and trace contaminant levels on the oxidation rates of formaldehyde, toluene, and 1,3-butadiene.* Environmental science & technology, 1995. **29**(5): p. 1223-1231

57. Shiraishi, F., K. Toyoda, and H. Miyakawa, *Decomposition of gaseous formaldehyde in a photocatalytic reactor with a parallel array of light sources: 2. Reactor performance.* Chemical Engineering Journal, 2005. **114**(1-3): p. 145-151.

58. R. Asahi, et al., *Visible-Light Photocatalysis in Nitrogen-Doped Titanium Oxides* Science, 2001. **293,**: p. 269-271.

59. Ihara, T., et al., *Visible-light-active titanium oxide photocatalyst realized by an oxygen-deficient structure and by nitrogen doping.* Applied Catalysis B: Environmental, 2003. **42**(4): p. 403-409.

60. LIPING YANG and Z. LIU, *Study on light intensity in the process of photocatalytic degradation of indoor gaseous formaldehyde for saving energy.* Energy conversion and management 2007. **48**(3): p. 882-889.

61. Salthammer, T. and F. Fuhrmann, *Photocatalytic Surface Reactions on Indoor Wall Paint.* Environmental science & technology, 2007. **41**(18): p. 6573-6578.

62. Liping Li, et al., *Surface doping for photocatlytic purposes, relations between particle size, surface modifications and photoactivity of SnO2:Zn2+ nanocrystals.* Nanotechnology, 2009. **20**: p. 155706.

63. Ullah, R., et al., *Wet-chemical Synthesis of InTaO4 for Photocatalytic Decomposition of Organic Contaminants in Air and Water with UV-vis Light.* Industrial & Engineering Chemistry Research, 2011: p. null-null.

64. Colón, G., et al., *Gas phase photocatalytic oxidation of toluene using highly active Pt doped TiO2.* Journal of Molecular Catalysis A: Chemical, 2010. **320**(1-2): p. 14-18.

65. Ravichandran, L., et al., *Photovalorisation of pentafluorobenzoic acid with platinum doped TiO2.* J Hazard Mater, 2009. **167**(1-3): p. 763-9.

66. Morikawa, T., et al., *Visible-light-induced photocatalytic oxidation of carboxylic acids and aldehydes over N-doped TiO2 loaded with Fe, Cu or Pt.* Applied Catalysis B: Environmental, 2008. **83**(1-2): p. 56-62.

67. Iliev, V., et al., *Photocatalytic properties of TiO2 modified with platinum and silver nanoparticles in the degradation of oxalic acid in aqueous solution.* Applied Catalysis B: Environmental, 2006. **63**(3-4): p. 266-271.

68. Xu, R., et al., *Photocatalytic degradation of organic dyes under solar light irradiation combined with Er3+:YAlO3/Fe- and Co-doped TiO2 coated composites.* Solar Energy Materials and Solar Cells, 2010. **94**(6): p. 1157-1165.

69. Hamal, D.B. and K.J. Klabunde, *Synthesis, characterization, and visible light activity of new nanoparticle photocatalysts based on silver, carbon, and sulfur-doped TiO2.* Journal of Colloid and Interface Science, 2007. **311**(2): p. 514-522.

70. Li, G., et al., *Composition dependence of the photophysical and photocatalytic properties of (AgNbO3)1-x(NaNbO3)x solid solutions.* Journal of Solid State Chemistry, 2007. **180**(10): p. 2845-2850.

71. Shi, H., et al., *2-Propanol photodegradation over nitrogen-doped NaNbO3 powders under visible-light irradiation.* Journal of Physics and Chemistry of Solids, 2009. **70**(6): p. 931-935.

72. OBEE T. N, B.R.T., *TiO2 photocatalysis for indoor air applications : effects of humidity and trace contaminant levels on the oxidation rates of formaldehyde, toluene, and 1,3-butadiene.* Environmental science & technology, 1995. **29**(5): p. 1223-1231

73. Shiraishi, F., et al., *Decomposition of gaseous formaldehyde in a photocatalytic reactor with a parallel array of light sources: 1. Fundamental experiment for reactor design.* Chemical Engineering Journal, 2005. **114**(1-3): p. 153-159.

74. F.B. Li, et al., *Enhanced photocatalytic degradation of VOCs using Ln3+–TiO2 catalysts for indoor air purification.* Chemosphere 2005. **59** p. 787–800.

75. Vu, A.T., et al., *Synthesis and characterization of TiO 2 photocatalyst doped by transition metal ions (Fe 3+ , Cr 3+ and V 5+).* Advances in Natural Sciences: Nanoscience and Nanotechnology, 2010. **1**(1): p. 015009.

76. Lee, B.-Y., et al., *Optical properties of Pt-TiO₂ catalyst and photocatalytic activities for benzene decomposition.* Korean Journal of Chemical Engineering, 2003. **20**(5): p. 812-818.

77. Ananpattarachai, J., P. Kajitvichyanukul, and S. Seraphin, *Visible light absorption ability and photocatalytic oxidation activity of various interstitial N-doped TiO2 prepared from different nitrogen dopants.* Journal of Hazardous Materials, 2009. **168**(1): p. 253-261.

78. Higashimoto, S., et al., *Effective photocatalytic decomposition of VOC under visible-light irradiation on N-doped TiO2 modified by vanadium species.* Applied Catalysis A: General, 2008. **340**(1): p. 98-104.

79. Ma, C.-M., et al., *Effects of Silver on the Photocatalytic Degradation of Gaseous Isopropanol.* Water, Air, & Soil Pollution, 2009. **197**(1): p. 313-321.

80. Ban, J.-Y., et al., *Highly concentrated toluene decomposition on the dielectric barrier discharge (DBD) plasma-photocatalytic hybrid system with Mn-Ti-incorporated mesoporous silicate photocatalyst (Mn-Ti-MPS).* Applied Surface Science, 2006. **253**(2): p. 535-542.

81. Bennani, J., et al., *Physical properties, stability, and photocatalytic activity of transparent TiO2/SiO2 films.* Separation and Purification Technology. **I**n Press, Corrected Proof.

82. Li, G.-S., D.-Q. Zhang, and J.C. Yu, *A New Visible-Light Photocatalyst: CdS Quantum Dots Embedded Mesoporous TiO2.* Environmental science & technology, 2009. **43**(18): p. 7079-7085.

83. Stodolny, M. and M. Laniecki, *Synthesis and characterization of mesoporous Ta2O5-TiO2 photocatalysts for water splitting.* Catalysis Today, 2009. **142**(3-4): p. 314-319.

84. Asahi, R., et al., *Visible-Light Photocatalysis in Nitrogen-Doped Titanium Oxides.* Science, 2001. **293**(5528): p. 269-271.

85. Kitano, M., et al., *Recent developments in titanium oxide-based photocatalysts.* Applied Catalysis A: General, 2007. **325**(1): p. 1-14.

86. Demeestere, K., et al., *Visible light mediated photocatalytic degradation of gaseous trichloroethylene and dimethyl sulfide on modified titanium dioxide.* Applied Catalysis B: Environmental, 2005. **61**(1-2): p. 140-149.

87. Auvinen, J. and L. Wirtanen, *The influence of photocatalytic interior paints on indoor air quality.* Atmospheric Environment, 2008. **42**(18): p. 4101-4112.

88. LIPING YANG, Z.L., *Study on light intensity in the process of photocatalytic degradation of indoor gaseous formaldehyde for saving energy.* Energy conversion and management, 2007. **48**(3): p. 882-889.

89. Sun, H., et al., *Room-light-induced indoor air purification using an efficient Pt/N-TiO2 photocatalyst.* Applied Catalysis B: Environmental, 2011. **108-109**(0): p. 127-133.

90. Tang, Y.-C., et al., *Nitrogen-Doped TiO2 Photocatalyst Prepared by Mechanochemical Method: Doping Mechanisms and Visible Photoactivity of Pollutant Degradation.* International Journal of Photoenergy, 2012. **2012**.

91. Bamwenda, G.R. and H. Arakawa, *Cerium dioxide as a photocatalyst for water decomposition to O2 in the presence of Ceaq4+ and Feaq3+ species.* Journal of Molecular Catalysis A: Chemical, 2000. **161**(1-2): p. 105-113.

92. Hernández-Alonso, M.D., et al., *EPR study of the photoassisted formation of radicals on CeO2 nanoparticles employed for toluene photooxidation.* Applied Catalysis B: Environmental, 2004. **50**(3): p. 167-175.

93. Coronado, J.M., et al., *EPR study of the radicals formed upon UV irradiation of ceria-based photocatalysts.* Journal of Photochemistry and Photobiology A: Chemistry, 2002. **150**(1-3): p. 213-221.

94. Leny Yuliati, et al., *Nonoxidative Coupling of Methane over Supported Ceria Photocatalysts.* The Jounral of Physical Chemistry C, 2008. **112**(18): p. 7223-7232.

95. Zhai, Y., S. Zhang, and H. Pang, *Preparation, characterization and photocatalytic activity of CeO2 nanocrystalline using ammonium bicarbonate as precipitant.* Materials Letters, 2007. **61**(8-9): p. 1863-1866.

96. Qian, L., et al., *Solvothermal synthesis, electrochemical and photocatalytic properties of monodispersed CeO2 nanocubes.* Materials Chemistry and Physics, 2009. **115**(2-3): p. 835-840.

97. Ohuchi, T., et al., *Liquid phase photooxidation of alcohol over niobium oxide without solvents.* Catalysis Today, 2007. **120**(2): p. 233-239.

98. Xinyi Chen, et al., *Enhanced Activity of Mesoporous Nb2O5 for photoctalytic Hydrogen Prodcution.* Applied Surface Science, 2007. **253**: p. 8500-8506.

99. In-Sun, C., et al., *Preparation, Characterization, and Photocatalytic Properties of CaNb₂O₆ Nanoparticles.* Journal of the American Ceramic Society, 2009. **92**(2): p. 506-510.

100. Zhang, G., et al., *Wet chemical synthesis and photocatalytic activity of potassium niobate K6Nb10.8O30 powders.* Journal of Solid State Chemistry, 2008. **181**(9): p. 2133-2138.

101. Chatrchyan, S., et al., *Measurement of the Inclusive Jet Cross Section in pp Collisions at sqrt[s]=7 TeV.* Phys Rev Lett, 2011. **107**(13): p. 132001.

102. Zou, Z., J. Ye, and H. Arakawa, *Structural properties of InNbO4 and InTaO4: correlation with photocatalytic and photophysical properties.* Chemical Physics Letters, 2000. **332**(3-4): p. 271-277.

103. Chang, H., et al., *Electronic structures of InTaO4, a promising photocatalyst.* Chemical Physics Letters, 2004. **398**(4-6): p. 449-452.

104. Matsushima, S., et al., *First-principles energy band calculation for undoped and N-doped InTaO4 with layered wolframite-type structure.* Journal of Physics and Chemistry of Solids, 2003. **64**(12): p. 2417-2421.

105. Hiroshi, I. and H. Kazuhito, *Visible Light-Sensitive InTaO₄-Based Photocatalysts for Organic Decomposition.* Journal of the American Ceramic Society, 2005. **88**(11): p. 3137-3142.

106. Ye, J., et al., *Correlation of crystal and electronic structures with photophysical properties of water splitting photocatalysts InMO4 (M=V5+,Nb5+,Ta5+).* Journal of Photochemistry and Photobiology A: Chemistry, 2002. **148**(1-3): p. 79-83.

107. Chen, H.-C., et al., *Sol-gel prepared InTaO4 and its photocatalytic characteristics.* Journal of Materials Research, 2008. **23**(05): p. 1364-1370.

108. Chiou, Y.-C., U. Kumar, and J.C.S. Wu, *Photocatalytic splitting of water on NiO/InTaO4 catalysts prepared by an innovative sol-gel method.* Applied Catalysis A: General, 2009. **357**(1): p. 73-78.

109. Yoshida, T., et al., *InTaO4-based nanostructures synthesized by reactive pulsed laser ablation.* Applied Physics A: Materials Science & Processing, 2008. **93**(4): p. 961-966.

110. Hu, C.-C. and H. Teng, *Influence of structural features on the photocatalytic activity of NaTaO3 powders from different synthesis methods.* Applied Catalysis A: General, 2007. **331**: p. 44-50.

111. Kato, H. and A. Kudo, *Water Splitting into H2 and O2 on Alkali Tantalate Photocatalysts ATaO3 (A = Li, Na, and K).* The Journal of Physical Chemistry B, 2001. **105**(19): p. 4285-4292.

112. Kato, H., H. Kobayashi, and A. Kudo, *Role of Ag+ in the Band Structures and Photocatalytic Properties of AgMO3 (M: Ta and Nb) with the Perovskite Structure.* The Journal of Physical Chemistry B, 2002. **106**(48): p. 12441-12447.

113. Gao, Y., et al., *Preparation and Photocatalytic Mechanism of Vanadium Doped NaTaO3 Nanoparticles.* Integrated Ferroelectrics, 2011. **127**(1): p. 106-115.

114. Fu, H., et al., *Visible-light-driven NaTaO3-xNx catalyst prepared by a hydrothermal process.* Materials Research Bulletin, 2008. **43**(4): p. 864-872.

115. Liu, M., et al., *Photocatalytic Water Splitting to Hydrogen over a Visible Light-Driven LaTaON2 Catalyst.* Chinese Journal of Catalysis, 2006. **27**(7): p. 556-558.

116. Lin Zhou, et al., *Bi2O3 Hierarchical Nanostructures: Controllable Synthesis, Growth Mechanism, and Their Application in Photocatalysis.* Chemistry A European Journal, 2008. **15**: p. 1776-1782.

117. Kako, T., et al., *Decomposition of Organic Compounds over NaBiO3 under Visible Light Irradiation.* Chemistry of Materials, 2006. **19**(2): p. 198-202.

118. Chang, X., et al., *Rapid photocatalytic degradation of PCP-Na over NaBiO3 driven by visible light irradiation.* Journal of Hazardous Materials, 2009. **166**(2-3): p. 728-733.

119. Belgiorno, V., et al., *Review on endocrine disrupting-emerging compounds in urban wastewater: occurrence and removal by photocatalysis and ultrasonic irradiation for wastewater reuse.* Desalination, 2007. **215**(1–3): p. 166-176.

120. Wols, B.A. and C.H.M. Hofman-Caris, *Review of photochemical reaction constants of organic micropollutants required for UV advanced oxidation processes in water.* Water Research, (0).

121. Kou, J., et al., *Photooxidation of Polycyclic Aromatic Hydrocarbons over NaBiO3 under Visible Light Irradiation.* Catalysis Letters, 2008. **122**(1): p. 131-137.

122. Yu, K., et al., *Visible Light-Driven Photocatalytic Degradation of Rhodamine B over NaBiO3: Pathways and Mechanism.* The Journal of Physical Chemistry A, 2009. **113**(37): p. 10024-10032.

123. Grover, D.P., et al., *Improved removal of estrogenic and pharmaceutical compounds in sewage effluent by full scale granular activated carbon: Impact on receiving river water.* Journal of Hazardous Materials, 2011. **185**(2–3): p. 1005-1011.

124. Johnson, A.C. and J.P. Sumpter, *Removal of Endocrine-Disrupting Chemicals in Activated Sludge Treatment Works.* Environmental Science & Technology, 2001. **35**(24): p. 4697-4703.

125. Zhang, J., et al., *Self-Assembled 3-D Architectures of BiOBr as a Visible Light-Driven Photocatalyst.* Chemistry of Materials, 2008. **20**(9): p. 2937-2941.

126. Zhang, X., et al., *Generalized One-Pot Synthesis, Characterization, and Photocatalytic Activity of Hierarchical BiOX (X = Cl, Br, I) Nanoplate Microspheres.* The Journal of Physical Chemistry C, 2008. **112**(3): p. 747-753.

127. Zhihui Ai, et al., *Efficient Photocatalytic Removal of NO in Indoor Air with Hierarchical Bismuth Oxybromide Nanoplate Microspheres under Visible Light.* Environ. Sci. Technol., 2009. **43**(11): p. 4143–4150.

128. Yildirim, N., et al., *Aptamer-Based Optical Biosensor For Rapid and Sensitive Detection of 17β-Estradiol In Water Samples.* Environmental Science & Technology, 2012. **46**(6): p. 3288-3294.

129. Zhang, Z., et al., *Degradation behavior of 17α-ethinylestradiol by ozonation in the synthetic secondary effluent.* Journal of Environmental Sciences, 2012. **24**(2): p. 228-233.

130. Shang, M., et al., *Bi2WO6 Nanocrystals with High Photocatalytic Activities under Visible Light.* The Journal of Physical Chemistry C, 2008. **112**(28): p. 10407-10411.

131. Li, Y., J. Liu, and X. Huang, *Synthesis and Visible-Light Photocatalytic Property of Bi2WO6 Hierarchical Octahedron-Like Structures.* Nanoscale Research Letters, 2008. **3**(10): p. 365-371.

132. Zhang, S., et al., *Bi2WO6 photocatalytic films fabricated by layer-by-layer technique from Bi2WO6 nanoplates and its spectral selectivity.* Journal of Solid State Chemistry, 2007. **180**(4): p. 1456-1463.

133. Luan, J., et al., *Structural, photophysical and photocatalytic properties of novel Bi2AlVO7.* Journal of Hazardous Materials, 2009. **164**(2-3): p. 781-789.

134. Luan, J., et al., *Structural characterization and photocatalytic properties of novel Bi2FeVO7.* Research on Chemical Intermediates, 2007. **33**(6): p. 487-500.

135. Shan, Z., et al., *Preparation and photocatalytic activity of novel efficient photocatalyst Sr2Bi2O5.* Materials Letters, 2009. **63**(1): p. 75-77.

136. Hu, X., C. Hu, and J. Qu, *Photocatalytic decomposition of acetaldehyde and Escherichia coli using NiO/SrBi2O4 under visible light irradiation.* Applied Catalysis B: Environmental, 2006. **69**(1-2): p. 17-23.

137. Maruyama, H., et al., *Removal of Bisphenol A and Diethyl Phthalate from Aqueous Phases by Ultrasonic Atomization.* Industrial & Engineering Chemistry Research, 2006. **45**(18): p. 6383-6386.

138. Kohtani, S., et al., *Photodegradation of 4-alkylphenols using BiVO4 photocatalyst under irradiation with visible light from a solar simulator.* Applied Catalysis B: Environmental, 2003. **46**(3): p. 573-586.

139. Li, G., D. Zhang, and J.C. Yu, *Ordered Mesoporous BiVO4 through Nanocasting: A Superior Visible Light-Driven Photocatalyst.* Chemistry of Materials, 2008. **20**(12): p. 3983-3992.

140. Li, H., G. Liu, and X. Duan, *Monoclinic BiVO4 with regular morphologies: Hydrothermal synthesis, characterization and photocatalytic properties.* Materials Chemistry and Physics, 2009. **115**(1): p. 9-13.

141. Tang, T., et al., *Adsorption Properties and Degradation Dynamics of Endocrine-Disrupting Chemical Levonorgestrel in Soils.* Journal of Agricultural and Food Chemistry, 2012.

142. Wang, L., et al., *FeCl3/NaNO2: An Efficient Photocatalyst for the Degradation of Aquatic Steroid Estrogens under Natural Light Irradiation.* Environmental Science & Technology, 2007. **41**(10): p. 3747-3751.

143. Sun, Q., et al., *Transformation of Bisphenol A and Alkylphenols by Ammonia-Oxidizing Bacteria through Nitration.* Environmental Science & Technology, 2012.

144. Liu, Z.-h., Y. Kanjo, and S. Mizutani, *Removal mechanisms for endocrine disrupting compounds (EDCs) in wastewater treatment — physical means, biodegradation, and chemical advanced oxidation: A review.* Science of The Total Environment, 2009. **407**(2): p. 731-748.

145. Mišík, M., et al., *Impact of ozonation on the genotoxic activity of tertiary treated municipal wastewater.* Water Research, 2011. **45**(12): p. 3681-3691.

146. Esperanza, M., et al., *Determination of Sex Hormones and Nonylphenol Ethoxylates in the Aqueous Matrixes of Two Pilot-Scale Municipal Wastewater Treatment Plants.* Environmental Science & Technology, 2004. **38**(11): p. 3028-3035.

147. Radošević, K., et al., *Comparison of Cytotoxicity Induced by 17<i>α</i>-Ethynylestradiol and Diethylstilbestrol in Fish CCO and Mammalian CHO-K1 Cell Lines.* Bulletin of Environmental Contamination and Toxicology, 2011. **86**(3): p. 252-257.

148. Ge, L., *Novel visible-light-driven Pt/BiVO4 photocatalyst for efficient degradation of methyl orange.* Journal of Molecular Catalysis A: Chemical, 2008. **282**(1-2): p. 62-66.

149. Zhang, X., et al., *Preparation of Ag doped BiVO4 film and its enhanced photoelectrocatalytic (PEC) ability of phenol degradation under visible light.* Journal of Hazardous Materials, 2009. **167**(1-3): p. 911-914.

150. Zhang, A. and J. Zhang, *Synthesis and characterization of Ag/BiVO4 composite photocatalyst.* Applied Surface Science. **256**(10): p. 3224-3227.

151. Martínez-de la Cruz, A. and U.M.G. Pérez, *Photocatalytic properties of BiVO4 prepared by the co-precipitation method: Degradation of rhodamine B and possible reaction mechanisms under visible irradiation.* Materials Research Bulletin. **45**(2): p. 135-141.

152. Xu, H., et al., *Synthesis, characterization and photocatalytic activities of rare earth-loaded BiVO4 catalysts.* Applied Surface Science, 2009. **256**(3): p. 597-602.

153. Chen, L.-C., et al., *In situ DRIFT and kinetic studies of photocatalytic degradation on benzene vapor with visible-light-driven silver vanadates.* Journal of Hazardous Materials, 2010. **178**(1-3): p. 644-651.

154. Huang, C.-M., et al., *Crystalline phases and photocatalytic activities of hydrothermal synthesis Ag3VO4 and Ag4V2O7 under visible light irradiation.* Applied Catalysis A: General, 2009. **358**(2): p. 164-172.

155. Kato, H. and A. Kudo, *Photocatalytic water splitting into H2 and O2 over various tantalate photocatalysts.* Catalysis Today, 2003. **78**(1-4): p. 561-569.

156. Takahara, Y., et al., *Mesoporous Tantalum Oxide. 1. Characterization and Photocatalytic Activity for the Overall Water Decomposition.* Chemistry of Materials, 2001. **13**(4): p. 1194-1199.

157. Yang, X., et al., *Enhanced photocatalytic activity of Eu2O3/Ta2O5 mixed oxides on degradation of rhodamine B and 4-nitrophenol.* Colloids and Surfaces A: Physicochemical and Engineering Aspects, 2008. **320**(1-3): p. 61-67.

158. Huang, H., et al., *Efficient Degradation of Benzene over LaVO4/TiO2 Nanocrystalline Heterojunction Photocatalyst under Visible Light Irradiation.* Environmental science & technology, 2009. **43**(11): p. 4164-4168.

159. Yanagida, S., et al., *Semiconductor Photocatalysis. Part 22. Visible-Light Induced Photoreduction of CO2 with CdS Nanocrystallites — Importance of the Morphology and Surface Structures Controlled through Solvation by N,N-Dimethylformamide.* Bulletin of the Chemical Society of Japan, 1997. **70**(9): p. 2063-2070.

160. Xing, C., et al., *Band structure-controlled solid solution of Cd1-x ZnxS photocatalyst for hydrogen production by water splitting.* International Journal of Hydrogen Energy, 2006. **31**(14): p. 2018-2024.

161. Sun, M., et al., *Photocatalyst Cd2Sb2O6.8 with High Photocatalytic Activity toward Benzene and Dyes.* The Journal of Physical Chemistry C, 2009. **113**(33): p. 14916-14921.

3

3 - Wet-Chemical Synthesis of $InTaO_4$ for Photocatalytic Decomposition of Organic Contaminants in Air and Water with UV-vis Light

Abstract

A wet-chemical technique was used to synthesize $InTaO_4$, $AgNbO_3$, $InNbO_4$ and various metal doped $InTaO_4$ catalysts. Their physicochemical properties were characterized by UV-vis diffusion reflectance spectroscopy, X-ray diffraction (XRD), scanning electron microscopy (SEM) and energy-dispersive X-ray spectroscopy (EDS). Photocatalytic activities of these materials were evaluated in liquid-phase decomposition of methylene blue and gas-phase degradation of toluene under UV-vis light. $InTaO_4$ exhibited higher activity than $AgNbO_3$ and $InNbO_4$ in photodecomposition of organic compounds in gas and liquid phases. Ni-doping could enhance the photocatalytic activities. Although commercial TiO_2-P25 had better activity, Ni-$InTaO_4$ showed more stable performance in catalytic oxidation of toluene.

3.1 Introduction

Recent investigations show that $InTaO_4$ is a good photocatalyst for splitting water to H_2 under UV light irradiation, and that it has better performance than commercial TiO_2-P25.[1, 2] Visible light photocatalysis for water splitting and/or organic contaminant decomposition using various tantalates and niobates have also been reported.[3-5] However, $InTaO_4$ and $InNbO_4$ only showed good performance in H_2 production via visible light irradiation but less activity in O_2 production. Three important factors; i) position of conduction/valence bands, ii) moment of photo-generated carriers, and iii) M-O-M angle, influence the photocatalytic activities of materials. The more negative/positive the conduction/valence band is the higher the redox potential and consequently the higher photocatalytic activity. The more closure M-O-M to 180º the higher the carrier mobility and consequently the better activity of the material is. Zou et al.[1] demonstrated that $InTaO_4$ and $InNbO_4$ are consisted of two octahedrons InO_6 and TaO_6 / NbO_6, where conduction bands were made of empty 5d and 4d orbitals of Ta and Nb, respectively and were positioned at different energy levels. However, valence bands which were made of O 2p orbitals of InO_6 in both the materials have the same potential level. Thus due to the lower conduction band position $InNbO_4$ band gap (2.5 eV) was smaller than that of $InTaO_4$ (2.6 eV), but hydrogen was evolved at lower rate on $InNbO_4$ than that evolved on $InTaO_4$ when irradiated with visible light in the presences of co-catalyst NiO. Higher photocatalytic activity of $InTaO_4$ than $InNbO_4$ was mainly attributed to the position of the conduction band, M-O-M angle valve and its subsequent effect on electron moment. It was found that Ta-O-Ta is more closure to 180°, which alleviates moment of electron in conduction band and thus resulting in increased photocatalytic activity.

Many attempts such as doping with cations (Mn, Fe, Co, Cu, and Ni,[6] Sc, V, Zn, Ti, and Cr,[7] and anions (N)[8, 9] have been made to enhance the photocatalytic efficiency of $InTaO_4$. A significant improvement in photocatalytic production of H_2/O_2

was achieved on 1% nickel coated $InTaO_4$, which was attributed to the alleviated electron moment caused by the change in M-O-M angle[10] a narrowed band gap by doping[2] and electron trapping of the NiO layer.[7]

Previously, all the above materials were prepared by solid state reaction. Some other techniques were also employed for synthesis of $InTaO_4$, such as an reactive pulsed LASER ablation method[9] and sol-gel techniques.[11] However, few investigations have been reported in wet-chemical synthesis of $InTaO_4$, $AgNbO_3$, which is usually facile and environmentally friendly, and their application for decomposition of organic contaminants[8]. Hiroshi et al.[8] found that $InTaO_4$ doped with vanadium could decompose gaseous isopropyl alcohol [12] into acetone and CO_2 at ultraviolet radiation but showed little activity under visible light irradiation. Chiou et al.[11] reported that $InTaO_4$ prepared by sol-gel techniques demonstrated higher photocatalytic activities for H_2 production because of a smaller band gap (2.62 eV), particle size (0.05-0.1μm) and more uniform crystalline phase than the one prepared by solid state reactions.

Photocatalytic decomposition of contaminants in gas and water is important in environmental remediation [13-15]. Many types of photocatalyst have been tested; however, few investigations have been reported using $InTaO_4$ systems. In this paper, we report synthesis of pristine $InTaO_4$, $AgNbO_3$, $InNbO_4$, and doped $InTaO_4$ by a simple wet-chemical technique. The synthesized materials were tested for photocatalytic decomposition of methylene blue in aqueous solution and toluene in gaseous phase under UV-Vis light.

3.2 Experimental section

3.2.1 Synthesis of various catalysts

Polycrystalline pristine $InTaO_4$, $AgNbO_3$, $InNbO_4$ and doped $InTaO_4$ photocatalysts were prepared by a solution method. All chemicals were obtained from Sigma-Aldrich at 99.99% purity and were used as received. In a typical synthesis, 10 mmol of indium

(III) nitrate hydrate ($In(NO_3)_3.xH_2O$) and 8 mmol of tantalum (V) chloride ($TaCl_5$) were dissolved separately in a 50 mL ethanol solution with continuously stirring and heating at 70 °C for 30 min to make solutions A and B, respectively. Dopant solution C was also prepared similarly by dissolving 0.01 mmol of dopant salt (cobalt (II) nitrate hexahydrate, copper (II) nitrate trihydrate, and nickel (II) nitrate hexahydrate, etc) in 30 mL ethanol. Both solutions A and B were then mixed and 0.5 - 1.0 mL concentrated nitric acid was added to the mixture. The mixture was kept heating at 80 °C for refluxing of 6-8 h. A clear solution without any precipitation was then aged for 12-24 h at room temperature and was kept in an oven at 50 – 60 °C till dried completely. After ground, the samples were calcined at 1150 °C for 24-30 h. $AgNbO_3$ and $InNbO_4$ were also prepared by the similar technique where niobium (V) chloride ($NbCl_5$) and silver nitrate ($AgNO_3$) were used as Nb and Ag precursors, respectively.

3.2.2 Characterization of catalysts

The crystal structures of samples were analyzed by X-ray diffractometer (Bruker D8 Advance equipped with a Lynx eye detector, Bruker-AXS, Karlsruhe, Germany) operated at 40 kV and 30 mA. The scanning rate was 0.2 sec/step with 2θ (10°- 90°) and step size of 0.02°. Cu Kα (λ = 1.54178 Å) was used as a X-ray source with divergent slit of 0.300 and 2.5° primary and secondary soller slits. The optical absorption of the samples was determined by UV-Vis absorbance spectroscopy using the diffuse reflectance method (JASCO V-670 Spectrometer). Morphology and chemical composition of the materials were examined by scanning electron microscopy (ZEISS NEON 40EsB) equipped with an energy dispersive spectrometer (SEM-EDS). Surface chemistry of catalyst samples was examined by X-ray photoelectron spectroscopy (XPS) analysis. FTIR, analysis was performed with PerkinElmer Model FTIR-100 with MIR detector. XPS data was acquired using a Kratos Axis ULTRA X-ray Photoelectron Spectrometer incorporating a 165mm hemispherical electron energy analyzer. The incident radiation was Monochromatic Al Kα X-rays (1486.6 eV) at

225W (15 kV, 15 mA). Survey (wide) scans were taken at analyzer pass energy of 160 eV and multiplex (narrow) high resolution scans at 40 eV. Survey scans were carried out over 1200.0 eV binding energy range with 1.0 eV steps and a dwell time of 100 ms. Narrow high-resolution scans were run with 0.05 eV steps and 250 ms dwell time.

3.2.3 Photocatalytic evaluation

Photocatalytic activities of prepared samples were evaluated in decomposition of methylene blue in water and toluene in air with UV-vis radiations. The light source was a 500 W Mercury-Xenon lamp (UXM-502MD, Ushio) with the average intensities of 5 mW/cm^2 at 220 – 280 nm, 38.5 mW/cm^2 at 280 - 400 nm, and 200 mW/cm^2 at > 400 nm. In a typical run of methylene blue decomposition in water, 10 ppm methylene blue solution with 100 mg catalyst particles were continuously stirred in a Pyrex glass reactor which was irradiated with the UV-vis light without filter. Temperature of the reactor was maintained by passing cooling water through the reactor continuously. Concentration of methylene blue was determined by taking one mL aliquots from the reactor at a regular interval. The aliquots were evaluated by measuring the absorbance at λ= 664 nm with a visible spectrophotometer (Spectronic Instruments Model 4001/4).

Toluene decomposition in gas was evaluated in a flow reactor connected with a gas chromatograph (Shimadzu GC-17A) fitted with a GS-GSPRO column of 60 m in length and 0.32 mm inner diameter. Oven temperature of the GC was 220 °C and FID detector temperature was kept at 250 °C. In a typical experiment, 200-300 mg of a photocatalyst was dispersed in 10 mL deionized water in a petri dish of 450 mm diameter and was dried in an oven overnight. The petri dish was kept inside an air-tight reactor fitted with a removable quartz sheet in order to allow UV-vis radiation in. A flow of toluene at 100 ppm was continuously passed into the reactor (1.08 L) at a flow rate of 60 mL/min. The temperature of the reactor was controlled at room temperature by continuously passing cooling water through the reactor and also by blowing the reactor with fresh air from outside.

3.3 Results and discussions

3.3.1 Characterization of catalysts

XRD analysis of the prepared $InTaO_4$ at varying temperatures (Figure 3.1) indicates that the sample without calcination presented an amorphous phase. However, crystallization could be observed at calcination of 300 °C and complete crystalline structure of $InTaO_4$ was obtained at elevated temperature of 1150 °C. At lower temperatures (300 -1000 °C), In_2O_3 and Ta_2O_5 at $2\boldsymbol{\theta}$ = 30.58°, 21.47° and $2\boldsymbol{\theta}$ = 22.820°, 28.267°, respectively, were observed. However, indium tantalum oxide ($InTaO_4$) was found to be the major product, which has a monoclinic structure with a = 5.150, b = 5.770, c = 4.821, α = 90°.0, β = 91.35°, γ = 90°.0, primitive - P2/a (13). This $InTaO_4$ has the similar crystal structure to those prepared by solid state reaction, but different space group of P2/c.[1]

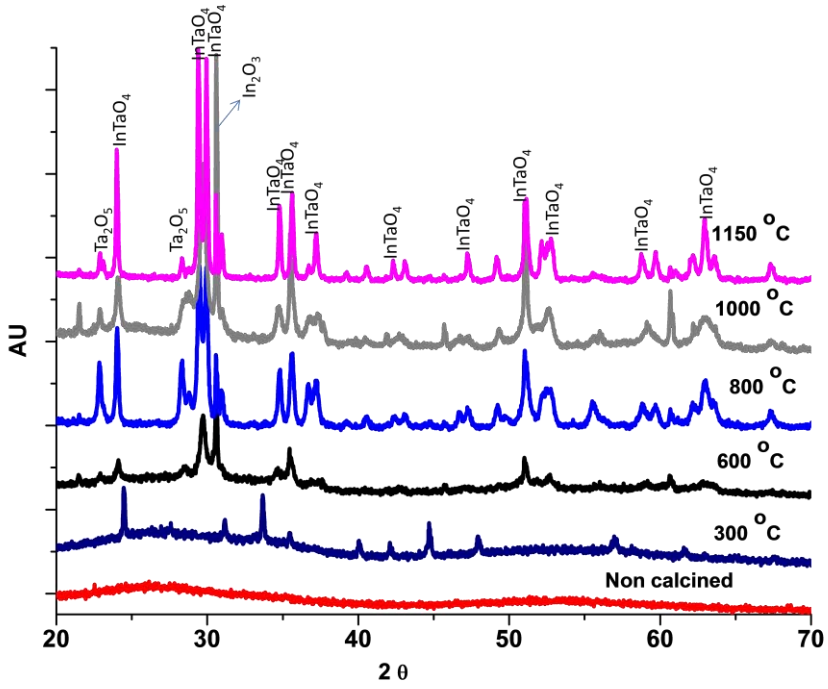

Figure: 3.1 XRD analysis of $InTaO_4$ synthesized at various temperatures.

In order to obtain a pure product of $InTaO_4$, molar ratios of the precursor salts (indium nitrate and tantalum chloride) were varied in preparation. It was found that the sample synthesized at the molar ratio of 1:0.5 (In : Ta) had very lower In_2O_3 and Ta_3O_5 impurities (Figure 3.2). Therefore, the molar ratio of In: Ta was kept at 1 : 0.5 for doped $InTaO_4$ synthesis. The metals of doping were Bi, Cu, Ag, V, and Ni at 1- 2%. XRD patterns (Figure 3.3) showed no significant structure change occurring on those doped samples. This revealed that 1 - 2% metal doping into pristine $InTaO_4$ may only bring about some physical changes but no changes in crystal structure or chemical phase.[2] Zou et al.[10] reported no modification in crystal parameters by doping $InTaO_4$ with Ag, Ni, Cu and Co. However, a slight decrease in crystal parameters (a = 4.833, b = 5.778, c = 5.157, γ = 90°.000, β= 91.380°, γ= 90°.000) was found in bismuth doped sample ($InTaO_4$: Bi). The steadiness of crystal structure and crystal parameters of $InTaO_4$ by doping with Ag^{2+}, Ni^{2+}, Cu^{2+} and Co^{2+} may be either due to their interstitial position or surface cover of the oxides on $InTaO_4$. Bismuth in the difference of ionic radius may cause the structural variation. Thus it is concluded that substitutional dopant could cause variations in crystal parameters if the dopant ionic size is different from that of the substituted ion while the interstitial doping of foreign elements may only change the physical properties such as an increase in defect sites and band gap modification.

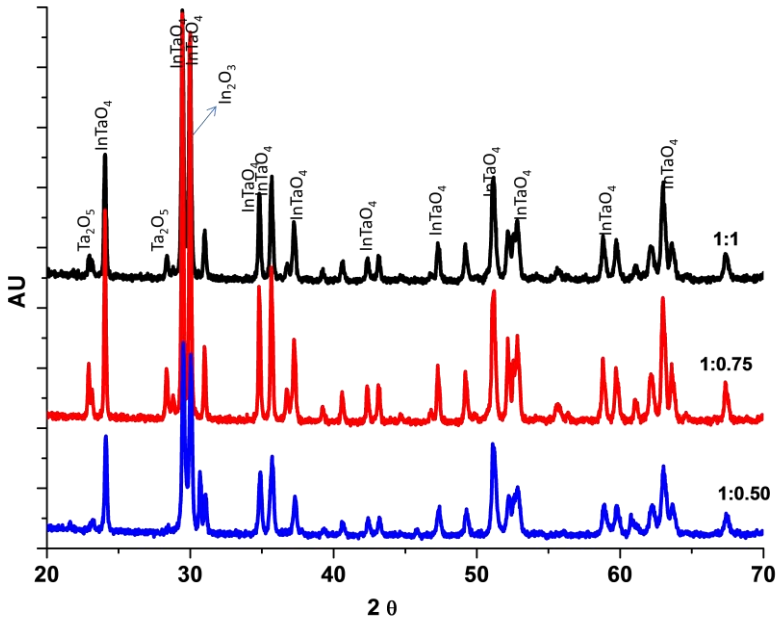

Figure: 3.2 XRD analysis of $InTaO_4$ synthesized at different ratios of In and Ta.

XRD analyses of $AgNbO_3$ and $InNbO_4$ (Figure 3.3) show that silver niobium oxide ($AgNbO_3$) has an orthorhombic structure with a = 5.602, b = 7.824, c = 5.540, α = 90.000, β = 90.000, γ = 90.0, primitive - Pnma (62). Indium niobium oxide has a monoclinic structure with a = 4.843, b = 5.773, c = 5.147, α = 90°.0, β = 91.230°, and γ = 90°.0 - Primitive. Chemical compositions of doped and non-doped samples determined by SEM-EDS show no dopant atoms. It can be deduced from EDS analyses that the concentration of the dopant atoms is high enough to modify the physical properties of the material ($InTaO_4$) but not to change its chemical composition.

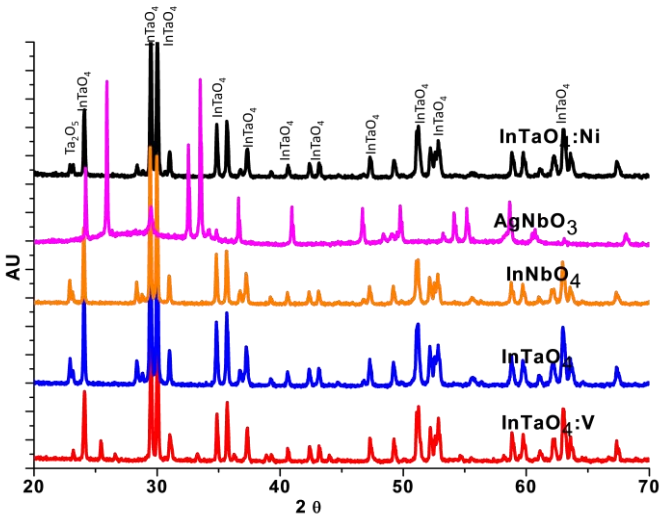

Figure: 3.3 XRD analysis of $AgNbO_3$, $InNbO_4$ and Ni-, V-doped $InTaO_4$ catalysts.

UV-vis diffuse reflectance spectra of non-doped (Figure 3.4) and doped $InTaO_4$ (Figure 3.5) indicate that dopant ions brought out a significant modification to the band gap of the material. Figure 3.4 shows that there is a shoulder peak between 284 and 340 nm in the optical absorption of pristine $InTaO_4$, which reveals that this material may have two band gaps. The absorption edge at around 284 nm is due to the electronic transition between conduction band and valence band, and another absorption edge at around 450 nm is because of the defect sites mostly being composed of oxygen vacancies. Hiroshi et al.[8] have also observed the similar effect of two onsets in the absorption spectrum of non-doped $InTaO_4$. The band gap of the non-doped $InTaO_4$ estimated with a formula[16] (Eg = 1239/λ (wavelength (nm)) was found to be 2.4 eV[17], however, Zou et al.[10] reported a band gap of 2.6 eV for a non-doped $InTaO_4$. Although there are different views[18] regarding the band gap due to the two onsets in the absorption spectrum of $InTaO_4$, however, based on its first absorption edge at lower wavelength, this material has a larger and indirect band gap of 4.3 eV[8, 9].

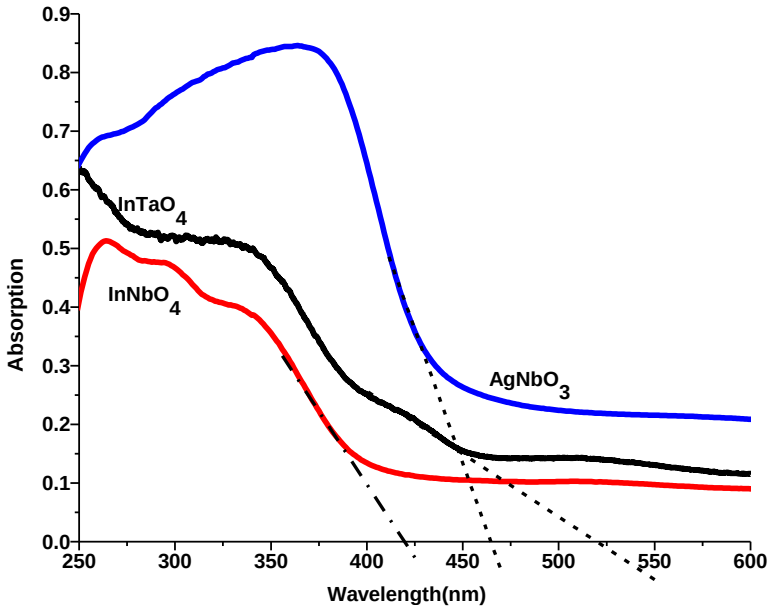

Figure: 3.4 UV-Vis diffusive reflectance spectra of $AgNbO_3$, $InNbO_4$, $InTaO_4$.

Figure 3.4 shows the optical absorption of $InTaO_4$, $AgNbO_3$ and $InNbO_4$. $InTaO_4$ and $AgNbO_3$ have an onset at 400 and 450 nm, respectively, while $InNbO_4$ has an absorption onset at lower wavelength of 380 nm. Unlike $InTaO_4$, $AgNbO_3$ has very sharp absorption, whereas $InNbO_4$ has slightly flat shoulder absorption between 280-380 nm. Band gaps of $InNbO_4$ and $AgNbO_3$ were found to be 2.9, and 2.8 eV, respectively. Ye et al.[19] reported a band gap of 2.5 eV for $InNbO_4$ and Li et al.[20] reported a similar band gap of 2.8 eV for $AgNbO_3$.

Doping Pt, Cu, Ag, Ni, Co, Fe, and Bi ions in $InTaO_4$ modified the optical absorption of $InTaO_4$ and shifted the absorption to the longer wavelength (Figure 3.5). This red-shift in doped $InTaO_4$ was also reported by other investigators.[7, 8] Dopants like Fe, V, Bi and Cu, enhanced the optical absorption significantly and produced a shift of absorption edge to the longer wavelength, while Ag doping had a worse effect on the optical absorption by reducing the overall optical absorption. Dopant ions like Bi, Fe, V, and Cu would substitute In ions in InO_6 octahedron and brought out changes to the

crystal structure in lattice parameters and reducing the band gap. The changes in lattice parameters also affected the volume of InO_6 octahedron producing defect sites and enhancing optical absorption.

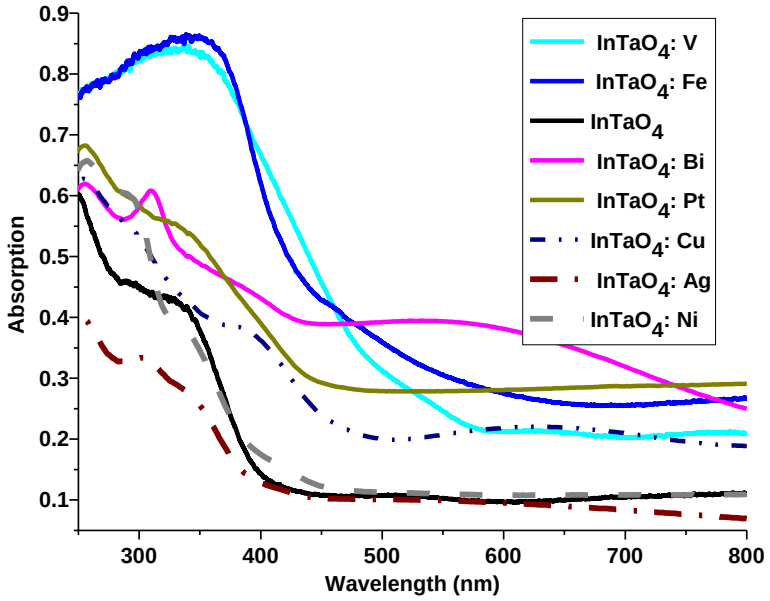

Figure: 3.5 UV-Vis diffusive reflectance spectra of metal-doped $InTaO_4$.

As illustrated in Scheme 3.1, dopants like Bi, Fe, V, and Cu introduced a narrow band just above the valence band of $InTaO_4$, and pushed the valence band toward more negative position, thus reducing the effective band gap of $InTaO_4$. Therefore, owing to the above two reasons, i.e. increase in defect sites, and formation of dopant band above the valence band, doped $InTaO_4$ absorbed more light in the visible range. Contrary to Bi, Fe, V, and Cu ions doping, Ni doping into $InTaO_4$ brought about very limited modification to the optical absorption while it induced a moderate increase in the UV light absorption (Figure 3.5). This effect of different absorption characteristic at longer or shorter wavelengths suggests that different dopant ions may have different positions (interstitial, substitution) in the crystal and thus produce defect states at various energy levels. We suggest that, Ni ion doping induces both deep and shallow defects states,

which promote the absorption mostly in shorter wavelength and minor changes at longer wavelengths. It must be noted that various reports[1, 2] on Ni doped $InTaO_4$ have suggested internal transitions in partially filled Ni 3d levels, which boosted absorption both in the longer and shorter wavelengths. However, XPS analysis (Figure 3.8) confirmed the presence of Ni 2p state, which meant that NiO is formed on the surface of $InTaO_4$. The presence of NiO on the surface acts as co-catalyst and traps the photo-generated electrons, thus reducing the electron-hole pair recombination. This electron trapping (Scheme 3.2) of the co-catalyst (NiO) could not produce a significant modification to the band gap but assist in suppression of recombination process.

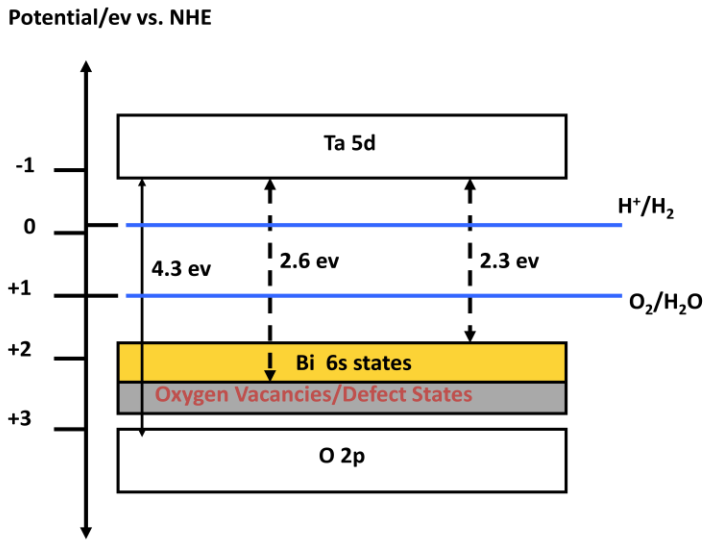

Scheme: 3.1 Band gap modification of $InTaO_4$ doped with various ions (Bi, Cu, Ni).

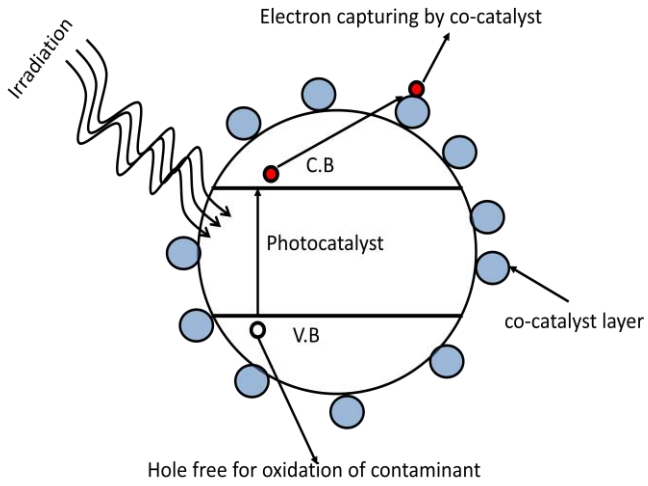

Scheme: 3.2 Diagram of Ni-doped $InTaO_4$ in photocatalysis.

SEM images (Figures 3.6 (a-d)) of non-doped $InTaO_4$ show the presence of varying geometrical shapes and particle sizes i.e. elongated, spherical and plate like structures. These images suggested the growth and agglomeration of $InTaO_4$. SEM images of Ni doped $InTaO_4$ (Figures 3.6 (e, f, g) show similar particles morphology and particle size as that of non-doped $InTaO_4$, suggesting that doping did not change the morphology of $InTaO_4$. SEM images (Figure 3.7) of $InNbO_4$ shows that this material crystallizes in plate like structure and has comparatively larger micro-size than that of $InTaO_4$.

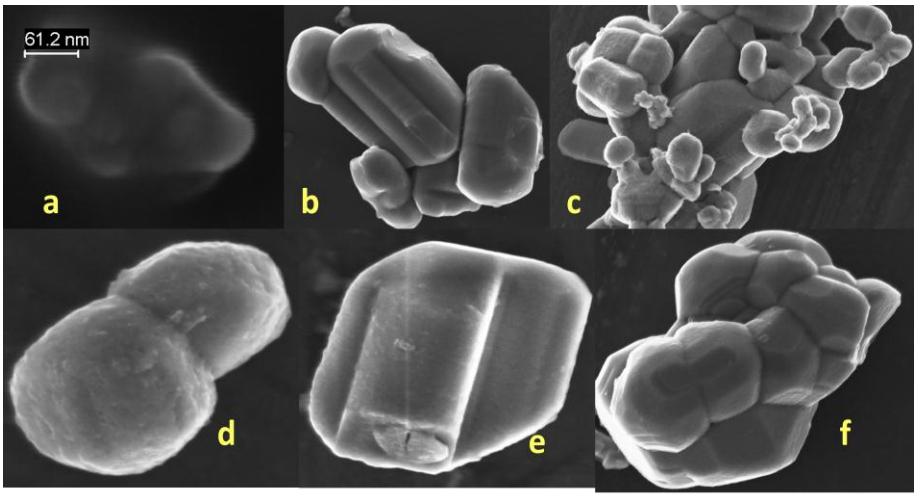

Figure: 3.6 SEM images of $InTaO_4$ (a-d) and Ni-doped $InTaO_4$ (e, f).

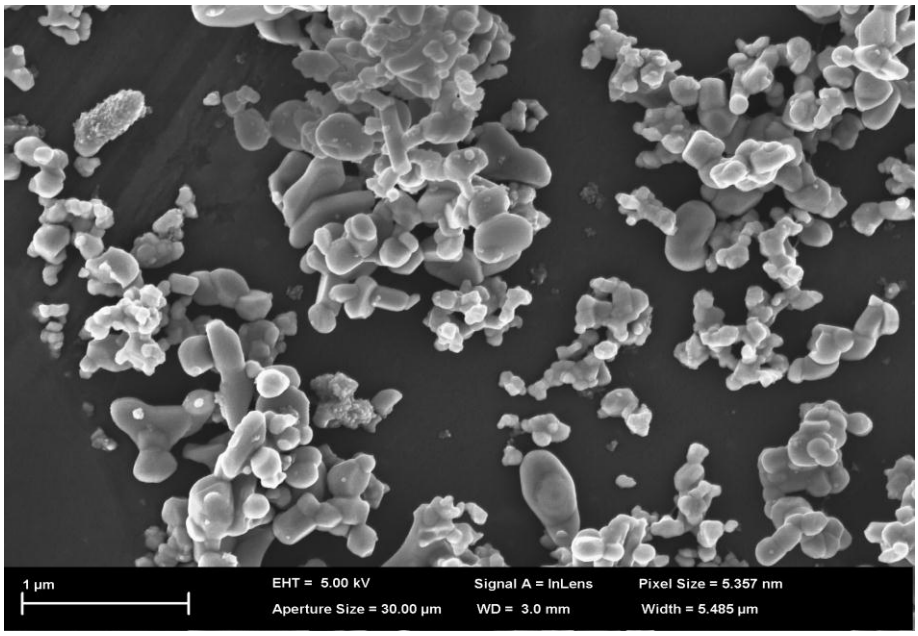

Figure: 3.6 (g) SEM images of Ni-doped $InTaO_4$.

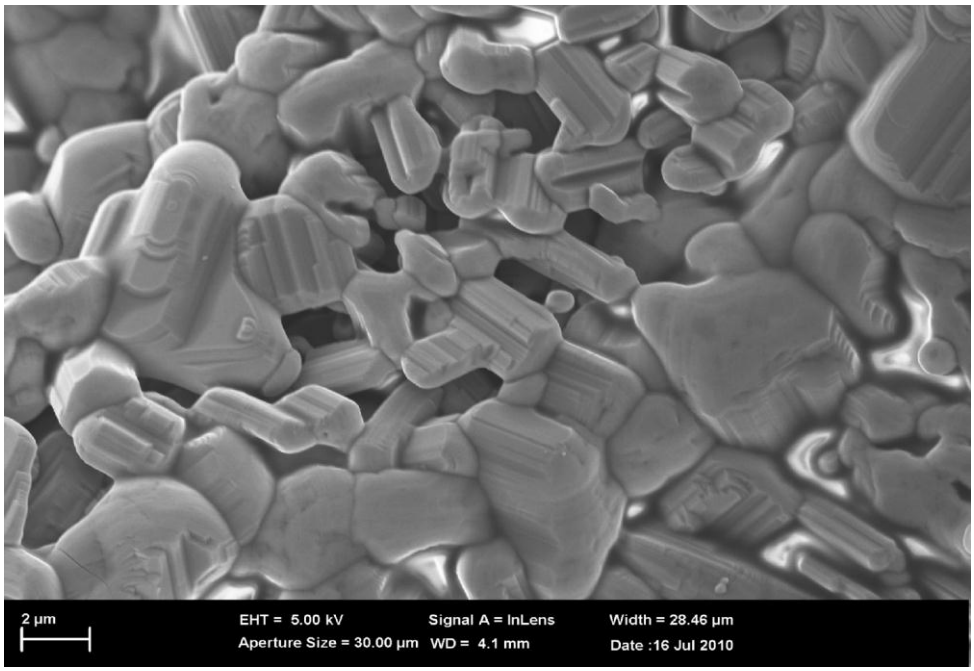

Figure: 3.7 SEM image of $InNbO_4$.

Although EDS (Figure 3.9) and XRD investigations could not detect Ni and/or NiO, however, X-ray photoelectron spectroscopy (XPS) of Ni doped $InTaO_4$ confirmed the existence of NiO. Since the concentration of Ni ions 2% w/w, which cannot be detected with EDS analysis. Ni $2p_{3/2}$ state of NiO was observed at binding energy of 855.5 eV [11] where its corresponding satellite peak is close to 861.0 eV. The satellite is about 6.0 eV higher than the main BE peak. Another peak observed at 873.6 eV can be assigned to Ni $2p_{1/2}$ states of NiO[21]. Chiou et al. [11] also observed the presence of metallic Ni at binding energy of 852.9 eV, of the sample reduced in H_2 environment. However, we could not observed existence of metallic Ni [22] in the Ni doped sample of $InTaO_4$.

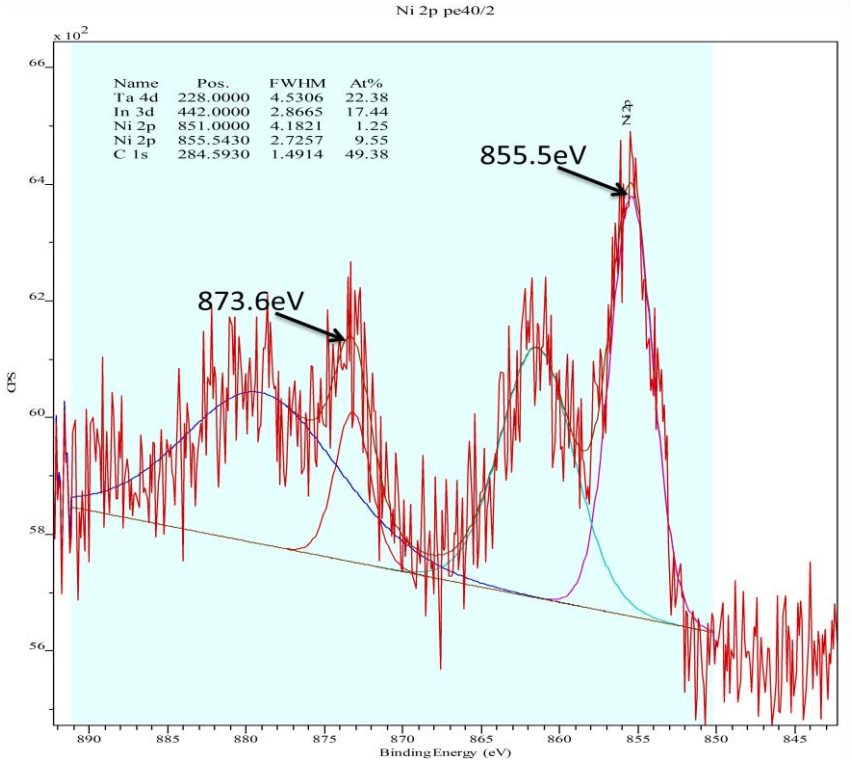

Figure: 3.8 XPS analysis of InTaO4: Ni

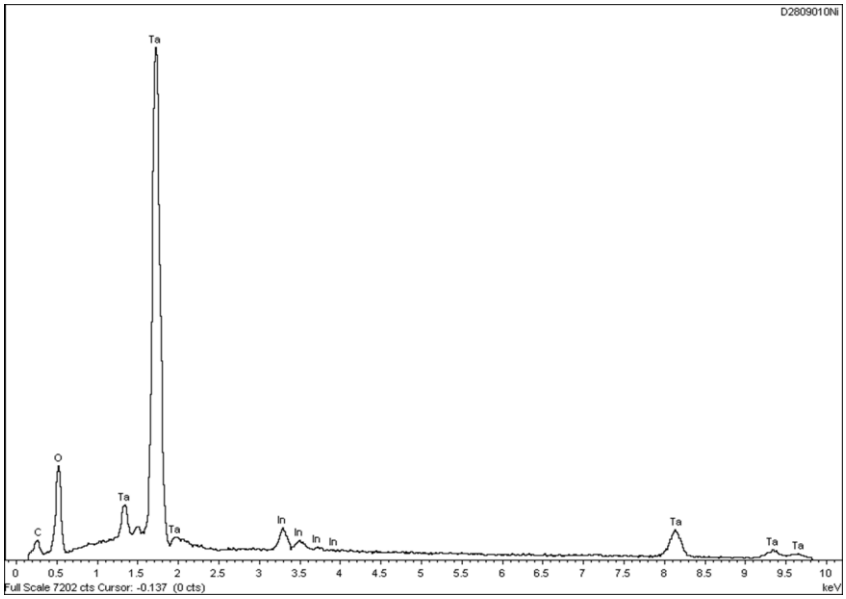

Figure: 3.9 EDS analysis of InTaO4:Ni.

3.3.2 Photocatalytic activities

Photocatalytic activities of $InTaO_4$, $InNbO_4$, $AgNbO_3$ and doped $InTaO_4$ in decomposition of toluene gas were determined in a closed continuous flow reactor irradiated with UV-vis light (Figure 3.10). TiO_2-P25 presented a fast decomposition of toluene at 50% in the first hour under UV-vis irradiation but strong deactivation afterwards. After 800 min, toluene decomposition efficiency was reduced to 20%. $InTaO_4$ exhibited a gradually increased efficiency of toluene degradation and reached 30% at the first hour and maintained the stable activity ever since. $InNbO_4$, and $AgNbO_3$[23] showed similar activities with decomposition of toluene at 10-15% within the first two hours.

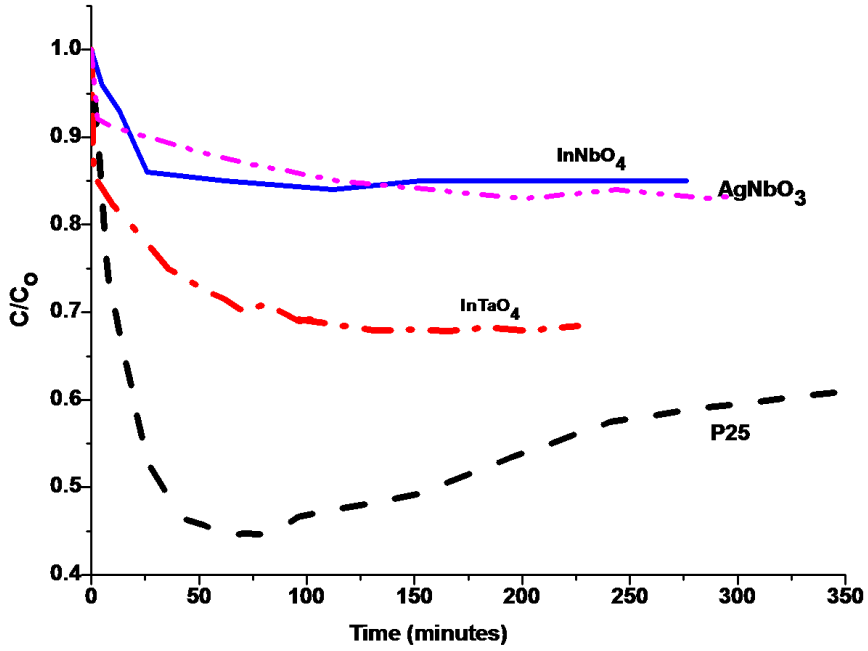

Figure: 3.10 Photocatalytic decomposition of toluene on various photocatalysts with UV-vis irradiation.

The deactivation of TiO_2-P25 was due to a strong affinity to water and reaction intermediates which covered the surface reactive sites for photocatalytic decomposition

of toluene. It was also found that TiO_2-P25 changed the color from white to black after reaction; however $InTaO_4$ showed a pale yellow color indicating much less intermediate adsorption on the surface. Adsorption of by-products and water on TiO_2 covered the reactive sites on material surface. So upon UV light irradiation, electron-hole pairs will not generate on material surface which cause the redox reaction. It may also be possible that due the adsorption of intermediates and water on TiO_2 surface, toluene molecules will not contact or touch the material surface which is one of the basic requirements for photocatalytic reaction and therefore, toluene will not decompose.

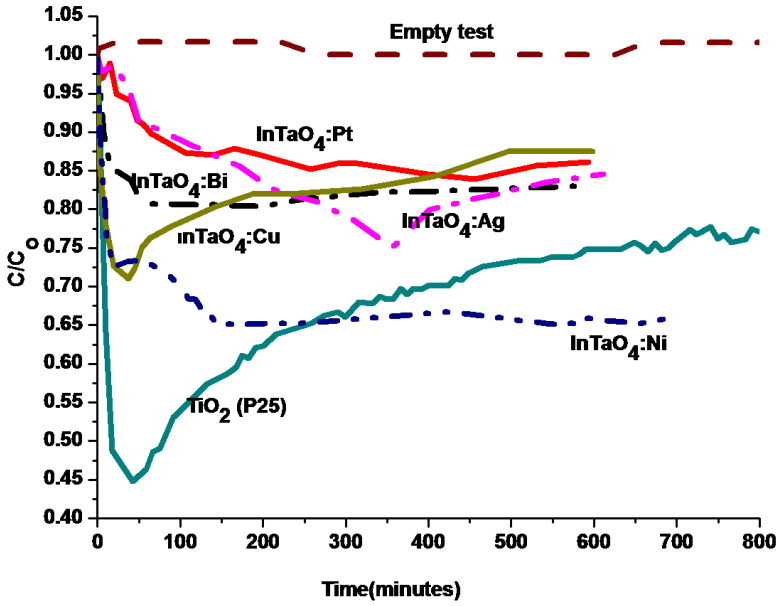

Figure: 3.11 Photocatalytic decomposition of toluene on metal-doped $InTaO_4$ with UV-vis irradiation.

Figure 3.12 shows FTIR analysis of P25 and $InTaO_4$ after using for photocatalytic oxidation of toluene under UV-vis light irradiation. Similar to other research work[24],[25],[26], strong water and intermediate adsorption was observed on TiO_2

surface. A broad and intense peak at 3600-2800 cm^{-1}, centered at 3350 cm^{-1} corresponds to the stretching mode of water molecules[24] whereas bands at 1700-1590 cm^{-1} centered at 1659 cm^{-1} corresponds to aromatic molecules of benzaldehyde. Another aromatic intermediate observed with a single band at 1420 cm^{-1} was found to be benzoic acid[24], [27]. It can be deduced from the FTIR analysis that strong adsorption of water molecules and aromatic intermediates cover the active sites of TiO_2 and caused the irreversible deactivation[27], [28]. However, such strong adsorption of water molecules and intermediates did not occur on doped and non-doped $InTaO_4$ surface and therefore they works longer than commercial TiO_2.

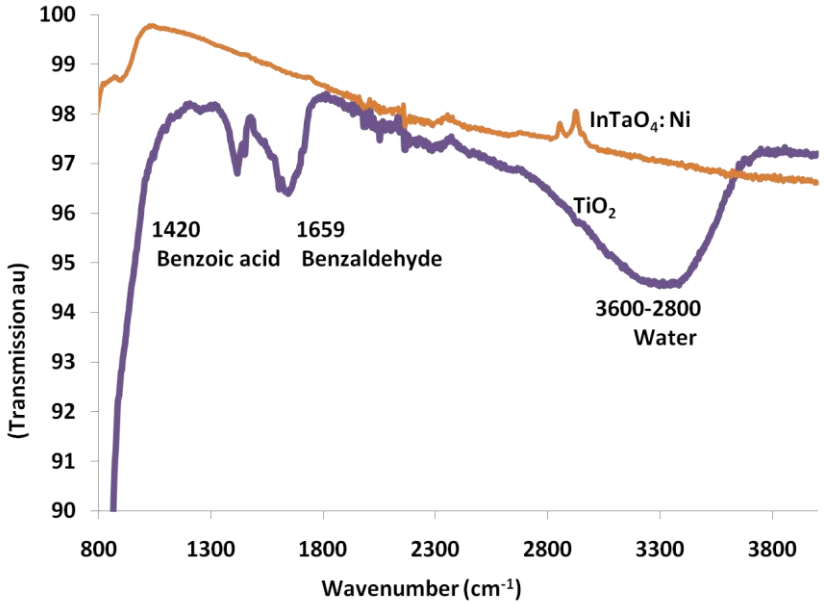

Figure: 3.12 FTIR analyses of used TiO_2 and $InTaO_4$.

Photocatalytic activity of Ni, Ag, Cu, Pt, and Bi doped $InTaO_4$ samples for toluene decomposition were also investigated (Figure 3.11). The order of photocatalytic activity in the first two hours was TiO_2-P25 > $InTaO_4$: Ni > $InTaO_4$: Cu> $InTaO_4$: Bi> $InTaO_4$: Ag > $InTaO_4$: Pt. As shown in Figure 3.11, the tests in a longer period indicated that Ni doped $InTaO_4$ was far better than the commercial TiO_2-P25. The

activity of $InTaO_4$: Ni remained unchanged in 14 h. In the second run after regeneration, TiO_2-P25 lost 90% of its efficiency, while $InTaO_4$: Ni maintained its photocatalytic activity. XRD analyses of $InTaO_4$: Ni after use (for 14 hours) (Figure 3.13) clearly indicates that the material is quite stable and did not change its structure. This strong stability of the material suggests that $InTaO_4$ doped with Ni can be a better alternative to commercial photocatalytic material. Zou et al.[2] found that TiO_2-P25 had better performance than Ni-doped $InTaO_4$ in H_2 production from water splitting under UV light irradiation. However, $InTaO_4$ doped with Mn, Co, and Ni showed better performance than TiO_2-P25 for H_2 production under visible light irradiation [2, 10]. Chiou et al. [11] have demonstrated that 3wt% Ni loading produced both NiO and NiOH on $InTaO_4$ surface. Upon reduction in H_2 environment metallic Ni shell on surface was created and acted as electron trapping centers, thus enhancing photocatalytic water splitting. Thus it is deduced that the better performance of $InTaO_4$: Ni is the combined effect of both the band gap contraction and electron capturing by NiO as explained in Scheme 3.2. Although doping of $InTaO_4$ with Ag, Cu, Pt, V and Bi produced red-shifts of the optical absorption but they did not make a cover on the $InTaO_4$ surface like NiO. These metal dopants reduced the optical band gap, but they may also enhance the electron-hole pair recombination, by creating mid-gap defect states. The generation of the defect states plays a detrimental role in recombination centers which may reduce the photocatalytic decomposition of toluene. Ni doping modified the band gap but suppressed the recombination via electron trapping on NiO, making it exhibiting better performance. Recently Shu et al.[23] have demonstrated a similar effect of electron trapping by NiO loaded on $AgNbO_3$ for methylene blue decomposition under UV irradiation.

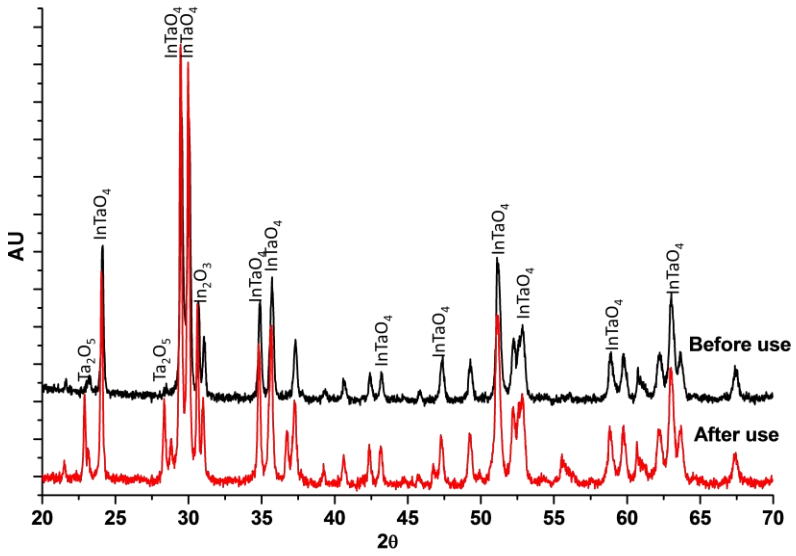

Figure: 3.13 XRD analysis of InTaO4: Ni before and after use for photocatalytic reaction.

Photocatalytic performance of non-doped and doped $InTaO_4$ materials in methylene blue decomposition in water with UV-vis light (Figure 3.14) showed that Ni doped $InTaO_4$ degraded methylene blue at a much faster rate than the others. $AgNbO_3$ had almost comparable performance as $InTaO_4$: Ni. $InTaO_4$: Ni, and $AgNbO_3$ were capable to decompose about 90% methylene blue within six hours, while Cu, Pt, V, and non-doped $InTaO_4$ could degrade about 60% methylene blue. It is noted that doped and non-doped $InTaO_4$ did not show the same trend in methylene blue decomposition as that in toluene decomposition; however, Ni doped $InTaO_4$ has demonstrated the best performance. Another test revealed that Ni doped $InTaO_4$ could also decompose about 75% of phenol within 3 hours (Figure not shown). As explained earlier, the better photocatalytic performance of Ni doped $InTaO_4$ among the others are mainly attributed to the dual effects of band gap reduction and electron trapping by NiO.

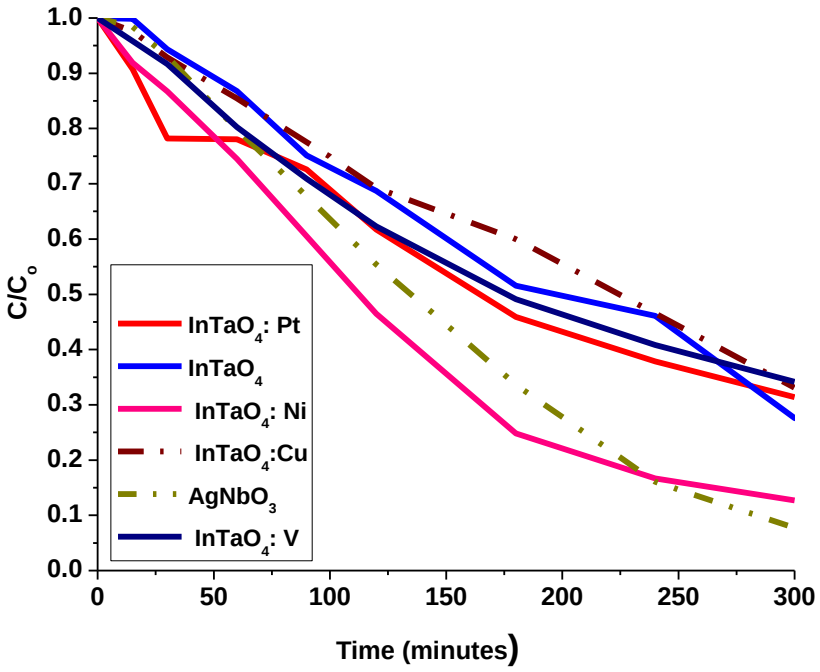

Figure: 3.14 Decomposition of methylene blue on various photocatalysts with UV-vis irradiation.

3.4 Conclusion

Tantalum and niobium based compounds such as $InTaO_4$, $InNbO_4$ and $AgNbO_3$ can be prepared by a simple wet-chemical technique. Most of these materials possess poly-crystalline structures and large size agglomerates. $InTaO_4$ exhibits better activity than $InNbO_4$ and $AgNbO_3$. The physical properties and photocatalytic activities of $InTaO_4$ are also influenced by doping with metals like Pt, Cu, Ag, V, Bi, and Ni. Bi doped $InTaO_4$ will result in more visible light absorption, but Ni doped $InTaO_4$ shows stronger UV absorption. $InTaO_4$: Ni can efficiently decompose all the contaminants of toluene, methylene blue and phenol in air or water under UV-vis light. The higher photocatalytic activity of $InTaO_4$: Ni is attributed to the band gap modification and

electron trapping centre of NiO. $InTaO_4$: Ni also has better performance in multiple uses and longer life time than the commercial TiO_2-P25.

3.5 References

1. Zou, Z., J. Ye, and H. Arakawa, *Structural properties of InNbO4 and InTaO4: correlation with photocatalytic and photophysical properties.* Chemical Physics Letters, 2000. **332**(3-4): p. 271-277.
2. Zou, Z., et al., *Photocatalytic hydrogen and oxygen formation under visible light irradiation with M-doped InTaO4 (M=Mn, Fe, Co, Ni and Cu) photocatalysts.* Journal of Photochemistry and Photobiology A: Chemistry, 2002. **148**(1-3): p. 65-69.
3. Yang, X., et al., *Enhanced photocatalytic activity of Eu2O3/Ta2O5 mixed oxides on degradation of rhodamine B and 4-nitrophenol.* Colloids and Surfaces A: Physicochemical and Engineering Aspects, 2008. **320**(1-3): p. 61-67.
4. Ohuchi, T., et al., *Liquid phase photooxidation of alcohol over niobium oxide without solvents.* Catalysis Today, 2007. **120**(2): p. 233-239.
5. Zhang, G., et al., *Wet chemical synthesis and photocatalytic activity of potassium niobate K6Nb10.8O30 powders.* Journal of Solid State Chemistry, 2008. **181**(9): p. 2133-2138.
6. Zhang, X., et al., *Generalized One-Pot Synthesis, Characterization, and Photocatalytic Activity of Hierarchical BiOX (X = Cl, Br, I) Nanoplate Microspheres.* The Journal of Physical Chemistry C, 2008. **112**(3): p. 747-753.
7. Ye, J. and Z. Zou, *Visible light sensitive photocatalysts In1-xMxTaO4 (M=3d transition-metal) and their activity controlling factors.* Journal of Physics and Chemistry of Solids, 2005. **66**(2-4): p. 266-273.

8. Hiroshi, I. and H. Kazuhito, *Visible Light-Sensitive InTaO4- Based Photocatalysts for Organic Decomposition.* Journal of the American Ceramic Society, 2005. **88**(11): p. 3137-3142.
9. Matsushima, S., et al., *First-principles energy band calculation for undoped and N-doped InTaO4 with layered wolframite-type structure.* Journal of Physics and Chemistry of Solids, 2003. **64**(12): p. 2417-2421.
10. Zou, Z., et al., *Direct splitting of water under visible light irradiation with an oxide semiconductor photocatalyst.* Nature, 2001. **414**(6864): p. 625-627.
11. Chiou, Y.-C., U. Kumar, and J.C.S. Wu, *Photocatalytic splitting of water on NiO/InTaO4 catalysts prepared by an innovative sol-gel method.* Applied Catalysis A: General, 2009. **357**(1): p. 73-78.
12. Chatrchyan, S., et al., *Measurement of the Inclusive Jet Cross Section in pp Collisions at sqrt[s]=7 TeV.* Phys Rev Lett, 2011. **107**(13): p. 132001.
13. Wang, S.B., H.M. Ang, and M.O. Tade, *Volatile organic compounds in indoor environment and photocatalytic oxidation: State of the art.* Environment International, 2007. **33**(5): p. 694-705.
14. Shukla, P., et al., *Photocatalytic generation of sulphate and hydroxyl radicals using zinc oxide under low-power UV to oxidise phenolic contaminants in wastewater.* Catalysis Today, 2010. **157**(1-4): p. 410-414.
15. Shukla, P.R., et al., *Photocatalytic oxidation of phenolic compounds using zinc oxide and sulphate radicals under artificial solar light.* Separation and Purification Technology, 2010. **70**(3): p. 338-344.
16. Zhang, K.L., et al., *Study of the electronic structure and photocatalytic activity of the BiOCl photocatalyst.* Applied Catalysis B-Environmental, 2006. **68**(3-4): p. 125-129.
17. Madhusudan Reddy, K., S.V. Manorama, and A. Ramachandra Reddy, *Bandgap studies on anatase titanium dioxide nanoparticles.* Materials Chemistry and Physics, 2003. **78**(1): p. 239-245.

18. Chang, H., et al., *Electronic structures of InTaO4, a promising photocatalyst.* Chemical Physics Letters, 2004. **398**(4-6): p. 449-452.
19. Ye, J., et al., *Correlation of crystal and electronic structures with photophysical properties of water splitting photocatalysts InMO4 (M=V5+,Nb5+,Ta5+).* Journal of Photochemistry and Photobiology A: Chemistry, 2002. **148**(1-3): p. 79-83.
20. Li, G., et al., *Composition dependence of the photophysical and photocatalytic properties of (AgNbO3)1-x(NaNbO3)x solid solutions.* Journal of Solid State Chemistry, 2007. **180**(10): p. 2845-2850.
21. Suwanwatana, W., S. Yarlagadda, and J.J.W. Gillespie, *Hysteresis heating based induction bonding of thermoplastic composites.* Composites Science and Technology, 2006. **66**(11-12): p. 1713-1723.
22. Dutta, R.S., et al., *Characterization of microstructure and corrosion properties of cold worked Alloy 800.* Corrosion Science, 2006. **48**(9): p. 2711-2726.
23. Shu, H., et al., *Structural characterization and photocatalytic activity of NiO/AgNbO3.* Journal of Alloys and Compounds, 2010. **496**(1-2): p. 633-637.
24. Barraud, E., et al., *Gas phase photocatalytic removal of toluene effluents on sulfated titania.* Journal of Catalysis, 2005. **235**(2): p. 318-326.
25. Martra, G., et al., *The role of H2O in the photocatalytic oxidation of toluene in vapour phase on anatase TiO2 catalyst: A FTIR study.* Catalysis Today, 1999. **53**(4): p. 695-702.
26. Augugliaro, V., et al., *Photocatalytic oxidation of gaseous toluene on anatase TiO2 catalyst: mechanistic aspects and FT-IR investigation.* Applied Catalysis B: Environmental, 1999. **20**(1): p. 15-27.
27. Marcì, G., et al., *Photocatalytic oxidation of toluene on irradiated TiO2: comparison of degradation performance in humidified air, in water and in water containing a zwitterionic surfactant.* Journal of Photochemistry and Photobiology A: Chemistry, 2003. **160**(1-2): p. 105-114.

28. Maira, A.J., et al., *Fourier Transform Infrared Study of the Performance of Nanostructured TiO2 Particles for the Photocatalytic Oxidation of Gaseous Toluene.* Journal of Catalysis, 2001. **202**(2): p. 413-420.

4

4 -Photocatalytic Decomposition of Water and Air Contaminants with Metal Doped $BiTaO_4$ Irradiated with Visible Light

Abstract

Various metal ions (Al, Nd, La, Ga, Ba, Sn, W, Fe, Co, Cr, Ce, Cu, Sb, Pb, Ni, and Ag) doped and undoped triclinic $BiTaO_4$ photocatalysts were synthesized using a solution method. Metal ion doping changed the photophysical properties, but did not alter the crystal structure of $BiTaO_4$. The newly prepared materials were characterized with high resolution transmission electron microscopy (HRTEM), scanning electron microscopy (SEM), Fourier transform infrared spectroscopy (FTIR), X-ray diffraction (XRD), energy dispersive X-ray spectroscopy (EDS), and UV-vis diffuse reflectance spectroscopy. $BiTaO_4$ doped with various metal ions were used for photocatalytic decomposition of water and air contaminants with both UV and visible light irradiation. Increased photocatalytic decomposition of toluene in air was observed for dopants such as Al, Nd, La, Ga, Ba, Sn, W, Fe, Sb, Ag, while other metal ions like Cu, Ce, Co, Pb, and Ni induced a detrimental effect on the photocatalytic performance. $BiTaO_4$ doped with La, Ga and Nd catalysts have shown much better and stable performance than TiO_2 in gaseous toluene decomposition with both UV and visible light. Metal ion doped $BiTaO_4$ also has shown good performance in methylene blue degradation in water.

4.1 Introduction

Since the discovery of photocatalysis processes as vital advanced oxidation techniques for decomposition of water [1] and volatile organic compounds [2, 3], large number of materials (metal oxides[4, 5], mixed oxides[6, 7], and metal sulphide[8-10] etc.) have been explored. However, the need for an efficient and visible light active photocatalytic material is still under way and requires further investigation[11]. Bismuth and group five elements based pyrochlore type materials, such as $BiVO_4$[12, 13], $BiNbO_4$[14, 15], and $BiTaO_4$ [16, 17] have been proven as efficient materials not only for microwave applications[18, 19] but also as alternative materials to the commercially known photocatalyst (TiO_2). Band gap excitation of a photocatalytic material through irradiation to generate electron-hole pair for the impending redox reaction is the main procedure of the photocatalytic reaction. Thus, for visible light active photocatalytic materials, (i) band gap must lie within the range of visible light energy i.e. below 2.8 eV, (ii) conduction band must be more negative than the oxidation potential of VOCs, (iii) and valence band must be more positive than the reduction potential. The landmark photocatalyst, TiO_2, fulfils the latter two conditions and is therefore the most suitable material; however it cannot be activated with visible light irradiation owing to its large band gap of 3.2 eV. Nevertheless, various techniques such as doping[20] with metals, non-metals[21, 22] and coupling[23]/coating[24] with other metals have been introduced to modify the band gap of TiO_2 making it a visible light active photocatalyst. Although some of these modifications were successful[25, 26] to reduce the band gap and activate TiO_2 with visible light, irreversible inactivation[27], lower life time, and lack of re-generation of TiO_2 made us to explore other materials which have stable activity and longer life time.

Since last decade much attention has been made to tantalates such as $InTaO_4$ [28], $NaTaO_3$[29, 30], and $BiTaO_4$ as visible light active photocatalytic materials, because conduction band of these materials is consisted of Ta 5d orbitals which are at more negative potential than Ti 3d orbitals. Tantalates are consisted of TaO_6 octahedrons, where M-O-M angle is close to 180° [29]. It has been reported that the

closer the M-O-M angle to 180°, the more distorted the structure of the material, and the higher the mobility of the carriers[31]. Among tantalates, $BiTaO_4$ has other benefits of i) direct and lower band gap of 2.75 eV, ii) higher oxidation potential than H_2O_2 and O_3, and iii) largely dispersed valence band which is made of Bi 6s and O 2p hybridized orbitals[32]. Mobility and life time of the photo-generated carriers strongly affect the photocatalytic process[33]. Unlike titanate and other tantalates such as $NaTaO_3$, mobility of photo-generated holes and electrons in valence and conduction bands of $BiTaO_4$ is higher due to the hybrid and distorted nature of these bands.

Based on these favourable properties of lower band gap, higher carrier mobility, suitable valence and conduction band positions and higher redox potential, we synthesized various metal ion doped $BiTaO_4$ catalysts via a solution method and tested them for decomposition of volatile organic compounds both in liquid and gaseous forms. We have shown that some metal ion doped $BiTaO_4$ materials have much better performance than TiO_2 under both ultraviolet [34] and visible light irradiation for toluene decomposition in gaseous form, while they have comparatively better activity in degradation of water contaminants.

4.2 Experimental

4.2.1 Material synthesis

Polycrystalline undoped and metal ion (Fe, Cu, V, Ba, Sn, Sb, La, Al, Ag, Ni, Co, Nd, and Ga) doped $BiTaO_4$ materials were prepared by wet-chemical techniques. All of chemicals were obtained from Sigma-Aldrich at 99.99% purity and were used as received. In a typical synthesis, 12 mmol of bismuth (III) nitrate hydrate ($Bi(NO_3)_3 \cdot 5H_2O$) and 8 mmol of tantalum (V) chloride ($TaCl_5$) were dissolved separately in a 50 mL ethanol solution with continuously stirring and heating at 70 °C for 30 min as solutions A and B, respectively. A dopant solution C was also prepared similarly by dissolving 0.01 mmol of dopant salt (Fe, Cu, V, Ba, Sn, Sb, La, Al, Ag, Ni, Ce, Nd, Cr, Co, and Ga) in 30 mL ethanol. Both the solutions A and B were then mixed and 0.5 - 1.0 mL concentrated nitric acid was added to the

mixture. After half hour, the dopant solution C was also added to the mixture, which was then kept heating at 80 °C for 6-8 h. The final solution with no precipitation was then aged for 12-24 h at room temperature and was kept in an oven at 50 – 60 °C till dried completely. Samples were ground by mortar and pestle and then calcined at 700 °C for 40-50 h. Undoped $BiTaO_4$ was also prepared by the similar technique where no dopant solution was added to the process. The synthesis procedure is given in the following flow chart.

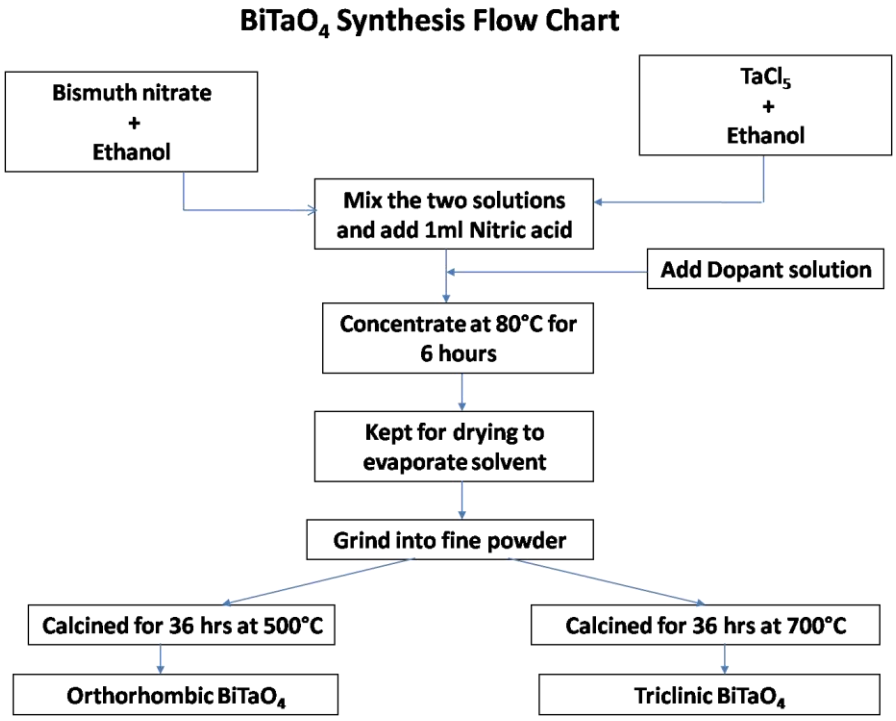

4.2.2 Characterization of catalysts

The crystal structures of samples were analysed by X-ray diffractometer (Bruker D8 Advance equipped with a Lynx eye detector, Bruker-AXS, Karlsruhe, Germany) operated at 40 kV and 30 mA. The scanning rate was 0.2 sec/step with 2θ (10- 90°) and step size of 0.02°. Cu Kα (λ = 1.54178 Å) was used as a X-ray source with divergent slit of 0.300 and 2.5° primary and secondary soller slits. The optical absorption of samples was determined by UV-Vis absorbance spectroscopy using the diffuse reflectance method (JASCO V-670 Spectrometer). Morphology and

chemical composition of the materials were examined by scanning electron microscopy (ZEISS NEON 40EsB) equipped with an energy dispersive spectrometer (SEM-EDS). Samples were directly coated on an aluminium stub where 3 nm platinum coating was used as a conducting material. FTIR analysis was performed on Perkin-Elmer Model FTIR-100 with a MIR detector. Transmission electron microscopy was performed to study the grain size, structure and detailed morphology of nanoparticles. A JEOL-300F TEM machine operated at 3000 kV was used, which has 50 K magnification and 0.1 nm resolution. Samples were evenly distributed on a carbon coated copper grid.

4.2.3 Photocatalytic evaluation

Photocatalytic activities of prepared samples were evaluated by decomposition gaseous toluene with both ultraviolet and visible light irradiations. Two different light sources; 300 W Mercury-Xenon lamps (UXM-502MD, Ushio) and Xenon lamp (UXL-306, Ushio) were used as UV and visible light sources, respectively. The average intensities of UV lamp were measured to be 19.1 mW/cm^2 at 220 – 280 nm, 19.0 mW/cm^2 (at 280 - 400 nm), and 27.5 mW/cm^2 (at > 400 nm), while the Xenon lamp has average intensities of 26.0 mW/cm^2 at (315 – 400 nm), 240.0 mW/cm^2 (at 400 – 1050 nm). Methylene blue was used as a model water contaminant. In a typical run of methylene blue decomposition in water, 10 ppm methylene blue solution with 100 mg catalyst particles were continuously stirred in a Pyrex glass reactor which was irradiated with UV-vis light without any filter. Temperature of the reactor was maintained by passing cooled water through the reactor continuously. Concentration of methylene blue was determined by taking one mL aliquots from the reactor at a regular interval. The aliquots were evaluated by measuring the absorbance at λ= 664 nm with a visible spectrophotometer (Spectronic Instruments Model 4001/4), and the sample was put back in the reactor to maintain the concentration of solution unchanged.

Toluene decomposition in gas was evaluated in a flow reactor connected with a gas chromatograph (Shimadzu GC-17A) fitted with a GS-GSPRO column of 60 m in

length and 0.32 mm in diameter. Oven temperature of the GC was 220 °C and FID detector temperature was kept at 250 °C. In a typical experiment, 300 mg of photocatalysts were dispersed in 10 mL deionised water in a Petri dish of 450 mm diameter and was dried in an oven overnight. The Petri dish was kept inside an air-tight stainless steel reactor fitted with a removable quartz sheet in order to allow both UV and visible radiation in. A flow of toluene at 100 ppm was continuously passed into the reactor (1.08 L) at a flow rate of 60 mL/min. The temperature of the reactor was controlled at room temperature by continuously passing cooling water through the reactor and also by blowing the reactor with fresh air from outside.

4.3 Results and discussions

4.3.1 Structure of materials

$BiTaO_4$ prepared with a solid state reaction method crystallized in two different forms i.e. triclinic (β-type) at high temperature (1200 ºC) and orthorhombic (α-type) at lower temperature (900 ºC)[35], respectively. X-ray diffraction patterns of $BiTaO_4$ prepared in this investigation at various temperatures are shown in Figure 4.1, and Table 4.1 gives the corresponding lattice parameters.

Table 4.1 Structural parameters of various $BiTaO_4$ catalysts.

Calcination temperature	Structure observed	a (Å)	b (Å)	c (Å)	α (Å)	β (Å)	γ (Å)
250	tetragonal	3.8910	3.89100	7.36900	90.00	90.00	90.00
500	tetragonal	3.8830	3.88300	7.34700	90.00	90.00	90.00
700	triclinic	7.6520	5.58400	7.77200	89.92	77.12	86.45
800	triclinic	7.6623	5.58707	7.78498	90.05	77.03	86.47
1150	triclinic	7.6623	5.58707	7.78498	90.05	77.03	86.47
800 [36]	triclinic	7.651	5.584	7.772	89.92	77.12	86.45
1100[32]	triclinic	5.297	7.674	7.779	102.98	89.95	93.47

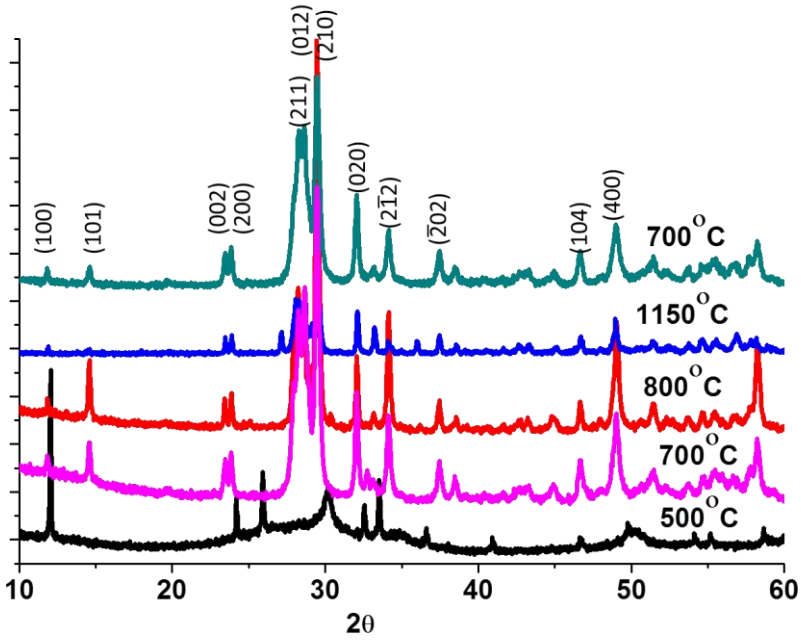

Figure: 4.1 XRD analysis of $BiTaO_4$ synthesized with various temperatures

It is evident from Figure 4.1 that the nucleation starts at 250 °C, but phase transformation begins at 500 °C, and realizes complete crystalline structure at 700 °C. Although Figure 4.1 shows the major peaks of $BiTaO_4$ at 500 °C, the material still contains chlorine ions, which form the structure of BiOCl. The chlorine originated from the parent chemical ($TaCl_5$) is completely eliminated at 700 °C and above. It is noted that solid state reaction at low sintering temperature produced orthorhombic $BiTaO_4$ [32], [35], [37], [38] however, the solution method would result in triclinic $BiTaO_4$ at lower and higher temperatures. As shown in Table 4.1, lattice parameters of all $BiTaO_4$ samples prepared at different temperatures (500 - 1150°C) correspond to only triclinic form without any orthorhombic structure. Murhurajan et al. [36] and Almeida et al. [39] also found similar triclinic structure of $BiTaO_4$ prepared (at lower sintering temperature) with co-precipitation and polymeric precursor method. However, in case of solid state reaction, transformation from orthorhombic to triclinic phase occurred at elevated temperature of 1100 °C[35], [40] and dopants [37]. The samples sintered at 700, 800 and 1150 °C have the same triclinic crystalline phases, the lattice parameters

increases with increasing temperature. The same trend of increased lattice parameters was not found when temperature increased from 800 to 1150 °C.

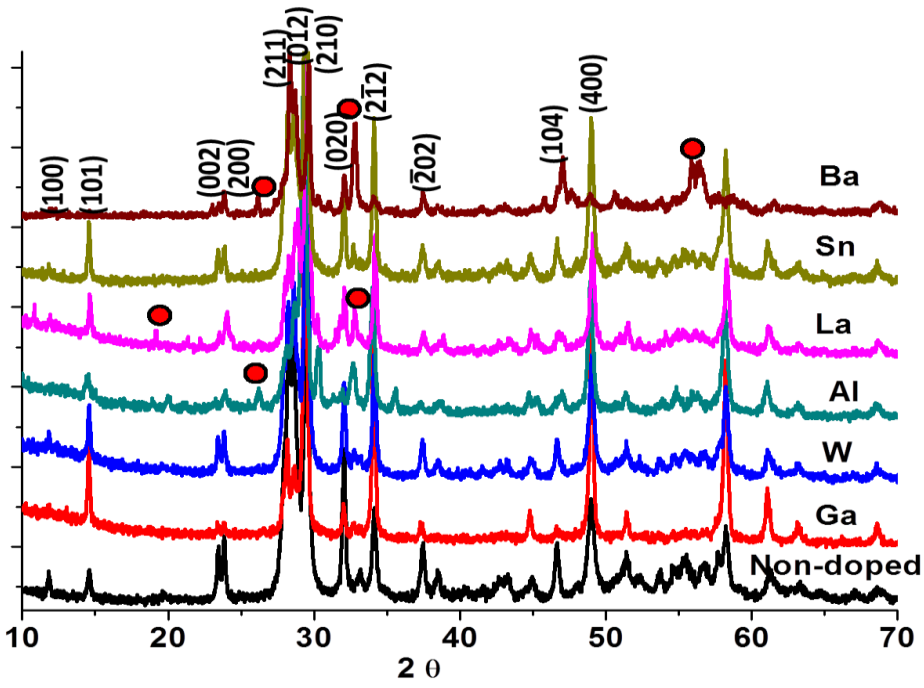

Figure: 4.2 XRD analysis of doped $BiTaO_4$ sintered with 700 °C.

Figure 4.2 shows XRD analysis of $BiTaO_4$ doped with various metal ions such as tin (Sn), barium (Ba), aluminium (Al), tungsten (W), gallium (Ga), and lanthanum (La). It is evident from Figure 4.2 that all these doped $BiTaO_4$ materials have been crystallized in triclinic form with minor variation in the lattice parameters. These samples were sintered at same temperature of 700 °C. There are various reports on phase alteration (triclinic to orthorhombic) due to variation in elemental ratio (Ta/Nb) [35], [40], [41], [42], however, none of the doped $BiTaO_4$ in this investigation and Cu doped $BiTa_{1-x}Cu_xO_4$ (x = 0.00-0.04) [16] has shown phase alteration to orthorhombic form due to doping and/or substituting different types of elements. There are some unidentified peaks (Figure 4.2) represented with red dots in the XRD patterns of doped $BiTaO_4$. These peaks arises either from the oxide of the dopant atoms or the weaker peaks of native $BiTaO_4$, which became more visible due to dopant atom substitution. Since the sizes of the dopant ions are different

from that of tantalum ions, therefore, substitution of dopant ions may slightly modify some of the crystallographic planes. These slight changes in crystal planes may introduce new peaks (as observed in Figure 4.2) and/or highlight the already existing weaker peaks in the XRD patterns of doped $BiTaO_4$. It can be deduced from the above discussion that triclinic form of both undoped and doped $BiTaO_4$ can be prepared at low sintering temperature with the solution method, while it requires elevated temperature in solid state reaction routes[35].

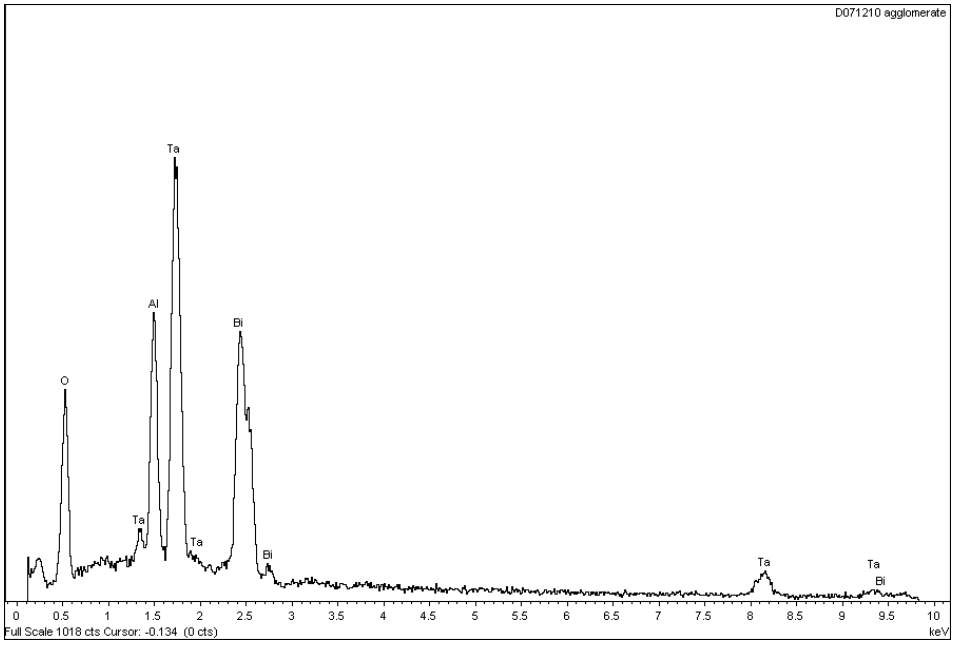

Figure: 4.3 EDS analysis of $BiTaO_4$: Ba.

EDS analysis (Figure 4.3) of $BiTaO_4$: Ba and $BiTaO_4$: Sn did not show the presence of dopant atoms in the crystal structure, indicating that 2% doping of foreign atoms could not induce a change in chemical structure due to low loading. Aluminium peak in the EDS analysis is originated from the stub, since the sample was directly dispersed on the aluminium stub.

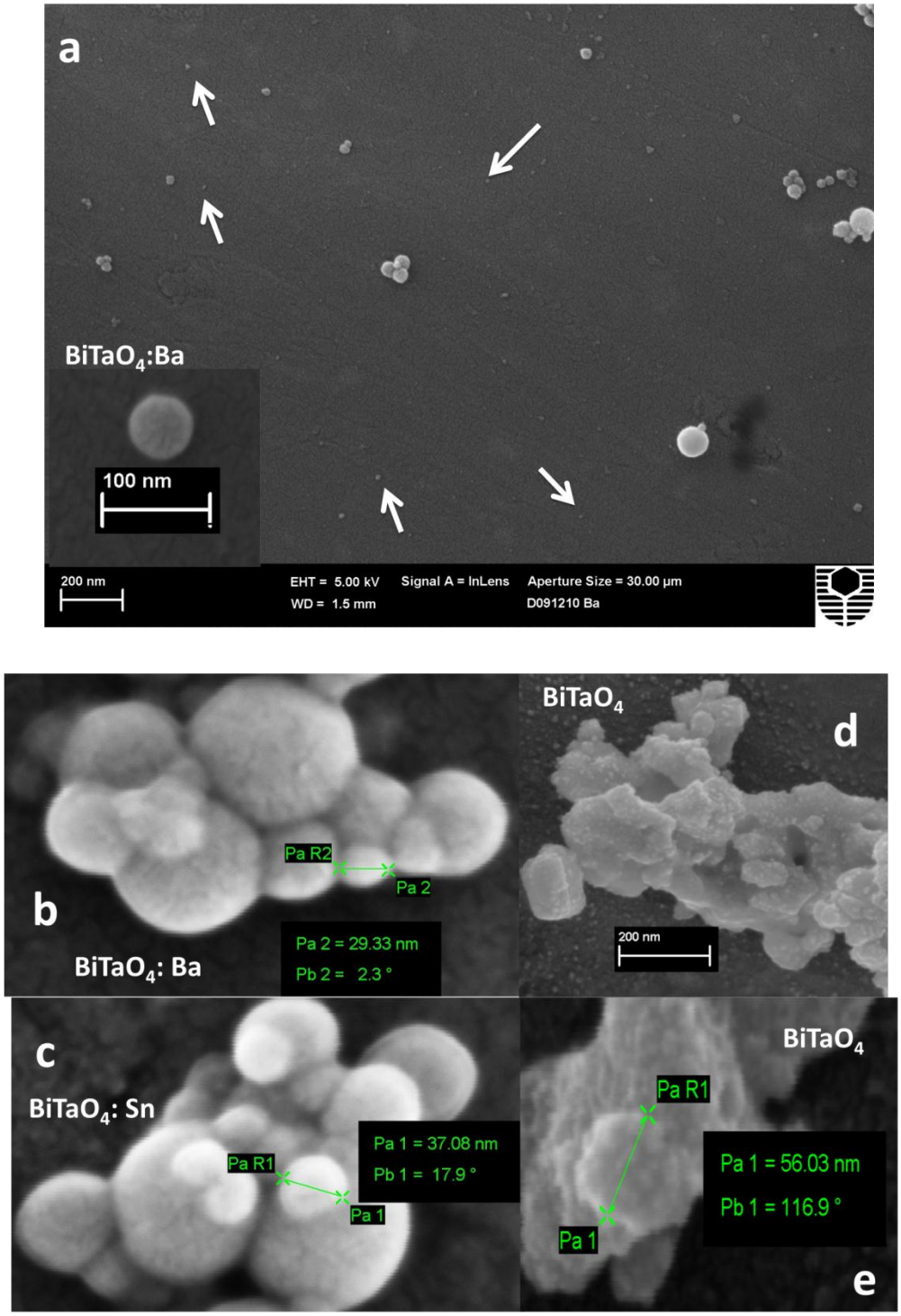

Figure: 4.4 SEM micrograph of $BiTaO_4$: Ba (a, b), $BiTaO_4$: Sn (C), and Undoped $BiTaO_4$ (d, e).

Morphology, shapes and crystalline sizes of doped and undoped $BiTaO_4$ was determined with scanning electron microscopy. Figure 4.4 shows the SEM micrographs of both doped and undoped samples. $BiTaO_4$ agglomerated in different sizes and shapes. The particle sizes were in nano-scale and the particles as small as 7 nm were observed. Although, undoped $BiTaO_4$ has bigger agglomerates than the doped samples, the average particle size was found to be less than 100 nm, unlike other research work[16], [32], [43].

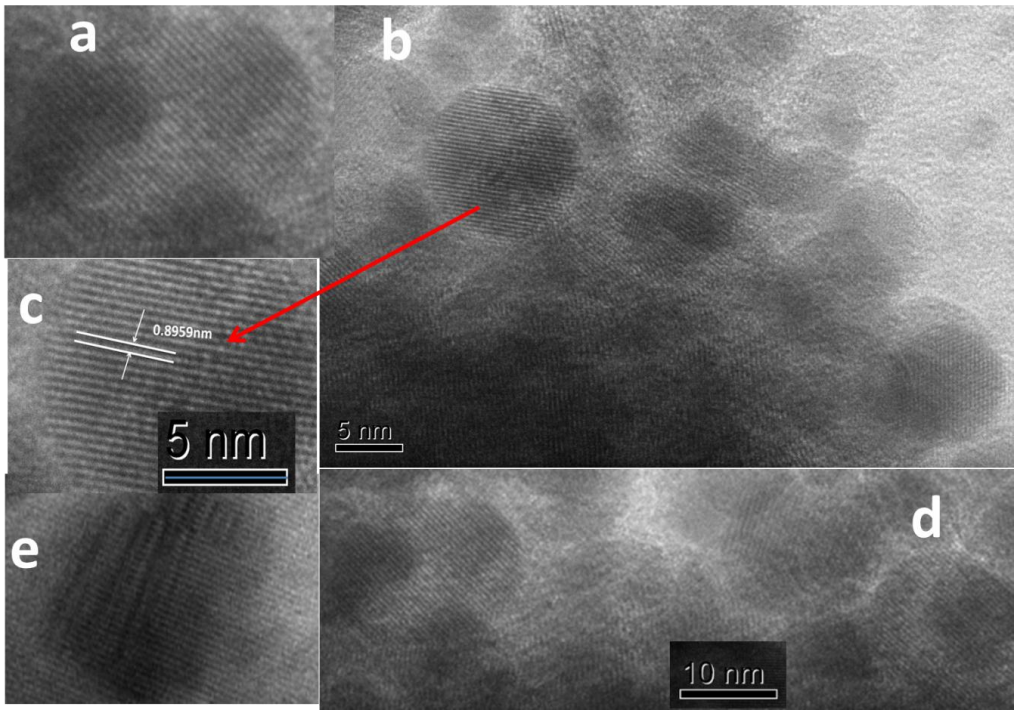

Figure: 4.5 TEM images of undoped $BiTaO_4$, (a) doped $BiTaO_4$ (b, c, d) and crystalline defects (e).

High resolution transmission electron micrographs (Figure 4.5) of prepared materials showed the crystal planes, indicating regularly arranged atomic layers in the crystallites. The average single crystallite size was 5 to 15 nm. Crystallographic planes of undoped (Figure 4.5a) and doped $BiTaO_4$ (Figures 4.5b, c, and d) were almost similar. Crystalline plane spacings were exactly corresponded to the planes of $BiTaO_4$ as observed by XRD analysis. Figure 5e shows some uneven distribution of atomic layers, which arise from the defects in the crystalline structures. These defects are caused by i) difference in the dopant ionic size[44], [45], ii) oxygen

vacanies [46], and iii) planes slipping. It must be noted that the presence of the defects are benefical [47] for photocatalytic processes, because they may serve as active sites[48], [44], where electron-hole pair can be easily generated by irradiation.

Table 4.2 Absorption and edge and band gap of doped $BiTaO_4$

Dopant	Concentration (% w/w)	Absorption edge (nm)	Band gap (eV)
Undoped	0	405	3.06
Gallium	2	413	3.00
Tungsten	2	425	2.92
Nickel	2	440	2.81
Aluminium	2	498	2.49
Chromium	2	500	2.48
Tin	2	502	2.47
Neodymium	2	505	2.46
Lanthanum	2	510	2.43
Barium	2	515	2.40
Silver	2	525	2.36
Lead	2	528	2.35
Copper	2	528	2.35
Cerium	2	570	2.18
Vanadium	2	575	2.16
Iron	2	600	2.10
Cobalt	2	650	1.91

The optical absorption of undoped and doped materials was determined by diffuse reflectance spectroscopy. As shown in Table 4.2 and Figure 4.6, undoped sample has absorption edge at 405 nm and therefore its response to visible light is very limited, while the absorption edges of doped materials are shifted to longer wavelengths. Since both the type and content of dopants have strong effects on the optical and electronic properties of the materials[49], therefore concentration of all the dopants ions in our case was kept constant (at 2% by mol). However, the effect

of various dopants on the optical and electrical properties of $BiTaO_4$ was different. In fact, these metal dopants i) have varying ionic sizes, ii) occupy different positions (substitution, interstitial) in the lattice structure, iii) contribute different energy levels to the conduction and valence bands of $BiTaO_4$, and iv) generate oxygen vacancies at various energy levels. Thus, each metal dopant responded independently to the optical absorption of $BiTaO_4$.

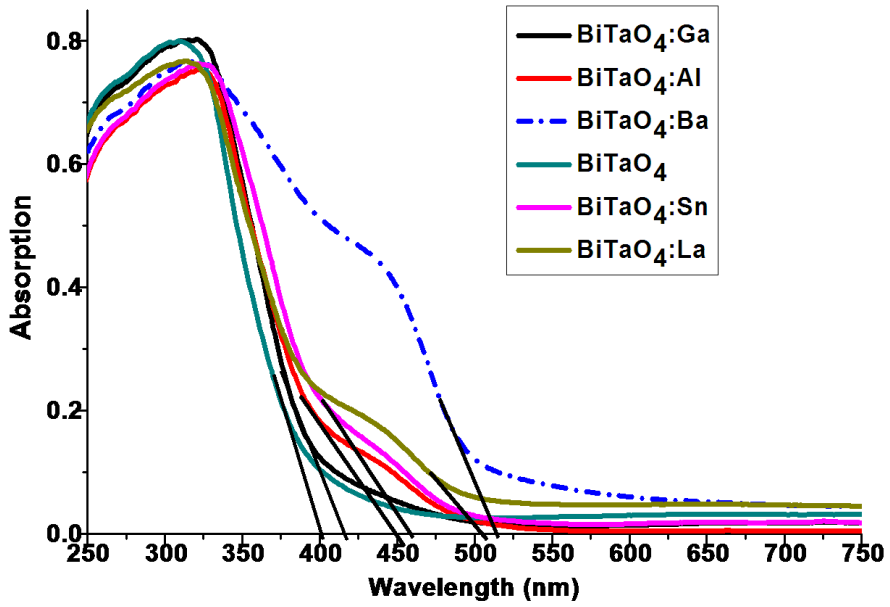

Figure: 4.6 UV-Vis diffuse reflectance spectroscopy of the selected materials.

Scheme 4.1 shows the proposed band gap miniaturization due to doping, where the apparent band gap of doped $BiTaO_4$ was reduced due to two main reasons i.e. addition of dopant energy level just above the valence band [50] and creation of large amount of oxygen vacancies[51], [52] at various energy positions. Additionally, formation of localized energy levels[53] (at the bottom of conduction band due to dopant 3d orbitals) [54], [55] and hybridization of the valence band (due to dopant's orbitals) are other two reasons, which contribute to band gap reduction. Obviously dopants like Ba, Ag, Pb, Cu, Ce, V, Fe and Co significantly increased the optical absorption in the visible range, but these dopants except Ba could not substantially increase the photocatalytic activities of doped $BiTaO_4$. Since

the conduction band of $BiTaO_4$ is mainly composed of Ta 5d, and Bi 6p along with a small contribution of O 2p orbitals [16]. We assume that 3d orbital of dopants like Ba, Ag, Pb, Cu, V, Fe, Co or 4f orbital of Ce [56] also contributes to the conduction band of $BiTaO_4$ and introduces a localized energy level just below the conduction band. As indicated by dotted arrows (Scheme 4.1) the electronic transition between the dopant states and localized energy levels results in huge visible light absorption. However, the localized energy states also serve as recombination centres [57], and have adverse effect on the photocatalytic performance of materials. Enhanced visible light absorption, but negative effect on photocatalytic performance of Cr, V [57], Co [58], Cu [51], and Fe doping have been also reported in TiO_2.

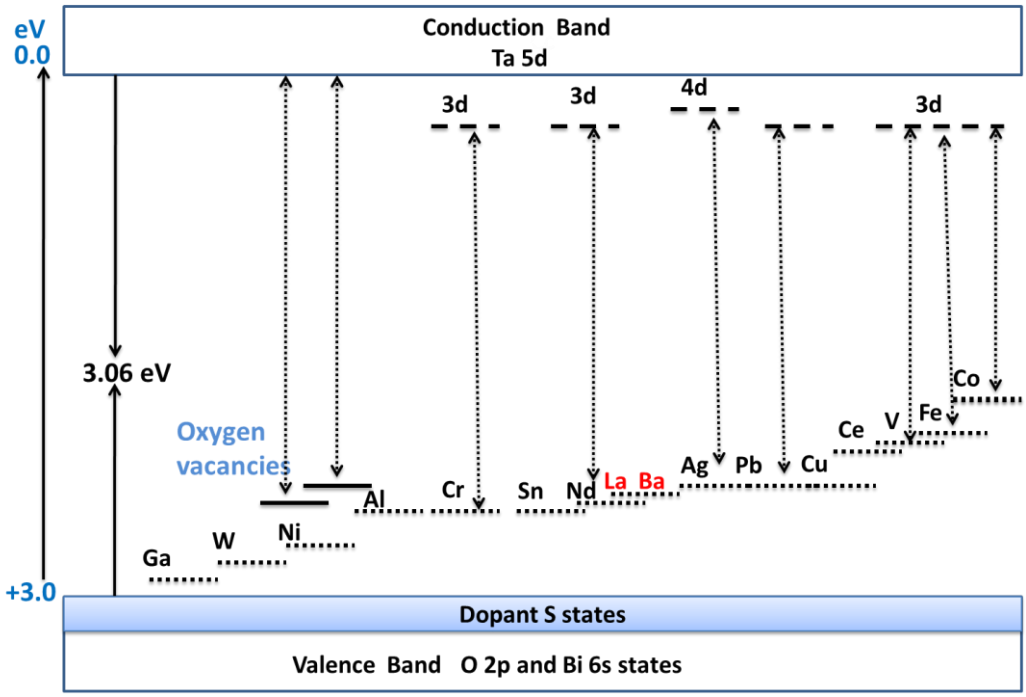

Scheme 4.1: Band gap modification of $BiTaO_4$ with various dopant ions.

We further assume that along with the creation of dopant level and oxygen vacancies, dopants like Nd, La, Ga, Sn, Al, Sb, and W also hybridize the valence band by tallying s orbitals. These dopants do not create localized energy states, which can cause recombination of photo-generated carriers. This valence band hybridization by s orbitals of dopants produces a red shift of the absorption, and

enhance the life time of photo-generated hole, which suppress the recombination process.

Fourier transform infrared analysis of doped and undoped $BiTaO_4$ shown in Figure 4.7 clearly indicates the presence of Bi-O, and Ta-O bindings. Sharp bands at 878-882 cm^{-1}[59] correspond to the vibration mode of Ta-O-Ta and the broad band at 1000-1100 cm^{-1} [6], [16] could be assigned to both Bi-O and Ta-O vibrations. The weak peak at 1618 cm^{-1} corresponded to the adsorbed water molecules on $BiTaO_4$ surface[60]. Figure 4.7 further reveals that both the doped and undoped samples have exactly the same behaviour.

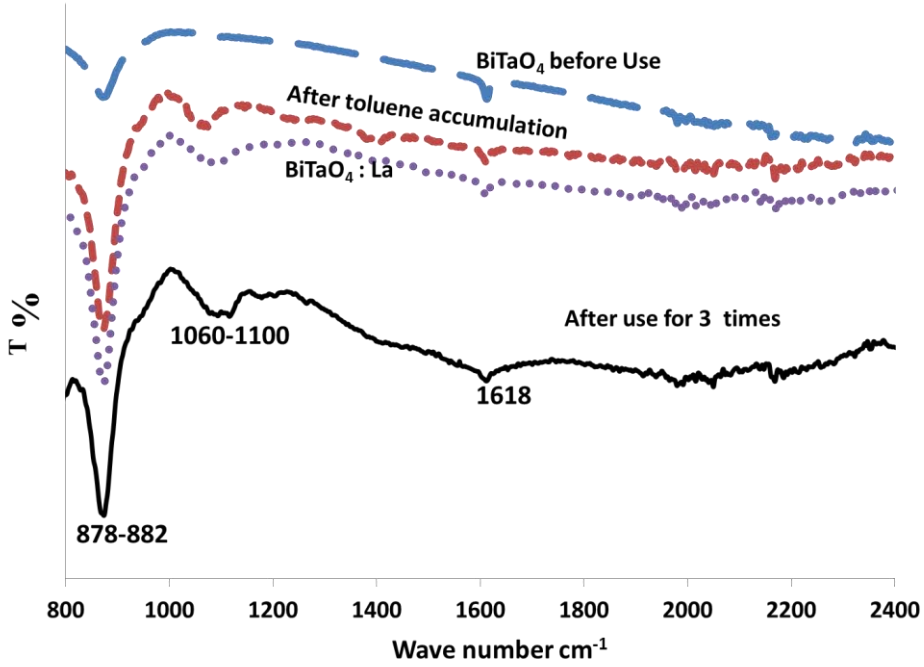

Figure: 4.7 FTIR analysis of BiTaO4, before and after use showing peaks for B-O, and water.

4.4 Photocatalytic activities

4.3.2 Toluene decomposition in air

Figure 4.8 and Table 4.3 show toluene decomposition with metal ion (La, Al, Nd, Ba, W, Sb, Pb, Co, Ag, Ga, Ni, Cr, V, Cu and Ce) doped $BiTaO_4$ under UV irradiation. Both Table 4.3 and Figure 4.8 reveal that dopants like La, Al, Nd, Sn,

Ga, and Ba have a promoting effect, while dopants like Ce, V, Cu, Ni, Pb, and Cr present an adverse effect on the photocatalytic performance. It has been found that La, Al, and Nd doped $BiTaO_4$ showed excellent performance and were capable to decompose about 40-48% of toluene within the first two hours of UV irradiation. Furthermore, $BiTaO_4$ doped with Al, La, and Nd presented better activity than undoped $BiTaO_4$ and TiO_2 in the initial 5 hours of UV irradiation. Although TiO_2 activity in the initial first hour was comparatively better, $BiTaO_4$ doped with Al, La, and Nd showed much stable performance than TiO_2 after 3 hours. Photocatalytic decomposition of toluene on doped $BiTaO_4$ materials irradiated with UV light shows the trend of La> Al> TiO_2> Nd> Ba> W> Sb> undoped> Pb> Co> Ag> Ga> Ni> Cr> V> Cu> Ce. Although the dopants like Ce, Cu, Cr, Fe, and Ni had a significant effect on the optical absorption of $BiTaO_4$, these dopant modified catalysts did not show toluene decomposition with UV irradiation. It was reported that TiO_2 doped with metal ions like Ce, Cu[51], Fe [57] , Cr [57] and Co[58] have reduced photocatalytic properties.

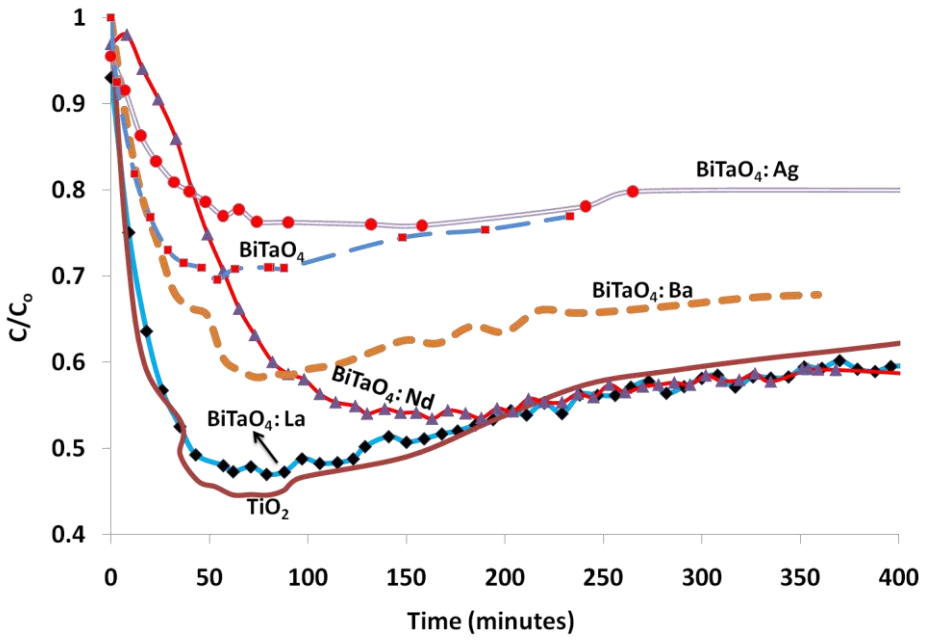

Figure: 4.8 Photocatalytic decomposition of toluene with various doped $BiTaO_4$ materials and UV irradiation.

Table 4.3: Photocatalytic decomposition of toluene with doped $BiTaO_4$ under UV and visible light.

Dopant	Concentration (%)	C/Co	
		Visible	UV
Undoped	None	15.58	24.39
Lanthanum	0.5	13.77	-
	1	2.02	13
	2	15.43	48
	5	8.72	12.12
Aluminium	1	12.54	12.28
	2	17.39	47
	3	5.78	22.85
Barium	0.5	0	10.13
	1	14.85	29.65
	2	11.45	34.62
	3	16.96	22.19
	5	15.64	31.0
Gallium	1	7.53	30
	2	7.42	18.10
	3	20.58	26
Tin	2	19.31	40.41
	3	6.94	21.34
Neodymium	2	13.97	33.10
	5	8.75	2.10
Antimony	2	0	27
Lead	2	0	23.12
Cobalt	2	3	21.03
Silver	2	14.39	19.64
Nickel	2	0	6.56
Iron	2	13.12	1.5
Chromium	2	4.31	0
Vanadium	2	0.88	0
Copper	2	0.69	0
Cerium	2	0	0

Figure 4.9 shows decomposition of toluene under visible light irradiation, where $BiTaO_4$ doped with 3% Ga has better performance than others, since this material

removed about 20.0% of toluene within initial two hours. However, toluene decomposition with doped (2%) materials irradiated with visible light have the trend of Sn>Al>W>La>undoped>Ag>Ne>Fe>Ba>Ga>TiO_2>Cr>Co>V>Cu, while lead, antimony, nickel, and cerium doped materials showed no activity under the similar conditions. This trend of photocatalytic activity is different from that at UV light. As shown in Table 4.3 under UV light irradiation $BiTaO_4$: La has better performance. An important observation is that the photocatalytic removal of toluene with $BiTaO_4$: La under UV light irradiation is more than doubled when irradiated with visible light. However, in case of $BiTaO_4$: Ga (3%), photocatalytic activity of the material under visible light is almost similar to that with UV light. As the content of dopants also affects the performance of materials, therefore, we used different dopant concentrations. Except gallium which has enhanced activity for 3 mol%, all other dopants showed enhanced activity, when doped at 2 mol%. Photocatalytic activities of the doped materials augmented by shifting the radiation's wavelength from higher to lower, since the intensity and energy of photo-generated electron-hole pair increases. However, $BiTaO_4$: Fe has very good photocatalytic activity with visible light, while its activity becomes extinct when irradiated with UV light. Further, it can be seen from Table 3 that $BiTaO_4$ doped with lead, antimony and cobalt are active under UV light while these materials are totally dull with visible light. The varying behaviour of doped materials under UV and visible light irradiation is attributed to the different type of changes which the dopant ions made to the parent materials. As explained in Scheme 4.1, each dopant ion i) generates dopant energy level at different positions, ii) generates oxygen vacancies of different energies, and iii) modifies the optical absorption differently.

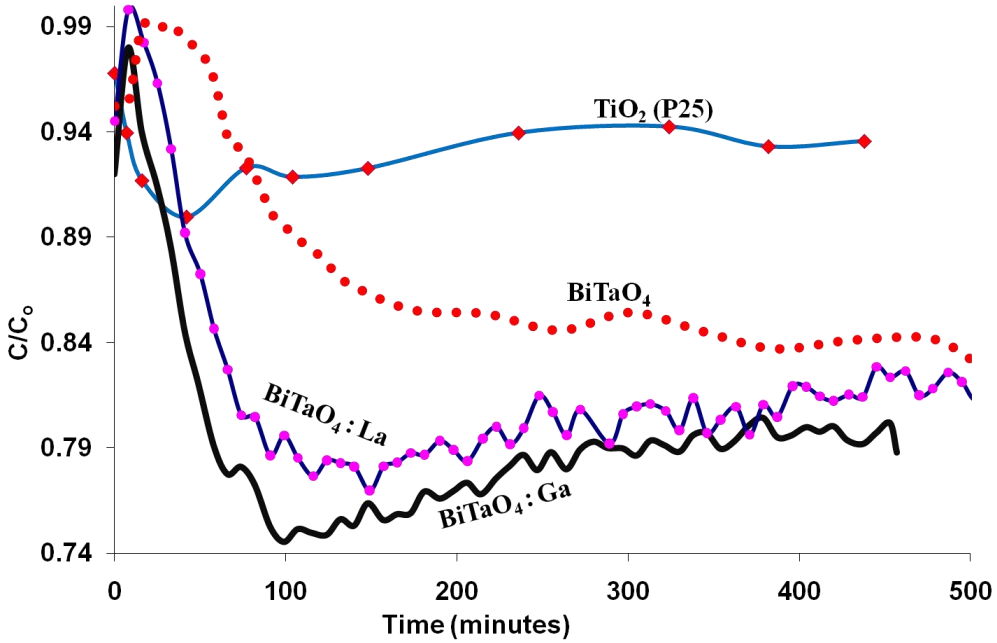

Figure: 4.9 Photocatalytic decomposition of toluene with various doped $BiTaO_4$ materials and visible.

In view of all these, $BiTaO_4$ materials doped with Cu, Ce, Cr, Ni, and V were not active under either UV light or visible light irradiation. Dopants like Ce^{4+}, Cu^{2+}, Ni^{2+}, Cr^{3+}, and V^{4+} may be reduced by capturing electrons on oxygen vacancies [56]. This reduction in the dopant ions resulted in deactivation of the oxygen vacancies, which are the main sites for photocatalytic activities. As suggested in Scheme 4.1 the localized energy levels generated by these dopants (Cu, Ce, Cr, Ni, and V) under the conduction band of the material serve as recombination centres. The photo-generated carriers are trapped by these localized energy levels and re-combination before participating in the useful reactions. So the reduced photocatalytic activity of Cu, Ce, Cr, Ni, and V doped materials is attributed to both the deactivation of the oxygen vacancies and enhanced recombination of photo-generated carriers by the localized energy levels. Although we have recently shown that Ni doping in $InTaO_4$ enhanced the photocatalytic properties of materials, it was mainly attributed to the existence of NiO on the surface of material, which was acting as electron trapping centres. These dopant oxides (NiO) on the surface trap photo-generated electrons and allow the holes for the preceding oxidation reactions. However, we presumably exclude existence of such dopant oxides in case of

$BiTaO_4$ doped with Cu, Ce, Cr, Ni, and V. On the other hand these dopants reduce the oxygen vacancies and generate recombination centres, which both are critical to the photocatalytic activity. The adverse effect of Cu [51], Co [58], Cr, and V[57] doping on photocatalytic activities has been also reported for TiO_2, where the lower activity of these doped materials was attributed to the enhanced recombination caused by the doping and closed electronic shell of Co. Although, Zhang et al. [16] reported an improved photocatalytic activity for Cu doped $BiTaO_4$, the material was coated with RuO_2, where the later acted as a co-catalyst. Similarly, NiO coated and La doped $NaTaO_3$ also showed better performance for water splitting[61].

As explain in Scheme 4.1 dopants like Nd, La, Ga, Sn, Al, Sb, and W create dopant levels above the valence band, produce oxygen vacancies at various energy positions and hybridize the valence band by tallying their s orbitals. This valence band hybridization by s orbitals of dopant produced red shift absorption, and enhanced the life time of photo-generated holes, which suppress the recombination process. Thus the enhanced photocatalytic performance of material doped with Nd, La, Ga, Sn, Al, Sb, Ba, and W is attributed to the combined effect of enhanced oxygen vacancies, hybridized valence band and reduced band gap.

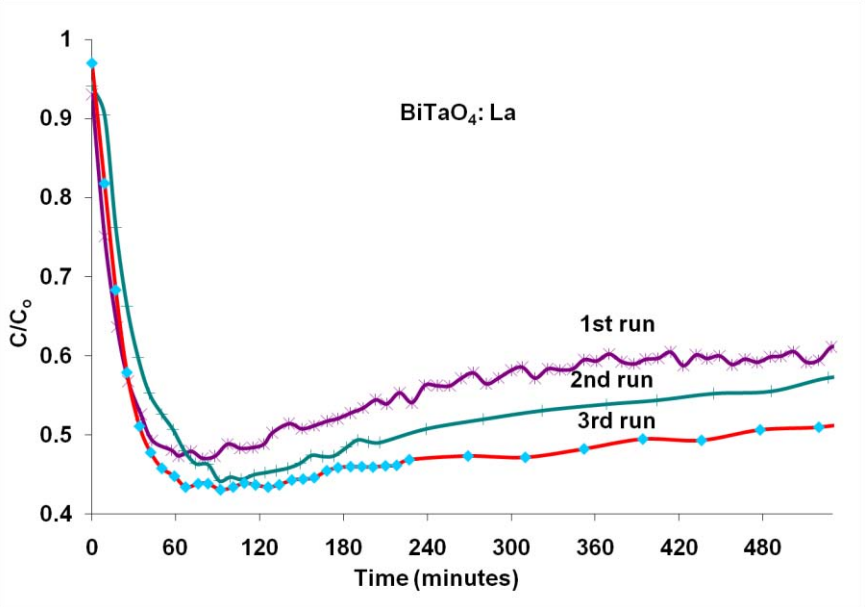

Figure: 4.10 Photocatalytic decomposition of toluene with $BiTaO_4$: La repeated three times under UV irradiation.

Stability, re-useability and life time of the photocatalytic materials have been a major concern for most of the photocatalytic materials. Interestingly we found that the photocatalytic activities of both undoped and doped with lanthanum and barium $BiTaO_4$ are increased in regenerated use. Figure 4.10 shows that photocatalytic activity of $BiTaO_4$: La increases at the second and third runs. This increase in the photocatalytic activity of the used $BiTaO_4$ has never been reported before. We assume that, some minor defects (such as oxygen vacancies) have been created each time when the material is exposed to irradiation. However, creation of these defects does not affect the crystal structure of the material. Figure 4.11 compares XRD patterns of the material before and after using for 3 times, which clearly indicates that the material is quite stable and remains unchanged even when used repeatedly. This strong stability and longer time utilization of $BiTaO_4$ has been reported in case of methylene blue degradation under UV irradiation[32].

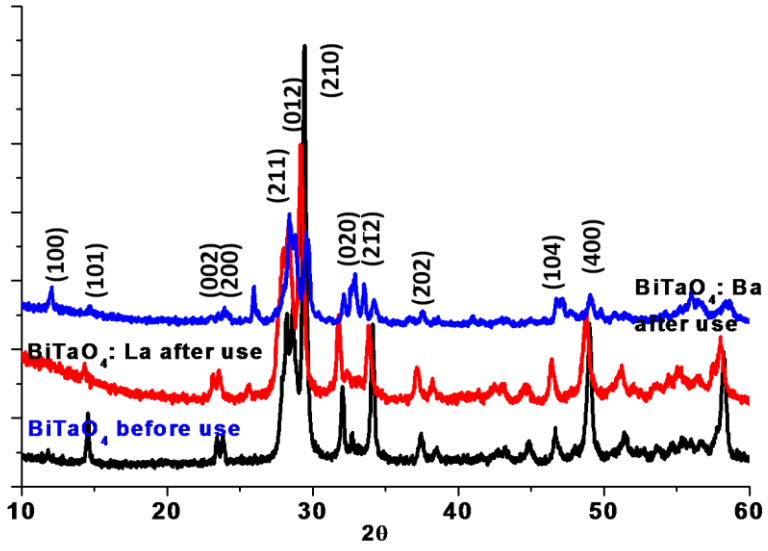

Figure 4.11

Figure 4.11 XRD analysis of doped and undoped $BiTaO_4$ before and after using for photocatalytic reaction.

Figure 4.12 shows that $BiTaO_4$ doped with aluminium and neodymium could be used for a long time as compared to TiO_2, since these two materials maintained

their activities for a longer time. Although the commercial photocatalyst TiO_2 exhibited better performance in the initial two hours, its immediate and irreversible deactivation reduced its photocatalytic activity. The deactivation and short life time of TiO_2 are due to the adsorption of intermediates on the active surface. FTIR analysis (Figure 4.13) confirmed the existence of intermediate products such as water, benzaldehyde and benzoic acid on TiO_2. However, no evidence of intermediate adsorption was observed on $BiTaO_4$ surface. These various types of analysis suggest that $BiTaO_4$ doped with various metal ions, particularly Al, La and Nd, not only have a longer life time but can also be used repeatedly without losing its activity. This everlasting stability, longer life time and re-activation of doped $BiTaO_4$ are mainly attributed to the lower adsorption of intermediates on its surface.

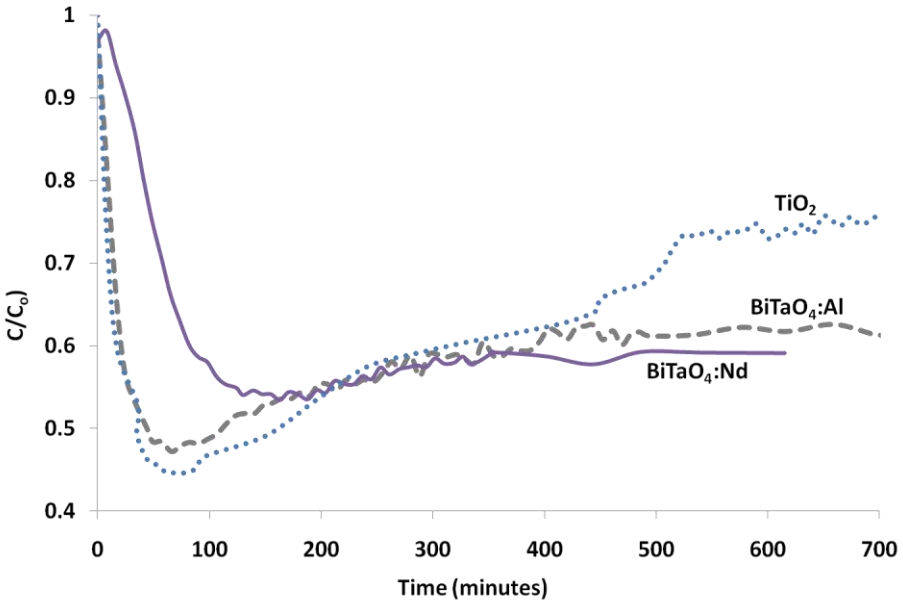

Figure: 4.12 Comparing photocatalytic performance of $BiTaO_4$ doped with Nd and La with that of TiO_2.

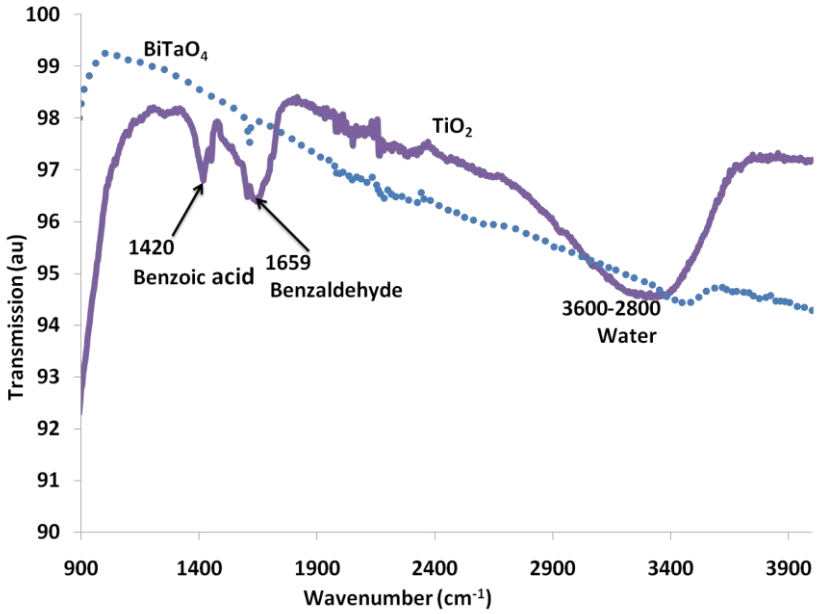

Figure: 4.13 FTIR analysis of used $BiTaO_4$ and TiO_2, showing adsorption of water and intermediates on TiO_2.

4.3.3 Methylene blue decomposition in water

Photocatalytic activities of metal ion doped $BiTaO_4$ were examined for decomposition of methylene blue (MB) both under UV and visible light irradiations as shown in Figure 4.14. $BiTaO_4$: Al decolorized methylene blue at a faster rate than undoped and other metal ion doped materials. Photocatalytic decomposition of methylene blue under UV irradiation did not follow the same trend as what was observed in the gaseous toluene decomposition. Under UV irradiation, the trend of methylene blue decomposition on various metal ion doped $BiTaO_4$ catalysts was $BiTaO_4$: Al> $BiTaO_4$: Sn> $BiTaO_4$> $BiTaO_4$: La > $BiTaO_4$: Nd> $BiTaO_4$: Ga> $BiTaO_4$: Ce> $BiTaO_4$: Fe> $BiTaO_4$: V. Although aluminium doped $BiTaO_4$ degraded methylene blue with much faster rate than the others, most of the doped materials except $BiTaO_4$: Ce, $BiTaO_4$: Fe and $BiTaO_4$: V have shown similar behaviour toward complete degradation of MB. It was observed that different ion doped materials along with the undoped $BiTaO_4$ completely decolorized MB within 5 h. However, efficacy of the materials reduced to 50% when irradiated with visible light. As shown in Figure 4.15, both $BiTaO_4$: Sn and $BiTaO_4$: Al degraded MB

under visible light irradiation with a slower rate. Since visible light absorption of the materials is mainly due to the existence of various types of defects, while the concentration of these defects are very limited, therefore, photo-generated electron-hole pairs will also be limited. Thus, visible light irradiation will generate less number of electron-hole pairs as compared to UV light irradiation. The smaller the number of electron-hole pair, the lower the concentration of reactive species and the lower the degradation rate of VOCs are. Figure 4.14 further reveals that vanadium, cerium and iron have a detrimental effect resulting in the lower photocatalytic activity. Such an effect of vanadium, cerium, and iron doping on photocatalytic properties of TiO_2 has also been reported [50]. Additionally we have recently found similar reduction in activity of vanadium doped $InTaO_4$ [44].

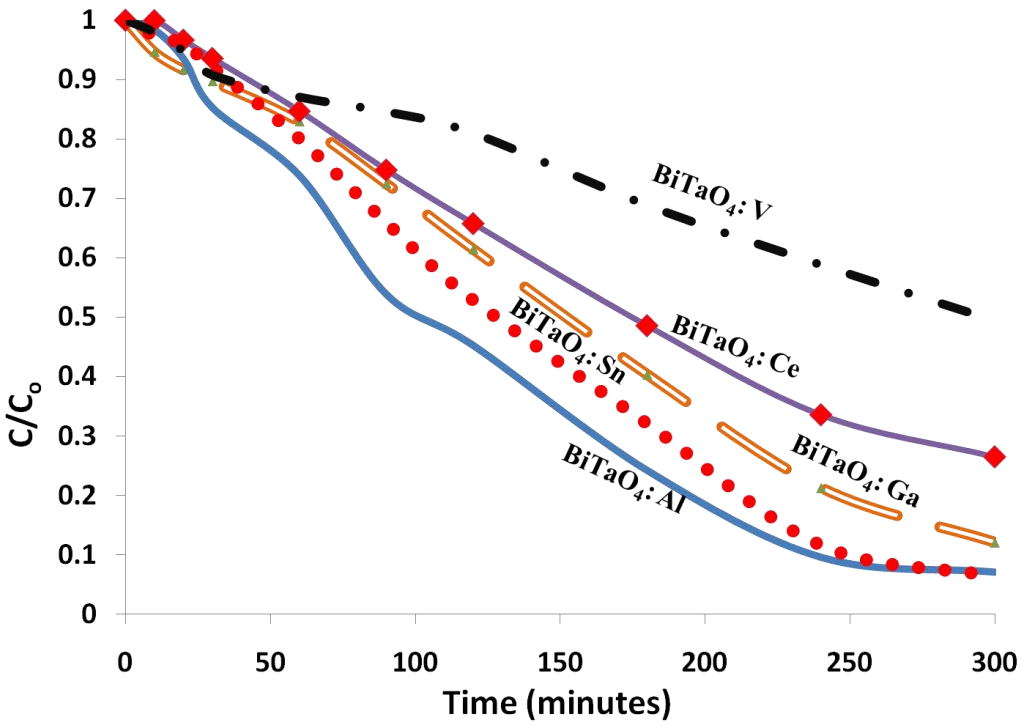

Figure: 4.14 Photocatalytic decomposition of methylene blue in water with doped $BiTaO_4$ and UV light irradiation.

As detailed in the section of characterization, some dopants like Fe^{2+}, Co^{2+}, and V^{3+} improve the optical absorption but could not increase the photocatalytic activities. Reduction in the photocatalytic activities of Ce, Fe, and V-doped $BiTaO_4$ is due to

increased recombination of electron-hole pairs. Since 3d orbitals of V, Fe, and 4f orbitals of Ce ions create localized energy level below the conduction band which act as recombination centres. Although, $BiTaO_4$: V, $BiTaO_4$: Fe, $BiTaO_4$: Ce have much improved absorption in the visible region, high recombination rate[57] of electron-hole pairs make these dopants (V, Ce, and Fe) detrimental to photocatalytic activities [50].

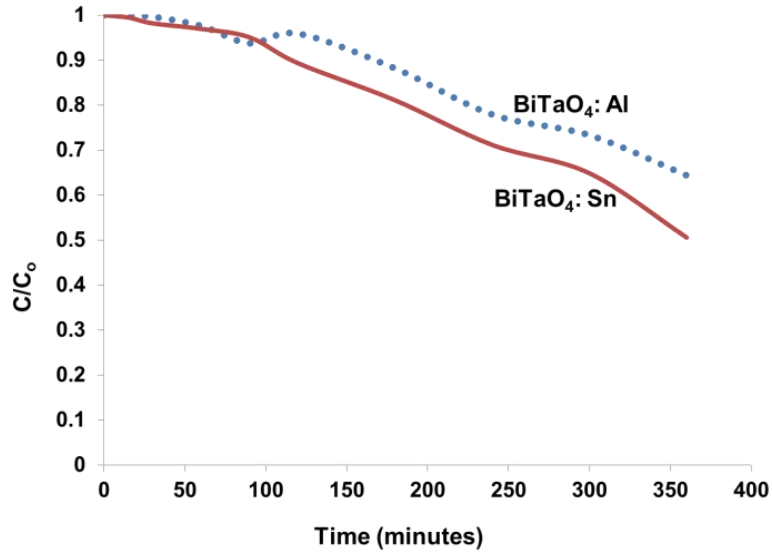

Figure: 4.15 Methylene blue decomposition with $BiTaO_4$ doped with Sn and Al irradiated with visible light.

By comparing the photocatalytic activity of doped $BiTaO_4$ with TiO_2-P25 for removal of VOCs in water, we found that, these materials have much lower activity than TiO_2, since the latter could degrade MB very quickly. The lower performance of doped $BiTaO_4$ than TiO_2 in liquid is mainly due to the; i) smaller surface area, ii) lower water adsorption, and iii) lower solid liquid interface of $BiTaO_4$.

4.5 Conclusion

Undoped triclinic $BiTaO_4$ and doped with various metal ion (Al, Nd, La, Ga, Ba, Sn, W, Fe, Co, Cr, Ce, Cu, Sb, Pb, Ni, Ag) catalysts have been successfully synthesized with a solution method at lower sintering temperature of 700 °C. The average particle size was in the range of nanometres. TEM micrograph showed the presence of defects on the surface of the materials, which are essential for enhanced

photocatalytic activity both under UV and visible light. Doping of $BiTaO_4$ with various metal ions not only enhanced the optical absorption but also increased the photocatalytic activities of the materials. Dopants like Cu, Cr, Ce, Ni, Pb, and Co were not successful to improve the photocatalytic activities, but La, Al, Ga and Nd significantly increased the performance in toluene decomposition. Metal dopants like Sn, Ba, Sb, Fe, and Ag were also successful to modify the photocatalytic properties of the materials. Most importantly, $BiTaO_4$ doped with La was found not only to be stable and have longer life time, but to be used repeatedly with increased performance. Upon comparing with TiO_2, $BiTaO_4$ doped with Nd, Al, and La were found to have better performance, longer life time and more stability for gaseous toluene decomposition. The enhanced photocatalytic activity of $BiTaO_4$ doped with metal ions (Al, Nd, La, Ga, Ba, Sn, W, Fe, Sb, and Ag) was mainly attributed to the large number of oxygen vacancies created by doping, reduced band gap and valence band hybridization. Unlike TiO_2, no intermediate and water adsorption was occurred on metal doped $BiTaO_4$. However, metal doped $BiTaO_4$ was found to have lower photocatalytic activity than TiO_2 when used for methylene blue decomposition in water. The lower photocatalytic activity for methylene blue in water is due the smaller surface area of $BiTaO_4$ than TiO_2. It can be summarized that metal doped $BiTaO_4$ can efficiently decompose air contaminants with both UV and visible light. These materials are also effective for removal of water contaminants.

4.6 Reference

1. Zou, Z., et al., *Direct splitting of water under visible light irradiation with an oxide semiconductor photocatalyst.* Nature, 2001. **414**(6864): p. 625-627.

2. Hui, A., et al., *Lifestyle intervention on diet and exercise reduced excessive gestational weight gain in pregnant women under a randomised controlled trial.* BJOG, 2011.

3. F.B. Li, et al., *Enhanced photocatalytic degradation of VOCs using Ln3+–TiO2 catalysts for indoor air purification.* Chemosphere 2005. **59** p. 787–800.

4. Barreca, D., et al., *Photoinduced superhydrophilicity and photocatalytic properties of ZnO nanoplatelets.* Surface and Coatings Technology, 2009. **203**(14): p. 2041-2045.

5. Demeestere, K., et al., *Visible light mediated photocatalytic degradation of gaseous trichloroethylene and dimethyl sulfide on modified titanium dioxide.* Applied Catalysis B: Environmental, 2005. **61**(1-2): p. 140-149.

6. Zhang, G., et al., *Synthesis of nanometer-size Bi3TaO7 and its visible-light photocatalytic activity for the degradation of a 4BS dye.* Journal of Colloid and Interface Science, 2010. **345**(2): p. 467-473.

7. Ye, J. and Z. Zou, *Visible light sensitive photocatalysts In1-xMxTaO4 (M=3d transition-metal) and their activity controlling factors.* Journal of Physics and Chemistry of Solids, 2005. **66**(2-4): p. 266-273.

8. Yan, H., et al., *Visible-light-driven hydrogen production with extremely high quantum efficiency on Pt-PdS/CdS photocatalyst.* Journal of Catalysis, 2009. **266**(2): p. 165-168.

9. Li, G.-S., D.-Q. Zhang, and J.C. Yu, *A New Visible-Light Photocatalyst: CdS Quantum Dots Embedded Mesoporous TiO2.* Environmental science & technology, 2009. **43**(18): p. 7079-7085.

10. Sun, M., et al., *Photocatalyst Cd2Sb2O6.8 with High Photocatalytic Activity toward Benzene and Dyes.* The Journal of Physical Chemistry C, 2009. **113**(33): p. 14916-14921.

11. Wang, S.B., H.M. Ang, and M.O. Tade, *Volatile organic compounds in indoor environment and photocatalytic oxidation: State of the art.* Environment International, 2007. **33**(5): p. 694-705.

12. Li, H., G. Liu, and X. Duan, *Monoclinic BiVO4 with regular morphologies: Hydrothermal synthesis, characterization and photocatalytic properties.* Materials Chemistry and Physics, 2009. **115**(1): p. 9-13.

13. Xu, H., et al., *Synthesis, characterization and photocatalytic activities of rare earth-loaded BiVO4 catalysts.* Applied Surface Science, 2009. **256**(3): p. 597-602.

14. Dunkle, S.S. and K.S. Suslick, *Photodegradation of BiNbO4 Powder during Photocatalytic Reactions.* The Journal of Physical Chemistry C, 2009. **113**(24): p. 10341-10345.

15. Subramanian, M.A. and J.C. Calabrese, *Crystal structure of the low temperature form of bismuth niobium oxide [[alpha]-BiNbO4]*. Materials Research Bulletin, 1993. **28**(6): p. 523-529.

16. Zhang, H., et al., *Electronic structure and water splitting under visible light irradiation of BiTa1-xCuxO4 (x = 0.00-0.04) photocatalysts.* International journal of hydrogen energy, 2009. **34**(9): p. 3631-3638.

17. Shi, H., et al., *2-Propanol photodegradation over nitrogen-doped NaNbO3 powders under visible-light irradiation.* Journal of Physics and Chemistry of Solids, 2009. **70**(6): p. 931-935.

18. Sleight, A., *Ferroelastic transitions in B-bismuth niobate (B-BiNbO4) and B-bismuth tantalate (B-BiTaO4).* Acta crystallographica. Section B, Structural crystallography and crystal chemistry, 1975. B31Acta Crystallogr., Sect. B(11): p. 2748.

19. Wang, N., M.-Y. Zhao, and Z.-W. Yin, *Effects of Ta2O5 on microwave dielectric properties of BiNbO4 ceramics.* Materials Science and Engineering B, 2003. **99**(1-3): p. 238-242.

20. Yuan, Z., et al., *Effect of metal ion dopants on photochemical properties of anatase TiO2 films synthesized by a modified sol-gel method.* Thin Solid Films, 2007. **515**(18): p. 7091-7095.

21. Ihara, T., et al., *Visible-light-active titanium oxide photocatalyst realized by an oxygen-deficient structure and by nitrogen doping.* Applied Catalysis B: Environmental, 2003. **42**(4): p. 403-409.

22. Liu, G., et al., *Band-to-Band Visible-Light Photon Excitation and Photoactivity Induced by Homogeneous Nitrogen Doping in Layered Titanates.* Chemistry of Materials, 2009. **21**(7): p. 1266-1274.

23. Stodolny, M. and M. Laniecki, *Synthesis and characterization of mesoporous Ta2O5-TiO2 photocatalysts for water splitting.* Catalysis Today, 2009. **142**(3-4): p. 314-319.

24. Huang, H., et al., *Efficient Degradation of Benzene over LaVO4/TiO2 Nanocrystalline Heterojunction Photocatalyst under Visible Light Irradiation.* Environmental science & technology, 2009. **43**(11): p. 4164-4168.

25. Asahi, R., et al., *Visible-light photocatalysis in nitrogen-doped titanium oxides* Science., 2001. **293**: p. 269-271.

26. Sun, H.Q., et al., *Halogen element modified titanium dioxide for visible light photocatalysis.* Chemical Engineering Journal, 2010. **162**(2): p. 437-447.

27. Shang, J., et al., *Comparative Studies on the Deactivation and Regeneration of TiO2 Nanoparticles in Three Photocatalytic Oxidation Systems: C7H16, SO2, and C7H16-SO2.* Journal of Solid State Chemistry, 2002. **166**(2): p. 395-399.

28. Hiroshi, I. and H. Kazuhito, *Visible Light-Sensitive InTaO4- Based Photocatalysts for Organic Decomposition.* Journal of the American Ceramic Society, 2005. **88**(11): p. 3137-3142.

29. Li, X. and J. Zang, *Facile Hydrothermal Synthesis of Sodium Tantalate (NaTaO3) Nanocubes and High Photocatalytic Properties.* The Journal of Physical Chemistry C, 2009. **113**(45): p. 19411-19418.

30. Fu, H., et al., *Visible-light-driven NaTaO3-xNx catalyst prepared by a hydrothermal process.* Materials Research Bulletin, 2008. **43**(4): p. 864-872.

31. Zou, Z., J. Ye, and H. Arakawa, *Structural properties of InNbO4 and InTaO4: correlation with photocatalytic and photophysical properties.* Chemical Physics Letters, 2000. **332**(3-4): p. 271-277.

32. Shi, R. and R. Shi, *Visible-Light Photocatalytic Degradation of BiTaO4 Photocatalyst and Mechanism of Photocorrosion Suppression.* The journal of physical chemistry. C, 2010. **114**(14): p. 6472.

33. Ye, J. and Z. Zou, *Visible light sensitive photocatalysts In1-xMxTaO4 (M=3d transition-metal) and their activity controlling factors.* Journal of Physics and Chemistry of Solids. **66**(2-4): p. 266-273.

34. Auvinen, J. and L. Wirtanen, *The influence of photocatalytic interior paints on indoor air quality.* Atmospheric Environment, 2008. **42**(18): p. 4101-4112.

35. Lee, C.-Y. and C. Lee, *Structural and spectroscopic studies of BiTa1-xNbxO4.* Journal of Solid State Chemistry, 2003. **174**(2): p. 310.

36. Muthurajan, H., *A co-precipitation technique to prepare BiTaO4 powders.* Materials Letters, 2008. **62**(3): p. 501.

37. Zou, Z., et al., *Photocatalytic and photophysical properties of a novel series of solid photocatalysts, BiTa1-xNbxO4* Chemical Physics Letters, 2001. **343**(3-4): p. 303-308.

38. Zou, Z. and Z. Zou, *Substitution effect of Ta5+ by Nb5+ on photocatalytic, photophysical, and structural properties of BiTaNbO4.* Journal of materials research, 2002. **17**(06): p. 1446.

39. Almeida, C.G., et al., *Synthesis of nanosized [beta]-BiTaO4 by the polymeric precursor method.* Materials Letters, 2010. **64**(9): p. 1088-1090.

40. Zou, Z. and Z. Zou, *Substitution effect of Ta5+ by Nb5+ on photocatalytic, photophysical, and structural properties of* BiTaNbO4. Journal of materials research, 2002. **17**(06): p. 1446.

41. Zou, Z., J. Ye, and H. Arakawa, *Optical and structural properties of the BiTa1-xNbxO4 compounds.* Solid State Communications, 2001. **119**(7): p. 471-475.

42. Zhou, D. and D. Zhou, *Phase composition and phase transformation in Bi(Sb,Nb,Ta)O4 system.* Solid State Sciences, 2009. **11**(11): p. 1894.

43. Almeida, C. and C.G.o.m.e.s. Almeida, *Synthesis of nanosized ÃŽÂ²-BiTaO4 by the polymeric precursor method.* Materials Letters, 2010. **64**(9): p. 1088.

44. Ullah, R., et al., *Wet-chemical Synthesis of InTaO4 for Photocatalytic Decomposition of Organic Contaminants in Air and Water with UV-vis Light.* Industrial & Engineering Chemistry Research, 2011: p. 10.1021/ie200544z.

45. Takata, T. and K. Domen, *Defect Engineering of Photocatalysts by Doping of Aliovalent Metal Cations for Efficient Water Splitting.* The Journal of Physical Chemistry C, 2009. **113**(45): p. 19386-19388.

46. Rodriguez, J.A., et al., *DeNOx Reactions on MgO(100), ZnxMg1-xO(100), CrxMg1-xO(100), and Cr2O3(0001): Correlation between Electronic and Chemical Properties of Mixed-Metal Oxides.* The Journal of Physical Chemistry B, 2001. **105**(23): p. 5497-5505.

47. Sun, H., et al., *Visible-light-driven TiO2 catalysts doped with low-concentration nitrogen species.* Solar Energy Materials and Solar Cells, 2008. **92**(1): p. 76-83.

48. Baruah, S. and et al., *Photocatalytic paper using zinc oxide nanorods.* Science and Technology of Advanced Materials, 2010. **11**(5): p. 055002.

49. Karvinen, S.M., *The Effects of Trace Element Doping on the Optical Properties and Photocatalytic Activity of Nanostructured Titanium Dioxide.* Industrial & Engineering Chemistry Research, 2003. **42**(5): p. 1035-1043.

50. Serpone, N., *Is the Band Gap of Pristine TiO2 Narrowed by Anion- and Cation-Doping of Titanium Dioxide in Second-Generation Photocatalysts?* The Journal of Physical Chemistry B, 2006. **110**(48): p. 24287-24293.

51. Jing, L., et al., *Effects of doping La and Cu on photoinduced charge properties of TiO₂ and its relationships with photocatalytic activity.* Science in China Series B: Chemistry, 2006. **49**(4): p. 345-350.

52. Kuznetsov, V.N. and N. Serpone, *On the Origin of the Spectral Bands in the Visible Absorption Spectra of Visible-Light-Active TiO2 Specimens Analysis and Assignments.* The Journal of Physical Chemistry C, 2009. **113**(34): p. 15110-15123.

53. Torres, G.R., et al., *Photoelectrochemical Study of Nitrogen-Doped Titanium Dioxide for Water Oxidation.* The Journal of Physical Chemistry B, 2004. **108**(19): p. 5995-6003.

54. Wang, J., Z. Zou, and J. Ye, *Surface modification and photocatalytic activity of distorted pyrochlore-type Bi2M(M=In, Ga and Fe)TaO7 photocatalysts.* Journal of Physics and Chemistry of Solids. **66**(2-4): p. 349-355.

55. Thimsen, E., et al., *Predicting the Band Structure of Mixed Transition Metal Oxides: Theory and Experiment.* The Journal of Physical Chemistry C, 2009. **113**(5): p. 2014-2021.

56. Iwaszuk, A. and M. Nolan, *Electronic Structure and Reactivity of Ce- and Zr-Doped TiO2: Assessing the Reliability of Density Functional Theory Approaches.* The Journal of Physical Chemistry C, 2011. **115**(26): p. 12995-13007.

57. Zhou, J., et al., *Photodegradation of Benzoic Acid over Metal-Doped TiO2.* Industrial & Engineering Chemistry Research, 2006. **45**(10): p. 3503-3511.

58. Choi, W., A. Termin, and M.R. Hoffmann, *The Role of Metal Ion Dopants in Quantum-Sized TiO2: Correlation between Photoreactivity and Charge*

Carrier Recombination Dynamics. The Journal of Physical Chemistry, 1994. **98**(51): p. 13669-13679.

59. Krishnan, R.R., et al., *Effect of doping and substrate temperature on the structural and optical properties of reactive pulsed laser ablated tin oxide doped tantalum oxide thin films.* Vacuum, 2010. **84**(10): p. 1204-1211.

60. Xi, X., et al., *Preparation and characterization of Ce-W composite nanopowder.* Materials Science and Engineering A, 2005. **394**(1-2): p. 360-365.

61. Kato, H., K. Asakura, and A. Kudo, *Highly Efficient Water Splitting into H2 and O2 over Lanthanum-Doped NaTaO3 Photocatalysts with High Crystallinity and Surface Nanostructure.* Journal of the American Chemical Society, 2003. **125**(10): p. 3082-3089.

5

5 - Visible Light Photocatalytic Activities on Nano-particles of Ternary Metal Oxides in Organics Degradation

Abstract

Various ternary metal oxides, Bi_2WO_6, $AgVO_3$, $AgTaO_3$, $BiTaO_4$, $Cd_2Ta_2O_7$, $InTaO_4$, $CoTa_2O_6$, $CeTaO_4$ and $EuTaO_4$, were synthesized with a solution method and were characterized by X-ray diffraction analysis (XRD), scanning electron microscopy (SEM), diffuse reflectance spectroscopy, and Fourier transform infrared spectroscopy (FTIR). All the materials were also tested for photocatalytic aqueous and gaseous VOCs decomposition. Results indicated that, tantalum based ternary compounds like $Cd_2Ta_2O_7$, $AgTaO_3$ and $BiTaO_4$ can decompose gaseous toluene under visible light irradiation with a much faster rate than TiO_2. These compounds also have very stable activity under UV light irradiation and showed no deactivation even when used for a longer time. Tantalum based compounds also decomposed methylene blue under UV-vis light irradiation but they have lower activity than Bi_2WO_6 and $AgVO_3$.

5.1 Introduction

Photocatalytic decomposition of volatile organic compounds (VOCs) has been under investigation since the discovery of advanced oxidation technologies. Heterogeneous photocatalysis has been considered as a vital and easily applicable technology owing to the adequacy of sunlight for operating the system at ambient temperature. Various metal oxides and sulphides have been examined for complete mineralization of VOCs with both ultraviolet light and visible light irradiations. Significant efforts have been made to explore some suitable semiconductor materials which can completely mineralize VOCs with purely visible irradiation under ambient temperature and pressure. Semiconductor metal oxides consisted of elements with 3d, 4d, and 5d orbitals have been investigated since their valence electrons can be excited with sunlight irradiation. Materials composed of modified transition metals, lanthanides, rare earth metals and alkali metals have also been examined for photocatalytic decomposition of VOCs and water splitting via UV light irradiation. Large numbers of mixed metal oxides containing tantalum (Ta)[1], [2, 3], vanadium (V)[4] [5, 6], silver (Ag)[7], [8], and tungsten (W)[9], [10], [11], [12] have been explored both for water splitting and VOCs disintegration. Mixed metal oxides such as $NaTaO_3$, $CoTa_2O_6$[13], and $CeTaO_4$[14] which contain higher d and f orbitals elements were assumed to have extended conduction bands[15] and valence bands. These extended conduction and valence bands increase the life time of photo-generated carriers, which facilitate the redox reaction on the material surface. It has been also investigated that most of tantalum based compounds have M-O-M bond angle close to 180° which has favourable[15] implications on the photocatalytic performance of these materials. Tantalum based compounds such $InTaO_4$ coated with NiO[16], $NaTaO_3$[17], and Ag ion modified materials could efficiently evolve hydrogen and oxygen through water splitting with visible light irradiation. Higher photocatalytic activities of these compounds were mainly attributed to the wider conduction band, the closeness of M-O-M angle to 180°, and band gap modification by Ag ions[18]. Bi_2InTaO_7 was found to have higher photocatalytic activity as compared to Bi_2MTaO_7 (M = Al, Ga, and Fe)[19], since

its M-O-M angle was more close to 180°. The closeness of M-O-M angle to 180° assists in the faster migration of photo-generated carrier to the corresponding reactive species on the material surfaces, which subsequently suppresses the recombination process and enhances the photocatalytic activities of these materials. Recombination was further reduced by coating Bi_2InTaO_7 with Pt, NiO and RuO_2, which resulted in efficient hydrogen production via UV light irradiation[20]. However, compositional variations of the constituent elements showed that $Bi_{0.5}In_{0.5}TaO_4$ has the lowest band gap among others and produced hydrogen with the highest rate under visible light irradiation[21].

It was also reported that requirements of co-catalyst for hydrogen production via photocatalysis can be excluded by introducing lanthanides into the layered perovskite tantalates, $RbLnTa_2O_7$ (Ln = Nd, Sm, La, Ce, Tb, Eu)[14]. The study revealed that, except Ce, Eu, and Tb lanthanides like Nd, Sm, and La have significant effects on the photocatalytic activities of layered $RbLnTa_2O_7$. The higher photocatalytic activities of these materials were mainly attributed to the addition of extra energy level within the band gap, caused by the 4f electrons of lanthanides. Combination of rare earth oxides[22] (Eu_2O_3) and tantalum oxide (Ta_2O_5) has suggested that tantalum based mixed oxide semiconductors have enhanced photocatalytic activities and can be considered for further exploration. Recent study on the rare earth tantalates has shown that tantalum based mixed oxides are energetically stable owing to the longer inter atomic distance between different metallic cations[23]. Stability, long lifetime, and exclusion of co-catalyst were among the few factors which excite us to further explore tantalum based ternary compounds, and compare their photocatalytic activities with vanadium and tungsten based photocatalyst materials. Therefore, we synthesized various types of materials through a solution method and examined their photocatalytic performance both in air and water under UV and visible light excitation.

5.2 Experimental

5.2.1 Material synthesis

Various ternary metal oxides including $AgTaO_3$, $Cd_2Ta_2O_7$, $EuTaO_4$, $CeTaO_4$, $CoTa_2O_6$, $BiTaO_4$, $InTaO_4$, $AgVO_3$, and Bi_2WO_6, with polycrystalline structures were prepared by solution techniques. All of chemicals were obtained from Sigma-Aldrich at 99.99% purity and were used as received. In a typical synthesis, 8 mmol of tantalum (V) chloride ($TaCl_5$) was dissolved in 50 mL ethanol at 70 °C, which made solution A. 12 mmol of each bismuth (III) nitrate hydrate ($Bi(NO_3)_3 \cdot 5H_2O$), silver nitrate ($AgNO_3$), cobalt(II) nitrate hexahydrate ($Co(NO_3)_2 \cdot 6H_2O$), cerium(III) nitrate hexahydrate ($Ce(NO_3)_3 \cdot 6H_2O$), europium(III) nitrate pentahydrate ($Eu(NO_3)_3 \cdot 5H_2O$), cadmium nitrate tetrahydrate ($Cd(NO_3)_2 \cdot 4H_2O$), and indium(III) nitrate hydrate ($In(NO_3)_3 \cdot xH_2O$) were dissolved separately in 50 mL ethanol with continuously stirring and heating at 70 °C for 30 min to make solutions B. Solution A and solution B were mixed together, where one mL nitric acid was added to the mixture. The mixture was heated at 80 °C with continuous refluxing and stirring for 6-8 h. The final solution with no precipitation was then aged for 12-24 h at room temperature and was kept in an oven at 50-60 °C till dried completely. Samples were ground by mortar and pestle and then calcined at 700 – 1150 °C for 40-50 h. $AgVO_3$ was prepared by a different method where each 3.0 mmol of ammonium meta-vanadates (NH_4VO_3) and 9 mmol of silver nitrate ($AgNO_3$) were dissolved in 50 mL de-ionized water. The two solutions were mixed and heated at 80 °C for 3 h. After aging for 12 h and drying in an oven, the dried sample was calcined at 300 °C for 4 h, which gave the final product of $AgVO_3$. Similarly, Bi_2WO_6 was also prepared by the solution method. In a typical synthesis process, 10 mmol of bismuth (III) nitrate hydrate ($Bi(NO_3)_3 \cdot 5H_2O$) and 5 mmol of tungsten tetra chloride (WCl_4) were dissolved in 50 mL ethanol. The two solutions were mixed and 0.5 mL nitric acid was added to the mixture, which was then heated for 6 h at 80 °C. After drying in the oven, the sample was calcined at 800 °C for 40 h, which gave the final product of Bi_2WO_6.

5.2.2 Characterization of catalysts

The crystalline structures of samples were analysed by X-ray diffractometer (Bruker D8 Advance equipped with a Lynx eye detector, Bruker-AXS, Karlsruhe, Germany) operated at 40 kV and 30 mA. The scanning rate was 0.2 sec/step with 2θ (10- 90°) and step size of 0.02°. Cu Kα (λ = 1.54178 Å) was used as a X-ray source with divergent slit of 0.300 and 2.5° primary and secondary soller slits. The optical absorption of samples was determined by UV-vis absorbance spectroscopy using the diffuse reflectance method (JASCO V-670 Spectrometer). Morphology and chemical composition of the materials were examined by scanning electron microscopy (ZEISS NEON 40EsB) equipped with an energy dispersive spectrometer (SEM-EDS). Samples were directly coated on an aluminium stub where 3 nm platinum coating was used as a conducting material. FTIR analysis was performed on a Perkin-Elmer Model FTIR-100 with a MIR detector.

5.2.3 Photocatalytic evaluation

Photocatalytic activities of prepared samples were evaluated in decomposition of gaseous toluene with both ultraviolet and visible light irradiations. Two different lamps, 300 W Mercury-Xenon lamp (UXM-502MD, Ushio) and Xenon lamp (UXL-306, Ushio), were used as UV and visible light sources, respectively. The average intensities of the UV lamp were measured as 19.1 mW/cm^2 at 220-280 nm, 19.0 mW/cm^2 (at 280-400 nm), and 27.5 mW/cm^2 (at > 400 nm), while the Xenon lamp has average intensities of 26.0 mW/cm^2 (at 315-400 nm), 240.0 mW/cm^2 (at 400-1050 nm). Methylene blue was used as a model of water contaminant and toluene was used as a model of gas compound.

In a typical run of methylene blue decomposition in water, 10 ppm methylene blue solution with 100 mg catalyst particles were continuously stirred in a Pyrex glass reactor which was irradiated with UV or visible light without any filter. Temperature of the reactor was maintained by passing cooled water through the reactor continuously. Concentration of methylene blue was determined by taking one mL aliquots from the reactor at a regular interval. The aliquots were evaluated

by measuring the absorbance at λ= 664 nm with a UV-visible spectrophotometer (Spectronic Instruments Model 4001/4), and the water sample was put back in the reactor to maintain the concentration of solution unchanged.

Toluene decomposition in gas was evaluated in a flow reactor connected with an on-line gas chromatograph (Shimadzu GC-17A) fitted with a GS-GSPRO column of 60 m in length and 0.32 mm in diameter. Oven temperature of the GC was 220 °C and FID detector temperature was kept at 250 °C. In a typical experiment, 300 mg of photocatalysts were dispersed in 10 mL deionized water in a Petri dish of 450 mm diameter and was dried in an oven overnight. The Petri dish was kept inside an air-tight stainless steel reactor fitted with a removable quartz sheet in order to allow both UV and visible radiation in. A flow of toluene at 100 ppm was continuously passed into the reactor (1.08 L) at a flow rate of 60 mL/min. The temperature of the reactor was controlled at room temperature by continuously passing cooling water through the reactor and also by blowing the reactor with fresh air from outside.

5.3 Results and Discussions

5.3.1 Structure of materials

XRD analysis of the as-prepared samples given in Figure 5.1 indicates that, all the materials ($AgTaO_3$, $Cd_2Ta_2O_7$ [24], [25], $EuTaO_4$[26], $CeTaO_4$[14], $CoTa_2O_6$ [13], [27], [28], $BiTaO_4$[29], $InTaO_4$[30], $AgVO_3$[4], and Bi_2WO_6[9, 31]) have exactly the same crystalline structures as previously reported. Except Bi_2WO_6 and $AgVO_3$, most of these Ta based materials have been synthesized through solid state reaction techniques. XRD analyses of all the samples prepared with the solution method are almost matched with that prepared by other techniques. However, due to the strong reaction of water with tantalum some materials have very few and weak peaks at 2θ = 22.28° and 28.26°, which correspond to tantalum oxide (Ta_2O_5). Even though some tantalum oxides are present but they are at extremely minor concentration and could not affect the performance of the required product materials.

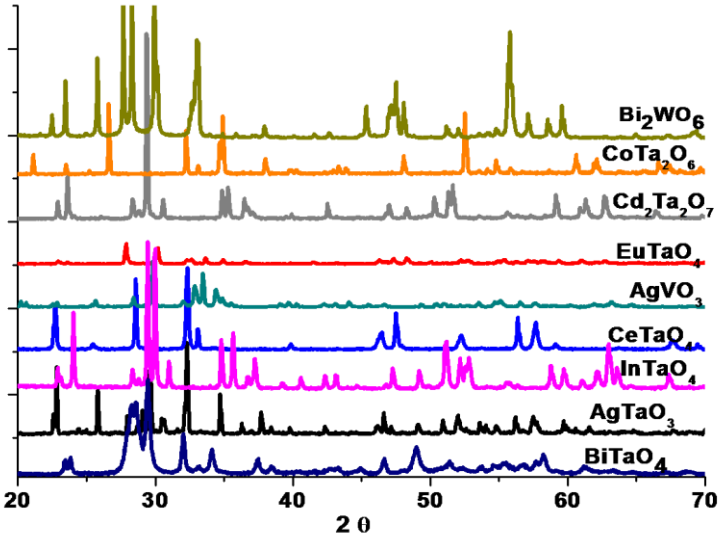

Figure: 5.1 X-ray diffraction (XRD) patterns of various materials prepared with solution method.

It must be noted that all the tantalum based compounds, $AgTaO_3$, $Cd_2Ta_2O_7$, $EuTaO_4$, $CeTaO_4$, $CoTa_2O_6$, $BiTaO_4$, $InTaO_4$ have pyro-tantalate type structures, with layered octahedral TaO_6 co-ordinated by other metallic ions like Cd [32], Ag, Co[33], Ce, Eu, Bi[34] and In[35]. Comparing the structures, phases and crystallinity of our tantalum based materials with the literature; all the materials prepared with the solution method have polycrystalline structures and different phases. The structures of $InTaO_4$, $EuTaO_4$, $BiTaO_4$, $Cd_2Ta_2O_7$, $CoTa_2O_6$, $CeTaO_4$, and $AgTaO_3$, were triclinic, monoclinic, triclinic, orthorhombic, trirutile, orthorhombic and triclinic, respectively. Although $BiTaO_4$, synthesized at temperature lower [36, 37] than 900 °C, has orthorhombic structures, however, in our case this material has triclinic structure synthesized either at 1150 °C or 700 °C. Drew et al. [38] observed phase transformation in $CeTaO_4$ synthesized at various temperatures, while in our case this material has orthorhombic structure when synthesized at 1150 °C. Phase transformation[24] from orthorhombic to triclinic and vice versa in most of these compounds occurs, both due to variation in sintering temperature[39] and variation in elemental ratio[40] of the constituent's metallic ions. Since surface of the materials play an important role in the photocatalysis[41],

where different phases of materials have varying surface properties[42]. However, more detailed and deep investigation is required to identify particular phase of these different materials, which is more suitable for photocatalytic process.

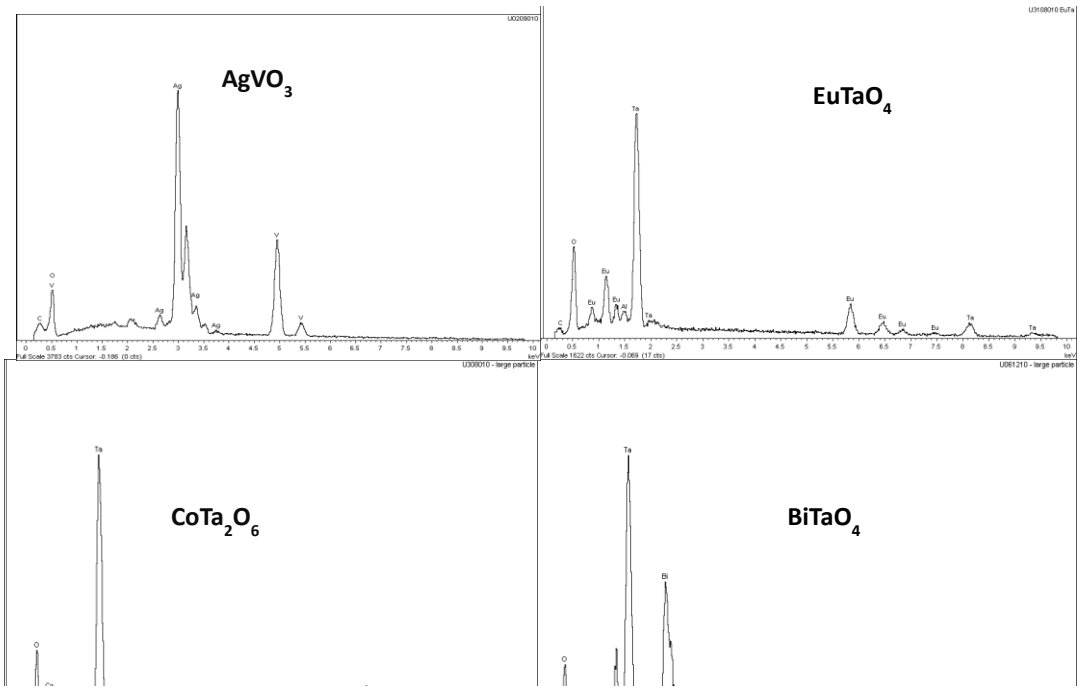

Figure: 5.2 Energy dispersive spectroscopy (EDS) of $AgVO_3$, $EuTaO_4$, $CoTa_2O_6$ and $BiTaO_4$ displaying the presence of corresponding elements in the materials.

Compositional analysis of the materials (Figure 5.2) performed with energy dispersive spectroscopy (EDS) shows that, all of these materials consisted of the corresponding constituents elements. Although EDS of only four samples are given in Figure 5.2, all of the samples were composed of the corresponding elements, and no contaminants were observed. As all the samples were directly coated on the aluminium stub, obviously some peaks of aluminium and carbon were observed.

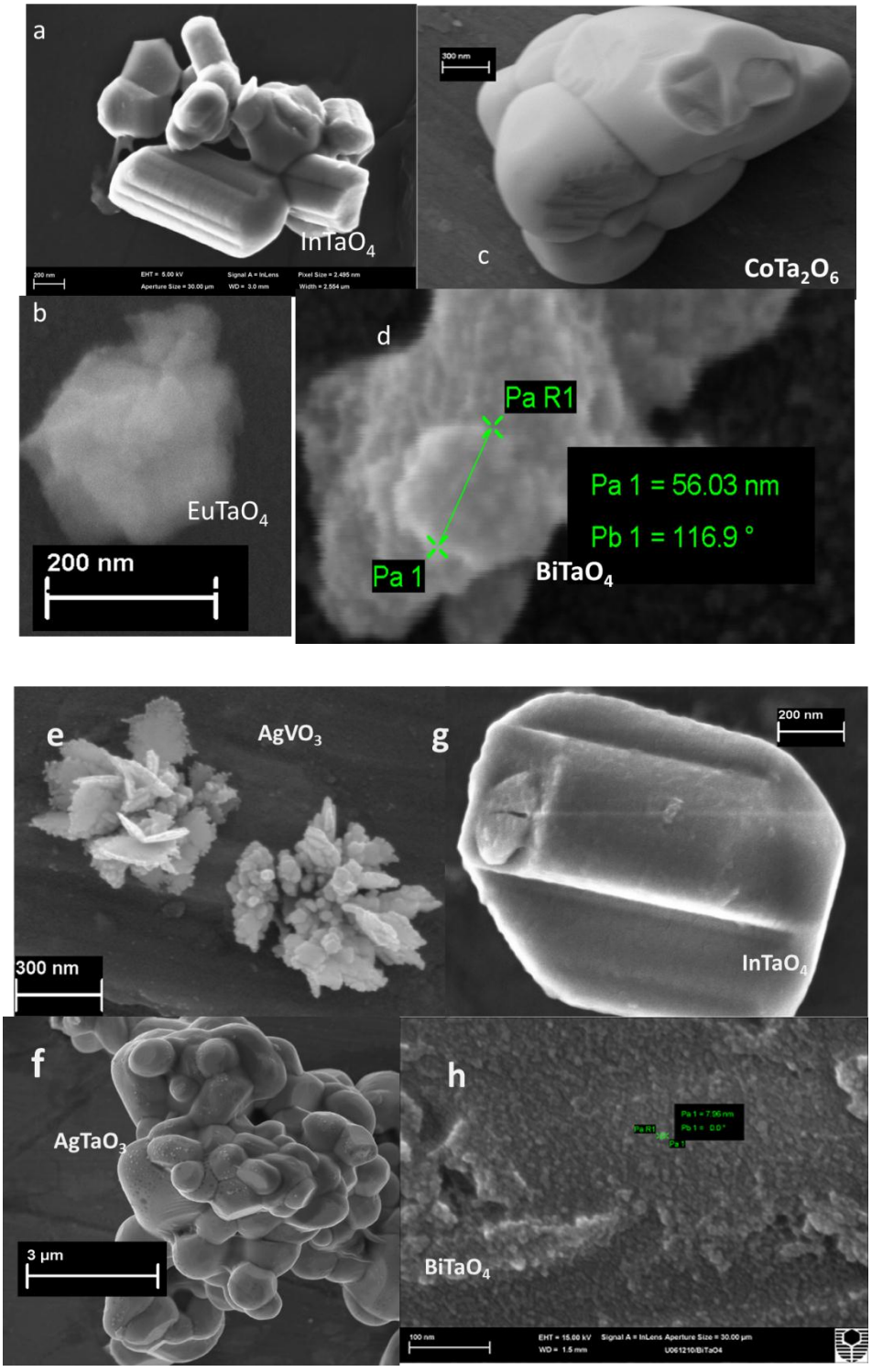

Figure: 5.3 Scanning electron micrograph images of various materials (a: $InTaO_4$, b: $EuTaO_4$, c: $CoTa_2O_6$, d: $BiTaO_4$, e: $AgVO_3$, f: $AgTaO_3$, g: $InTaO_4$, h: $BiTaO_4$).

Figure 5.3 shows scanning electron micrograph (SEM) images of some selected materials. It can be seen from Figure 5.3 that, $BiTaO_4$, $InTaO_4$, $CoTa_2O_6$, $AgVO_3$, and $EuTaO_4$ have particle sizes in nano-meter range. $BiTaO_4$ has the smallest particle size and crystallites up to 7.0 nm in dimension were observed. It is also evident from Figure 5.3 that different materials have varying shapes, sizes and morphologies. Large agglomerates with spherical, cylindrical, and plate-like structures were observed in various materials indicating stacking of nano-sized particles. Some defect sites can be clearly seen in Figure 5.3a, 5.3c, and 5.3g. These defects sites play dual roles in gap carrier generation centres, and recombination centres. Defect sites at suitable energy positions are beneficial for photocatalytic process, since large number of electron-hole pairs can be generated upon UV/visible light irradiation. However, some defects play a very crucial role as recombination centres, and suppress the photocatalytic process. It's very challenging at this stage to identify the role of these defect sites to see whether they recombine the electron-hole pairs or generate the carriers. We suggest that those defect sites which are positioned exactly at the mid of energy band gap are playing as carrier sinks and have a worst effect on the photocatalytic process. These defects significantly reduce the life time of photo-generated carriers, by providing a sink during the carrier moments toward the reactive sites on the particle surface. However, the defect sites which have energy positions in the vicinity of valence band and/or conduction band can mostly generate electron-hole pairs which are easily transferred to the reactive sites on the particle surfaces. Most often these defects can either be originated from oxygen vacancies or generated through cation and/or anion doping of the materials.

SEM images of silver based materials ($AgVO_3$ and $AgTaO_3$) shown in Figure 5.3e and 5.3f respectively have totally different morphology from other ternary compounds, where $AgVO_3$ has flower-like structure with different petal sizes agglomerated in spherical structures. However, $AgTaO_3$ has large size micrographs with different sub-particle sizes, where such large particle sizes were also reported by others [43].

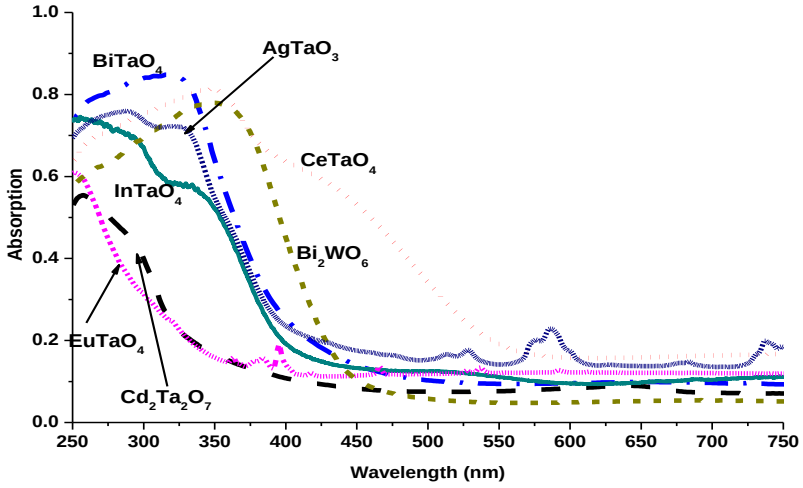

Figure: 5.4 UV Visible diffuse reflectance spectroscopy of various materials.

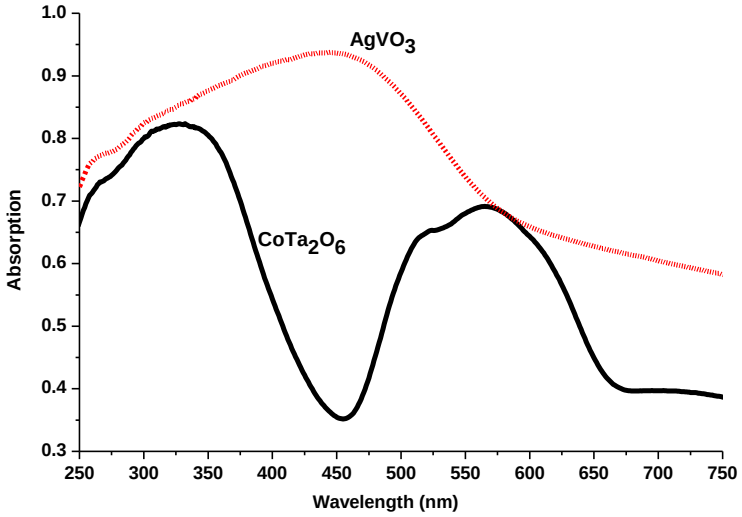

Figure: 5.5 UV Visible diffuse reflectance spectroscopy of $AgVO_3$ and $CoTa_2O_6$ showing absorption in the visible region.

Optical absorption of materials was determined with diffuse reflectance spectroscopy, as shown in Figure 5.4 and 5.5. It is evident that, except $EuTaO_4$ and $Cd_2Ta_2O_7$, all other ternary compounds have absorption edge beyond 400 nm, indicating a huge absorption in visible region of the spectrum. $EuTaO_4$ and

$Cd_2Ta_2O_7$ have absorption edges in the wavelength range lower than 350 nm indicating lower absorption in visible region. The optical absorption of $AgVO_3$ and $CoTa_2O_6$ are totally different where the latter has two distinct absorption edges in the visible region. This may be attributed to the dual contribution of cobalt 3d orbitals to the lower edge of the conduction band and upper edge of the valence band (as indicated in the Scheme 5.1). Band gap of all materials shown in Schematic 5.1 indicates conduction band and valence band positions of these materials. Table 5.1 shows the absorption edges of all the materials along with their corresponding band gaps. Energy band gap of all the materials was calculated using the formula [44].

$$Eg = \frac{1240}{\lambda}$$

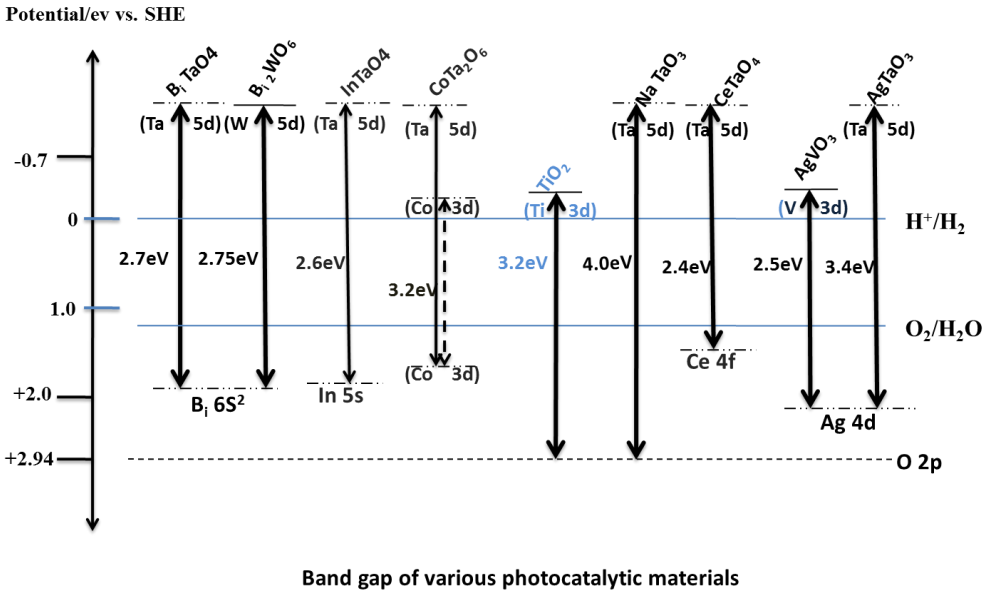

Scheme 5.1: Band gap representation of various materials.

Table 5.1: Absorption edges and calculated band gaps of all the newly synthesized materials.

Materials	Absorption edge (nm)	Band gap (eV)	
		Calculated	Literature
$AgVO_3$	725	1.71	2.5[10]
$CeTaO_4$	580	2.13	2.4[45]
Bi_2WO_6	455	2.72	2.75
$CoTa_2O_6$	450	2.75	3.2
$AgTaO_3$	430	2.88	3.4[43]
$BiTaO_4$	420	2.95	2.6
$EuTaO_4$	420	2.95	2.47
$InTaO_4$	400	3.1	3.1
$Cd_2Ta_2O_7$	350	3.54	?

Conduction bands of these ternary compounds are mainly consisted of 5d and 3d orbitals of tantalum, tungsten and vanadium, respectively, whereas valence bands are mainly made of O 2p orbitals, which are also hybridized by Bi 6s, In 5s, Co 3d, Ce 4f and Ag 4d orbitals. Obviously this valence band hybridization reduces the effective band gap by extending the valence band to more negative position as shown in Scheme 5.1. Extension in conduction/valence band width is assumed to increase the life time of photo-generated carriers and suppress their fast recombination.

5.3.2 Photocatalytic activities of materials

Photocatalytic activities of tantalum based materials ($InTaO_4$, $EuTaO_4$, $BiTaO_4$, $Cd_2Ta_2O_7$, $CoTa_2O_6$, $CeTaO_4$, and $AgTaO_3$), Bi_2WO_6 and $AgVO_3$ were evaluated in toluene decomposition under both UV and visible light irradiation and compared with that of TiO_2 (P25). Figure 5.6 shows the photocatalytic decomposition of toluene over tantalum based ternary metal oxides irradiated with UV light. Figure 5.6 clearly shows that $InTaO_4$ can decompose toluene at much faster rate than all others materials with UV irradiation. Comparing photocatalytic activities of all materials, it can be seen that, Bi_2WO_6, $AgVO_3$, $CeTaO_4$ (data not shown) and

$CoTa_2O_6$ could not decomposition toluene even within 6 h of UV irradiation. Although these materials absorb more visible light than other materials, they could not decompose toluene under UV light. We assume that UV irradiation produces high energetic electron-hole pairs which recombine very quickly due to the smaller band gap of these materials (Bi_2WO_6, $AgVO_3$, and $CoTa_2O_6$). Such lower photocatalytic activities of the materials (with smaller band gaps) under UV irradiation have also been observed in case of ZnO. The overall trend of tantalum based ternary compounds (excluding $CoTa_2O_6$ and $CeTaO_4$) toward the photocatalytic decomposition of toluene was found to be $InTaO_4$> $BiTaO_4$> $EuTaO_4$> $AgTaO_4$> $Cd_2Ta_2O_7$. It must be noted that these materials also absorb UV light in a similar trend as observed for toluene decomposition with UV irradiation. Thus it can be deduced that materials with high UV light absorption generate large number of electron-hole pairs and therefore have high photocatalytic activity under UV light irradiation. However, such materials may not have the same trend of photocatalytic activity under visible light irradiation.

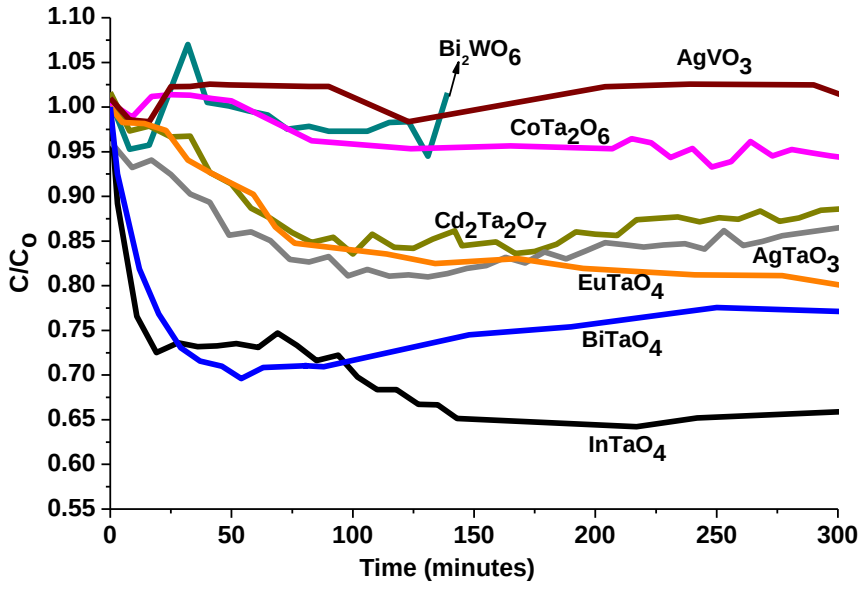

Figure: 5.6 Photocatalytic decomposition of toluene with various materials and UV light irradiation.

Though $InTaO_4$, $BiTaO_4$, $AgTaO_3$ and $Cd_2Ta_2O_7$ were capable of decomposing toluene with UV irradiation, these materials were not as efficient as a commercial TiO_2 (P25) under similar conditions. As shown in Figure 5.7, TiO_2 produces better performance than other materials in the initial few hours, however, its deactivation begins very rapidly and the photocatalytic decomposition of toluene drops very quickly. Figure 5.7 further reveals that photocatalytic activity of TiO_2 lasts only for 10-12 hours which indicates that this commercial material has very short life time as a photocatalyst and requires regeneration. Deactivation is mainly attributed to the adsorption of water and intermediates on TiO_2 surface which has been detailed in our previous study[46]. In chapter 3 we have critically analysed existence of water and intermediates on TiO_2 through FTIR analysis. There was a considerable evidence of water and intermediates adsorption on TiO_2 after the reaction. A weak evidence of toluene adsorption was also observed on TiO_2 surface before the reaction. Adsorption and desorption processes were observed in some cases (of TiO_2 but not for other materials) during the initial half an hour of irradiation. After achieving the equilibrium condition of 100 ppm toluene in reactor the light was turn on to initiate the photocatalytic reaction. Upon light irradiation a sharp increase in toluene concentration (above than 100 ppm) was first observed during first 10-30 minutes of irradiation. This was clearly indicating desorption of toluene within initial time of irradiation. However, this effect of adsorption and desorption was not a common process, since it was only observed on TiO_2. Adsorption of toluene, intermediates and water on TiO_2 is logical because this material is hygroscopic and likes to attract water. On the other hand, no such adsorption was observed before the reaction while toluene was passed through the samples such as $BiTaO_4$, $AgTO_3$, $Cd_2Ta_2O_7$ and $InTaO_4$. For these materials we could not observed adsorption of water and intermediates or even toluene when the samples were analysed through FTIR before and after the reaction. As per our analysis and understanding, adsorption of toluene on $BiTaO_4$, $AgTO_3$, $Cd_2Ta_2O_7$ and $InTaO_4$ surfaces can be excluded.

Even though tantalum based ternary compounds ($InTaO_4$, $BiTaO_4$, $AgTaO_3$ and $Cd_2Ta_2O_7$) have lower photocatalytic activity than TiO_2 in the initial few hours, they have very stable performance when used for a longer time. Unlike TiO_2, a small reduction was observed in the photocatalytic activities of these materials at longer period of time.

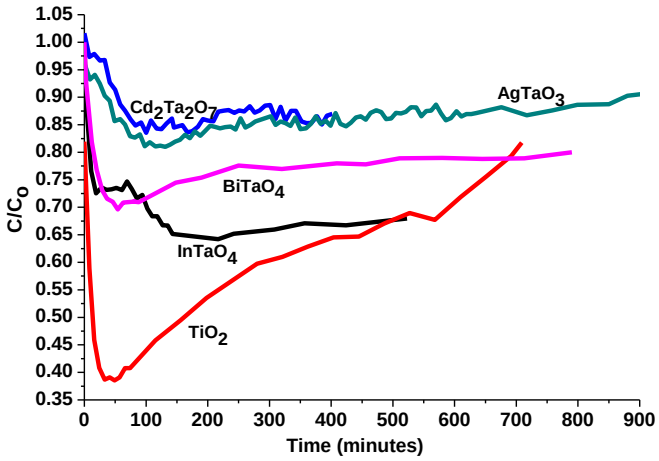

Figure: 5.7 Comparison of photocatalytic activities of selected materials with TiO_2 under UV light irradiation

Photocatalytic decomposition of toluene over $InTaO_4$, $EuTaO_4$, $BiTaO_4$, $Cd_2Ta_2O_7$, $CoTa_2O_6$, $CeTaO_4$, $AgTaO_3$, Bi_2WO_6 and $AgVO_3$ was also investigated under visible light irradiation. Figure 5.8 shows toluene decomposition efficiencies on some selected materials irradiated with visible light. Interestingly photocatalytic performance of these materials under visible light irradiation was totally reversed as compared to that under UV light irradiation. The trend of the photocatalytic decomposition of toluene with visible light is as $Cd_2Ta_2O_7$> $AgTaO_3$> $BiTaO_4$> Bi_2WO_6> $InTaO_4$> TiO_2, not similar to that observed for UV light irradiation. It must be noted that the materials like $CoTa_2O_6$, $CeTaO_4$, $AgVO_3$, and $EuTaO_4$ did not decompose toluene with visible light irradiation. Diffuse reflectance spectroscopy has shown that, these materials absorb more visible light than others, but they could not decompose toluene under visible light irradiation. The nil

performance of these materials for photocatalytic process may be attributed to the following reasons. Firstly, the band gap of these materials is much lower, therefore the photo-generated carriers may not have enough potential to produce powerful hydroxyl radical ($OH^{\bullet}$), which would be energetically strong to disintegrate toluene molecules. Secondly, due to the lower band gap, the photo-generated carriers may also have high chance of recombination. It has been reported that, 3d orbitals of Co contribute to both the valence and conduction band (as shown in Scheme 5.1) which may result in two band gap [27] of $CoTa_2O_6$ as seen from the optical absorption. These two band gaps have a detrimental effect on the photocatalytic process, because all of the photo-generated carriers recombine at the energy state which acts as a sink for photo-generated carriers. $EuTaO_4$ and $CeTaO_4$ have hybridized valence bands with Eu and Ce f orbitals on the top of their bands respectively. We assume that these f orbitals could reduce the band gaps, but they also generate an in-gap energy level[45] which serves as a recombination centre .

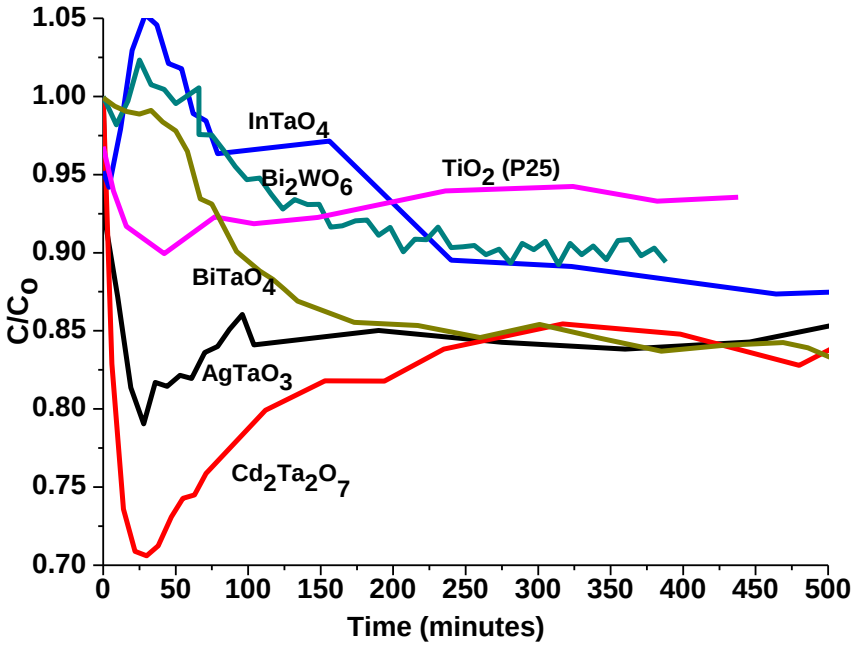

Figure: 5.8 Photocatalytic decomposition of toluene with various materials and visible light irradiation.

Figure 5.9 shows that among the four best materials ($Cd_2Ta_2O_7$, $AgTaO_3$, $BiTaO_4$ and $InTaO_4$) which decompose toluene with visible light irradiation, $AgTaO_3$, and $BiTaO_4$ have longer life time showing higher stability and decomposing a considerable amount of toluene. $Cd_2Ta_2O_7$ has better photocatalytic performance than others but like TiO_2 this material also showed deactivation and could not be used for long time.

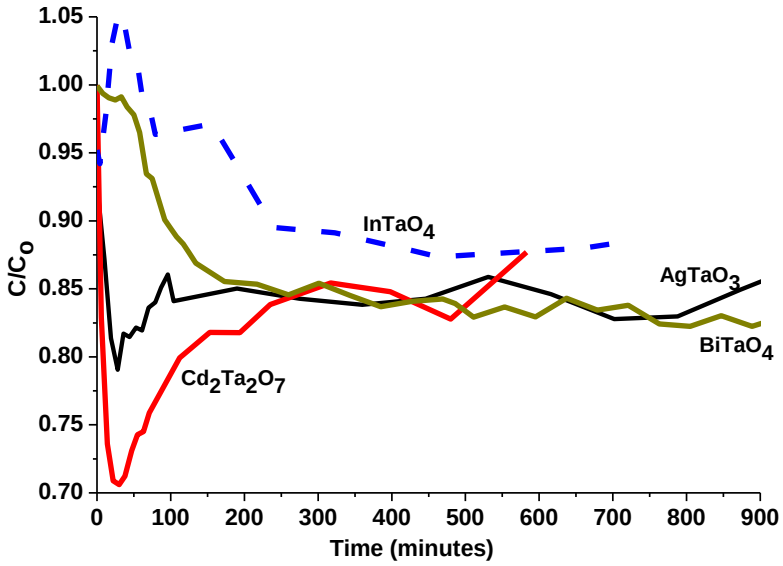

Figure: 5.9 Longer time photocatalytic activities of selected materials irradiated with visible light.

Interestingly the band gaps of $Cd_2Ta_2O_7$, $AgTaO_3$ and $BiTaO_4$ (as calculated from the absorption edge) were 3.54, 2.95 and 2.88 eV, respectively, where their visible light photocatalytic activities were as $Cd_2Ta_2O_7$ > $AgTaO_3$ >$BiTaO_4$. As can be seen these materials have large band gap and absorb small portion of visible light, however, they showed much better perform under visible light irradiation. This unusual behaviour of these materials may be attributed to following reasons. Since $BiTaO_4$ has smallest particle size as observed by SEM analysis, this material may have high surface area and more defect sites on the surface, which both enhance the photocatalytic activities. It has been reported that $AgTaO_3$ has large number of defect sites originated from Ag^+[47], the M-O-M angle of this material is also close

to 180°[43], moreover Ag 4d orbitals contribute to the valence band by pushing the valence band toward more negative position. All these properties have significant effects on the photo-physical properties of $AgTaO_3$, which results in enhanced photocatalytic activities under visible irradiation. $Cd_2Ta_2O_7$, which is the most efficient among all newly synthesized tantalum based compounds, has been tested for the first time for photocatalytic decomposition of VOCs. Although this material has been prepared by various methods[24], [48] and has been used for hydrogen production[49] via co-catalyst assisted system it has never been reported in pure form. We suggest that $Cd_2Ta_2O_7$ has enough number of defect sites associated with Cd^{2+} which produce electron-hole pairs with required potential to produce highly oxidative radicals on the surface.

Table 5.2: The overall photocatalytic performances of all the materials both with UV and visible light irradiation.

Material	Band gap (eV)	Toluene decomposition	
		UV light	Visible light
$Cd_2Ta_2O_7$	3.54	7.23	25.31
$AgTaO_3$	2.88	14.0	16.20
$InTaO_4$	3.1	2.7	0.9
$BiTaO_4$	2.95	25.2	16.6
$EuTaO_4$	2.95	11.0	nil
$AgVO_3$	1.71	1.0	nil
$CoTa_2O_6$	2.75	3.0	nil
Bi_2WO_6	2.72	1.6	2.5
$CeTaO_4$	2.13	1.0	nil
TiO_2	3.2	57.0	8.0

Overall performance of all the materials for photocatalytic decomposition of toluene with both UV and visible light has been summarized in Table 5.2. It is evident that

at UV light irradiation, TiO_2 has much better performance for the initial two hours and decomposed almost 60% toluene whereas $BiTaO_4$ and $AgTaO_3$ were the 2nd and 3rd better materials which removed about 25% and 14% toluene under similar condition. It must also be noted that TiO_2 has the lowest activity with visible light while $Cd_2Ta_2O_7$, $BiTaO_4$ and $AgTaO_3$ decomposed 26%, 16.5% and 16.0% toluene, respectively with visible light irradiation. Generally all the tantalum based compounds and particularly $BiTaO_4$, and $AgTaO_3$ have shown much stable performance since no deactivation was observed for these materials. Stability and longer time useability were evaluated by FTIR and XRD analyses of the materials after being used for the reactions. Figure 5.10 shows XRD of $AgTaO_3$ before and after photocatalytic reaction, which clearly indicates that this material is quite stable since no modification was observed in the XRD peaks of the materials. Figure 5.11 shows FTIR analysis of $AgTaO_3$ before and after photocatalytic reaction. No evidence of water and/or intermediate adsorption was observed on the tantalum based compounds. However, strong adsorption of water and intermediates were observed on TiO_2. This could be the reason for TiO_2 deactivation during photocatalytic process, while tantalum based compounds like $AgTaO_3$, $BiTaO_4$ and $InTaO_4$ did not adsorb intermediates, leading to deactivation.

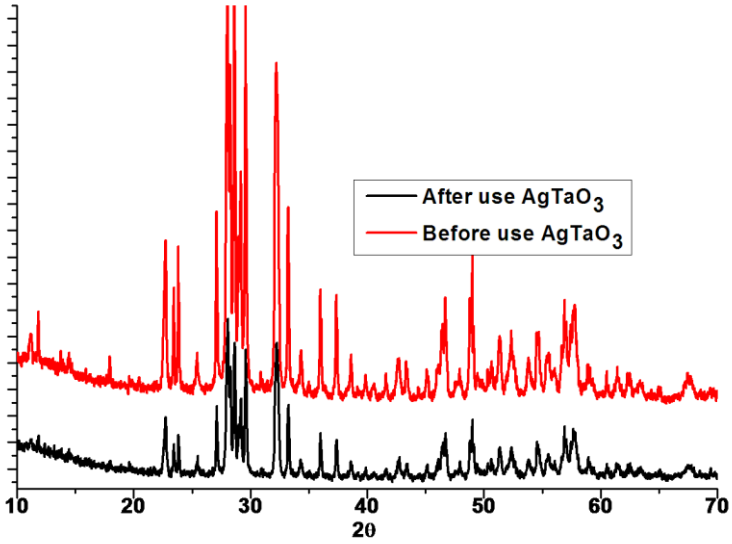

Figure: 5.10 XRD pattern of $AgTaO_3$ before and after use for photocatalytic reactions.

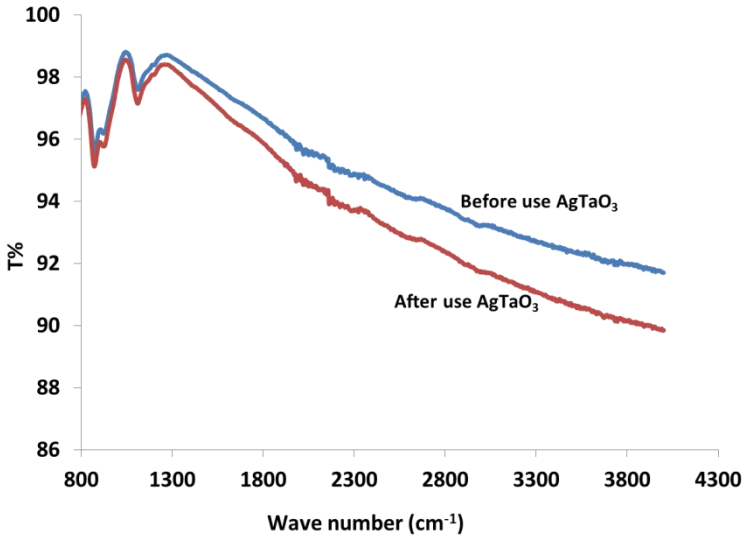

Figure: 5.11 FTIR analysis of $AgTaO_3$ before and after use for photocatalytic reactions.

The newly synthesized materials were also tested for photocatalytic removal of methylene blue in water. Figure 5.12 shows methylene blue decomposition with all

tantalum based materials, Bi_2WO_6 and $AgVO_3$ irradiated with UV-visible light. It is important to note that, unlike gas phase decomposition of toluene, the latter two materials, Bi_2WO_6 and $AgVO_3$, have shown better performance than tantalum based compounds. Similar to toluene decomposition in gas phase, $CeTaO_4$, $CoTa_2O_6$, and $EuTaO_4$ have demonstrated the worst activity for methylene blue bleaching. Nevertheless tantalum based compounds which include $AgTaO_3$, $Cd_2Ta_2O_7$ and $BiTaO_4$ were found to capable to decompose methylene blue in water with almost similar rate. TiO_2 has found to degrade methylene blue with much faster rate as compared to all other materials. The higher photocatalytic activity of TiO_2 for methylene blue bleaching is attributed to high adsorption of water onto the TiO_2 surface and its high surface area. The photocatalytic decomposition trend of methylene blue of all the materials was as Bi_2WO_6> $AgVO_3$>$AgTaO_3$> $BiTaO_4$>$Cd_2Ta_2O_7$> $InTaO_4$> $CoTa_2O_6$> $CeTaO_4$> $EuTaO_4$.

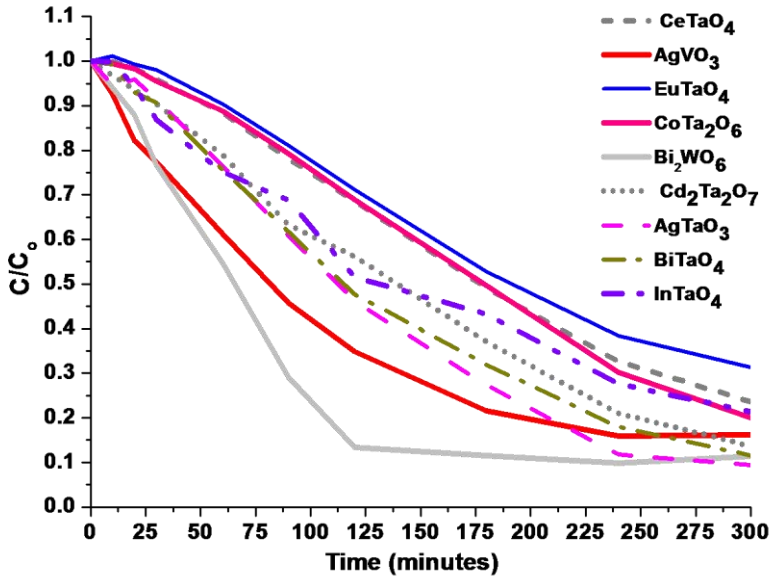

Figure: 5.12 Photocatalytic degradation of methylene blue with various ternary metal oxides irradiated with UV light.

5.4 Conclusion

Various materials (Bi_2WO_6, $AgVO_3$, $AgTaO_3$, $BiTaO_4$, $Cd_2Ta_2O_7$, $InTaO_4$, $CoTa_2O_6$, $CeTaO_4$ and $EuTaO_4$) were successfully prepared with solution techniques and were tested for photocatalytic decomposition of VOCs both in air and water. Among these tantalum containing compounds like $Cd_2Ta_2O_4$, $AgTaO_4$ and $BiTaO_4$ were found to decompose gaseous toluene with visible light irradiation more efficiently than other materials. These three compounds have very stable performance and have showed much better activity than commercial photocatalyst TiO_2 under visible light irradiation. However, TiO_2 degraded both gaseous toluene and methylene blue in water with UV irradiation efficiently than these compounds. $AgTaO_3$, $BiTaO_4$ and $Cd_2Ta_2O_7$ also degraded methylene blue with faster rate than other tantalum containing compounds. Bi_2WO_6 and $AgVO_3$ could not remove gaseous toluene, but they were the most efficient to degrade MB with UV irradiation in water. Thus $Cd_2Ta_2O_7$, $AgTaO_3$, $BiTaO_4$ can be assumed as the most efficient photocatalysts materials, since they removed gaseous toluene under visible light, have long life time and did not show deactivation due to intermediate adsorption, and degraded methylene blue in water with UV light. However, detail study is still required to comprehensively investigate $Cd_2Ta_2O_7$ and $AgVO_3$, as these materials has better overall performance and can be used as potential photocatalytic materials.

5.5 References

1. Ullah, R., et al., *Wet-chemical Synthesis of InTaO4 for Photocatalytic Decomposition of Organic Contaminants in Air and Water with UV-vis Light, DOI: 10.1021/ie200544z.* Industrial & Engineering Chemistry Research, 2011: p. 10.1021/ie200544z.

2. Zou, Z., J. Ye, and H. Arakawa, *Structural properties of InNbO4 and InTaO4: correlation with photocatalytic and photophysical properties.* Chemical Physics Letters, 2000. **332**(3-4): p. 271-277.

3. Zou, Z. and H. Arakawa, *Direct water splitting into H2 and O2 under visible light irradiation with a new series of mixed oxide semiconductor photocatalysts.* Journal of Photochemistry and Photobiology A: Chemistry, 2003. **158**(2-3): p. 145-162.

4. Ren, J., et al., *Photocatalytic activity of silver vanadate with one-dimensional structure under fluorescent light.* Journal of Hazardous Materials, 2010. **183**(1-3): p. 950-953.

5. Martínez-de la Cruz, A. and U.M.G. Pérez, *Photocatalytic properties of BiVO4 prepared by the co-precipitation method: Degradation of rhodamine B and possible reaction mechanisms under visible irradiation.* Materials Research Bulletin. **45**(2): p. 135-141.

6. Li, H., G. Liu, and X. Duan, *Monoclinic BiVO4 with regular morphologies: Hydrothermal synthesis, characterization and photocatalytic properties.* Materials Chemistry and Physics, 2009. **115**(1): p. 9-13.

7. Doucet, N., et al., *Kinetics of photocatalytic VOCs abatement in a standardized reactor.* Chemosphere, 2006. **65**(7): p. 1188-1196.

8. Arney, D., et al., *Flux synthesis of AgNbO3: Effect of particle surfaces and sizes on photocatalytic activity.* Journal of Photochemistry and Photobiology A: Chemistry, 2010. **214**(1): p. 54-60.

9. Fu, H., et al., *Visible-Light-Induced Degradation of Rhodamine B by Nanosized Bi2WO6.* The Journal of Physical Chemistry B, 2005. **109**(47): p. 22432-22439.

10. Fu, H., et al., *Synthesis, characterization and photocatalytic properties of nanosized Bi2WO6, PbWO4 and ZnWO4 catalysts.* Materials Research Bulletin, 2007. **42**(4): p. 696-706.

11. Shang, M., et al., *Bi2WO6 Nanocrystals with High Photocatalytic Activities under Visible Light.* The Journal of Physical Chemistry C, 2008. **112**(28): p. 10407-10411.

12. Zhang, S., et al., *Bi2WO6 photocatalytic films fabricated by layer-by-layer technique from Bi2WO6 nanoplates and its spectral selectivity.* Journal of Solid State Chemistry, 2007. **180**(4): p. 1456-1463.

13. Mulla, I.S., et al., *A coprecipitation technique to prepare CoTa2O6 and CoNb2O6.* Materials Letters, 2007. **61**(11-12): p. 2127-2129.

14. Machida, M., J.-i. Yabunaka, and T. Kijima, *Synthesis and Photocatalytic Property of Layered Perovskite Tantalates, RbLnTa2O7 (Ln = La, Pr, Nd, and Sm).* Chemistry of Materials, 2000. **12**(3): p. 812-817.

15. Eng, H.W., et al., *Investigations of the electronic structure of d0 transition metal oxides belonging to the perovskite family.* Journal of Solid State Chemistry, 2003. **175**(1): p. 94-109.

16. Zou, Z., et al., *Direct splitting of water under visible light irradiation with an oxide semiconductor photocatalyst.* Nature, 2001. **414**(6864): p. 625-627.

17. Fu, H., et al., *Visible-light-driven NaTaO3-xNx catalyst prepared by a hydrothermal process.* Materials Research Bulletin, 2008. **43**(4): p. 864-872.

18. Kato, H., H. Kobayashi, and A. Kudo, *Role of Ag+ in the Band Structures and Photocatalytic Properties of AgMO3 (M: Ta and Nb) with the Perovskite Structure.* The Journal of Physical Chemistry B, 2002. **106**(48): p. 12441-12447.

19. Torres-Martinez, L.M., et al., *Photocatalytic performance of pyrochlore-type structure compounds, Bi2MTaO (M = Al, Ga, Fe or In), on alizarin red S degradation*, in *Proceedings of the 2nd WSEAS international conference on Nanotechnology*. 2010, World Scientific and Engineering Academy and Society (WSEAS): UK. p. 73-78.

20. Wang, J., Z. Zou, and J. Ye, *Surface modification and photocatalytic activity of distorted pyrochlore-type Bi2M(M=In, Ga and Fe)TaO7 photocatalysts.* Journal of Physics and Chemistry of Solids. **66**(2-4): p. 349-355.

21. Luan, J., et al., *Structural, optical and photocatalytic properties of new solid photocatalysts, BixIn1-xTaO4 (0 < x < 1).* Materials Chemistry and Physics, 2006. **98**(2-3): p. 434-441.

22. Yang, X., et al., *Enhanced photocatalytic activity of Eu2O3/Ta2O5 mixed oxides on degradation of rhodamine B and 4-nitrophenol.* Colloids and Surfaces A: Physicochemical and Engineering Aspects, 2008. **320**(1-3): p. 61-67.

23. Forbes, T.Z., et al., *The energetics of lanthanum tantalate materials.* Journal of Solid State Chemistry, 2010. **183**(11): p. 2516-2521.

24. Sleight, A.W. and J.D. Bierlein, *Phase transition in Cd2Ta2O7 and the Cd2Nb2-xTaxO7 series.* Solid State Communications, 1976. **18**(1): p. 163-166.

25. Lukaszewicz, K., et al., *Temperature dependence of the crystal structure and dynamic disorder of cadmium in cadmium pyroniobates [Cd2Nb2O7 and Cd2Ta2O7]*. Materials Research Bulletin, 1994. **29**(9): p. 987-992.

26. Zinchenko, V.F., N.P. Efryushina, and O.G. Eryomin, *Optical absorption of Eu3+ and Eu2+ in europium oxides and europium fluorides.* Proc. SPIE-Int. Soc. Opt. Eng., 2002. **4766**(Copyright (C) 2011 American Chemical Society (ACS). All Rights Reserved.): p. 43-46.

27. Li, D.-F., et al., *Role of d electrons in oxide semiconductor CoTa2O6 on photocatalytic and photophysical properties.* Research on Chemical Intermediates, 2005. **31**(4): p. 521-527.

28. Yamamoto, A., et al., *Metal oxide catalysts for oxygen-oxidation/reduction devices and electrodes using the catalysts*. 2003, Sony Corp., Japan . p. 12 pp.

29. Shi, R. and R. Shi, *Visible-Light Photocatalytic Degradation of BiTaO4 Photocatalyst and Mechanism of Photocorrosion Suppression.* The journal of physical chemistry. C, 2010. **114**(14): p. 6472.

30. Hiroshi, I. and H. Kazuhito, *Visible Light-Sensitive InTaO₄-Based Photocatalysts for Organic Decomposition.* Journal of the American Ceramic Society, 2005. **88**(11): p. 3137-3142.

31. Chen, Y., et al., *The gas-phase photocatalytic mineralization of benzene over visible-light-driven Bi2WO6-C microspheres.* Catalysis Communications, 2010. **12**(4): p. 247-250.

32. Fischer, M., et al., *Structure and stability of Cd2 Nb2 O7 and Cd2 Ta2 O7 explored by ab initio calculations.* Physical Review B, 2008. **78**(1): p. 014108.

33. Kinast, E.J., et al., *Magnetic structure of the quasi-two-dimensional compound CoTa2O6.* Journal of Alloys and Compounds, 2010. **491**(1-2): p. 41-44.

34. Muthurajan, H., *A co-precipitation technique to prepare BiTaO4 powders.* Materials Letters, 2008. **62**(3): p. 501.

35. Ye, J., et al., *Correlation of crystal and electronic structures with photophysical properties of water splitting photocatalysts InMO4*

(M=V5+,Nb5+,Ta5+). Journal of Photochemistry and Photobiology A: Chemistry, 2002. **148**(1-3): p. 79-83.

36. Muktha, B. and Muktha, *Crystal structures and photocatalysis of the triclinic polymorphs of BiNbO4 and BiTaO4.* Journal of Solid State Chemistry, 2006. **179**(12): p. 3919.

37. Muthurajan, H., et al., *A co-precipitation technique to prepare BiTaO4 powders.* Materials Letters, 2008. **62**(3): p. 501-503.

38. Drew, G., et al., *Reversible Oxidation/Reduction in the CeTaO4+[delta]System: a TEM and XRD Study.* Journal of Solid State Chemistry, 1998. **140**(1): p. 20-28.

39. Zhang, G., et al., *Synthesis of nanometer-size Bi3TaO7 and its visible-light photocatalytic activity for the degradation of a 4BS dye.* Journal of Colloid and Interface Science, 2010. **345**(2): p. 467-473.

40. Santos, E.G. and et al., *Magnetic phases of the quasi-two-dimensional compounds Fe x Co 1 − x Ta 2 O 6.* Journal of Physics: Condensed Matter, 2010. **22**(49): p. 496004.

41. Shi, L. and D. Weng, *Highly active mixed-phase TiO2 photocatalysts fabricated at low temperatureand the correlation between phase compositionand photocatalytic activity.* Journal of Environmental Sciences, 2008. **20**(10): p. 1263-1267.

42. Su, W., et al., *Surface Phases of TiO2 Nanoparticles Studied by UV Raman Spectroscopy and FT-IR Spectroscopy.* The Journal of Physical Chemistry C, 2008. **112**(20): p. 7710-7716.

43. Kato, H., H. Kobayashi, and A. Kudo, *Role of Ag+ in the Band Structures and Photocatalytic Properties of AgMO3 (M: Ta and Nb) with the Perovskite Structure.* The Journal of Physical Chemistry B, 2002. **106**(48): p. 12441-12447.

44. Sun, H., et al., *Halogen element modified titanium dioxide for visible light photocatalysis.* Chemical Engineering Journal, 2010. **162**(2): p. 437-447.

45. Machida, M., et al., *Photocatalytic Property and Electronic Structure of Lanthanide Tantalates, LnTaO4 (Ln = La, Ce, Pr, Nd, and Sm).* The Journal of Physical Chemistry B, 2001. **105**(16): p. 3289-3294.

46. Ullah, R., et al., *Wet-chemical Synthesis of InTaO4 for Photocatalytic Decomposition of Organic Contaminants in Air and Water with UV-vis Light.* Industrial & Engineering Chemistry Research, 2011: p. 10.1021/ie200544z.

47. Kako, T., N. Kikugawa, and J. Ye, *Photocatalytic activities of AgSbO3 under visible light irradiation.* Catalysis Today, 2008. **131**(1-4): p. 197-202.

48. Guo, L., et al., *Method for preparing nanoscale cadmium tantalate photocatalyst*. 2008, Xi'an Jiaotong University, Peop. Rep. China . p. 20pp.

49. Chen, Y.-B., et al., *Effects of cocatalysts on photocatalytic properties of La doped Cd2TaGaO6 photocatalysts for hydrogen evolution from ethanol aqueous solution.* Int. J. Hydrogen Energy, 2010. **35**(Copyright (C) 2011 American Chemical Society (ACS). All Rights Reserved.): p. 7029-7035.

6

6 - Removal of Gaseous Volatile Organic Compounds via Doped $BiNbO_4$ Irradiated with Artificial Sunlight

Abstract

$BiNbO_4$, metal-doped and N-doped $BiNbO_4$ catalysts were obtained at lower sintering temperature of 700 °C using a solution method. Both undoped and metal ion (Ba, Ga, Sn, La, and Al) doped $BiNbO_4$ have multi-phase structures; while the nitrogen doped material has only triclinic structure. The materials were characterized by XRD, SEM, FTIR, and diffuse reflectance spectroscopy, and used for photocatalytic decomposition of gaseous toluene under either UV or visible light. Among the materials, $BiNbO_4$: Ga showed higher performance, much better than commercial TiO_2 and decomposed more than 50% toluene (100 ppm) in the initial two hours at UV irradiation. However, under visible light irradiation, $BiNbO_4$: Ba was better than others and degraded 12% toluene within initial two hours. All the materials also exhibited quite stable performance under UV or visible light.

6.1 Introduction

Pyrochlore $BiNbO_4$ has been extensively studied for piezoelectric, ferroelectric[1], and electro-optical applications such as microwave[2], micro-electro-mechanical systems (MEMS)[3] and optoelectronics[4] due to its tuneable crystal and electronic structure prepared at different sintering temperatures[5] and synthesis processes[6, 7]. Detailed investigations of the electronic structure[8] suggested that conduction and valence bands of $BiNbO_4$ are positioned at appropriate energy levels, and the material can be used for redox reactions if irradiated with visible light. Various reports have shown that $BiNbO_4$ can be crystallized in orthorhombic and triclinic phases at lower (1000 °C) [9] and higher (1150 °C) temperatures[10], respectively, using solid state reactions. The triclinic $BiNbO_4$ can also be obtained at lower temperature in non-solid-state reaction routes such as sol-gel techniques[5, 10], polymeric precursor techniques[6] and co-precipitation[7, 11]. Using the aqueous solutions of precursors, pure triclinic phase of $BiNbO_4$ was obtained at 700 °C, which was then transformed to orthorhombic phase at elevated temperature of 1000 °C[12]. Additionally, type and concentration of dopant[13] atoms also cause phase alteration in $BiNbO_4$. Obviously these two phases of $BiNbO_4$ possess different properties and can be used for different applications. The orthorhombic (α form, sintered at lower temperature) $BiNbO_4$ has better dielectric properties[14], smaller band gap, better performance in photocatalytic activities[15]. The orthorhombic $BiNbO_4$ also has a lower band gap of 2.6 eV, being suitable for hydrogen production via water splitting irradiated with UV and/or sunlight[16]. The band gap energy can be further reduced by cation and anion doping because these ions may generate oxygen vacancies, defect sites and energy levels below and above the conduction and valence bands[8]. It has been reported that doping of $BiNbO_4$ with Zn^{2+}[17], and lanthanides (Ln = Dy^{3+}, Gd^{3+}, Nd^{3+} or La^{3+})[2] produced a large number of oxygen vacancies and charge defects in the structure of material owing to the difference in ionic size. The dielectric properties of $BiNbO_4$ were significantly modified after cation-doping[17]. Photocatalytic degradation of azo dyes with $BiTaO_4$ and $BiNbO_4$ under UV irradiation has suggested that, triclinic

$BiNbO_4$ (β form) demonstrated a better selectivity toward the aromatic compounds and therefore, can be considered for further investigation[18]. Various studies have indicated that preparation of materials using non-solid state reaction techniques[19] at low sintering temperature has resulted in various advantages including large number of defect sites on the surface[20], controllable grain growth[21], and enhanced surface area[5, 22]. In this study we report the synthesis of undoped and doped $BiNbO_4$ with a solution technique and low sintering temperature and their photocatalytic performance in gas oxidation.

6.2 Experimental

6.2.1 Material synthesis

Polycrystalline non-doped and metal ion (Ba, Sn, La, Al, and Ga) doped $BiNbO_4$ materials were prepared using dissolved precursor salts in ethanol. All chemicals were obtained from Sigma-Aldrich at 99.99% purity and were used as received. In a typical synthesis, 12 mmol of bismuth (III) nitrate hydrate ($Bi(NO_3)_3.5H_2O$) and 12 mmol of niobium (V) chloride ($NbCl_5$) were dissolved separately in 50 mL ethanol with continuously stirring and heating at 70 °C for 30 min to make solutions A and B, respectively. Dopant solution C was also prepared by dissolving 0.01 mmol of dopant salt (Ba, Sn, La, Al, and Ga) in 30 mL ethanol. Both the solutions A and B were then mixed and 0.5 - 1.0 mL concentrated nitric acid was added to the mixture. After half hour mixing, the dopant solution C was added to the mixture, which was then kept heating at 80 °C for 6 h. The final solution with no precipitation was then aged for 24 h at room temperature and was kept in an oven at 60 °C till dried completely. The sample was ground by mortar and pestle and then calcined at 700 °C for 45-50 h. Non-doped $BiNbO_4$ was also prepared by the similar technique where no dopant solution was added to the process.

Nitrogen doping was performed by using another setup, where mist of nitrogen gas and ammonia was passed on through the sample fitted in a tube furnace at 500 °C for 5 hours. In particular setup nitrogen gas was flown at 100 mL/min through ammonia solution (28%) which was heated at about 100 °C to make and pass the

ammonia vapours through the sample. It must be noted the prepared $BiNbO_4$ was used for treatment in nitrogen environment. It was assumed that such a treatment in nitrogen environment may substitute oxygen with the nitrogen and make it nitrogen doped $BiNbO_4$.

6.2.2 Characterization of catalysts

Crystalline structure of materials was analyzed by X-ray diffractometer (Bruker D8 Advance equipped with a Lynx eye detector, Bruker-AXS, Karlsruhe, Germany) operated at 40 kV and 30 mA. The scanning rate was 0.2 sec/step with 2θ (10- 90°) and step size of 0.02°. Cu Kα (λ = 1.54178 Å) was used as a X-ray source with divergent slit of 0.300 and 2.5° primary and secondary soller slits. The optical absorption of samples was determined by UV-vis absorbance spectroscopy using the diffuse reflectance method (JASCO V-670 Spectrometer). Morphology and chemical composition of the materials were examined by scanning electron microscopy (ZEISS NEON 40EsB) equipped with an energy dispersive spectrometer (SEM-EDS). Samples were directly coated on an aluminium stub where 3 nm platinum coating was used as a conducting material. FTIR analysis was performed on a Perkin-Elmer Model FTIR-100 with a MIR detector.

6.2.3 Photocatalytic evaluation

Photocatalytic activities of both undoped and doped $BiNbO_4$ samples were evaluated in decomposition of gaseous toluene with ultraviolet and visible light irradiations. Two different lamps, 300 W Mercury-Xenon lamp (UXM-502MD, Ushio) and Xenon lamp (UXL-306, Ushio), were used as UV and visible light sources, respectively. The average intensities of the UV lamp were measured as 19.1 mW/cm^2 (at 220-280 nm), 19.0 mW/cm^2 (at 280-400 nm), and 27.5 mW/cm^2 (at > 400 nm), while the Xenon lamp has average intensities of 26.0 mW/cm^2 at 315-400 nm, 240.0 mW/cm^2 at 400-1050 nm. Gaseous toluene was used as a model air contaminant at a concentration of 100 ppm in air.

Toluene decomposition was evaluated in a flow reactor connected to an on-line gas chromatograph (Shimadzu GC-17A) fitted with a GS-GSPRO column of 60 m in

length and 0.32 mm in diameter. Oven temperature of the GC was 220 °C and FID detector temperature was kept at 250 °C. In a typical experiment, 300 mg of photocatalysts were dispersed in 10 mL deionized water on a Petri dish of 450 mm diameter and was dried in an oven overnight. The Petri dish was kept inside an air-tight stainless steel reactor fitted with a removable quartz sheet in order to allow both UV and visible radiation in. A flow of toluene at 100 ppm was continuously passed into the reactor (1.08 L) at a flow rate of 60 mL/min. The temperature of the reactor was controlled at room temperature by continuously passing cooling water through the reactor and also by blowing the reactor with fresh air from outside. Complete set up for toluene decomposition under both UV and visible light irradiation is shown in Figure 6.1.

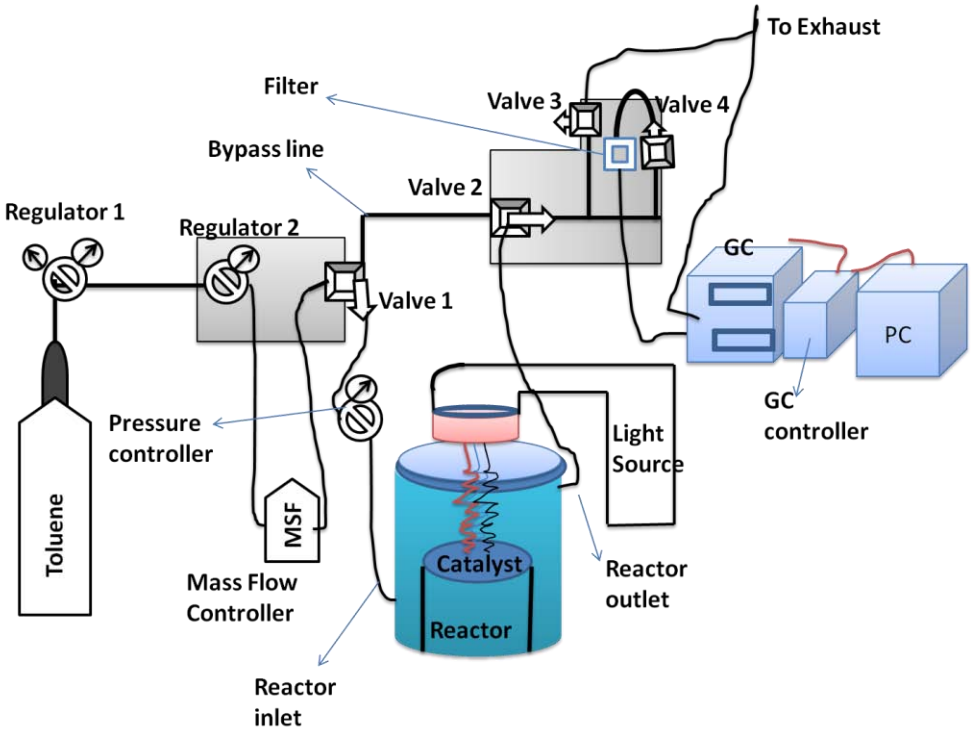

Figure: 6.1 Experimental set up for toluene decomposition.

6.3 Results and discussions

6.3.1 Material structure

X-ray diffraction analysis of undoped and metal ion (Ba, Sn, La, Al, and Ga) doped $BiNbO_4$ shown in Figure 6.2 indicates that the as-prepared materials have multi-crystalline structures with both orthorhombic and triclinic polymorphs. It has been reported that orthorhombic $BiNbO_4$ obtained at 900 °C in solid state reaction can be transformed to triclinic phase after heating at above 1020 °C[23, 24]. However, triclinic phase could also be obtained at 700 - 750 °C via co-precipitation techniques[25] and citrate reaction method[26]. In our case the observed lattice parameters of triclinic phase were a = 5.538, b = 7.618, c = 7.932, α = 102.56°, β = 90.14° and γ = 92.78°, primitive, while those for orthorhombic structure are a = 4.980, b = 11.700, c = 5.675, α = 90.00°, β = 90.00° and γ = 90.00°, F30. The two different polymorphs synthesized with the solution method were exactly matched with the polymorphs prepared by solid state reaction method[27] and non-solid state reaction[25]. Although, Subramanian et al. [11] has reported an irreversible phase transition between the two polymorphs of $BiNbO_4$, recent findings indicated that the phase transition is possible from β to α form if the material is synthesized with non-solid state reaction techniques[26]. As can be seen from Figure 6.2, introduction of metal dopants into $BiNbO_4$ did not modify the crystal structure of material significantly. Very few extra peaks of Bi_2O_3 were observed in $BiNbO_4$: La, where intensities of some peaks were reduced both in Ba and La doped $BiNbO_4$ indicating a minor effect of doping. It can be deduced from XRD analysis that the newly prepared metal ion doped and undoped $BiNbO_4$ have both the orthorhombic and triclinic phases.

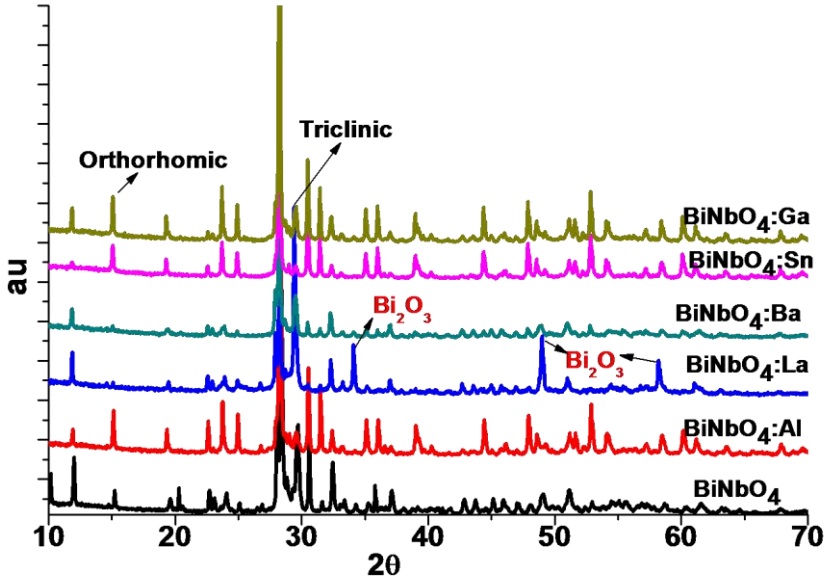

Figure: 6.2 X ray diffraction analysis of undoped and metal doped $BiNbO_4$.

Figure 6.3 shows XRD analysis of $BiNbO_4$ treated in ammonia and N_2 gas, which was referred as nitrogen doped material i.e. $BiNbO_4$: N. It is evident that nitrogen doping significantly modify the crystal structure of $BiNbO_4$, since most of the major peaks were shifted toward lower angles. Importantly the material has only triclinic phase with the same lattice parameters (a = 5.538, b = 7.618, c = 7.932, α = 102.56°, β = 90.14° and γ = 92.78°, primitive) as undoped $BiNbO_4$. This obviously suggest that, unlike metal ion doping, substitution of oxygen with nitrogen affected the atomic co-ordination of sheets of NbO_6 octahedral[28] by keeping the vertices oxygen/nitrogen along the c-axis. This will always maintain the NbO_6 sheet along the bc plane separated by the layers of Bi^{3+} which is co-ordinated with eight oxygen atoms[24].

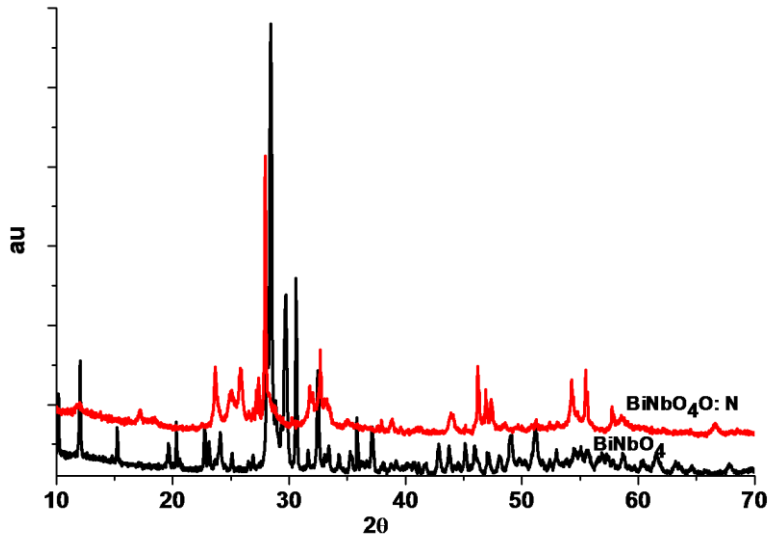

Figure: 6.3 X ray diffraction analysis of nitrogen doped $BiNbO_4$.

Elemental analysis of the metal doped materials was also performed. Figure 6.4 shows EDS analysis of four samples, undoped, La-, Ba-, Sn-doped $BiNbO_4$. It was found that all the materials have only Bi, Nb and O atoms, where no dopant atom was identified. This was due to lower dopant concentration, which could only modify the physical properties of $BiNbO_4$ material but not amend the composition of material. Since the material was directly coated on the stub, therefore some major peaks of Al were observed in the EDS analysis of the samples.

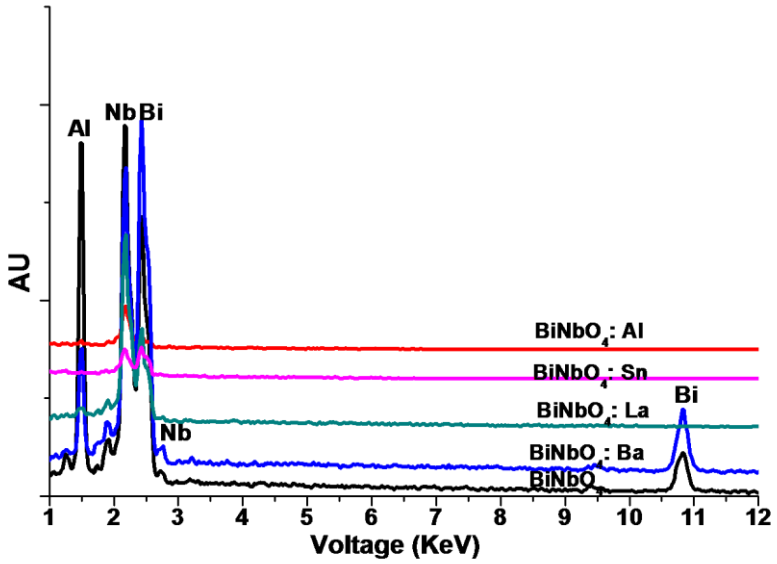

Figure: 6.4 EDS analysis of undoped and metal doped $BiNbO_4$.

Figure 6.5 shows scanning electron micrographs of undoped (a) and metal [(b) La, (c) Al, (d) Sn, (e) Ba] doped $BiNbO_4$. Figure 6.5 indicates that the undoped and doped materials have various morphologies with different shapes and particle sizes. All the materials have very small sized particles in a range of few nano-meters. As shown in Figures 6.5b, and 6.5c, La and Al doped $BiNbO_4$ present very uniformed and regular shapes, however the size of the agglomerates are comparatively larger than that of undoped, Ba, and Sn doped $BiNbO_4$. Furthermore, La and Al doped $BiNbO_4$ have few nanosized particles deposited on large agglomerates. The morphology of undoped, Ba, and Sn doped $BiNbO_4$ is different from Al, and La doped materials. The undoped, Ba, and Sn doped materials have a large number of nano sized particles residing on the layered like structures. These layered like structures and nano sized particles are advantageous for the photocatalytic process. The existence of the structure introduces defects in the materials at various energy levels which will enhance UV and visible light absorption. Previous investigations reported $BiNbO_4$ particles in micro-size [2, 26, 29], however, the average particle size of undoped and doped $BiNbO_4$ in this report is in the range of a few nanometres to hundred nanometres.

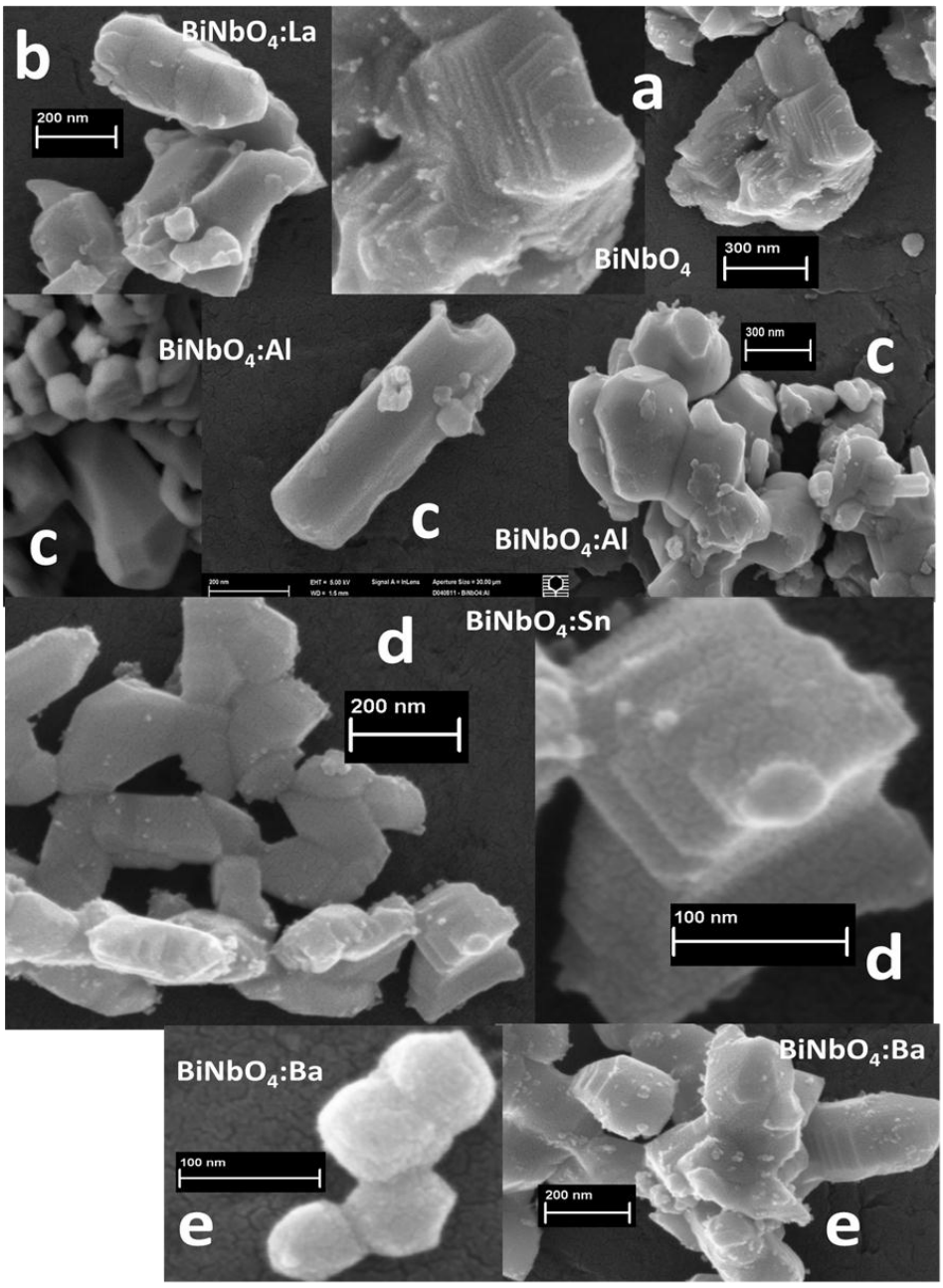

Figure: 6.5 Scanning electron micrographs of a) undoped $BiNbO_4$, b) $BiNbO_4$: La, c) $BiNbO_4$: Al, d) $BiNbO_4$: Sn and e) $BiNbO_4$: Ba.

It has been reported that conduction and valence bands of $BiNbO_4$ which contain octahedral $M(Nb)O_6$ are mainly composed of Nb 4d electrons, O 2p and Bi 6s electrons, respectively[30]. Contribution of Bi 6s orbitals extends the valence band

toward the higher energies, making the valence band more positive than that of TiO_2. The conduction band of $BiNbO_4$ is also more distorted than that of TiO_2 where the photo-generated carriers will have longer life time and will not be recombined quickly. As suggested[8] band gap of $BiNbO_4$ can be further modified through cation and anion doping. Therefore, nitrogen and metal ions will modify the band gap and make the material capable to work under visible light irradiation.

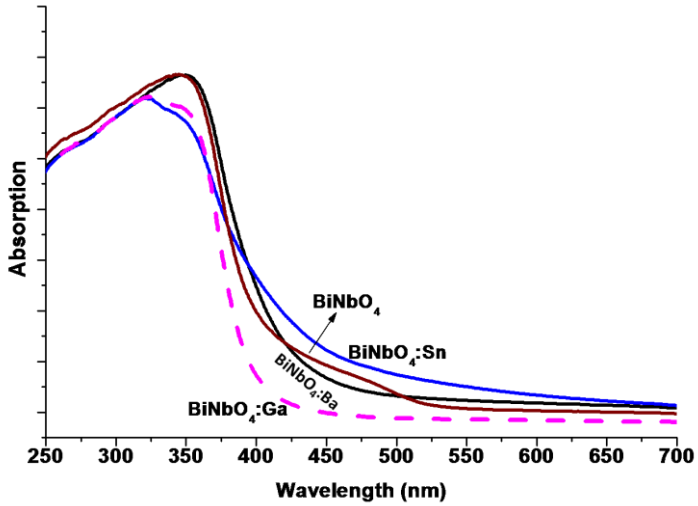

Figure: 6.6 Diffuse reflectance spectroscopy of selected materials.

Figure 6.6 shows the diffuse reflectance absorption spectroscopy of undoped and metal ion doped $BiNbO_4$. It can be seen that absorption edges of doped materials except $BiNbO_4$: Ga presented a red-shift as compared to that of undoped $BiNbO_4$ (Table 6.1). This indicated that dopant ions have different effects on the photo-physical properties of the doped materials. Band gaps were calculated from the corresponding absorption edges. The band gap of undoped orthorhombic and triclinic $BiNbO_4$ are reported 3.5 eV [31] and 3.39 eV [12], respectively. The calculated band gap of undoped $BiNbO_4$ in this investigation was 2.93 eV. Unconventionally, a blue shift in Ga doped material revealed that $BiNbO_4$: Ga absorbs more black light than visible light. This blue shift in the band gap may be attributed to the smaller particle size of materials and generation of defect states at higher energies due to Ga ion doping.

Table 6.1: Band gap and absorption edge of doped $BiNbO_4$.

Dopant	Absorption edge (nm)	Band gap (eV)
Ga	405	3.06
Undoped	423	2.93
Ba	425	2.91
La	445	2.79
Al	448	2.77
Sn	485	2.56

The ionic sizes of the dopants, Ba^{3+}(1.35 Å), Sn^{2+}(0.69 Å), Ga^{3+}(0.62 Å), Al^{3+}(0. 535Å), and La^{3+}(1.061 Å), are different from that of Bi^{3+}(1.02 Å). They may take different positions and cause different effects [32]. Based on their substitutional and/or interstitial positions, dopant ions can introduce the change of particle growth, oxygen vacancies at various energy levels, produce charge defects, and/or cause plane dislocations in the crystal structure of $BiNbO_4$. Consequently, these various dopant ions modify the physical properties of the material e.g. substitution of Bi^{3+} with La^{3+} reduced the number of defect sites[2], Ga^{3+} reduced particle growth, and Sn^{2+} increased the number of oxygen vacancies and defect states.

6.3.2 Photocatalytic decomposition of toluene

Photocatalytic activities of doped and undoped $BiNbO_4$ were investigated in toluene decomposition with both UV and visible irradiations. Figure 6.7 shows gaseous toluene decomposition profiles over various $BiNbO_4$ catalysts under UV irradiation. Both metal and nitrogen doped $BiNbO_4$ catalysts showed a faster rate in toluene degradation than that of undoped one. Metals like Ga, Sn, Ba, and Al have improved photocatalytic decomposition of toluene with UV light in terms of conversion and stability while La has an adverse effect on the photocatalytic activity of $BiNbO_4$. Photo-degradation of toluene on $BiNbO_4$ doped with Ga, and Sn is much better than that of $BiNbO_4$: N.

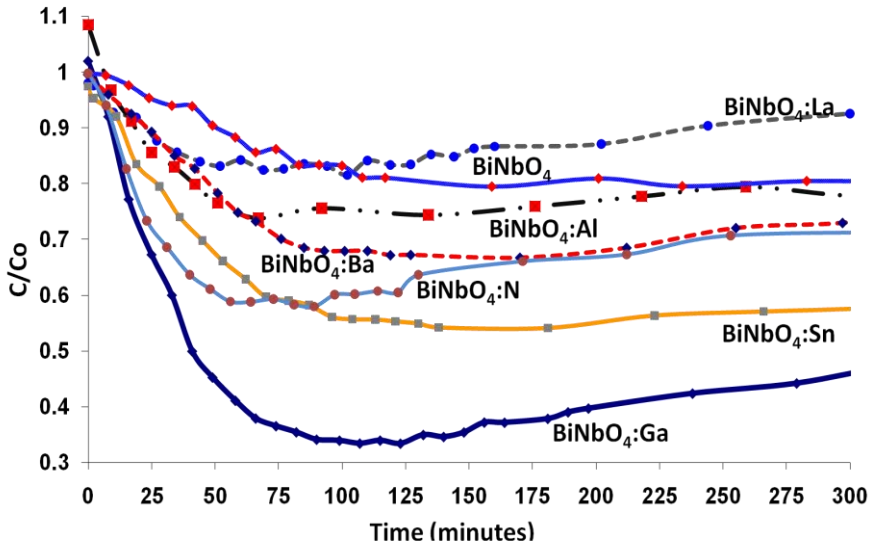

Figure: 6.7 Photocatalytic activities of materials with UV light irradiation.

Figure 6.8 compares photocatalytic performance of $BiNbO_4$: Ga, $BiNbO_4$: Sn, $BiNbO_4$: N and the commercial TiO_2 (P25) under UV light irradiation. It can be seen that $BiNbO_4$: Ga and $BiNbO_4$: Sn have much higher activity than TiO_2, while the activity of $BiNbO_4$: N is similar to that of TiO_2. Figures 6.7 and 6.8 further reveal that undoped and doped $BiNbO_4$ showed very stable performance while TiO_2 deactivated very rapidly. Although TiO_2 has better performance in the initial half an hour, its photocatalytic activity started decreasing after 40 min of irradiation. $BiNbO_4$ doped with Ga, Sn and N displayed very stable activity and no deactivation was observed. Photocatalytic decomposition of toluene under UV light irradiation on all materials was in an order of $BiNbO_4$: Ga > $BiNbO_4$: Sn > TiO_2 > $BiNbO_4$: N > $BiNbO_4$: Ba > $BiNbO_4$: Al > $BiNbO_4$ > $BiNbO_4$: La.

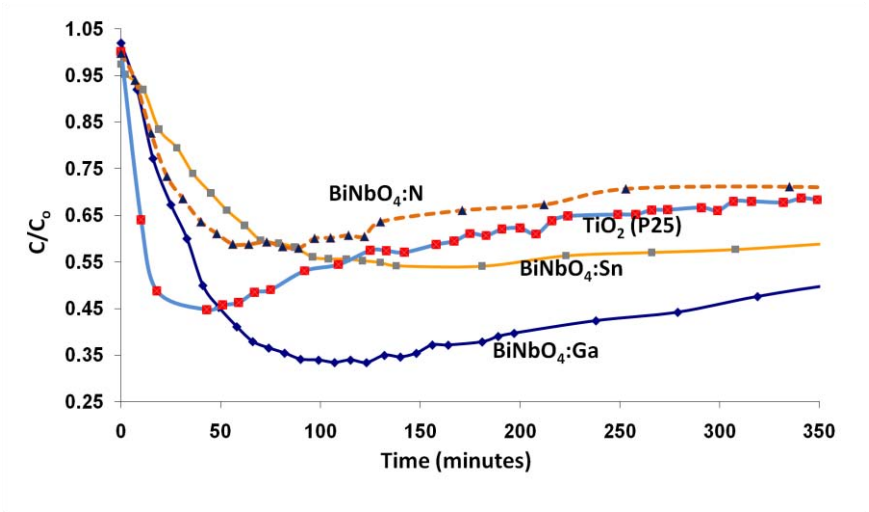

Figure: 6.8 Comparing photocatalytic activities of doped and undoped $BiNbO_4$ with TiO_2 under UV irradiation.

The effect of dopant concentration on the photocatalytic activities of doped $BiNbO_4$ was also investigated. Detailed photocatalytic activities of all the materials at UV and visible light irradiation are given in Table 6.2. It can be seen that, not only the type of dopants but concentration[33] of dopants in parent material also amends photocatalytic decomposition of toluene. Large numbers of studies on the photocatalytic performance of materials doped with anion and/or cation have identified a suitable concentration of dopant ions [34]. However, the optimum concentration of dopant ions showing the maximum photocatalytic activities was not identical instead it was dopant type dependent [30, 35, 36]. $BiNbO_4$ doped with 1 wt% Sn, 2 wt% Ba, and 2 wt% Ga have better performance than other dopant concentrations (0.5 wt%, and 1 wt%). We believe that dopant concentration lower than 2 wt% (in case of Ga, and Ba) could not create significant number of vacancies (oxygen and charge) and defect states, which are the sources of electron hole pairs upon UV/visible light irradiation.

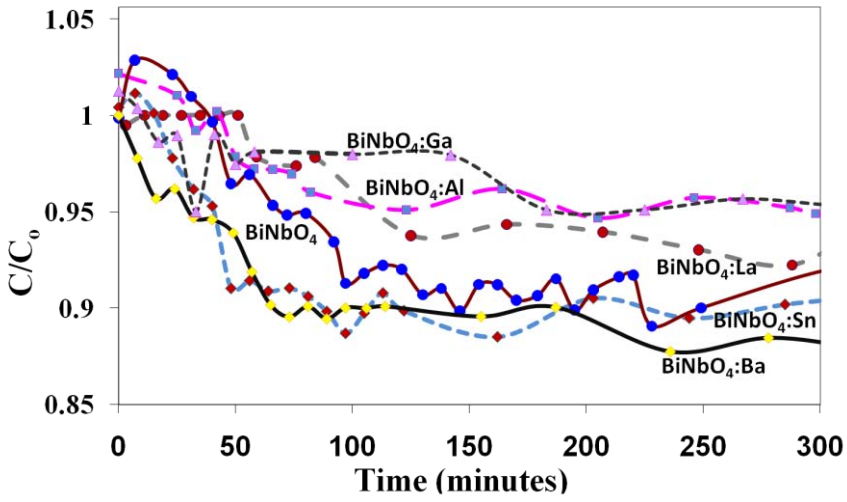

Figure: 6.9 Photocatalytic decomposition of toluene with doped $BiNbO_4$ irradiated with sun light from solar simulator.

The main objective of this study was to explore a new material which can decompose gaseous VOCs with visible light. Therefore, undoped and doped $BiNbO_4$ were also examined for the photocatalytic decomposition of toluene using visible light from a solar simulator. Figure 6.9 shows conversion of toluene over the undoped and doped $BiNbO_4$ irradiated with visible light from the solar simulator. It can be seen that $BiNbO_4$: Ba and $BiNbO_4$: Sn could decompose toluene faster than undoped $BiNbO_4$, whereas $BiNbO_4$: Ga, $BiNbO_4$: La and $BiNbO_4$: Al were found to be slower in toluene decomposition. Within the initial three hours of irradiation, $BiNbO_4$: Ba and $BiNbO_4$: Sn showed almost similar performance toward toluene conversion, the former having more stability and long life time. $BiNbO_4$: Ba has a maximum toluene conversion of about 13- 15% among all materials when irradiated with the solar simulator. It must be noted that $BiNbO_4$: Ga showing the best performance under UV light displayed the lowest activity at visible light. Similarly, activity of La, and Al doped $BiNbO_4$ is also very weak and lower than undoped $BiNbO_4$. The overall performance of undoped and doped materials with visible light irradiation was listed as $BiNbO_4$: Ba> $BiNbO_4$: Sn > $BiNbO_4$ > $BiNbO_4$: La> $BiNbO_4$: Al > $BiNbO_4$: Ga. Interestingly, this trend of photocatalytic activities is reverse to the order under UV light irradiation. $BiNbO_4$: Ba has the lowest activity with UV light irradiation, while it has the best activity

with visible light. It is noted that, neither TiO_2 nor $BiNbO_4$: N could decompose toluene under visible light irradiation.

There are few reports indicating that modified TiO_2 [37] and ZnO [38] have higher activity at visible light than that of black light. As stated earlier, the type and content of dopants produced different changes to the physical properties of the materials based on the positions occupied by the dopant ions. Since the reactive centres (oxygen vacancies, defect states, and charge vacancies) produced by the dopants ions have different energy levels, and therefore respond to the UV/visible light irradiation in different manners. The material like $BiNbO_4$: Ba has a large number of reactive centres within the energy range of visible light, therefore, it responds to the light at required energy for excitation. However, the response of such a material to UV light irradiation is lower, since radiation with higher energy either passes through the reactive centres swiftly or generates highly energetic electron hole pairs with a short life time and recombines before participating in the redox reaction. On the other hand materials like $BiNbO_4$: Ga has reaction centres (oxygen vacancies, defect states, and charge vacancies) within the energy range of UV light, which generates electron-hole pair with a longer life time. Obviously these types of materials either response very weakly or behave totally inert to visible light due to the lower energy of radiation.

Thus it can be deduced that various defect states, oxygen vacancies and mid gap impurities which have different energies can only produce electron-hole pairs when irradiated with the light having suitable energy. Radiations having energy lower or higher than the reactive centres are either energetically incapable to generate carriers, or over energetic to produce carriers with short life time and cause recombination.

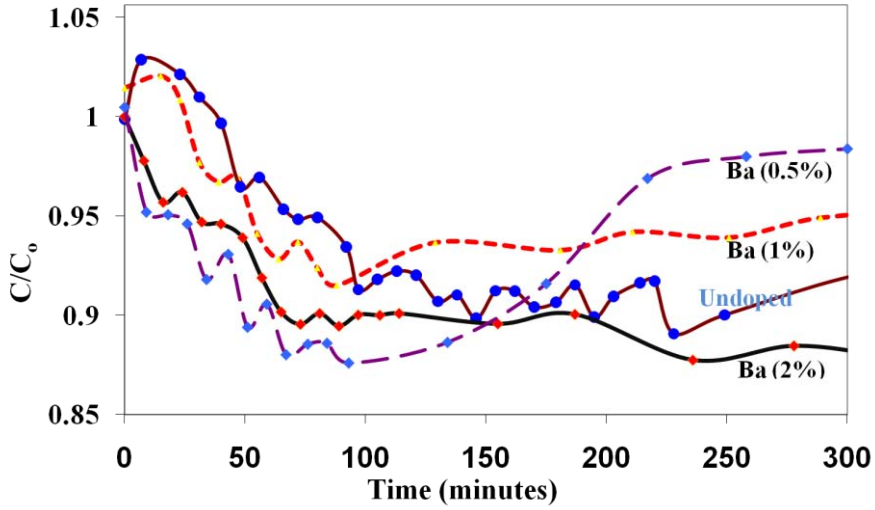

Figure: 6.10 Variation of photocatalytic activities with dopant (Ba) concentration.

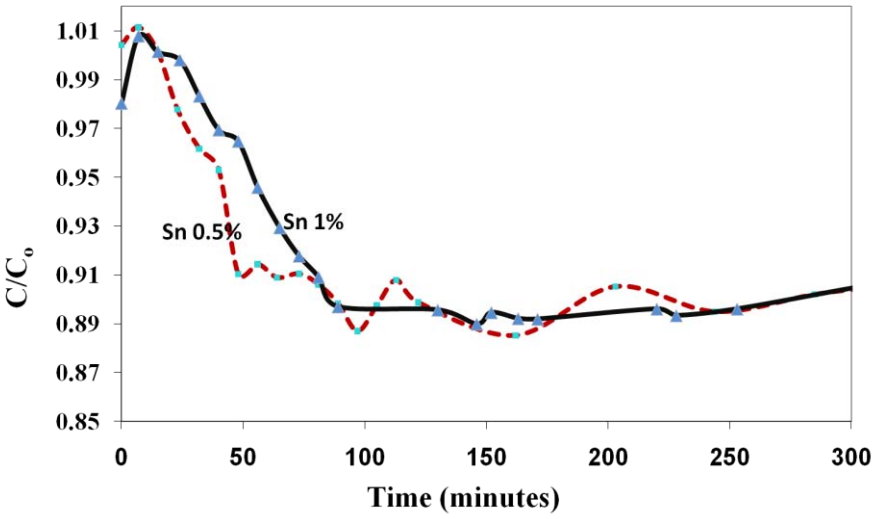

Figure: 6.11 Variation of photocatalytic activities with dopant (Sn) concentration.

Figure 6.11 illustrates the effect of dopant content on the photocatalytic decomposition of toluene with visible light irradiation. Variation in Sn concentration has a weak effect on the photocatalytic performance of $BiNbO_4$: Sn, while Ba concentration has a significant effect on the photocatalytic activities of $BiNbO_4$: Ba. At 0.5% dopant concentration $BiNbO_4$: Ba has shown better performance in the initial two hours, however, at 2% concentration $BiNbO_4$: Ba has

very stable activity and long life time. In general, $BiNbO_4$: Ba at 2 % dopant (Figure 6.10) concentration exhibited better activity under UV and visible light irradiation.

Table 2: Overall performance of all the materials with UV and visible light.

Materials	Dopant concentration (W/w %)	Conversion (C/C_o)	
		Visible light	UV light
$BiNbO_4$	0	7.12	10.49
$BiNbO_4$:Sn	0.5	6.57	18.11
$BiNbO_4$:Sn	1	6.36	29.98
$BiNbO_4$:Ba	0.5	8.34	13.52
$BiNbO_4$:Ba	1	5.31	22.0
$BiNbO_4$:Ba	2	11.91	6.86
$BiNbO_4$:La	2	3.0	13.58
$BiNbO_4$:Al	2	2.91	15.48
$BiNbO_4$:Ga	2	3.0	53
$BiNbO_4$:N	?	10.26	32.62
TiO_2	0	6.0	46.0

Comparing overall performance of all the materials, it can be deduced that, $BiNbO_4$: Al, and $BiNbO_4$: La have the lowest photocatalytic activities with both UV and visible light, while $BiNbO_4$: Ba (2%), and $BiNbO_4$: Ga have the best performance with visible light and UV light respectively. Previously, lower photocatalytic activities of doped materials were attributed to the looseness of crystallinity in structure due to doping[33], however, in our case the lower activities of La, and Al doped materials are attributed to lack of nano-sized particles on the large agglomerates, lack of lapped structures and reduction of defect states[2]. As can be seen in the SEM images of the doped materials, both Al, and La doped materials have very large sized agglomerates without any nano-sized particles and layers on

the surfaces, therefore these materials have very limited number of reactive centres/defects[2] and would very poorly respond to UV-visible light irradiation. Choi et al.[39] found Al doping produced the worst effect on the photocatalytic activities of TiO_2. Lanthanides doped $BiNbO_4$ [2] has enhanced conductivity and dielectric properties due to large number of defect states introduced by various lanthanides ions (dopants) but La[32] doping has significantly small number of defect states which reduced the conductivity of the material. Therefore, we suggest that Al and La doping in $BiNbO_4$ reduced the defect states and oxygen vacancies in the structure and consequently lowered the photocatalytic activities of $BiNbO_4$.

Higher photocatalytic activities of $BiNbO_4$, $BiNbO_4$: Ga, $BiNbO_4$: Sn, $BiNbO_4$: Ba and $BiNbO_4$: N are mainly attributed to the existence of nano-sized particles on the surface of large agglomerates and existence of various reactive centres (oxygen vacancies, charge vacancies, and defect sites). It must be noted that dopants other than La, and Al increase reactive centres and therefore, have higher activities than undoped $BiNbO_4$. Ba, Sn, Al, and La doping increased the optical absorption, but Ga showed a blue shift of the absorption toward the lower wavelength. Co^{3+} and Fe^{3+} doped TiO_2 also absorbed more visible light than others but their photocatalytic activities were worsen[40]. Thus enhancement in the optical absorption by doping semiconductor photocatalysts with metals and/or non-metals is not the determined parameter to improve the photocatalytic activities of materials. There are some other parameters, such as particle size, crystal structure, phase of the crystal structures, defect states, oxygen vacancies, position of these defects and impurity states introduced by dopants, could also modify the photocatalytic activities of materials. Blue shifts in the absorption edge of $BiNbO_4$: Ga ensure more UV absorption, which subsequently enhance the photocatalytic activity of this material when irradiated with UV light. Similar effect of larger band gap and higher activity was also observed in Bi_2M (Ga, In, Fe)TaO_7 when Ga was used as a dopant[41].

Stability, life time, intermediate adsorption, re-useability and regeneration are important in photocatalytic performance of materials. Although, various

photocatalyst materials including benchmark TiO_2 have higher photocatalytic efficiency and perform very well initially, their activities last in a short time and decline immediately. Therefore, we compare the photocatalytic activity of undoped and doped $BiNbO_4$ to that of TiO_2. As shown in Figure 6.8, initially TiO_2 decomposed toluene very fast with UV light, however, the activity saturated very quickly and then declined immediately. TiO_2 has been reported to be stable[42] under UV irradiation where no photo-corrosion and/or variation in crystal has been observed, its affinity to intermediates and water significantly reduced its activity. This high adsorption of reaction intermediates[43] and water on TiO_2 surface reduced its life time, by covering the active sites and making TiO_2 impractical for repeated use and/or re-generation[44]. These are the main drawbacks of TiO_2 as a photocatalyst. Nevertheless, doped $BiNbO_4$ has shown much better performance than TiO_2, since the former has very less affinity for intermediates adsorption and therefore its photocatalytic activities are much stable for a long time. Unlike TiO_2 (Figures 6.8), very small reduction in photocatalytic performance of $BiNbO_4$: Ga was observed. Figure 6.12 compares multiple use of $BiNbO_4$: Ga, which clearly indicates that the photocatalytic performance of the doped material is better than undoped one even after being used for three times. Figure 6.12 further reveals that the activity of $BiNbO_4$: Ga is almost similar in the first two runs, but declines after used in the 3rd time. However, this reduction in activity is recoverable if the material is regenerated properly by complete removal of intermediates adsorbed on the active surface.

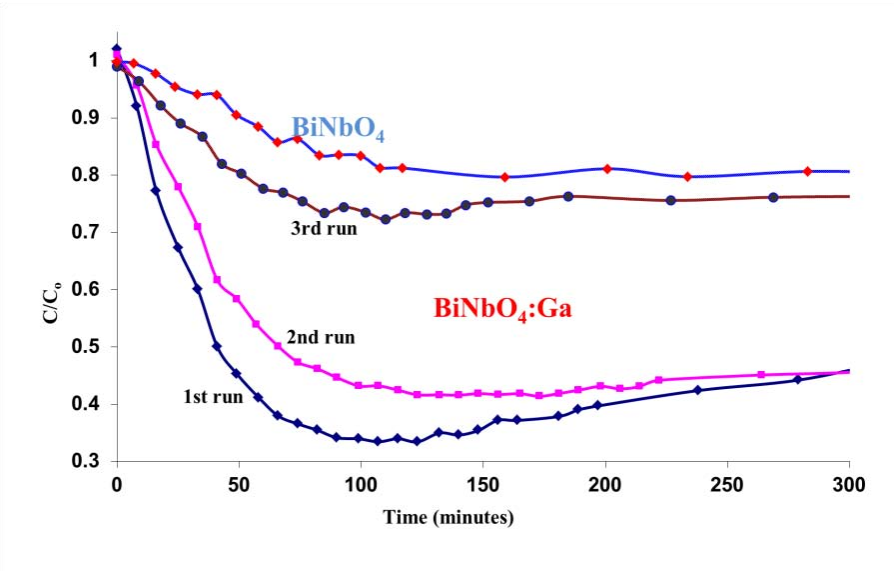

Figure: 6.12 Comparison of repeated use of $BiNbO_4$: Ga, with undoped $BiNbO_4$ with UV light irradiation.

FTIR analysis of used TiO_2[19] has shown strong adsorption of water and three main by-products; benzoic acid, benzaldehyde, and benzyl alcohol[45, 46]. However, none of these intermediates or water was detected on the used undoped and doped $BiNbO_4$ (Figure 6.13). This low adsorption of by-products and/or intermediates on $BiNbO_4$ surface enhanced the life time of the materials much higher than TiO_2 and makes this material capable to withstand its performance for longer time.

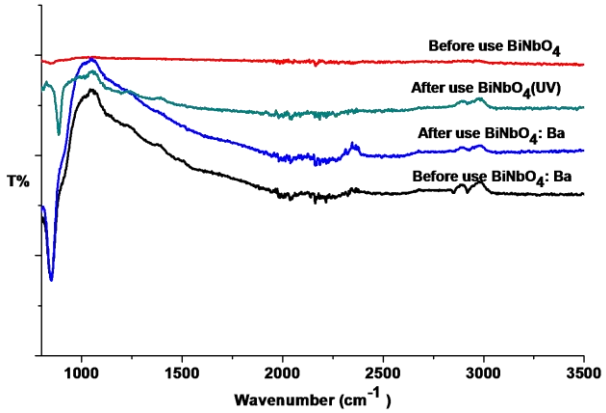

Figure: 6.13 FTIR analysis of used $BiNbO_4$ materials

Although there are few reports[18] on photo-degradation of $BiNbO_4$, however, in our case both the undoped and doped materials were quite stable and no photo-corrosion was observed neither with UV light nor visible light. XRD analysis (Figure 6.14) of undoped $BiNbO_4$ and $BiNbO_4$: Ga (after used four times) clearly indicates that, the crystal structure of the materials is quite stable and no modification in the XRD pattern was detected before and after use. Dunkle et al. [47] has detected a thin layer of only Bi on the surface of $BiNbO_4$, indicating degradation of the material. However, XRD analysis could not detect any Bi formation in our samples. These findings in stability, inertness, longer life time, multiple usage of undoped and doped $BiNbO_4$ and higher photocatalytic activities than TiO_2 under UV and visible light irradiations have proved a new material in the photocatalysis.

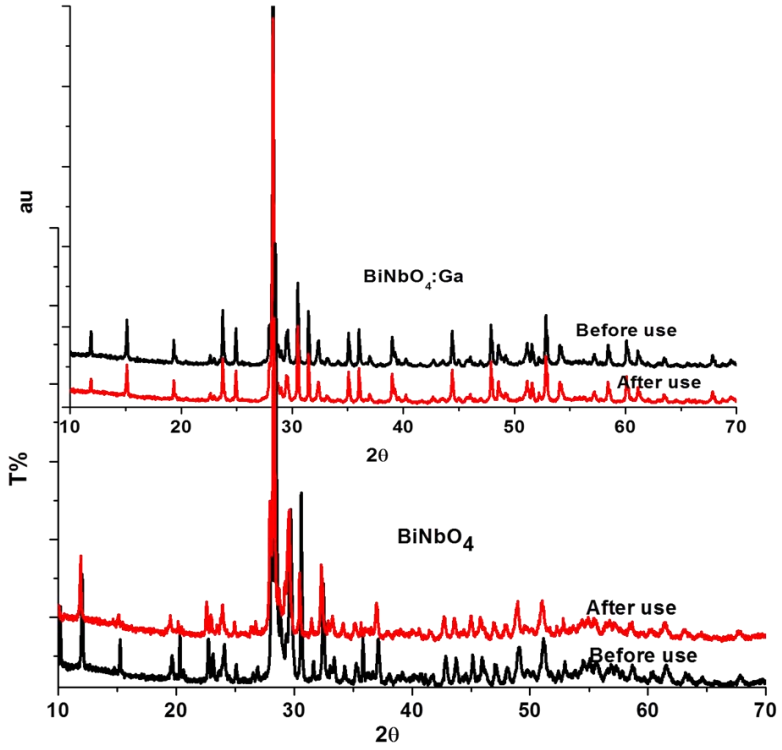

Figure: 6.14 XRD analysis of used and non-used materials

6.4 Conclusion

Multi-phase crystallites of $BiNbO_4$ composed of orthorhombic and triclinic structures were successfully prepared with a solution method. $BiNbO_4$ was also doped with various metals (such as Ga, Ba, Sn, Al and La) and nitrogen for the first time. XRD patterns of metal doped $BiNbO_4$ matched with that of undoped, however a small deviation was observed in nitrogen doped material. All the materials, undoped, metal doped and nitrogen doped samples were tested for photocatalytic decomposition of gaseous toluene with both UV and visible light irradiation. Results demonstrated that Ba, Sn, Ga have improved photocatalytic properties under UV and visible light, however La, and Al doping produced the worse effect on the photocatalytic performance of the materials. $BiNbO_4$: Ba (2%) presented better performance than others for toluene decomposition with visible light irradiation. The photocatalytic performance of $BiNbO_4$: Ga was significantly higher than others and TiO_2 under UV irradiation, however this material has the lowest activity when irradiated with sun light from a solar simulator. Since $BiNbO_4$: Ga has the largest band gap among all doped materials, therefore, it absorbed more UV light showing higher photocatalytic activity at UV light and lower activity at visible light. SEM micrographs of doped and undoped materials have shown layered like structure and large number of nano-sized particles on large agglomerates, which are responsible for catalytic activity. Both undoped and metal doped $BiNbO_4$ has shown much stable and longer time performance both with UV and visible light irradiation. Photocatalytic decomposition of toluene with $BiNbO_4$: Ga and UV irradiation was much faster and stable than TiO_2. Both undoped and doped $BiNbO_4$ are quite stable and no photo-corrosion was observed, suggesting very bright future of these materials.

6.5 References

1. Shihua, D., Y. Xi, and Y. Yong, *Dielectric properties of B2O3-doped BiNbO4 ceramics.* Ceramics International, 2004. **30**(7): p. 1195-1198.

2. Butee, S., et al., *Effect of lanthanide ion substitution on RF and microwave dielectric properties of BiNbO4 ceramics.* Journal of Alloys and Compounds, 2010. **492**(1-2): p. 351-357.

3. Setter, N. and R. Waser, *Electroceramic materials.* Acta Materialia, 2000. **48**(1): p. 151-178.

4. Kang, Y.J., et al., *Optical properties of bismuth niobate thin films studied by spectroscopic ellipsometry.* Thin Solid Films, 2010. **518**(22): p. 6526-6530.

5. Liou, Y.-C., W.-C. Tsai, and H.-M. Chen, *Low-temperature synthesis of BiNbO4 ceramics using reaction-sintering process.* Ceramics International, 2009. **35**(6): p. 2119-2122.

6. Almeida, C.G., et al., *Synthesis of nanosized [beta]-BiTaO4 by the polymeric precursor method.* Materials Letters, 2010. **64**(9): p. 1088-1090.

7. Radha, R., et al., *A co-precipitation technique to prepare BiNbO4 powders.* Ceramics International, 2008. **34**(6): p. 1565-1567.

8. Nisar, J., et al., *Mo- and N-doped BiNbO4 for photocatalysis applications.* Appl. Phys. Lett., 2011. **99**(Copyright (C) 2011 American Chemical Society (ACS). All Rights Reserved.): p. 051909/1-051909/3.

9. Keve, E.T. and A.C. Skapski, *The crystal structure of triclinic β-BiNbO4.* Journal of Solid State Chemistry, 1973. **8**(2): p. 159-165.

10. Wang, N., et al., *Low-temperature synthesis of [beta]-BiNbO4 powder by citrate sol-gel method.* Materials Letters, 2003. **57**(24-25): p. 4009-4013.

11. Subramanian, M.A. and J.C. Calabrese, *Crystal structure of the low temperature form of bismuth niobium oxide [α-BiNbO4].* Materials Research Bulletin, 1993. **28**(6): p. 523-529.

12. Li, A.-D. and A. Li, *Ferroelectric and photocatalytical properties of Ta-based and Nb-based oxide ceramics and powders from environmentally friendly water-soluble tantalum and niobium precursors.* Materials science forum, 2010. **654-656**(Pt): p. 2029.

13. Zhou, D. and D. Zhou, *Phase composition and phase transformation in Bi(Sb,Nb,Ta)O4 system.* Solid State Sciences, 2009. **11**(11): p. 1894.

14. Rao, K.S. and S. Buddhudu, *Structural, Thermal and Dielectric Properties of BiNbO4 Ceramic Powder.* Ferroelectrics Letters Section, 2010. **37**(6): p. 101-109.

15. Zou, Z., et al., *Photocatalytic and photophysical properties of a novel series of solid photocatalysts, BiTa1-xNbxO4.* Chemical Physics Letters, 2001. **343**(3-4): p. 303-308.

16. Zou, Z. and H. Arakawa, *Direct water splitting into H2 and O2 under visible light irradiation with a new series of mixed oxide semiconductor photocatalysts.* Journal of Photochemistry and Photobiology A: Chemistry, 2003. **158**(2-3): p. 145-162.

17. Yang, Y., S. Ding, and X. Yao, *Study on the relationship between the defect and dielectric properties of ZnO-doped BiNbO4 ceramic.* Ceramics International, 2004. **30**(7): p. 1335-1339.

18. Muktha, B. and Muktha, *Crystal structures and photocatalysis of the triclinic polymorphs of BiNbO4 and BiTaO4.* Journal of Solid State Chemistry, 2006. **179**(12): p. 3919.

19. Ullah, R., et al., *Wet-chemical Synthesis of InTaO4 for Photocatalytic Decomposition of Organic Contaminants in Air and Water with UV-vis Light.* Industrial & Engineering Chemistry Research, 2011: DOI. 10.1021/ie200544z.

20. Arney, D., et al., *Flux synthesis of AgNbO3: Effect of particle surfaces and sizes on photocatalytic activity.* Journal of Photochemistry and Photobiology A: Chemistry, 2010. **214**(1): p. 54-60.

21. Li, X. and J. Zang, *Facile Hydrothermal Synthesis of Sodium Tantalate (NaTaO3) Nanocubes and High Photocatalytic Properties.* The Journal of Physical Chemistry C, 2009. **113**(45): p. 19411-19418.

22. Shi, L. and D. Weng, *Highly active mixed-phase TiO2 photocatalysts fabricated at low temperatureand the correlation between phase compositionand photocatalytic activity.* Journal of Environmental Sciences, 2008. **20**(10): p. 1263-1267.

23. Kim, E.S. and W. Choi, *Effect of phase transition on the microwave dielectric properties of BiNbO4.* Journal of the European Ceramic Society, 2006. **26**(10-11): p. 1761-1766.

24. Zhou, D., et al., *Phase transformation in BiNbO4 ceramics*. Vol. 90. 2007: AIP. 172910.

25. Muthurajan, H., *A co-precipitation technique to prepare BiTaO4 powders.* Materials Letters, 2008. **62**(3): p. 501.

26. Zhai, H.-F., et al., *Abnormal phase transition in BiNbO4 powders prepared by a citrate method.* Journal of Alloys and Compounds. DOI: 10.1016/j.schres.2011.09.029.

27. Wang, N., M.-Y. Zhao, and Z.-W. Yin, *Effects of Ta2O5 on microwave dielectric properties of BiNbO4 ceramics.* Materials Science and Engineering B, 2003. **99**(1-3): p. 238-242.

28. Keve, E.T. and A.C. Skapski, *The structure of triclinic BiNbO4 and BiTaO4.* Chemical Communications (London), 1967(6): p. 281-283.

29. Li, A.-D., et al., *Ferroelectric and Photocatalytical Properties of Ta-based and Nb-based Oxide Ceramics and Powders from Environmentally Friendly Water-soluble Tantalum and Niobium Precursors*, in *Pricm 7, Pts 1-3*, J.F.M.A. Nie, Editor. 2010. p. 2029-2032.

30. Zou, Z. and Z. Zou, *Substitution effect of Ta5+ by Nb5+ on photocatalytic, photophysical, and structural properties of BiTa1-xNbxO4.* Journal of materials research, 2002. **17**(06): p. 1446.

31. Wiegel, M., W. Middel, and G. Blasse, *Influence of ns2 ions on the luminescence of niobates and tantalates.* Journal of Materials Chemistry, 1995. **5**(7): p. 981-983.

32. Wang, N., et al., *Effects of complex substitution of La and Nd for Bi on the microwave dielectric properties of BiNbO4 ceramics.* Materials Research Bulletin, 2004. **39**(3): p. 439-448.

33. Yu, J.C., et al., *Effects of F- Doping on the Photocatalytic Activity and Microstructures of Nanocrystalline TiO2 Powders.* Chemistry of Materials, 2002. **14**(9): p. 3808-3816.

34. Akpan, U.G. and B.H. Hameed, *Parameters affecting the photocatalytic degradation of dyes using TiO2-based photocatalysts: A review.* Journal of Hazardous Materials, 2009. **170**(2-3): p. 520-529.

35. Ye, J. and Z. Zou, *Visible light sensitive photocatalysts In1-xMxTaO4 (M=3d transition-metal) and their activity controlling factors.* Journal of Physics and Chemistry of Solids. **66**(2-4): p. 266-273.

36. Ye, J., et al., *Correlation of crystal and electronic structures with photophysical properties of water splitting photocatalysts InMO4 (M=V5+,Nb5+,Ta5+).* Journal of Photochemistry and Photobiology A: Chemistry, 2002. **148**(1-3): p. 79-83.

37. Chuang, H.-Y. and D.-H. Chen, *Fabrication and photocatalytic activities in visible and UV light regions of Ag-TiO 2 and NiAg-TiO 2 nanoparticles.* Nanotechnology, 2009. **20**(10): p. 105704.

38. Ullah, R. and J. Dutta, *Photocatalytic degradation of organic dyes with manganese-doped ZnO nanoparticles.* Journal of Hazardous Materials, 2008. **156**(1-3): p. 194-200.

39. Choi, W., A. Termin, and M.R. Hoffmann, *The Role of Metal Ion Dopants in Quantum-Sized TiO2: Correlation between Photoreactivity and Charge Carrier Recombination Dynamics.* The Journal of Physical Chemistry, 1994. **98**(51): p. 13669-13679.

40. Bouras, P., E. Stathatos, and P. Lianos, *Pure versus metal-ion-doped nanocrystalline titania for photocatalysis.* Applied Catalysis B: Environmental, 2007. **73**(1-2): p. 51-59.

41. Wang, J., Z. Zou, and J. Ye, *Surface modification and photocatalytic activity of distorted pyrochlore-type Bi2M(M=In, Ga and Fe)TaO7 photocatalysts.* Journal of Physics and Chemistry of Solids. **66**(2-4): p. 349-355.

42. Sun, H., et al., *Visible-light-driven TiO2 catalysts doped with low-concentration nitrogen species.* Solar Energy Materials and Solar Cells, 2008. **92**(1): p. 76-83.

43. Guo, T., et al., *Influence of relative humidity on the photocatalytic oxidation (PCO) of toluene by TiO2 loaded on activated carbon fibers: PCO rate and intermediates accumulation.* Applied Catalysis B: Environmental, 2008. **79**(2): p. 171-178.

44. Carneiro, J.T., J.A. Moulijn, and G. Mul, *Photocatalytic oxidation of cyclohexane by titanium dioxide: Catalyst deactivation and regeneration.* Journal of Catalysis, 2010. **273**(2): p. 199-210.

45. d'Hennezel, O., P. Pichat, and D.F. Ollis, *Benzene and toluene gas-phase photocatalytic degradation over H2O and HCL pretreated TiO2: by-products and mechanisms.* Journal of Photochemistry and Photobiology A: Chemistry, 1998. **118**(3): p. 197-204.

46. Sleiman, M., et al., *Photocatalytic oxidation of toluene at indoor air levels (ppbv): Towards a better assessment of conversion, reaction intermediates and mineralization.* Applied Catalysis B: Environmental, 2009. **86**(3-4): p. 159-165.

47. Dunkle, S.S. and K.S. Suslick, *Photodegradation of BiNbO4 Powder during Photocatalytic Reactions.* The Journal of Physical Chemistry C, 2009. **113**(24): p. 10341-10345.

7

7 - Effect of nitrogen doping on the photocatalytic activities of Ta_2O_5 and Nb_2O_5 Nanoparticles

Abstract

Nb_2O_5, Nb_4N_5, Ta_2O_5 and nitrogen doped Ta_2O_5 were prepared at moderate sintering temperature of 700 °C using a solution method. Most of the materials were multi crystalline with orthorhombic and monoclinic structures. The materials were characterized by X-ray diffraction analysis (XRD), scanning electron microscopy (SEM), Fourier transform infra-red spectroscopy (FTIR), and diffuse reflectance spectroscopy. All the materials were used for photocatalytic decomposition of gaseous toluene irradiated with artificial solar light and pure visible light. Undoped Ta_2O_5 and nitrogen doped (Ta_2O_5: N (Lab)) have shown much better performance than niobium based materials. We have found that laboratory made nitrogen doped material Ta_2O_5: N (Lab) decomposed gaseous toluene with much higher rate than all other materials irradiated with artificial sun light. Ta_2O_5: N (Lab) decomposed about 70 % toluene with artificial sun light while 30 % with pure visible light. All the materials exhibited very stable performance with artificial sunlight and pure visible light.

7.1 Introduction

Visible light photocatalysis has been thoroughly investigated for water splitting, oxidation of volatile organic compounds, and CO_2 reduction using various types of photocatalytic materials. Recent investigations showed that heavy metal oxide semiconductors such as Ta_2O_5 and Nb_2O_5 have almost comparable photo-physical properties as a land mark photocatalyst TiO_2. These materials and their modified forms may have the opportunities to be activated only with visible light and could display better performance than the commercial photocatalyst material. However, large band gaps (3.9 eV and 3.4 eV) are the major concerns which inhibit activation of these compounds with visible light irradiation. Nevertheless, band gap modification through nitrogen doping has been proven as a successful technique to induce redshifts of the optical absorption of these materials and make them capable to operate only with visible light irradiation. Highly mesoporous structure of these materials is advantageous for the efficient transition of photo-generated carriers to the adsorbed species on the surface. Structure porosity, pore wall thickness, stability and hydrophobicity of these compounds are strongly dependent on the preparation methods[1]. Although porosity of Ta_2O_5 prepared with neutral surfactant tempalting method (NST) and sintering temperature of 800 °C is weaker than the material sintered at 700 °C prepared with ligand assisted tempalting method (LAT), however, NST material has more stability and also more hydrophobicity. Porosity of Nb_2O_5 prepared with various sintering temperatures (400 °C, 450 °C, 500 °C) was reduced with increased calcination temperature [2], indicating pore collapse and particle aggregation at high sintering temperature. Although Nb_2O_5 prepared at higher temperature has lower band gap (3.02 eV) than that prepared at lower temperature, the latter one has better photocatalytic activity for H_2 production mainly attributed to the thinner pore wall. The material prepared at higher temperature has a thicker pore wall which affects electron migration and electron hole pair recombination. Kominami et al. [3] have reported that amorphous Nb_2O_5 due to its high surface area possessed better photocatalytic activity both for hydrogen production and mineralization of acetic acid than that of crystalline

material and commercial Nb_2O_5. Although Nb_2O_5 can be used as an efficient photocatalyst with a better selectivity for aerobic oxidation of various types of amines[4] and alcohols[4, 5] under visible light irradiation, its photocatalytic performance was lower than TiO_2. Carbon [6] in carbonate species adsorbed on Nb_2O_5 was successful to modify the surface and optical absorption of the material, consequently enhanced its photocatalytic activities under visible light irradiation.

Ta_2O_5 annealed at 700 °C in ammonia environment was doped with nitrogen [7] whereas annealing at 850 °C transformed the material to TaON phase. UV/visible spectroscopy have shown a red shift in the optical absorption which clearly indicated that doped nitrogen substitutes oxygen and reduces band gap of the material. Photocatalytic activities of all the materials evaluated with gaseous 2 propanol (both under UV and visible light irradiation) revealed that nitrogen doped Ta_2O_5 decomposed IPA to CO_2 and acetone at a faster rate than non-doped Ta_2O_5; however, TaON was not active under visible light irradiation and could not decompose gaseous 2 – propanol, although the band gap of TaON [8] prepared with sol-gel techniques was observed to be 2.4 eV.

Sato et al.[9] have reported reduction of CO_2 to HCOOH via visible light photocatalytic reaction using p-type N–doped Ta_2O_5 as a photocatalyst, triethanol-amine (TEOA) as an electron donor and Ru complex as a metal complex. In this system upon visible light irradiation, electrons were photo-excited to the conduction band of Ta_2O_5, transferred efficiently to the metal complex adsorbed on the surface of the semiconductor material and reduced CO_2 to HCOOH. The difference in potential energies of conduction band minimum of semiconductor and CO_2 reduction potential energy of metal complex was the main reason for reduction of CO_2. It was further detailed[10] that in case of N-doped Ta_2O_5 photo-excited electrons trapped at deep defect sites, after being excited at shallow defect states. However, for Ru loaded N-doped Ta_2O_5, electronic transition occurred from shallow defect states to the adsorbed Ru complex.

Various studies[2], [11] have shown that phase of Ta_2O_5 changes to p-type nitrogen doped Ta_2O_5[12], TaON, and Ta_3N_5 at increased annealing temperature above 700 °C in nitrogen environment [13]. Band gaps and conduction band edges of Ta_2O_5, TaON and Ta_3N_5 determined with ultraviolet photoelectron spectroscopy (UPS) were measured to be 3.9, 2.4, 2.1 eV, and -3.93, -4.1 and -4.14 eV, respectively. Valence bands energies of TaON (-6.6 eV) and Ta_3N_5 (-6.02 eV) were much higher than that (-7.93 eV) of Ta_2O_5. Valence bands of Ta_2O_5, TaON and Ta_3N_5 were consisted of O 2p, O 2p + N 2p, and only N 2p orbitals respectively, whereas conduction bands of all these materials are made of Ta 5d orbitals. The latter two compounds have more absorption in the visible region, and might be suitable for photocatalytic reaction. Ho et al. [14] have attempted to prepare colloidal Ta_3N_5 nanoparticles via different synthesis techniques for enhanced H_2 production via visible light irradiation, however, very minute increase in the band gap of the nanoparticles was not promising for enhancement of efficiency. Zhang et al.[13] have found that band gap of Ta_3N_5 prepared by nitriding amorphous Ta_2O_5 is crystal size dependent with the average value of 2.04 eV. The material has shown better performance than nitrogen doped TiO_2 for methylene blue decomposition with visible light irradiation.

Herein we report wet-chemical synthesis of Nb_2O_5, Nb_4N_5, undoped and nitrogen doped Ta_2O_5. Nitrogen doped Ta_2O_5 has shown much better performance than both undoped Ta_2O_5 and commercial TiO_2 for gaseous toluene decomposition with artificial solar light and visible light irradiation.

7.2 Experimental

7.2.1 Material synthesis

Polycrystalline non-doped Ta_2O_5 and Nb_2O_5 materials were prepared by dissolving the precursor salts in ethanol. All of chemicals were obtained from Sigma-Aldrich at 99.99% purity and were used as received. In a typical synthesis, 20 mmol of Tantalum (V) chloride ($TaCl_5$)/Niobium (V) chloride ($NbCl_5$) were dissolved separately in 80 ml ethanol, mixed with 0.5 - 1.0 mL concentrated nitric acid with

continuously stirring and heating at 80 °C for 6 hours. The final solution with no precipitation was then aged for 24 h at room temperature and was kept in an oven at 60 °C till dried completely. Sample was ground by mortar and pestle and then calcined at 700 °C for 40 h in air/nitrogen to obtained undoped Ta_2O_5 and Nb_2O_5, respectively.

Raw Ta_2O_5 /Nb_2O_5 after grinding were annealed at 700 °C in a tube furnace, where N_2 gas was passed through enclosed flask containing 28% ammonia solution, and was continuously heated at temperature below boiling point of ammonia solution. Mist of ammonia and N_2 gas was then passed through the sample (fitted in tube furnace) with flow rate of 100 mL/min. Ammonia solution mist was continuously passed through the sample for 40 hours and was stopped when temperature of the furnace starts cooling down to room temperature naturally. To insure and maintained proper quantity of nitrogen, ammonia solution was refreshed after every ten hours.

7.2.2 Characterization of catalysts

Crystalline structure of materials were analysed by X-ray diffractometer (Bruker D8 Advance equipped with a Lynx eye detector, Bruker-AXS, Karlsruhe, Germany) operated at 40 kV and 30 mA. The scanning rate was 0.2 sec/step with 2θ (10- 90°) and step size of 0.02°. Cu Kα (λ = 1.54178 Å) was used as a X-ray source with divergent slit of 0.300 and 2.5° primary and secondary soller slits. The optical absorption of samples was determined by UV-vis absorbance spectroscopy using the diffuse reflectance method (JASCO V-670 Spectrometer). Morphology and chemical composition of the materials were examined by scanning electron microscopy (ZEISS NEON 40EsB) equipped with an energy dispersive spectrometer (SEM-EDS). Samples were directly coated on an aluminium stub where 3 nm platinum coating was used as a conducting material. FTIR analysis was performed on a Perkin-Elmer Model FTIR-100 with a MIR detector.

7.2.3 Photocatalytic evaluation

Photocatalytic activities of both undoped and doped samples were evaluated in decomposition of gaseous toluene with artificial solar light irradiations. Xenon lamp (UXL-306, Ushio) was used as an artificial sun light source. The average intensities of the solar simulator with a quartz sheet were 26.0 mW/cm^2 (at 315-400 nm), and 240.0 mW/cm^2 (at 400-1050 nm). However, the intensity of light was reduced to 99.0 mW/cm^2 (at 400-1050 nm) with a soda glass filter. Gaseous toluene was used as a model air contaminant, with a concentration of 100 ppm in air.

Toluene decomposition was evaluated in a flow reactor connected with an on-line gas chromatograph (Shimadzu GC-17A) fitted with a GS-GSPRO column of 60 m in length and 0.32 mm in diameter. Oven temperature of the GC was 220 °C and FID detector temperature was kept at 250 °C. In a typical experiment, 300 mg of photocatalysts were dispersed in 10 mL deionized water in a Petri dish of 450 mm diameter and was dried in an oven overnight. The Petri dish was kept inside an air-tight stainless steel reactor fitted with a removable quartz sheet in order to allow both UV and visible radiation in. A flow of toluene at 100 ppm was continuously passed into the reactor (1.08 L) at a flow rate of 60 mL/min. Temperature of the reactor was controlled by continuously passing cooling water through the reactor and also by blowing fresh air on to the reactor from outside.

7.3 Results and discussions

7.3.1 Material structure

Multi-crystalline phases of Nb_2O_5 containing orthorhombic and monoclinic structures were obtained by sintering the raw mixture at 700 °C for 40 hours. The XRD patterns of the newly prepared material shown in Figure 7.1 exactly matched with that reported by the literature[15]. Lin et al.[16] recently observed phase transformation from amorphous to crystallite started at 500 °C and detected major characteristic peaks of Nb_2O_5 at higher temperature of 650 °C. Nb_2O_5 crystallizes in various forms (T-, B-, H-, N-, and P- forms) depending on the preparation method and sintering temperature[17]. The material prepared at low temperature is meta-

stable, while the one prepared at higher temperature (>1100 °C) has higher stability. Nb_2O_5 prepared at lower temperature (up to 600 °C) in short time has some forms of oxy-chloride [18]. Therefore, we calcined the raw material at medium temperature [18] of 700 °C to obtain the pure and highly crystalline mesoporous Nb_2O_5. The crystalline parameters of our samples for orthorhombic (a = 6.1750 °A, b = 29.1750 °A, c = 3.930 °A, α = 90.00°, β = 90.00°, and γ = 90.00°) and monoclinic (a = 3.9830 °A, b = 3.8260 °A, c = 12.790 °A, α = 90.00°, β = 90.75°, and γ = 90.00°) structures were similar to that observed for TT phase and T-phase, respectively[19]. Figure 7.1 also shows XRD patterns of Nb_4N_5 which was obtained by sintering amorphous Nb_2O_5 in nitrogen environment at 700 °C for 40 hours. Patel et al. [20] also obtained similar diffraction patterns of Nb_4N_5 by annealing sample at 765 °C.

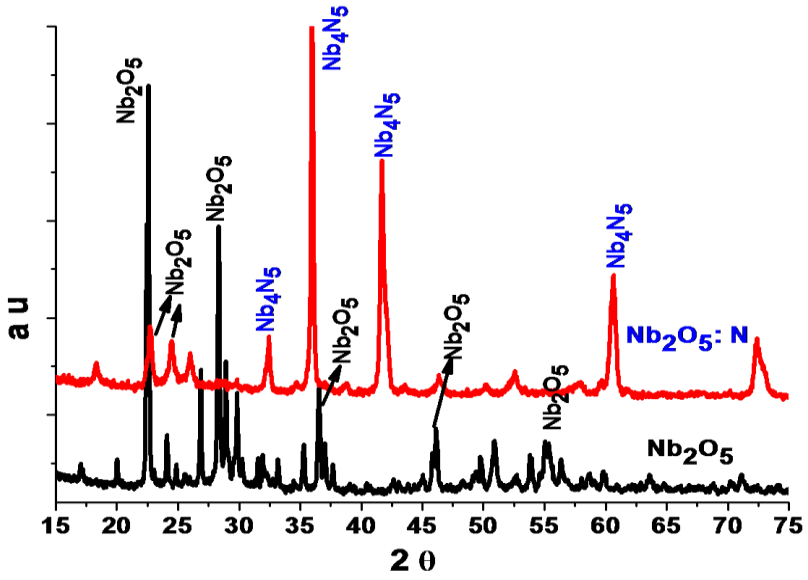

Figure: 7.1 XRD patterns of Nb_2O_5 and Nb_4N_5 calcined at 700 °C.

Figure 7.2 shows XRD patterns of undoped and nitrogen doped Ta_2O_5 calcined at 700 °C for 40 hours. XRD patterns of nitrogen doped Ta_2O_5 were also compared with that of unmodified commercial Ta_2O_5 and nitrogen treated commercial material. All the major peaks of the newly prepared materials observed at 2θ =

22.70°, 28.19°, 36.58°, 46.68°, and 55.54° corresponding to (001), (100), (101), (002), and (102)[21] were exactly matched with that of the commercial material. Unlike high temperature sintered materials H-Ta_2O_5[22] and L-Ta_2O_5[23], undoped and nitrogen doped Ta_2O_5 have orthorhombic[21] structure with lattice parameters as a = 43.977 °A, b = 3.894 °A, c = 6.209 °A, α = 90.0°, β = 90.0°, and γ = 90.0°, Primitive, Pmm2. Most of the XRD patterns of undoped and nitrogen doped materials were similar, however, three weak peaks observed at 2θ = 25.45°, 32.74°, and 42.82° showed formation of TaON.

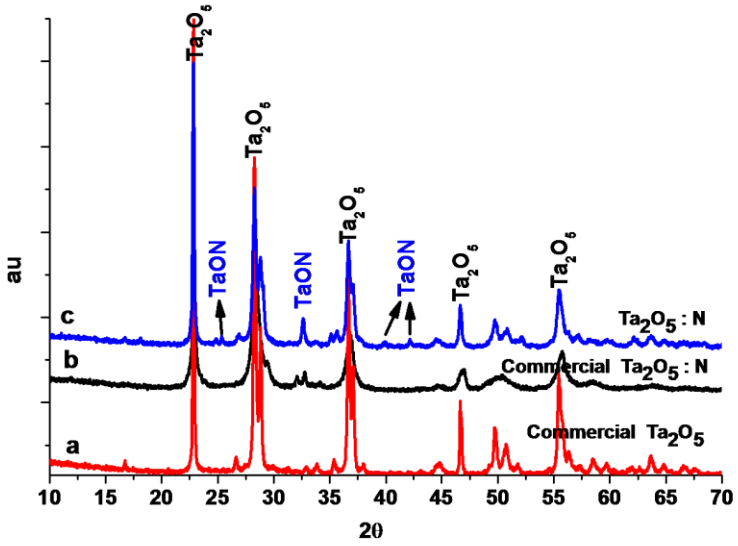

Figure: 7.2 XRD patterns of undoped (a) commercial Ta_2O_5, (b) commercial Ta_2O_5 treated in nitrogen, and (c) nitrogen doped Ta_2O_5.

This weak evidence of TaON was observed for both the commercial and laboratory made materials even for the samples treated for 20 hours in nitrogen environment (Figure 1.1 of appendix 1). However, by increasing the annealing time to 40 hours neither extra peaks nor increase in the three peaks (shown by arrows in Figure 7.2) for TaON was detected.

Ta_2O_5 has distorted structure made of octahedra TaO_6 and pentagonal bipyramids TaO_7. Each tantalum atom in the structure is attached to seven oxygen atoms with the average tantalum-oxygen bond distance of about 2.04 Å[22]. Theoretical and

experimental analyses have confirmed existence of large number of oxygen vacancies at energy positions (which lie within the visible region) in TaO_6 octahedron [24, 25]. Therefore, we prepared undoped and nitrogen doped orthorhombic Ta_2O_5 and use these materials for photocatalytic decomposition of toluene in air.

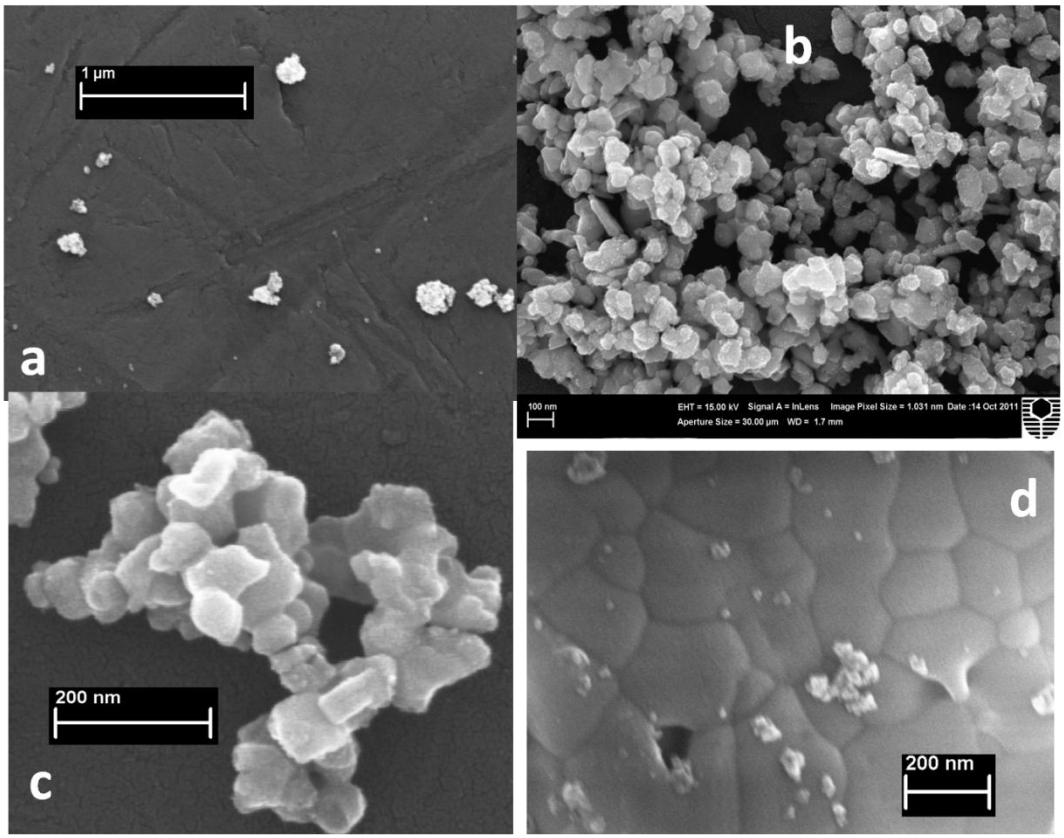

Figure: 7.3 SEM micrographs of Ta_2O_5: N.

Figure 7.3 (a-d) shows SEM images of nitrogen doped Ta_2O_5 calcined at 700 °C for 40 hours. SEM micrographs reveal that nitrogen doped Ta_2O_5 crystallizes in various morphologies and sizes. Most of the particles have average size in the range of few nano-meters, which then aggregated into large agglomerates. Gou et al. [26] have recently observed almost similar morphologies of Ta_2O_5 but with smaller particle size (than in our case) annealed at 700 °C for 4 hours. Obviously the 10 times larger annealing time in our case promotes the particle aggregation, however, large

numbers of nanoparticles residing on aggregated structures are highly beneficial for photocatalytic reactions. Figure 7.3 c and d, clearly shows tiny particles[27] on the agglomerated surfaces which increase the active surface area for the photocatalytic reaction.

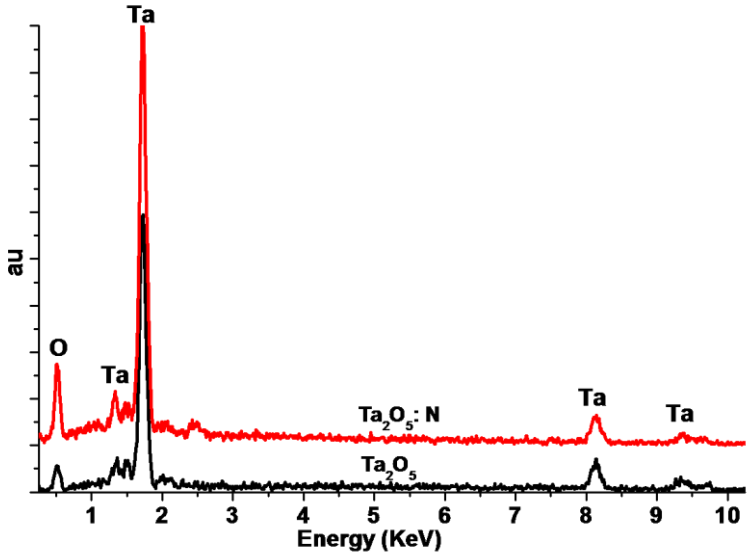

Figure: 7.4 Energy dispersive spectroscopy of Ta_2O_5 and Ta_2O_5: N

EDS analysis of undoped and nitrogen doped Ta_2O_5 showed in Figure 7.4 clearly indicates existence of Ta and oxygen atoms. Since the structure of Ta_2O_5 consisted of TaO_6 octahedra and pentagonal TaO_7 oxygen atoms, therefore, more strong peaks for Ta than O can be observed in the ED analysis. However, neither any contaminants nor nitrogen was detected by EDS in the nitrogen doped Ta_2O_5. Although XRD analysis has shown some minor peaks for TaON, but due to the very low concentration, nitrogen cannot be detected by EDS analysis.

Figure 7.5 compares the optical of undoped Ta_2O_5 and undoped Nb_2O_5 with that of commercial Ta_2O_5. It is evident from the Figure that the undoped and commercial Ta_2O_5 have exactly the same absorption edge of 330 nm, whereas the absorption edge of Nb_2O_5 is at 420 nm suggesting absorption in the visible range. However, absorption onset of Nb_2O_5 prepared at 500 °C and Ta_2O_5 annealed at 650 °C were 385 nm [28] and 315 nm[27] respectively. Since we annealed samples (Nb_2O_5 and

Ta_2O_5) at higher temperature for longer time, therefore large number of oxygen vacancies' may have been introduced in these materials, which red-shifted the optical absorption.

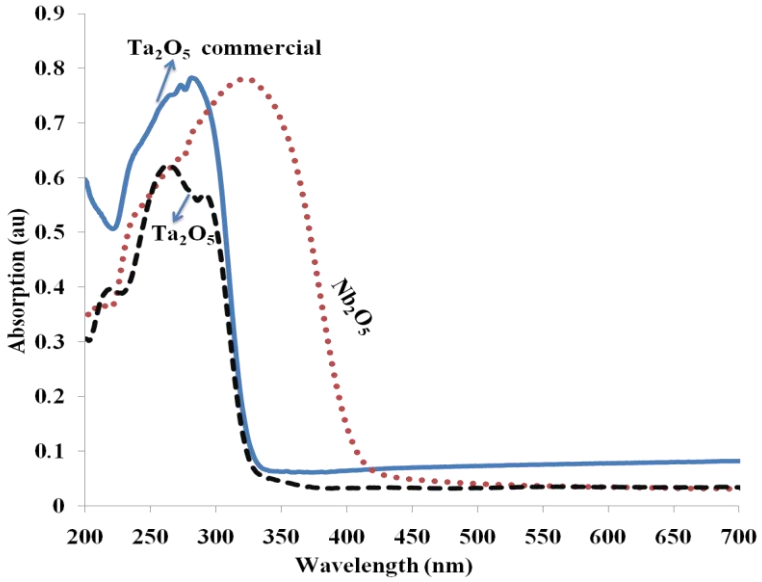

Figure: 7.5 Defuse reflectance spectroscopy of undoped Ta_2O_5, commercial Ta_2O_5, and undoped Nb_2O_5.

Figure 7.6 shows diffusive reflectance spectroscopy of the undoped and nitrogen doped Ta_2O_5, which clearly indicates effect of doping on the optical absorption of the material. Figure 7.6 further reveals that commercial Ta_2O_5 treated in nitrogen environment has two absorption onsets at 330 nm and 550 nm, while the laboratory made nitrogen doped Ta_2O_5 has a single absorption starting at 545 nm. The laboratory made Ta_2O_5: N absorbs more visible light than the commercial Ta_2O_5: N. The absorption edges and the corresponding calculated band gaps [29], [30] of all the materials are given in Table 7.1. It must be noted that a similar effect of two absorption edges for nitrogen doped Ta_2O_5 has been observed by Ho et al.[31]. The two absorption edges are obviously originated from the two main sources i.e. i) electronic excitation from conduction band to valence band of the martial, and ii) electronic excitation at the various defect sites such as oxygen vacancies and reduced Ta metal defects[31].

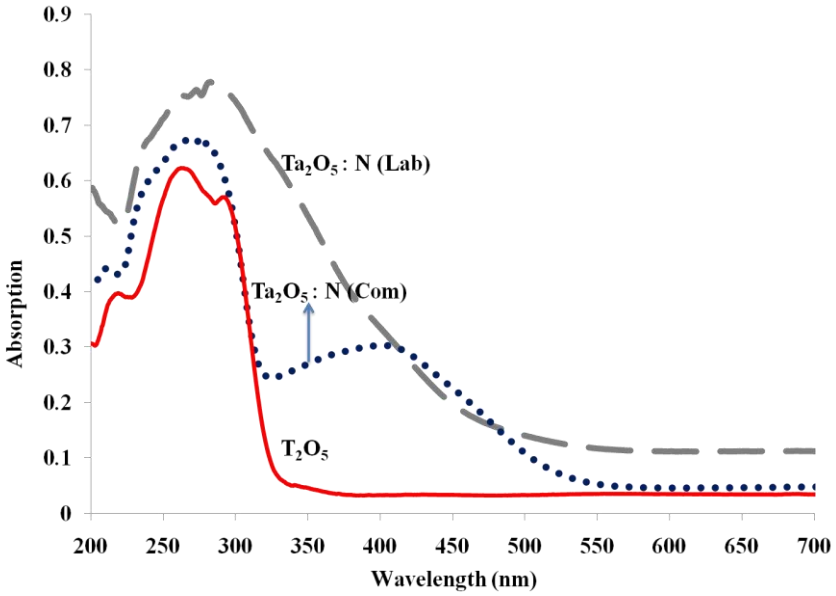

Figure: 7.6 Defuse reflectance spectroscopy of undoped Ta_2O_5 (laboratory made) nitrogen doped Ta_2O_5: N (Lab) and Ta_2O_5: N (Com).

Various studies have shown that conduction band of pristine Ta_2O_5 composed of Ta 5d orbitals with an energy position of -7.3 eV and valence band consisted of O 2p orbitals with energy position of -3.4 eV, thus resulting in a wide band gap of 3.9 eV[11]. Even though the pristine Ta_2O_5 has a wide band gap, but it still has very prominent photoluminescence at visible light. This huge photoluminescence of pristine Ta_2O_5 is originated both from shallow (350 – 450 nm)[32] and deep (500 - 650 nm) defect states[25], which are mainly attributed to the existence of oxygen vacancies and Ta defect sites. We believe that heat treatment of Ta_2O_5 in the reduced environment (i.e. N_2 environment in our case) further increases the defect states by producing new oxygen vacancies at shallow energy levels (350 – 500 nm) [25]. Definitely the new defect states at the shallow energy levels resulted in a significant optical absorption which is clearly seen in Figure 7.6 for Ta_2O_5: N (com). Unlike treated commercial material, the laboratory made Ta_2O_5: N has very smooth optical absorption starting from 545 nm. This indicates that the defect states in Ta_2O_5: N (Lab) are extended to a broad energy bands[33] rather than the discrete energy levels originated from particular defect states. As shown in Figure 7.5 undoped Ta_2O_5 (both laboratory made and commercial) have exactly same optical

absorption, where no evidence of longer wavelength absorption can be seen. This indicates there exists very limited number of defect states in pristine Ta_2O_5 which can give a rise to photoluminescence but they are not enough to absorb significant amount of visible light. However, nitrogen doping in Ta_2O_5 contributes to the optical absorption of material by two ways i.e. increases the number of defect states and producing an energy level above the valence band originated from N 2p orbital. Chun et al.[11] have calculated the conduction and valence band positions of the undoped and nitrogen doped Ta_2O_5 and suggested that contribution of N 2p orbitals shifted the valence band to the higher energy level and reduced the effective band gap of Ta_2O_5 to 2.4 eV.

Table 7.1: Absorption edges and band gaps of materials

Material	Absorption edge	Band gap (eV)
Ta_2O_5	330	3.76
Ta_2O_5	330	3.76
Ta_2O_5 : N (Com)	330, 550	3.76, 2.25
Ta_2O_5 : N (Lab)	545	2.28
Nb_2O_5	420	2.97

Theoretical[34] and experimental[35] investigations have confirmed that pristine Ta_2O_5 has defect states originated mainly from oxygen vacancies. These defect states are the main reasons for the photoluminescence [36] and photocatalytic performance of this material. Additionally various studies have also shown that the number of these defect states can be further enhanced by doping Ta_2O_5 with nitrogen. Our laboratory made nitrogen doped Ta_2O_5 has significant optical absorption confirming contribution of both the large number of defect states and N 2p orbitals to the optical and electronic properties [34] of the material.

7.3.2 Photocatalytic decomposition of gaseous toluene

Photocatalytic performance of all the materials (Nb_2O_5, Nb_4N_5, Ta_2O_5 (Lab), Ta_2O_5: N (Com), and Ta_2O_5: N (Lab)) examined by decomposition of gaseous toluene and compared with commercial Ta_2O_5. Figure 7.7 shows photocatalytic decomposition

of toluene with all these materials irradiated with artificial solar light. It is evident from figure that Nb based compounds (Nb_2O_5, and Nb_4N_5) were almost inactive under solar light because they only decompose 5- 10 % toluene within the first few hours of irradiation. The commercial non-treated Ta_2O_5 was comparatively better than the Nb based compounds and decomposed about 30% of toluene within similar time of irradiation. However, introducing nitrogen into the crystal structure of commercial Ta_2O_5 by annealing the sample in nitrogen environment was considerably effective. Consequently commercial Ta_2O_5 doped with nitrogen (Ta_2O_5: N (Com)) removed almost 60 % toluene within initial two hours of solar light irradiation. The laboratory made undoped Ta_2O_5 was also efficient than Nb_2O_5, Nb_4N_4, and undoped commercial Ta_2O_5 materials which has decomposed about similar amount of toluene as Ta_2O_5: N (Com). The laboratory made nitrogen doped material Ta_2O_5: N (Lab) was found to be the most efficient among all the materials since it has decomposed more than 70% toluene within initial one and half hour of artificial solar light irradiation.

Furukawa et al.[4] have recently reported selective oxidation of various amines to imines using Nb_2O_5 as a heterogeneous photocatalyst irradiated with UV light (330 – 390 nm). NiO, and Pt coated Nb_2O_5[2], [16] have been also used for hydrogen production with UV light irradiation (λ = 360 nm). Acidic Nb_2O_5 irradiated with UV light has been attempted for degradation of 1-pentanol[19]. It must be noted that in all above mentioned studies Nb_2O_5 exhibited better photocatalytic performance only with UV light irradiation [37]. However, in our case neither Nb_2O_5 nor Nb_4N_5 was capable to decompose gaseous toluene. The malfunctioning of these materials for toluene decomposition was due to the lower energy of the irradiated light. Since, we used light from a solar simulator which mostly lies within the visible region and has very low UVA radiation. Band gap and surface defect states are other two important factors which have significant influence on the photocatalytic activities of materials. Neither the band gap of Nb_2O_5 is suitable for visible light excitation nor does the material has enough defect states to generate

electron hole pairs with visible light. Therefore, Nb_2O_5 is not capable for photocatalytic reaction with visible light irradiation.

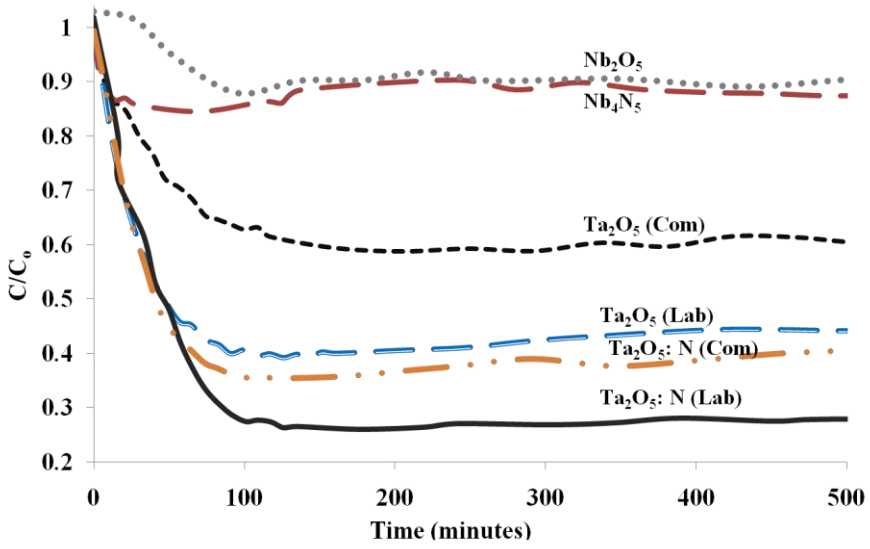

Figure: 7.7 Photocatalytic decomposition of toluene with various materials irradiated with solar simulator.

Even though, pristine Ta_2O_5 has larger band gap than Nb_2O_5 but the former has a large number of defect states mainly originated from oxygen vacancies. The solar light photocatalytic activity of the pristine Ta_2O_5 can be mainly attributed to the existence of these defect states which lie below the conduction band at energy level of 2.1 eV and 2.7 eV, respectively[32, 38].

Figure 7.8 further shows the photocatalytic performance of commercial undoped Ta_2O_5, Ta_2O_5: N (Com), laboratory made Ta_2O_5, and Ta_2O_5: N (Lab) at visible light. It is evident that commercial pristine Ta_2O_5 was unable to convert toluene with pure visible light (λ> 400 nm), however, nitrogen treated commercial material Ta_2O_5: N (Lab) was capable to decompose up to 10 % of toluene with visible light irradiation. Laboratory made undoped Ta_2O_5 has much better performance than Ta_2O_5: N (Com), since the former decomposed about 15 % toluene with pure visible light. The laboratory made nitrogen doped material (Ta_2O_5: N (Lab)) has shown excellent performance under visible light and decomposed up to 30 % toluene. It must be noted that Ta_2O_5: N (Lab) has better photocatalytic activity for gaseous

toluene decomposition both with artificial solar light and visible light. The higher photocatalytic activities of Ta_2O_5: N (Lab) are mainly attributed to the smaller band gap of the material, existence of large number of defect states, and oxygen vacancies on the material surface.

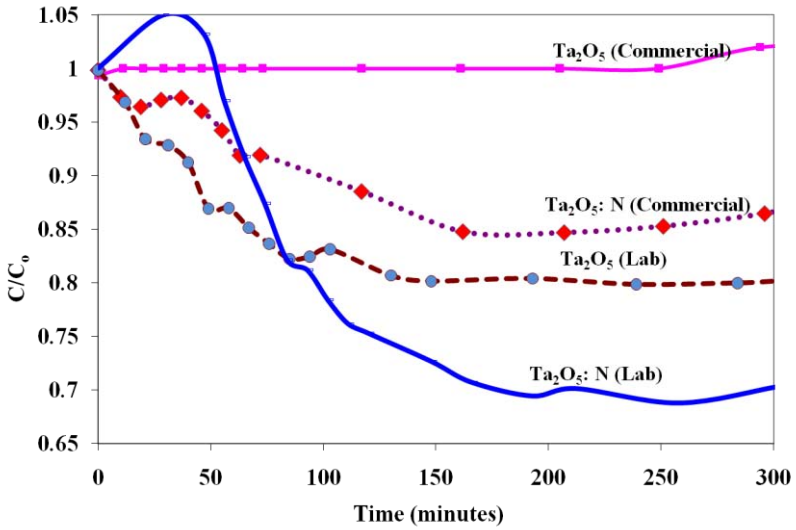

Figure: 7.8 Photocatalytic decomposition of toluene with undoped and nitrogen doped Ta_2O_5 irradiated visible light.

Nitrogen doped Ta_2O_5 has been recently investigated for photocatalytic oxidation of organic compounds [7], water splitting[39] into hydrogen/oxygen [39] and CO_2 reduction[9] to methanol with UV and solar light irradiation. The higher photocatalytic hydrogen production of mesoporous Ta_2O_5 was mainly attributed to the efficient charge transfer due to the thinner pore wall of the material[40]. In addition the photocatalytic hydrogen production with visible light was also attributed to the combined effect of NiO coating on Ta_2O_5 surface [41], [42]. However, other studies have found large number of defect states, and oxygen vacancies [24] which lay within the range of visible light, making the material showing photoluminescence [43]. Although band gap of Ta_2O_5 is higher and even larger than the land mark TiO_2, the material possesses excellent photoluminescence due to the existence of defect states at lower energy levels. Additionally, the number of these defect states [25] reportedly increased with nitrogen doping, which

also enhanced the photocatalytic properties of this material. Photoluminescence arises from the recombination of photo-generated electron hole pairs and nitrogen doping will further enhance the recombination of carriers. However, we suggest that the electron hole pairs after generation by incident light quickly react with surface species before undergoing recombination and produce the hydroxyl radicals. We further assume that recombination of electron hole pairs requires more energy than that needed for formation of hydroxyl radical. Although the photo-generated carriers have enough energy to recombine but photo-generated hole participate immediately in hydroxyl radical formation due to the lower energy requirement for the process. The photo-excited electrons also leave a hole at the trap centre of a cap oxygen vacancy between TaO_6 octahedra and TaO_7 bipyramids[44]. Thus we assume that the lower energy requirement of hydroxyl radical than the recombination process and the photo-generated hole left at the trap centre are the two main reasons, which enhance the photocatalytic activities of nitrogen doped Ta_2O_5. It must be noted that both of these processes depend upon the defect states and oxygen vacancies which are increasing with nitrogen doping.

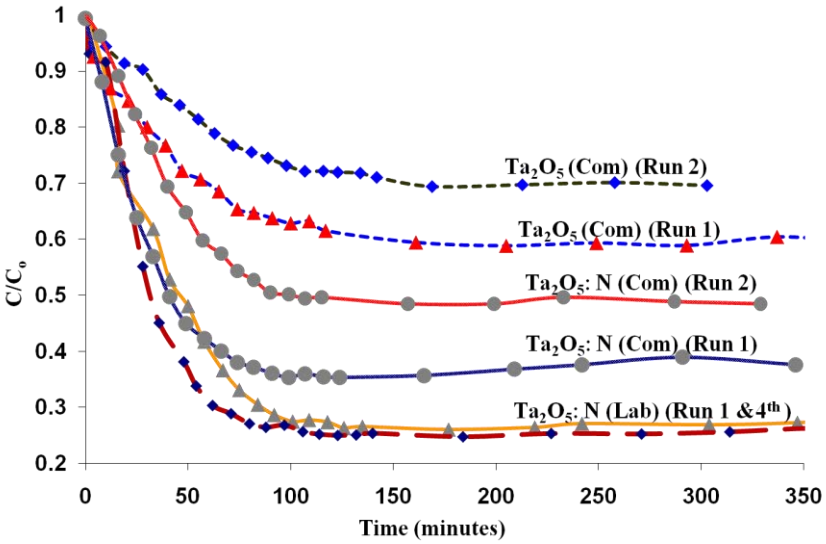

Figure: 7.9 Repeated use of materials for photocatalytic decomposition of toluene with solar light.

Intermediate adsorption, photocatalyst stability and reusability are other important factors influencing the photocatalytic performance of various materials. All the samples were used for repeated runs after being mixed with DI water and dried in an oven for more than 24 hours at 100 °C. Figure 7.9 shows the performance of commercial Ta_2O_5, nitrogen doped Ta_2O_5 and laboratory made nitrogen doped Ta_2O_5 in several runs. Figure 7.9 shows that the photocatalytic activities of commercial non-doped (Ta_2O_5) and nitrogen doped (Ta_2O_5: N (Com)) significantly reduced after being used repeatedly. The activity of Ta_2O_5: N (Com) reduced from 60 % toluene removal to 40 % removal when used for the second time. Non-treated Ta_2O_5 also exhibited similar trend in activity reduction when used for second run. It is worth mentioning that Ta_2O_5: N (Lab) has shown much stable performance and its activity remained unmodified even after use for 4 times.

Nitrogen doped Ta_2O_5: N (Lab) has shown higher, stable and prolonged performance for toluene decomposition with solar light irradiation. XRD analysis (shown in Figure 7.10) of the materials used for photocatalytic reaction clearly indicates that the structure of the materials remain unchanged. This revealed that Ta_2O_5: N (Lab) has much stronger stability under solar light irradiation where no photo-corrosion or other crystal instability occurred.

Intermediate adsorption on the photocatalyst surface plays a major role in degradation of photocatalytic activities of the materials. Along with carbon dioxide and water, toluene decomposition through photocatalytic oxidation resulted in formation hydrocarbons such as benzaldehyde[45], benzoic acid, and benzyl alcohol. In case of TiO_2[46], intermediates and water molecules [47] strongly adsorbed on the photocatalyst surface which consequently covered the active sites and reduced the performance of the material. Photocatalyst (TiO_2) regeneration through UV irradiation and washing with water was not successful to recover the performance of material.

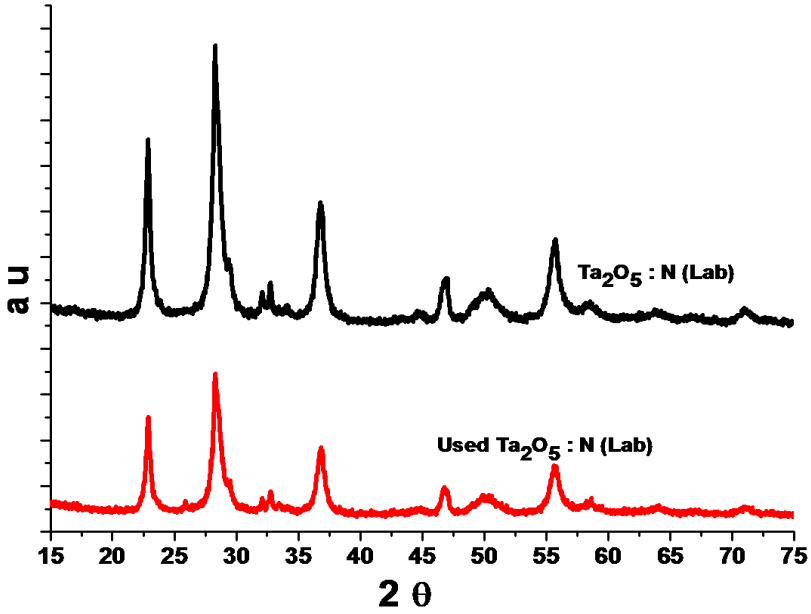

Figure: 7.10 XRD analysis of Ta_2O_5: N (Lab) before and after using for photocatalytic reaction.

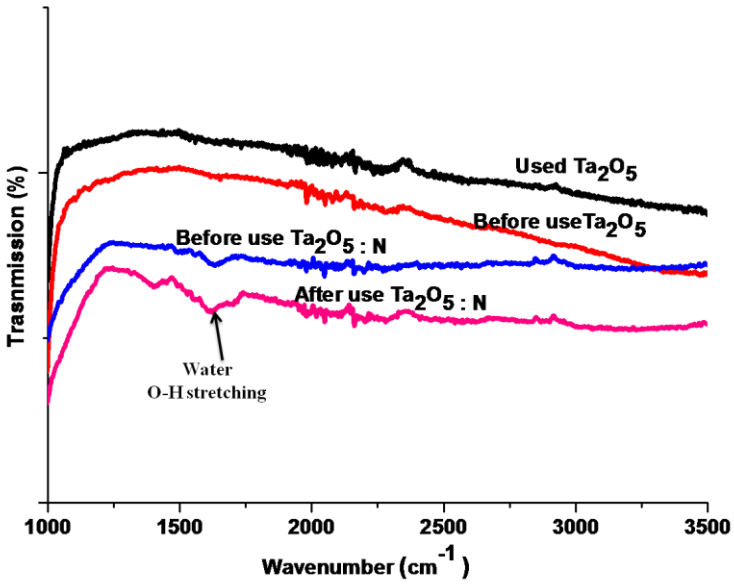

Figure: 7.11 FTIR analysis of Ta_2O_5 and Ta_2O_5: N (Lab) before and after the photocatalytic reaction.

Figure 7.11 shows FTIR analysis of the fresh and used materials, where no intermediate adsorption was detected on both Ta_2O_5 and Ta_2O_5: N. However, very week peak at 1632 cm^{-1} was observed on Ta_2O_5: N (Lab) indicating water adsorption[48]. We suggest that water vapour from atmosphere may be attached to the material which is insufficient to significantly affect the performance of Ta_2O_5: N (Lab). Contrary to Ta_2O_5: N (Lab) large amount of water and intermediates were adsorbed on TiO_2 (Figure 1.2 of appendix 1) surface, which obviously reduced its photocatalytic activity. Similar evidence of water and intermediate adsorption on TiO_2 and their effect on the photocatalytic activities have been observed somewhere else[48]. The overall performances of the laboratory made nitrogen doped Ta_2O_5: N (Lab) for toluene decomposition with artificial sun light and visible light irradiation were better than other materials including undoped Ta_2O_5, and commercial Ta_2O_5 treated in nitrogen environment.

7.4 Conclusions

It can be concluded that, Ta_2O_5 was successfully prepared by a solution method and was doped with nitrogen by passing mist of N_2 gas and ammonia solution through the amorphous material at 700 °C. Commercial Ta_2O_5 was also doped with nitrogen by a similar annealing process. All the materials; undoped Ta_2O_5, commercial Ta_2O_5, nitrogen doped commercial (Ta_2O_5: N (Com)) and laboratory made (Ta_2O_5: N (Lab)) decomposed toluene with artificial solar light. Ta_2O_5: N (Lab) was the most efficient, since it converted more than 70 % toluene with artificial solar light. This material was also capable to remove 30 % toluene with pure visible light irradiation. Laboratory made nitrogen doped Ta_2O_5 has also shown very stable and long life performance and maintained its activity after being used for several times. The higher photocatalytic performance of Ta_2O_5: N (Lab) under artificial sun light and pure visible light was attributed mainly to the large number of defect states and oxygen vacancies. This material may have the opportunity of efficient photocatalytic material and can be used for other photocatalytic reactions.

7.5 References

1. Kondo, J.N., et al., *Synthesis and Property of Mesoporous Tantalum Oxides.* Topics in Catalysis, 2002. **19**(2): p. 171-177.

2. Chen, X., et al., *Enhanced activity of mesoporous Nb2O5 for photocatalytic hydrogen production.* Applied Surface Science, 2007. **253**(20): p. 8500-8506.

3. Kominami, H., et al., *Novel solvothermal synthesis of niobium() oxide powders and their photocatalytic activity in aqueous suspensions.* Journal of Materials Chemistry, 2001. **11**(2): p. 604-609.

4. Furukawa, S., et al., *Selective Amine Oxidation Using Nb2O5 Photocatalyst and O2.* ACS Catalysis, 2011. **1**(10): p. 1150-1153.

5. Shishido, T., et al., *Mechanism of Photooxidation of Alcohol over Nb2O5.* The Journal of Physical Chemistry C, 2009. **113**(43): p. 18713-18718.

6. Ge, S., et al., *First observation of visible light photocatalytic activity of carbon modified Nb2O5 nanostructures.* Journal of Materials Chemistry, 2010. **20**(15): p. 3052-3058.

7. Murase, T., H. Irie, and K. Hashimoto, *Visible Light Sensitive Photocatalysts, Nitrogen-Doped Ta2O5 Powders.* The Journal of Physical Chemistry B, 2004. **108**(40): p. 15803-15807.

8. Ho, C.-T., et al., *Formation of Sol–Gel-Derived TaOxNy Photocatalysts.* Chemistry of Materials, 2011.

9. Sato, S., et al., *Visible-Light-Induced Selective CO2 Reduction Utilizing a Ruthenium Complex Electrocatalyst Linked to a p-Type Nitrogen-Doped Ta2O5 Semiconductor.* Angewandte Chemie International Edition, 2010. **49**(30): p. 5101-5105.

10. Yamanaka, K.-i., et al., *Photoinduced Electron Transfer from Nitrogen-Doped Tantalum Oxide to Adsorbed Ruthenium Complex.* The Journal of Physical Chemistry C, 2011. **115**(37): p. 18348-18353.

11. Chun, W.-J., et al., *Conduction and Valence Band Positions of Ta2O5, TaON, and Ta3N5 by UPS and Electrochemical Methods.* The Journal of Physical Chemistry B, 2003. **107**(8): p. 1798-1803.

12. Morikawa, T., *Dual functional modification by N doping of Ta2O5: p-jour conduction in visible-light-activated N-doped Ta2O5*. Appl. Phys. Lett., 2010. **96**(14): p. 142111.

13. Zhang, Q. and L. Gao, *Ta3N5 Nanoparticles with Enhanced Photocatalytic Efficiency under Visible Light Irradiation.* Langmuir, 2004. **20**(22): p. 9821-9827.

14. Ho, C.-T., et al., *Synthesis and Characterization of Semiconductor Tantalum Nitride Nanoparticles.* The Journal of Physical Chemistry C, 2010. **115**(3): p. 647-652.

15. Luo, H., M. Wei, and K. Wei, *Synthesis of Nb2O5 Nanorods by a Soft Chemical Process.* Journal of Nanomaterials, 2009. **2009**.

16. Lin, H.-Y., H.-C. Yang, and W.-L. Wang, *Synthesis of mesoporous Nb2O5 photocatalysts with Pt, Au, Cu and NiO cocatalyst for water splitting.* Catalysis Today, 2011. **174**(1): p. 106-113.

17. Schäfer, H., R. Gruehn, and F. Schulte, *The Modifications of Niobium Pentoxide.* Angewandte Chemie International Edition in English, 1966. **5**(1): p. 40-52.

18. Filonenko, V.P. and I.P. Zibrov, *High-Pressure Phase Transitions of M2O5(M = V, Nb, Ta) and Thermal Stability of New Polymorphs.* Inorganic Materials, 2001. **37**(9): p. 953-959.

19. Ohuchi, T., et al., *Liquid phase photooxidation of alcohol over niobium oxide without solvents.* Catalysis Today, 2007. **120**(2): p. 233-239.

20. Patel, U., et al., *Synthesis and superconducting properties of niobium nitride nanowires and nanoribbons.* Applied Physics Letters, 2007. **91**(16): p. 162508-3.

21. Huang, H.-C. and T.-E. Hsieh, *Preparation and characterizations of tantalum pentoxide (Ta2O5) nanoparticles and UV-curable Ta2O5-acrylic nanocomposites.* Journal of Applied Polymer Science, 2010. **117**(3): p. 1252-1259.

22. Stephenson, N.C. and R.S. Roth, *The crystal structure of the high temperature form of Ta2O5.* Journal of Solid State Chemistry, 1971. **3**(2): p. 145-153.

23. Grey, I.E., W.G. Mumme, and R.S. Roth, *The crystal chemistry of L-Ta2O5 and related structures.* Journal of Solid State Chemistry, 2005. **178**(11): p. 3308-3314.

24. Ramprasad, R., *First principles study of oxygen vacancy defects in tantalum pentoxide.* Journal of Applied Physics, 2003. **94**(9): p. 5609-5612.

25. Shin, H., et al., *Defect energy levels in Ta2O5 and nitrogen-doped Ta2O5.* Journal of Applied Physics, 2008. **104**(11): p. 116108-116108-3.

26. Guo, G. and J. Huang, *Preparation of mesoporous tantalum oxide and its enhanced photocatalytic activity.* Materials Letters, 2011. **65**(1): p. 64-66.

27. Sreethawong, T., et al., *Nanocrystalline mesoporous Ta2O5-based photocatalysts prepared by surfactant-assisted templating sol–gel process for photocatalytic H2 evolution.* Journal of Molecular Catalysis A: Chemical, 2005. **235**(1-2): p. 1-11.

28. Xinyi Chen, et al., *Enhanced Activity of Mesoporous Nb2O5 for photoctalytic Hydrogen Prodcution.* Applied Surface Science, 2007. **253**: p. 8500-8506.

29. Ye, J. and Z. Zou, *Visible light sensitive photocatalysts In1−xMxTaO4 (M=3d transition-metal) and their activity controlling factors.* Journal of Physics and Chemistry of Solids. **66**(2-4): p. 266-273.

30. Kudo, A., et al., *Nickel-loaded K4Nb6O17 photocatalyst in the decomposition of H2O into H2 and O2: Structure and reaction mechanism.* Journal of Catalysis, 1989. **120**(2): p. 337-352.

31. Ho, C.-T., et al., *Formation of Sol–Gel-Derived TaOxNy Photocatalysts.* Chemistry of Materials, 2011. **23**(21): p. 4721-4725.

32. Lau, W.S., et al., *Detection of oxygen vacancy defect states in capacitors with ultrathin Ta_2O_5 films by zero-bias thermally stimulated current spectroscopy* Applied Physics Letters, 2003. **83**(14): p. 2835-2837.

33. Alers, G.B., et al., *Nitrogen plasma annealing for low temperature Ta[sub 2]O[sub 5] films.* Applied Physics Letters, 1998. **72**(11): p. 1308-1310.

34. Sawada, H. and K. Kawakami, *Electronic structure of oxygen vacancy in Ta2O5.* Journal of Applied Physics, 1999. **86**(2): p. 956-959.

35. Ivanov, M.V., et al., *Electronic structure of delta -Ta2O5 with oxygen vacancy: ab initio calculations and comparison with experiment.* Journal of Applied Physics, 2011. **110**(2): p. 024115-5.

36. Di Franco, F., et al., *The Influence of Nitrogen Incorporation on the Optical Properties of Anodic Ta_2O_5.* Electrochimica Acta, (0).

37. Furukawa, S., et al., *Reaction Mechanism of Selective Photooxidation of Hydrocarbons over Nb2O5.* The Journal of Physical Chemistry C, 2011. **115**(39): p. 19320-19327.

38. Thomas Iii, J.H., *Defect photoconductivity of anodic Ta2O5 films.* Applied Physics Letters, 1973. **22**(8): p. 406-408.

39. Arakawa, H. and K. Sayama, *Solar hydrogen production. Significant effect of Significant effect of Na2CO3 addition on water splitting using simple oxide semiconductor photocatalysts addition on water splitting using simple oxide semiconductor photocatalysts.* Catalysis Surveys from Japan, 2000. **4**(1): p. 75-80.

40. Nakajima, K., et al., *Synthesis and application of thermally stable mesoporous Ta2O5 photocatalyst for overall water decomposition*, in *Studies in Surface Science and Catalysis*, N.Ž. J. Čejka and P. Nachtigall, Editors. 2005, Elsevier. p. 1477-1484.

41. Zou, J.-J., C.-J. Liu, and Y.-P. Zhang, *Control of the Metal−Support Interface of NiO-Loaded Photocatalysts via Cold Plasma Treatment.* Langmuir, 2006. **22**(5): p. 2334-2339.

42. Parida, K.M., et al., *Fabrication of NiO/Ta2O5 composite photocatalyst for hydrogen production under visible light.* International Journal of Energy Research, 2011: p. n/a-n/a.

43. Zhu, M., Z. Zhang, and W. Miao, *Intense photoluminescence from amorphous tantalum oxide films.* Applied Physics Letters, 2006. **89**(2): p. 021915-3.

44. Devan, R.S., et al., *Enhancement of green-light photoluminescence of Ta2O5 nanoblock stacks.* Physical Chemistry Chemical Physics, 2011. **13**(29): p. 13441-13446.

45. Maira, A.J., et al., *Gas-phase photo-oxidation of toluene using nanometer-size TiO2 catalysts.* Applied Catalysis B: Environmental, 2001. **29**(4): p. 327-336.

46. d'Hennezel, O., P. Pichat, and D.F. Ollis, *Benzene and toluene gas-phase photocatalytic degradation over H2O and HCL pretreated TiO2: by-products and mechanisms.* Journal of Photochemistry and Photobiology A: Chemistry, 1998. **118**(3): p. 197-204.

47. Ullah, R., et al., *Wet-chemical Synthesis of InTaO4 for Photocatalytic Decomposition of Organic Contaminants in Air and Water with UV-vis Light.* Industrial & Engineering Chemistry Research, 2011: p. 10.1021/ie200544z.

48. Wei, Z., et al., *Removal of gaseous toluene by the combination of photocatalytic oxidation under complex light irradiation of UV and visible light and biological process.* Journal of Hazardous Materials, 2010. **177**(1-3): p. 814-821.

8

8 -Conclusion and Future Work

8.1 Concluding comments

The two major objectives of this research were to prepare nano-photocatalysts and decompose gaseous volatile organic compounds by irradiating the new materials with visible light. The outlined objectives were successfully achieved as per the scheduled timeline. Various types of metal oxides and complex metal oxide nano-materials were synthesized with a solution method and used for gaseous toluene decomposition with UV and artificial solar light. Metal oxides such as $InTaO_4$, $BiTaO_4$, $InNbO_4$, $BiNbO_4$, $AgNbO_4$, $AgNbO_3$, Bi_2WO_6, $AgVO_3$, $AgTaO_3$, $BiTaO_4$, $Cd_2Ta_2O_7$, $InTaO_4$, $CoTa_2O_6$, $CeTaO_4$ and $EuTaO_4$, where Ta_2O_5 were prepared with different methods. Some of these photocatalyst materials like $InTaO_4$, $BiTaO_4$, and $BiNbO_4$ were also modified by doping with various metal ions such as aluminium (Al), silver (Ag), bismuth (Bi), barium (Ba), gallium (Ga), lanthanum (La), tin (Sn), platinum (Pt), copper (Cu), lead (Pb), Chromium (Cr), cobalt (Co), cadmium (Cd), nickel (Ni), iron (Fe), cerium (Ce), vanadium (V), neodymium (Nd), antimony (Sb) and tungsten (W). All of these photocatalyst materials were examined (and compared with TiO_2 (P25)) for gaseous toluene decomposition with UV and visible irradiation. Some of the new materials were also tested for methylene blue degradation in water. Among various new materials pristine and nitrogen doped Ta_2O_5 have shown excellent performance for photocatalytic decomposing of toluene with artificial solar light, which removes more than 80% toluene within half an hour. The major outcomes of this research thesis are outlined as below.

8.2.1 Effect of Ni doping on photocatalytic activities of $InTaO_4$

1) $InTaO_4$, $InNbO_4$ and $AgNbO_3$ were successfully prepared by a simple wet-chemical technique. Most of the materials have poly-crystalline structures and large size agglomerates. $InTaO_4$ exhibited better activity than $InNbO_4$ and $AgNbO_3$ for toluene decomposition with ultraviolet light. The photo-physical properties and photocatalytic activities of $InTaO_4$ were significantly influenced by doping with metals like Pt, Cu, Ag, V, Bi, and Ni. Bi doped $InTaO_4$ absorbed more visible light than Ag, V, Cu, and Pt doped materials. However, Ni doped $InTaO_4$ showed strong UV absorption.
2) Comparing the photocatalytic performance of three materials, $InTaO_4$, $InNbO_4$ and $AgNbO_3$, the former one showed much higher activity with UV irradiation for decomposition of toluene in air, methylene blue and phenol in water. Among the metal doped materials, $InTaO_4$: Ni showed much higher photocatalytic activity. This higher activity was attributed to the band gap modification and electron trapping centre of NiO. $InTaO_4$: Ni also has better performance in multiple uses and longer life time than the commercial TiO_2-P25.

8.2.2 Photocatalytic activities of metal ion doped $BiTaO_4$

1) Undoped and metal ion doped triclinic $BiTaO_4$ were prepared with a solution method at lower sintering temperature of 700 °C. Various metal ions like Al, Nd, La, Ga, Ba, Sn, W, Fe, Co, Cr, Ce, Cu, Sb, Pb, Ni, and Ag were successfully doped in $BiTaO_4$, which modified the optical absorption of the material. The average particle size of doped and undoped $BiTaO_4$ was in the range of nanometres. TEM micrographs showed the presence of defects on the surface of the materials, which are essential for the enhanced photocatalytic activity under UV and visible light.
2) Dopants like La, Al, Ga and Nd significantly increased the performance of materials for toluene decomposition. However, dopants like Cu, Cr, Ce, Ni,

Pb, and Co were not successful to modify the photocatalytic activities of $BiTaO_4$. A significant increase in photocatalytic activities of $BiTaO_4$: La was found with much higher stability, longer life time and re-useability. Upon comparing with TiO_2, $BiTaO_4$ doped with Nd, Al, and La were found to have better performance, longer life time and more stability for gaseous toluene decomposition under UV light irradiation.

3) The enhanced photocatalytic activity of $BiTaO_4$ doped with metal ions (Al, Nd, La, Ga, Ba, Sn, W, Fe, Sb, and Ag) was mainly attributed to the large number of oxygen vacancies created by doping, reduced band gap and valence band hybridization. Unlike TiO_2, no adsorption of intermediates and water was observed on metal doped $BiTaO_4$. It can be summarized that metal doped $BiTaO_4$ can efficiently decompose air contaminants and have better performance than TiO_2 with UV and visible light irradiation. These materials are also effective for removal of water contaminants but have lower performance than TiO_2.

8.2.3 Performance of ternary metal oxides

1) Various materials such as Bi_2WO_6, $AgVO_3$, $AgTaO_3$, $BiTaO_4$, $Cd_2Ta_2O_7$, $InTaO_4$, $CoTa_2O_6$, $CeTaO_4$ and $EuTaO_4$ were successfully prepared with solution techniques and tested for photocatalytic decomposition of VOCs both in air and water. Tantalum containing compounds like $Cd_2Ta_2O_4$, $AgTaO_4$ and $BiTaO_4$ have shown better performance for decomposition of gaseous toluene with visible light irradiation. These three compounds have very stable performance and have showed much better activity than commercial photocatalyst TiO_2 under visible light irradiation. However, TiO_2 degraded both gaseous toluene and methylene blue in water with UV irradiation efficiently than these compounds. $AgTaO_3$, $BiTaO_4$ and $Cd_2Ta_2O_7$ also degraded methylene blue with faster rate than other tantalum containing compounds. Although Bi_2WO_6 and $AgVO_3$ were most efficient in case of MB degradation with UV light irradiation, they were not capable to remove gaseous toluene at all.

2) Materials like $Cd_2Ta_2O_7$, $AgTaO_3$ and $BiTaO_4$ were assumed as the most efficient photocatalyst materials, since they removed gaseous toluene under visible light, have a long life time and did not show deactivation due to intermediate adsorption, and degraded methylene blue in water with UV light.

8.2.4 Removal of gaseous toluene with doped $BiNbO_4$

1) $BiNbO_4$ nanoparticles composed of orthorhombic and triclinic structures were prepared with a solution method. $BiNbO_4$ was doped with nitrogen and various metal ions such as Ga, Ba, Sn, Al and La. $BiNbO_4$ doped with Ba, Sn, and Ga decomposed toluene with UV and visible light efficiently than undoped material. However, La, and Al doping has the adverse effect on the photocatalytic performance. $BiNbO_4$: Ba (2%) presented better performance than others for toluene decomposition with visible light irradiation.
2) The photocatalytic performance of $BiNbO_4$: Ga was significantly higher than others and TiO_2 under UV irradiation, however this material has the lowest activity when irradiated with artificial sun light. The higher photocatalytic activities of $BiNbO_4$: Ga was attributed to the more UV light absorption. $BiNbO_4$: Ga has larger band gap than others and therefore absorb more UV light and has higher photocatalytic activity at UV light but lower activity at visible light.
3) SEM micrographs of doped and undoped $BiNbO_4$ materials have shown layered like structure and large number of nano-sized particles spread over large agglomerates. Both undoped and metal doped $BiNbO_4$ have shown much stable and longer time activity with UV and visible light irradiation. Photocatalytic decomposition of toluene with $BiNbO_4$: Ga and UV irradiation was much faster and stable than TiO_2. Both undoped and doped $BiNbO_4$ are quite stable and no photo-corrosion was observed, suggesting very bright future of these materials.

8.2.5 Photocatalytic activities of nitrogen doped Ta_2O_5

1) Ta_2O_5 prepared with the solution method has multi-crystalline orthorhombic structure. This material has absorption onset in the lower wavelength range, suggesting very high band gap. However, this material posses the highest photocatalytic decomposition of toluene with artificial solar light. The material was found to be the most efficient for toluene decomposition and has shown the excellent performance by removing 80% toluene within a half hour.
2) Nitrogen doped Ta_2O_5 has a similar crystal structure as the pristine material, however, optical absorption onset was significantly red shifted. This huge enhancement in the optical absorption was also helpful to further enhance the photocatalytic properties of this material. The material has higher stability, longer life time and capability of repeated use without any loss in performance. Both the undoped and nitrogen doped Ta_2O_5 has similar properties except the difference in the band gap and photocatalytic performance. Nitrogen doped Ta_2O_5 was also capable to decompose toluene with pure visible light irradiation.

8.2 Recommendations for future work

This research study focused on the photocatalytic removal of volatile organic compounds in air. We have shown that VOCs can be successfully disintegrated into by-products using various complex metal oxide nano-photocatalysts irradiated with UV and visible light. However, detailed study is still required to comprehensively investigate various aspects of this technology for full commercialization. Based on these research studies we recommend the following few steps and measures which require further attention for proficient use of this technology.

8.2.1 Photocatalytic material selection

Our research indicates that group five element compounds such as Ta_2O_5 $BiTaO_4$ and $BiNbO_4$ are the best alternatives to TiO_2 based on their

performance, stability and nil/lower adsorption of intermediates. However, like TiO_2, both $BiTaO_4$ and $BiNbO_4$ crystallize in two different phases (i.e. triclinic and orthorhombic) and it is still not very clear which crystalline phase is responsible for the photocatalytic reaction. Therefore, further investigations are necessary to co-relate the better photocatalytic performance of these two compounds with the particular crystalline phase. Cation and anion doping of these two compounds significantly modify their photo-physical properties but it still requires more investigation to optimize the dopant content and types for the improved visible light photocatalytic activities.

Although absorption onset of Ta_2O_5 was at short wavelength range suggesting a very high band gap, the material has shown the best photocatalytic performance for toluene decomposition with artificial solar light. Therefore, some detailed structural investigations and surface analyses are required to identify the main reasons for enhanced photocatalytic activities of this material. We believe that, based on its excellent performance, Ta_2O_5 can be a best photocatalytic material and can be used for hydrogen production and carbon dioxide reduction via photocatalysis. Since nitrogen doped Ta_2O_5 has more optical absorption and improved toluene decomposition thus there are opportunities for band gap modification through anion/cation doping which could further improve the photocatalytic properties of Ta_2O_5 toward the longer wavelength.

Coupling and/or coating of (lower band gap co-catalyst such as) NiO on Ta_2O_5 would be another possibility to further improve the activity of this material. We suggest that a synergetic effect of nitrogen doping and co-catalyst would probably enhance the photocatalytic properties of Ta_2O_5.

The preliminary results indicate that $Cd_2Ta_2O_7$ and $AgVO_3$ would be other possible photocatalyst materials that can work with visible light irradiation to degrade VOCs both in water and air.

8.2.2 Reaction by-products and intermediates adsorption

Preliminary investigations of the by-products and intermediates adsorption on the photocatalyst surface have confirmed that some non-degraded by-products and intermediates were adsorbed on TiO_2 surface. However, no such evidence of intermediates adsorption on the newly synthesized materials ($InTaO_4$, $BiTaO_4$, $BiNbO_4$ and Ta_2O_5) was observed. We suggest that, detailed investigation is highly required to determine both the intermediates and their adsorption on the photocatalyst surface.

8.2.3 Reaction parameters and mechanism

We used a continuous flow reactor for toluene decomposition via photocatalysis, where all the parameters were set once and used for new materials. However, in-depth details of toluene decomposition require further investigation to optimize the fundamental parameters such as contaminant pressure, flow rate, effect of humidity, temperature and pressure. It is extremely important to further investigate the effects of contaminant types, quantity, light intensity, and wavelength since these are the major parameters influencing the real and large scale application of this technology. Since, the concentration of individual VOC (discussed in the introduction part) is very limited and in the range of few ppb. Therefore, we suggest instead using total volatile organic compounds (TVOCs) which would be useful to investigate the real efficiency of new photocatalysts particularly nitrogen doped Ta_2O_5.

It is also highly required to investigate the reaction pathway of toluene decomposition and other aromatic hydrocarbons for comprehensive understanding and large scale application of this technology.

8.2.4 Photocatalyst stability and re-generation

Our findings have shown that almost all of the newly prepared materials were quite stable and the structures of the materials were unchanged after the photocatalytic reaction. None of the materials have shown structure deformation and/or other modification even if the materials were used

repeatedly. The activity of some materials (like $BiTaO_4$: La, $BiNbO_4$: Ga and Ta_2O_5) were further increased when used for 2^{nd} and 3^{rd} runs. Detailed investigation of the surface of the used materials is still needed for the increased activity of the repeatedly used materials.

Activities of some newly photocatalyst materials were reduced significantly, but the XRD analysis of those materials did not show any structural modification. Therefore some surface investigation is required to identify the root cause of the reduction in the photocatalytic activities.

Appendix -1

Table: 1.1 Photocatalytic Materials and their Operating Parameters

Catalyst	Co-Catalyst	Quantity used (gm)	Band gap Eg (eV)	H_2/O_2 Production (µmol/h)	Contaminants Type/Quantity	Aqueous/Gaseous	Wavelength (λ)(nm)	Power (Watt) /Lamp	Irradiation time (Hours)	Authors/Year
CeO_2	Fe^{3+} and Ce^{4+}	0.4-1.6	2.9	?/66.8	water Decomposition	Aqueous	>330	500/ Xe	10 hours	G. R. Bamwenda et
CeO_2			2.9		Toluene/1200ppmv	gaseous	<400	?		M. D. Hernandez-
CeO_2/TiO_2		0.030-0.040	2.94		Toluene/1200ppmv	gaseous	>365	6/T5		J.M. Coronado et al/2002
CeO_2	supported on SiO_2 and	0.2	2.95	0.32 and 1.23/?	Methane/200µmol	Gaseous	220-300, 310-400,	300/Xe	3 hours	L. Yuliati, T. Hamaiima et
CeO_2		.002-0.008			Acidic black 10B/10m	Aqueous	Solar radiation	?	2 hours	Y. Zhai et al./2007
CeO_2		0.0105			MO/?	Aqueous	visible			L. Qian et al./2009
Nb_2O_5	Pt+	0.1	3.2	1235.1	water Decomposition	Aqueous	200-600	400/Hg	7h	X. Chen, Tao Yu et.al/2007
Nb_2O_5		0.1	3.2		1-pentanol/?	liquid	?	?	?	T. Ohuchi et al./2007
$K_6Nb_{10.8}O_{30}$		0.15	2.92		Acid red G/?	Aqueous	>254			G. Zhang et al./2008
$CaNb_2O_6$	NiO	0.3	3.46	49/?	water Decomposition	Aqueous	uv	450/Xe		I. Sun Cho et al./2008
$LiNbO_3$		0.2	3.9	185/?	Formic acid/water	Aqueous	200-600	150/Hg		B. Zielinska et al./2008
$(AgNbO_3)_{1-x}(NaNbO_3)_x$		0.4	2.97-3.4	acetone production	IPA/370ppm	gaseous	400-500		?	G. Li et al./2007
N-doped $NaNbO_3$		0.4	<3.4		2-Propanol(IPA)/196ppm	Gaseous	>400	300/Xe	118 hours	H. Shi et al./2009
$InNbO_4$, $InTaO_4$	NiO	0.5	2.6, 2.5	4.0 & 3.5/Nil	water Decomposition	Aqueous	>420	300/Xe		Z. Zou et al./2009
$In_{1-x}Ni_xTaO_4$		0.5	Undoped 2.6, doped 2.3	3.1/?	water Decomposition	Aqueous	>420	400/Hg	24hours	Z. Zou et al./2009

Ni doped $InTaO_4$	Pt+	0.5	2.6	6.0/1.1	methanol, AgNO3/water	Aqueous	<400	300/Xe		Z. Zou et al./2002
$InTaO_4$, N-$InTaO_4$, V-		0.03	3.2		2-propanol/300ppm	Gaseous	400-530, 300-400	?	?	H. Irie et al./2005
$InTaO_4$, $InVO_4$, $InNbO_4$	NiO, Pt, Ru	0.5 in 270 ml	2.6, 1.9, 2.5	3.5, 5.0, 4.0	water Decomposition	Aqueous	>420nm		4 hours	J. Ye, et al./2002
$InTaO_4$,doped with Sc, Ti, V,			2.5	3.1/1.1	water Decomposition	Gaseous	>420			J. Ye et al./2005
$InTaO_4$	NiO	0.2	2.62-2.73	14.9/4.0	water Decomposition	Aqueous	>400	?	6-8 hours	Y. C. Chiou et al./2009
$NaTaO_3$		1	4.1 - 3.9	7600/3000	water Decomposition	Aqueous		400/Hg		C. C. Hu et al./2007
$NaTaO_3$, $KTaO_3$,		0.1	3.96,3.42, 3.08,3.14	36750, 1040,950,	Methanol/Water	Aqueous	UV			J. W. Liu et al./2007
$NiO/ATaO_3$ (A= Li, Na, K)			4.7, 4.0, 3.6	See table 2 for details		Gaseous	UV	400/Hg		H. Kato et al./2001
$AgTaO_3$, $AgNbO_3$	Pt+, NiO	0.15-0.3	3.4, 2.8	600/280, Ni/240	Methanol/Water, silver nitrate/Water	Aqueous, Vapors	< 300	300/Xe		H. Kato et al./2002
$NaTaO_3$:La	NiO/NaOH	1.0g	4.09	19800/9660	water Decomposition	Aqueous/CH_3OH	<400	400/Hg		H. Kato et al./2003
RE^+ doped $NaTaO_3$		0.5	4.03	See table 2 for details				400/Hg		A. Iwas et al./2002
$NaTaO_{3-x}N_x$	Nil	?	3.69		Formaldehyde	Gaseous	>400	500/Xe	12 hours	H. Fu et al./2008
$LaTaON_2$	Ru, Pt/ $AgNO_3$	0.3	2.1	38	water Decomposition	Aqueous	>400	?	?	L. Meiying et al./2006
$Bi2O_3$		0.5	2.93-3.10		RHB dye	Aqeous	> 420			L. Zhou et al./2008
$NaBiO_3$		0.4	2.6		2-Propanol/600ppm	Gaseous	>400		1hour	T. Kako et al./2006
$NaBiO_3$		0.3	2.6		MB	Aqueous	>400		1hour	T. Kako et al./2006
$NaBiO_3$		100m	2.3		PCP-Na/150ml	Aqueous	>400		1hour	X. Chang et al./2009
$NaBiO_3$		0.05	2.6		PAHC/0.003		>400		2 hours	J. Kou et al./2008
$NaBiO_3$		1	2.6		RHB dye/20mg/L	Aqueous	>400	500/Xe	2hours	Yu et al./2009
BiOCl		0.2	3.46		MO/10mg/L	Aqueous	<365	300 W Hg Lamp	12 minutes	K.-L. Zang et al./2006

BiOBr		0.4	2.54		Methyl Orange/400ml (10mg/L)	Aqueous	>420	300 W Xe	5hours	J. Zhang et al./2008
BiOX(X= Cl, Br, I)		0.1	3.22, 2.64, 1.77		MO/100ml	Aqueous	<400	500/Hal	3hours	X. Zhang et al./2008
BiOBr		0.2			NO/48ppm	Gaseous	310-400, >420	300/Hal	10 minutes	Zhihui AJ et al./2009
Bi_2WO_6		0.5	2.7		RHB dye/1x10-5M	Aqueous	254	12/Hg	1 hours	H. Fu et al./2006
Bi_2WO_6		0.1 in 100ml of	2.5		Rhodamine B (RHB)dye	Aqueous	>420		one hour	M. Shang et al./2008
Bi_2WO_6		0.5g/L	2.74		RHB dye/2x10-5M	Aqueous	>400	300/Xe	1 hours	Y. Li et al./2008
Bi_2WO_6		0.6-01m	2.7		RHB dye/2x10-5M	Aqueous	>245	25/Hg	1 hours	S. Zhang et la./2008
$BiWO_6$, $ZnWO_4$,		0.05	2.70, 3.31,2.43		RHB dye/2x10-5M	Aqueous	254, 290, 420, 490	12/Hg		H.Fu et al./2007
Bi_2WO_6:F		0.1	2.5		RHB dye/2x10-5M	Aqueous	>290	12/Hg	1 hours	H. Fu et al./2008
Bi_2AlVO_7, Bi_2InTaO_7		0.3	2.06, 2.81		MB/0.0506mmole/L	Aqueous	>400	300/Xe	3 hours	J. Luan et al./2009
Bi_2FO_7		0.3	2.22	39.7/19.6	Water, MB/0.0506mmole/L	Aqueous	>400, 390	300/Xe, 400/Hg	3 hours	J.Luan et al./2007
$BiCu_2VO_5$	Fe^{3+} and Ag^+	0.5	2.1	?/55	water	Aqueous	>400	300/Xe		H. Liu et al./2005
$ZnBiGaO_4$	NaOH	0.5	2.8	3030	H2S/0.50M	KOH/H2S	>400	?	?	B. B. Kale et al./2009
$Sr_2Bi_2O_5$, $SrBi_2O_4$,		0.3/L	2.87, 2.51, 2.34		MO/10mg/L	Aqueous	>400,<365		one hour	Z. Shan et al./2009
$BiVO_4$		1	2.4	?/421	water/AgNO3	Aqueous	>420	300/Xe		A. Kudo et al./1999
$BiVO_4$		0.1	2.4		4-Alkylphenols/2x10-4M	Aqueous	400	1000/Xe		S. Kohtani et al./2003
$BiVO_4$		0.2, 0.08	2.2		NO/400ppb,MB/100ppm	Aqueous /Gaseous	>400	300/Hal	1 hour	G. Li et al./2008
$BiVO_4$	$AgNO_3$	0.05	2.4	?/137	water Decomposition	Aqueous	>400	450/Hg	5 hours	S.S. Dunkle et al./2009
$BiVO_4$		0.5	2.39-2.46		MO/10mg/L	Aqueous			4hours	H. Li et al./2009
$Co_2O_3/BiVO_4$		3g/L	2.28-2.07		phenol/18mg/L	Aqueous	>400	1000/Xe	3 hours	M. Long et al.

Fe_2O_3,Co_3O_4, CuO/$BiVO_4$		0.2	2.33		MB/10mg/L	Aqueous	>420	300/H, 250/Hg		H. Xu et al./2008
$BiVO_4$	Pt^+	0.2	2.24		MO/10mg/L	Aqueous	>400	12	3 hours	L. Ge et al./2008
Ag doped $BiVO_4$		Film			Phenol	Aqueous	>400	150/ Xe		X. Zhang et al./2009
Ag/$BiVO_4$		0.2	?		MO/10mg/L	Aqueous	>420	500/Xe		A. Zhang et al./2009
$BiVO_4$		0.25	2.27-2.31		RHB dye/5m/L	Aqueous	>390, >365	Xe		A. Martinez-de la Cruz et
RE doped $BiVO_4$		0.2	2.5-2.4		MB/10mg/L	Aqeous	>400	150/Hal	5 hours	H. Xu et al./2009
Ta_2O_5	NiO	0.5	4	515/272	water	Aqueous	UV	450/Hg		Y. Takahara et al./2001
Eu_2O_3/Ta_2O_5		0.2	4		RB and 4-NP	Aqueous	>313	50/Hg		X.Yang et al./2008
Ta_2O_5	Pt	?	3.1-3.3	4450/?	water/CH3OH	Aqueous	>300	300/Vitaluc bulb	2 hours	M. Stodonly et al./2009
$K_3Ta_3Si_2O_{13}$, $K_3Nb_3Si_2O_{13}$,	NiO (See table 2 for	1.0g	4	368/188	Water	Aqueous/NaOH	<400	400/Hg	?	H. Kato et al./2003
$Cd_{1-x}Z_xS$		100m		16.32 and 2007			300, and <420	300/Hg	300min (UV)	C. Xing et al./2005
Pt-PdS/CdS	Pt, PdS	0.3	2.3	8.77mmol/h	water	NaS/Na2SO3/H2O	>420	300/Xe	25 hours	H. Yan et al./2009
		0.1	?		NO/48ppm	Gaseous	>400	300/Hg		G. Li et al./2009
		0.08	?		MB/10ppm	Aqueous	>400	300/Hg		G. Li et al./2009
CdS/TiO_2		0.08	?		4-Chlorophenol/0.1mmol	Aqueous	>400	300/Hg		G. Li et al./2009
$Cd_2Sb_2O_{6.8}$		0.3, 0.06, 0.06	3.9		Benzene /210ppm, RhB, MO	gaseous/Aqueous	>254	4/G4 T5		M. Sun et al./2009
V_2O_5		0.02	2.18-2.20		RHB dye	Aqueous	<365	125/Hg		Hai-Long Fei et al./2008
V_2O_5/LaF_3		5	composite material		acetone	Gaseous	>320, >380	500/Hg	5 hours	J. Wang et al./2008
$LaVO_4/TiO_2$		1.2	2.1-3.2(composite)		Benzene/250ppm	Gaseous	400-900	500/Xe		H. Huang et al./2009
$In_2O_3/Ba_2In_2O_5$		0.05	In_2O_3 = 2.88, $Ba_2In_2O_5$= 3.02		MB/10ppm	Aqueous		500/Xe		W. Ku-Chang et al./2009

$AgSbO_3$		0.5	2.5-2.7		Methylene Blue/150ml	Aqueous	<400, 400-800		3hours	J. Singh et al./2009
		0.3	2.8		Alizarin Red (AR)/16mg/L	Aqueous	>400	Xe	2hours	S. Ouyang et al./2006
$AgAlO_2$		0.3	2.8		Acetaldehyde/1270ppm	Gaseous	>400		2hours	S. Ouyang et al./2006
RE^{3+} Ag_3VO_4		0.075	2.34,		RHB dye/10mg/L	Aqueous	>400	30/Hal		H. Xu et al./2009
Ag_3VO_4	NiO		2.14		ARB dye	Aqueous	>400	350/Xe		Hu et al./2007
SnO_2:Zn^{2+}		0.05	3.8 -4.0		Methylene Blue	Aqueous	254	20/Hg		L. Li et al./2009
In_2TO_5		0.5	3.02		MO/10mg/L	Aqueous	>365	300/Hg	1 hour	W.-D. Wang et al./2007
$Cs_{0.68}Ti_{1.8}3O_{4-x}N_x$ and		0.1	2.73/2.85		RhG/4x10-5mol/L	Aqueous	>400	300/Xe		L. Wang et al./2009
Gold nanoparticles	Supported on ZrO_2				Formaldehyde	Gaseous	400 - 500			X. Chen et al./2008
CdS-DMF		2.5mMole	?	1.1μmol	CO2	Aqueous	>420		10 hours	S. Yanagida/1997
$InTaO_4$	NiO	0.3	2.6		CO2	Aqueous	<400	Fluorescent lamp		H.-C. Chen et al./2008

Appendex-1

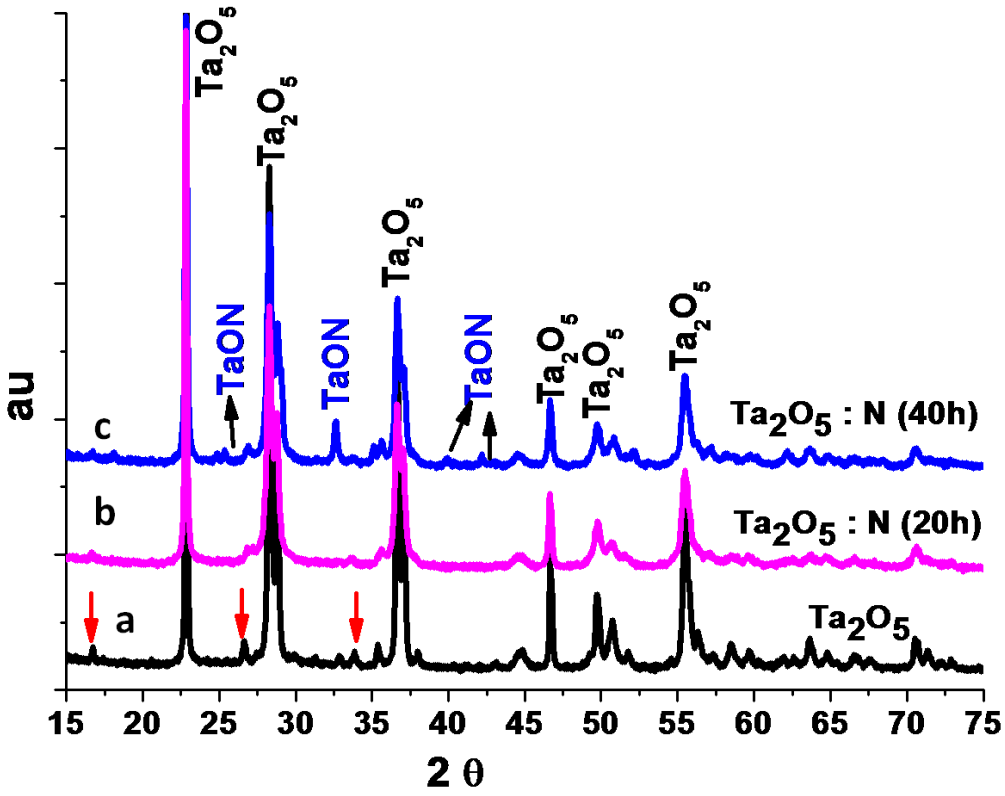

Figure 1.1 XRD analysis of commercial Ta_2O_5 a) non-treated, b) treated in nitrogen environment for 20 hours, and c) treated for 40 hours

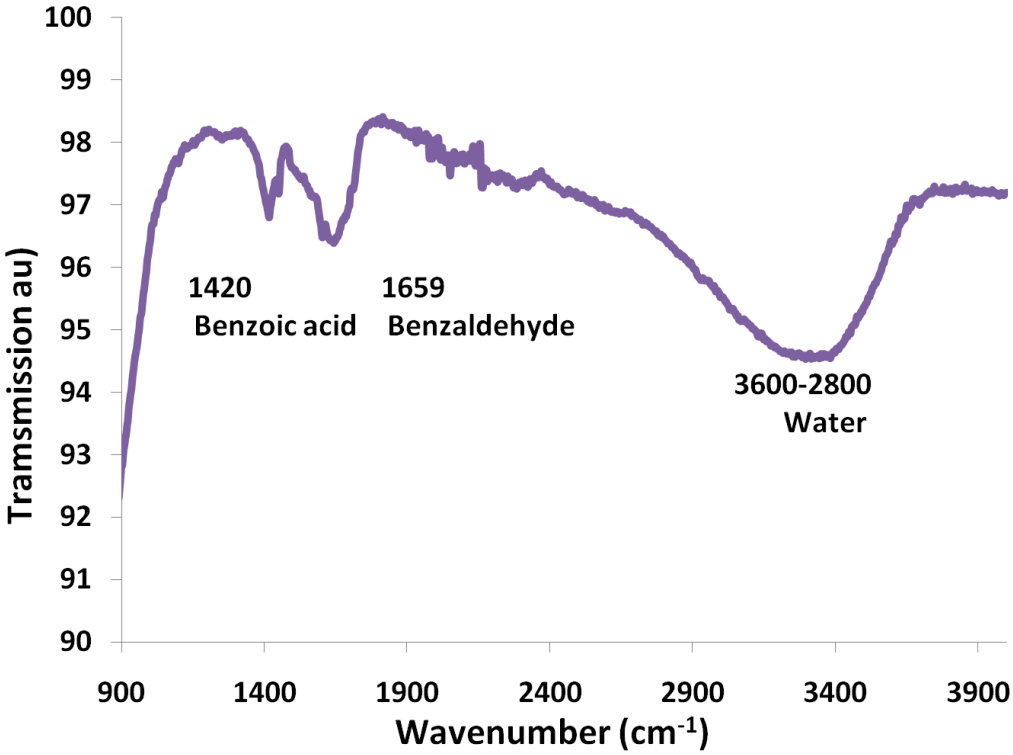

Figure 1.2 FTIR analysis of TiO_2 (P25) used for toluene decompositions indicating adsorption of intermediates at 1420 cm-1, 1659 cm-1 and 3600-2800 cm-1 which corresponds to benzoic acid, benzaldehyde and water.